Department of Mechanical Engineering

Understanding the effect of skin mechanical properties on the friction of human finger-pads

Xiaoxiao Liu

Submitted for the degree
of
Doctor of Philosophy

March 2013

Department of Mechanical Engineering

Understanding the effect of skin mechanical properties on the friction of human finger-pads

Xiaoxiao Liu

Submitted for the degree of Doctor of Philosophy
March 2013

The aim of this work is to achieve an understanding of the effect of skin mechanical properties on the friction of human finger-pads. This project primarily concentrates on gaining a more fundamental understanding of the frictional properties of skin. To achieve this, various parameters (epidermis thickness, sweat-gland counts, etc.) affecting skin friction were evaluated using an *in-vivo* technique, Optical Coherence Tomography (OCT) and a friction testing device. This project is also interested in investigating how those parameters alter the friction for different ages, genders, ethnicities and different contact conditions, such as moisture, temperature, loads, etc.

Experimental studies were conducted to investigate the skin frictional behaviour. The findings showed that the skin friction obeys a two-term relationship. The skin friction was found to be strongly associated with its Young's modulus.

Tests on the skin structural properties showed the moisture level of the skin, skin thickness and skin morphological properties play important roles in determining the skin friction. The findings gained can be applied to explain how the skin friction varies among different participants. Further tests showed that physico-chemical properties of the skin can have a significant effect on the skin friction.

The OCT system was combined with a multi-axis force plate to measure the contact area between fingers and smooth surfaces. Static measurement showed both apparent and real contact area increase with normal load following a power-law relationship. This is associated with the skin mechanical properties. The dynamic contact area was investigated using a Digital Image Correlation (DIC) method. As a finger was sliding along a flat surface, the dynamic apparent contact area was found to decrease with time.

There was a “bell curve” response observed in the skin friction when a finger was soaked in water for 400 s. This is thought to be due to the water absorption. It was achieved by investigating the structural and the mechanical properties of skin. The mechanism of water absorption reduced skin stiffness, which resulted in a rise of the contact area.

Finally a pilot study on sub-surface deformation *in-vivo* at human fingers during movement was conducted using combined OCT and friction measurements. This study provided some knowledge of the effect of the skin lateral Young’s modulus on the skin friction.

Keywords: Skin tribology, OCT, Skin structure, Skin mechanical properties, Contact area, Hydration, DIC.

Acknowledgements

First of all, I would like to thank my excellent PhD supervisors, Dr Roger Lewis and Dr Matt Carré, not only for offering me the opportunity to pursue my Doctor studies but also for their support, inspiration and encouragement throughout the past three years. I would also like to give my deep thanks to my third supervisor, Dr Steve Matcher. Without their help, I could not have completed my dissertation.

I would like to thank the many people who have help during my PhD, including; Dr Zenghai Lu for help with the OCT system, Jamie Booth and Chris Grigson for their technical support in equipment design; Daneil Gad for help on experiments; and all PhDs and RAs at the Mechanical Engineering Department for their kind help in this research.

I would also like to thank my husband, Qian Zhang, whose patience, love and encouragement allowed me to accomplish this degree.

Finally, I would like to thank my great parents, my sisters and brothers, to whom this thesis is dedicated, for their love and constant support through my life.

Contents

List of Figures

List of Tables

Abbreviations

AU	Arbitrary Units
CCD	Charge Coupled Device
COF	Coefficient of Friction
COP	Centre of Pressure
DAQ	Data Acquisition Unit
DIC	Digital Image Correlation
MRI	Magnetic Resonance Imaging
NMF	Natural Moisturizing Factor
NCOR	Normalised Correlation Coefficient
OCT	Optical Coherence Tomography
RTV	Room Temperature Vulcanizing
SC	Stratum Cornuem
SD	Sweat Duct
SEMM	Scanning Electron Microscope Mirror
TEWL	Transepidermal Water Loss

Nomenclature

A	contact area (m^2)
A_H	Hamaker constant (J)
A_o	apparent contact area (m^2)
A_P	area of the probe of cutometer (m^2)
A_{re}	real contact area (m^2)
a	radius of the circle of contact (m^2)
B	constant
b	contact specific constant
C	Capacitance (f)
c	specific contact area exponent
D	Distance (m)
d	distance between molecules (m)
d_j	contact length for individual skin ridge (m)
d_p	distance between negative and positive poles (m)
E	reduced Young's modulus (N/m^2)
E_l	lateral Young's modulus of skin (N/m^2)
E_{skin}	Young's modulus of skin (N/m^2)
E_{sub}	Young's modulus of a contacting substance (N/m^2)
E_v	normal Young's modulus of skin (N/m^2)
E_{xx}	strain value in xx direction
E_{yy}	strain value in yy direction
E_{xy}	total strain value
E'	Green-Lagrange strain tensor
e	constant
F	friction force (N)
F_{ad}	adhesion force (N)
F_{chem}	force due to chemical bonds and acid-base interactions (N)
F_{de}	deformation force (N)
F_{el}	electrostatic force (N)
F_{hy}	Hysteresis friction force (N)
F_i	force due to chemical bonds (N)
F_{int}	interlocking friction force (N)
F_0	force due to no-specific interaction (N)
F_{vdW}	van der Waals force (N)
F_x	friction force in x direction (N)
F_y	friction force in y direction (N)
F_z	friction force in z direction (N)
F'	deformation tensor

f	pressure coefficient
G	van der Waals energy (W)
g	length of the semi-minor axis of ellipse-shape contact area (m)
H	constant
h_{ridge}	height of a ridge (m)
i	length of the semi-major axis of ellipse-shape contact area (m)
j	number of skin ridge
k	proportionality constant
L	length of the contact area (m)
L_{ap}	total contact length (m)
L_{re}	real contact length (m)
m	constant
N	normal load (N)
N'	resultant force (N)
n	constant
n_{ap}	exponent related to the static area of apparent contact
n_{re}	exponent related to the static area of real contact
p	contact pressure (N/m^2)
Q	electronic charge (C)
q_{stick}	traction in the stuck area (N)
R	radius of sphere (m^2)
R^2	square of the correlation coefficient
Ra	finger surface roughness (μm)
R_0	immediate skin extensibility (U_e)
R_2	gross elasticity of skin (U_a/ U_f) (N/m^2)
R_5	net elasticity of skin (U_r/ U_e) (N/m^2)
R_6	portion of the viscoelasticity on extensibility (U_v/ U_e)
R_7	biological elasticity of skin (U_r/ U_f) (N/m^2)
${r_s}^2$	stick ratio of the struck region area to the total contact area
S	skin stiffness (N/m)
S_l	lateral stiffness of skin (N/m)
S_v	normal stiffness of skin (N/m)
s	size of sensor surface
t	estimated standard error of a regression
U	constant
U_a	recovery of skin after remove vacuum of cutometer
U_f	skin distensibility
U_r	skin immediate retraction
U_v	skin viscoelasticity
V	sliding velocity (m/s)
W	elastic work done (W)
v_{skin}	Poissons ratio of skin
v_{sub}	Poissons ratio of a contacting substance

β	viscoelastic hysteresis loss fraction
δ	penetration depth of skin (m)
ε_{skin}	dielectric constant for skin
ε_1	dielectric constant for medium delectirc
ε_0	dielectric constant for air
ρ	constant
η	viscosity of fluid ($Pa.\ s$)
τ	the interfacial shear stress (N/m^2)
τ_0	intrinsic interfacial shear strength (N/m^2)
θ	angle of a ridge
λ	distance between each ridge (m)
μ	skin dynamic friction coefficient
μ_{ad}	adhesion component of friction coefficient
μ_{def}	friction coefficient due to deformation mechanism
μ_s	static friction coefficient
$\mu_{viscous}$	friction coefficient due to hydrodynamic lubrication

Chapter 1

Introduction

1.1 Background

The term of "biotribology" was introduced by Dowson and Wight in the early 1970s (Dowson & Wight, 1973), and embraces all concepts of lubrication, wear, and friction concerned with biological systems. Biotribology is an interdisciplinary subject that draws on a range of rheology, biomechanics, chemistry, material science, etc. The subject has grown enormously and become one of the most exciting research areas in past decades. The range of research topics covers biological attachment and friction in animal world to human joints, replacement and soft-tissue friction (Dowson, 2012), which can be classified into two groups (Stachowiak & Batchelor, 2005):

a) the frictional processes that naturally occur in tissues and organs of animals or humans.

b) the frictional processes that arise after implantations of artificial organs or medical devices in human body.

Initially, studies of friction in natural biological systems were carried out on a wide range of sliding and frictional interfaces. With respect to most of these interfaces, lubrication is essential to successful functional operations in humans or animals. One of the most typical examples is the articular interfaces of synovial joints lubricated by *a* mixed lubrication. There is some contact and wear generally takes place in these synovial joints during movements of human or animals, such as running, walking, and jumping. In order to meet these functional needs, some boundary lubricating films are required to reduce friction, wear, and provide good protection to these

cartilage surfaces. In addition, natural friction processes are also found in other biological systems, such as the interactions between eyelids and corneas in humans, the contact between skin and external objects in humans or animals, and the motion of combing hair (Gohar & Rahnejat, *2008;* Dowson, *2012*). The application of tribology relating to implantations of artificial devices in the human body is one of the main research areas in biotribology. This subject has been extensively studied with aims to protect the implanted devices from wearing down and creating pain due to friction, and give them longer functional life. Consequently, these studies are specifically concerned with several aspects of this frictional process, including the tribology of artificial joints replacements, wear of screws and plates in bone fractures repair, wear of denture and restorative materials, and wear of replacement heart valves (Davim, 2010). Skin is the largest organ in human body, it acts as a protective shell between the internal and external environments, preventing all kinds of physical and chemical damage to the inner organs, maintaining water balance and regulating body temperature. As the first line of defence, skin is always exposed to the external environment, and has to directly contact with a variety of surfaces in human daily activities. Many problems from the physical or chemical interactions between human skin and contacting materials have been reported. For example, sweating during exercise can result in a slippery surface and cause sports injuries. This could be prevented by adding powder on the contact interface or using sports equipments with non-slip surfaces to provide high friction force. It is not always necessary to retain high friction coefficient in human daily tasks. For instance, high friction forces between human skin and the blades of a hair shaver can lead to a large skin deformation and cause skin cutting. Therefore, a lower friction coefficient is required in this case. Consequently, in order to satisfy human needs and improve the quality of human life, knowledge of these problems is required. In recent years, the tribology of human skin has become one of the key topics in the study of biotribology. This topic is also an interdisciplinary subject and closely related to many research areas.

1.2 Motivation for this Research

To date, the study of bio-tribological properties of skin at human finger-pads has attracted much attention, which is attributed to its importance in human daily life. A good understanding of skin friction is generally believed to have potential benefits to

the performance of conducting tasks, but also the prevention of pain and discomfort (for instance, a good understanding of the mechanism between skin and various materials could help avoid the chance of getting blisters on human hands). As a finger comes into contact with surfaces and start to move, there are four key factors that appear to strongly influence the skin friction between the finger-pad and the contacting surfaces, including the complex interplay of materials, properties of finger-pad skin, contact conditions and environmental conditions (see Figure 1.1). The current knowledge of the tribology of finger-pad skin is mainly focused on skin in touch with various materials under various testing conditions. The mechanical properties of skin related to cosmetic or skin-care products have been fully examined using various techniques. However, very few studies have addressed on the contribution of skin mechanical properties on its frictional properties.

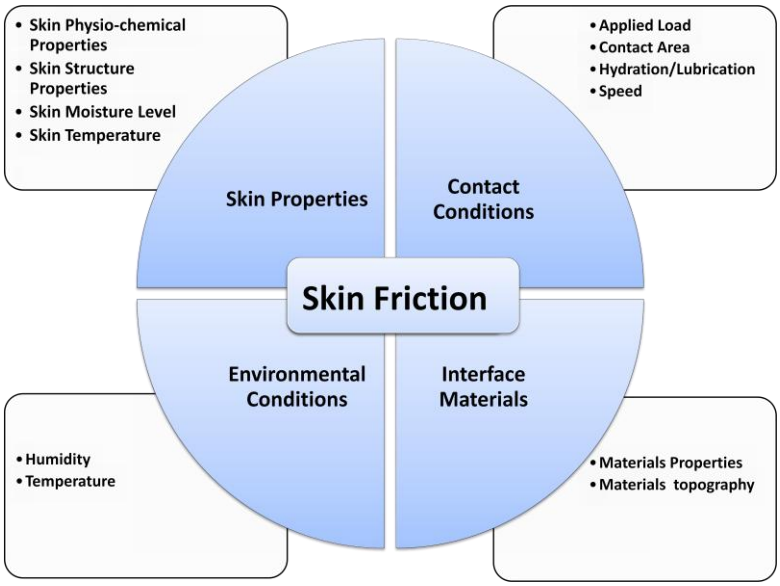

Figure 1.1: Important factors affecting human skin friction

The mechanical properties of skin were found to be strongly dependent on its structural properties (Peter, 1991; Frederick et al., 2001). Geerligs et al. (2011) developed a finite element model to estimate the Young's modulus of a tested sample with different thicknesses based on a NeoHookean model. They found that the Young's modulus is inversely proportional to the thickness of samples. Therefore, an understanding of mechanical and structure properties can be achieved by examining the morphological features and internal structures of skin. It would be very helpful if

these external and internal geometries of human skin could be directly imaged. In order to characterise skin properties and their effects on skin friction, it is necessary to characterise skin's mechanical properties (i.e. Young's modulus), structural properties and physico-chemical properties. In previous research, it was found that the skin friction coefficient varies widely from person to person, and even within the same person at different anatomical regions (Cua et al., 1990; Zhang & Mak, 1999; Sivamani et al., 2003; Derler et al., 2009; Zhu et al., 2011, Veijen et al., 2012). It is believed that investigation of the skin structure may help to explain the wide spread of friction data found among test candidates and anatomical regions.

Skin friction is found to not only depend on the skin's properties and the contact materials, but on its contact parameters (e.g. contact area, sliding speed, and sliding direction) (Tomlinson et al., 2007; Terekhov & Hayward, 2011). By examining the area of contact between human skin and surfaces, it is believed, the understanding of the friction mechanisms can be improved. A study of surface area between fingertip and surfaces conducted by Terekhov and Hayward (2011), suggested that the total contact area could divided into a shrinking, stuck region and a growing, slip region. The minimal surface adhesion area is considered to be associated with the dynamic friction coefficient. An experimental model has been developed by Bowden & Tabor (1964) with aims to explain the relationship between the friction force and the contact area. However, measuring the area of contact between the skin and objects under a certain load is difficult due to the current limited techniques. A number of different techniques have been applied to analyse the contact area, such as an ink stamping method (Childs, 2006; Warman & Ennos, 2009; Tomlinson, 2009), optical method (Andre´ et al., 2008; Soneda & Nakano, 2010), and electrical resistance (Tomlinson, 2009). However, most of those methods described only allow measurement of the area of contact statically. In addition, there were also big errors occurred in some measurements due to the drawbacks of ink spread, noise effects and threshold value setting in later image processing. Thus, exploration of a new method for measuring dynamic contact area is desirable.

From previously published literature, it is also noted that the friction of skin is sensitive to different environmental conditions, e.g. hydration, temperature, etc. (Adam et al., 2007; Tomlinson et al., 2007; Andre´ et al., 2008; Gerhardt et al., 2008;

Soneda & Nakano, 2010; Hendriks & Franklin, 2010, Veijen et al., 2012). Three possible mechanisms were proposed for the friction increase: water absorption, viscous shearing of liquid bridges formed and capillary adhesion (Dinc et al., 1991). With respect to the mechanism of water absorption, Tomlinson et al. (2010) attribute the changes of skin friction to the changes of skin mechanical parameters (e.g. stiffness, Young's modulus) and some contact parameters (e.g. contact area, sliding speed) caused by water being absorbed through the skin. Therefore, investigating the changes to the skin structure provides another effective way to study the effects of hydration on skin friction.

1.3 Aims and Objectives

The aim of this study is to gain a further understanding of the frictional properties of human finger-pads. The results of the study will contribute to fundamental knowledge that is required in those studies related to human-object interactions. For example, knowledge of the friction involved an interaction between human fingers and objects under different conditions can be fed into product design and development for different backgrounds. In addition, this research could be used to evaluate skin care or cosmetic products as the Optical Coherence Tomography (OCT) allows accurate in-vivo assessment of morphological properties of human skin, as well as the internal structure.

The objectives of the thesis proposal are summarised as:

- Investigating the influence of mechanical properties of human skin on frictional properties of finger-pads.
- Investigating potential relationships between skin structural parameters and skin friction.
- Measuring both the static and dynamic contact area of finger-pads, and determining the relationship between contact area and skin friction.
- Studying the mechanism of water absorption and its effect on friction of human finger-pads.
- Assessing the in-plane deformation properties of finger-pad skin during finger sliding.

1.4 Contributions of the Thesis

The main contributions of this thesis are of following:

- The relationship between the skin friction coefficient of finger-pads and normal loads has been investigated using different techniques. A two-part model has been proposed to describe the frictional properties of finger-pads skin.
- Skin friction of human finger-pads is found to be strongly dependent on its mechanical properties (i.e. Young's modulus).
- An Optical Coherence Tomography system (OCT) approach has been used to measure structural properties of finger-pad skin. The effects of skin structural properties on the friction of finger-pads have also been investigated, which could help to explain the wide spread of skin friction of finger-pads among subjects.
- Different methods have been developed to measure the static and dynamic contact areas between finger-pads and contacting surfaces, in particular real contact area, including a finger-print ink method, an OCT method, and a Digital Image Correlation method (DIC). The relationship between contact area and skin friction has been investigated using both theoretical and experimental data.
- The proposed mechanism of water absorption concerned with skin hydration has been studied via investigating the thickness of stratum corneum (SC) of finger-pad skin and contact area.
- In order to study the in-plane deformation properties of finger-pad skin, a 2D DIC method has been developed.

1.5 Structure of the Thesis

The thesis is organised into eight chapters that address the key aspects of this research:

Chapter 2 presents a review of the current knowledge of the tribology of human skin, including the basic concepts relating to human skin structure, skin mechanical

properties, theoretical background of skin friction, and the influences of skin properties, contact materials and contact parameters on skin friction. The later part of this section also describes various techniques used for measuring skin friction and skin structure in previous studies.

Chapter 3 outlines equipment and testing procedures that have been developed for investigating the structure, mechanical, and frictional properties of human finger-pad skin at The University of Sheffield and Philips Applied Technologies in the current study.

Chapter 4 describes the comparison of different techniques used to measure the human skin friction in order to select the most suitable device for the measurement of the skin friction coefficient of finger-pads in this research. Experimental studies on investigating the relationship between friction coefficient and normal load have also been carried out. The frictional properties of human skin are further studied using artificial fingers. Finally, it discusses the influence of age, gender and ethnicity on skin friction of finger-pads.

Chapter 5 presents work on assessing the physical parameters of finger-pad skin, which is expected to help explain the wide spread of friction data among tested subjects. The relationship between the superficial serum/sweat of skin on skin friction is studied by a tape stripping method. A skin rubbing method is also introduced to examine the effect of the stratum corneum thickness on skin friction.

Chapter 6 describes two different techniques used to measure the contact areas between finger-pads and contacting surfaces, including a fingerprint ink method and an Optical Coherence Tomography method. However, these two methods are restricted to static measurements, and cannot be used to investigate the relationship between contact area and skin friction. Further studies describe a new Digital Image Correlation method (DIC) method to determine dynamic contact area during finger sliding.

Chapter 7 investigates the mechanism of water absorption that has been proposed to explain the changes on the skin friction related to skin hydration. This study has been completed by analysing the morphology and mechanical properties of skin when the

tested finger was soaked in water. In addition, the effect of water absorption on the contact areas has also been carried out.

Chapter 8 describes a new approach (2D DIC) to study the in-plane deformation of finger-pad skin in vivo during finger sliding. The full field maps of the displacement and the strain are presented, which is believed to assess the deformation behaviour of finger-pad skin with respect to different stages of movements as well as different loads.

Chapter 9 describes the details of key findings resulting from this research and discusses future work.

Chapter 2

Literature Review

In this chapter, the current findings and fundamental concepts of skin frictional behaviour are presented. It starts with an overview on the anatomy and histology of the skin, as well as its mechanical properties for individual layers. Then, a general introduction to the theoretical background of skin friction is given, followed by the influences of the skin properties and complex interplay of materials on skin friction since they are intimately associated with the skin friction. Some other parameters such as load, contact area, hydration, lubrication and speed are important for the skin friction and are investigated in this chapter, particularly contact area and hydration. Finally, various techniques with respect to the skin friction measurement and the study of skin structure are discussed.

2.1 Structure of Skin

Skin is the largest organ in the body and it is also the first line of defence to the exterior to protect humans against inhospitable environment and damages. In the mean time, it is very important for maintaining the human body in a balanced and healthy condition through its principle processes, including absorption, thermoregulation, sensation, etc. Skin consists of an approximate area of 1.5 m^2 to 2 m^2 in an adult and 0.2 m^2 to 1 m^2 in child; most of it is 2 *mm* to 4 *mm* thick depending on the anatomic location on the body, as well as age, gender and other factors. The skin on palm and the soles of feet is relatively thicker than other parts of body, while the thinnest skin is found on the eyelid (approximate 0.5 *mm*) (Wood & Bladon, 1985; Jones & Lederman, 2006; Schlangen & Nuijs, 2000). Areas of thick skin are “glabrous” (having no hair) and covered with a pattern of ridges. Sometimes

termed “friction skin”, it improve the performance involved in physical activities (e.g. grasping) (Jones & Lederman, 2006).

Human skin is mainly composed by two distinct layers: the epidermis and the dermis, as shown in Figure 2.1. The outside layer is the epidermis, which directly contacts with the environment. The epidermis is also divided into five layers, which are, in descending order: stratum corneum, stratum lucidum, stratum granulosum, stratum spinsum and stratum basale. The stratum corneum consists of dead cells without a nucleus that are divided and transferred from the inner stratum basale. In the sub-division process of cells in the stratum basale, half new-borne cells move towards the surface and begin a maturation process, while the other half new-borne cells remain on the basement and continuously divide. Once those new-borne cells enter the stratum spinsum layer, they synthesize a kind of protein, keratin. These keratins start to lose their nuclear and become dead and dry cells as they migrate towards the outmost surface of the skin (Wood & Bladon, 1985; Jones & Lederman, 2006). The thickness of the stratum corneum is found to be only 0.06 *mm* to 0.1 *mm* in most regions of the body. The thickest stratum corneum is found on the palm and feet soles which help to give them additional protection since they are involved in daily activities more frequently compared with other parts of the body. The stratum corneum is also covered by a film of serum that is result of secretion from sebaceous glands, water and sweat. This film of serum acts as a barrier to prevent water loss and moisten skin.

Beneath the epidermis is the dermis, it consists of papillary and reticular layers, and is much thicker than the epidermis (5-7 times higher). The papillary layer is the interface between epidermis and dermis. In the skin of palm and feet soles, the pattern of ridges in the epidermis is formed based on its dermal papillae structure. Additionally, the papillary layer contains a large amount of connective tissues cells, and small and loose of collagen and elastin fibres. Compared to the papillary layer, the reticular layer contains a high density of collagens, elastin and the extrafibrillar matrix, which provides strong support to the skin and gives skin its properties of elasticity and extensibility. With aging, the elastins gradually lose elasticity, and in this case, skin becomes looser and wrinkles appear. As can be seen in Figure 2.1, there are lots of blood vessels, nerves endings and various glands can be found in the

dermis, which provide nourishment to the epidermis, and also help remove waste generated from the body and regulate the body temperature (Jones & Lederman, 2006; Schlangen & Nuijs, 2000).

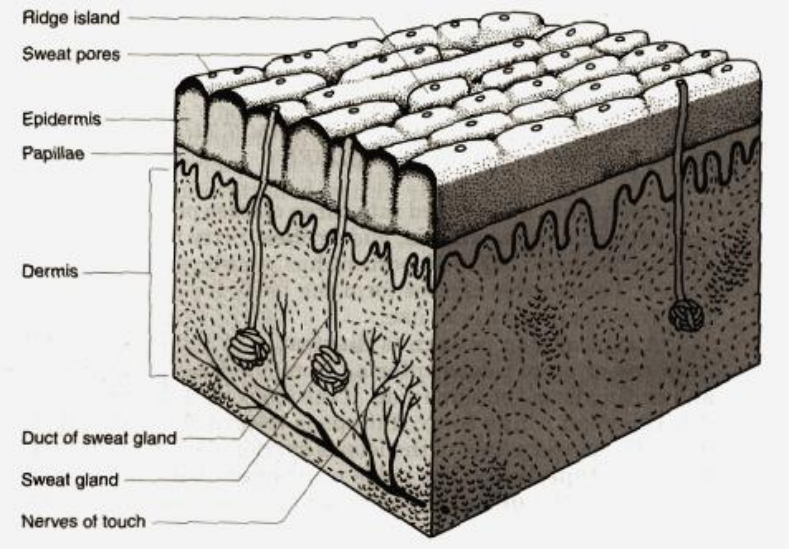

Figure 2.1: Structure of finger skin (Katz, 2005).

2.2 Skin Mechanical Properties

Unlike normal solids, human skin exists as a heterogeneous, anisotropic and a non-linear viscoelastic material that is very similar to rubber (Hendriks, 2005; Delalleau et al., 2008). The skin's mechanical properties include both elastic and viscous properties and are intimately associated with its complex structure (Payne, 1991). As discussed above, each layer of skin is made of various types of tissue, and possesses different mechanical properties. For example, in the dermis, collagen and elastin fibres form a network that not only supports the structure of skin, but also provides its elasticity. Viscous properties of skin are related to delayed recovery from deformation which attribute to viscous sliding of fibrous networks. Therefore, the mechanical behaviour of the skin is ascribed to the contribution of dermis in most research and generally characterised by a non-linear stress-strain relationship. The ratio of stress over strain is considered the elasticity of the skin (Young's modulus). This stress-strain relationship can be split into three stages (see Figure 2.2). In stage I, the stress-strain follows a linear relationship with a Young's modulus of 5 kPa, which is due to the fact that the elastins in the dermis provide a resistance "buffer" to

skin deformation. In the second stage, collagen fibres involved gradually stretch instead of elastin fibres, resulting in a non-linear stress relationship for strains greater than 0.3. In the third stage, all collagen fibres are stretched, contributing to the stress-strain behaviour appearing as a straight line again, and the corresponding slope of the straight line becomes steeper, thus skin becomes more stiff (Silver et al., 2001; Hendriks, 2005; Holzapfel, 2000).

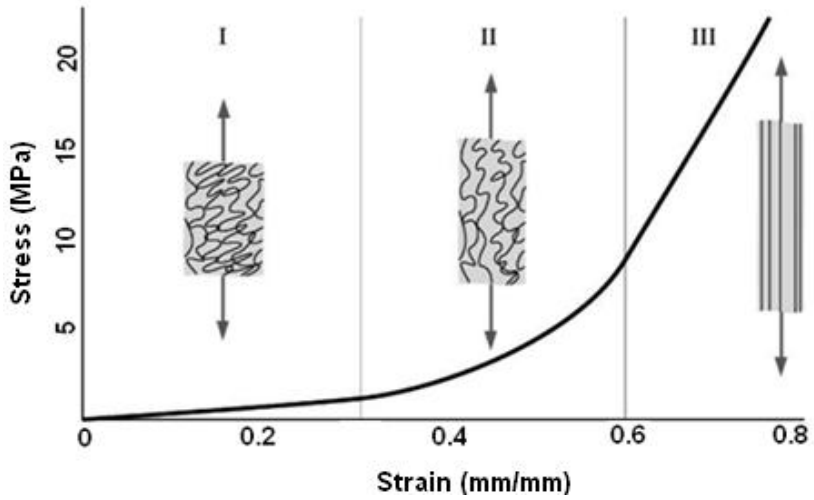

Figure 2.2: The stress-strain relationship for normal human skin related to a tension test, modified from Holzapfel (2000).

In contrast to the dermis, the epidermis is mainly composed of keratinocytes and is relatively thin in most regions of the body. In previous studies, some researchers believed that the contribution of the epidermis to the overall mechanical properties of skin is so small that it can be neglected (Peter, 1991; Hendriks, 2005), except for the palm and the feet soles. However, the epidermis is considered important in determining the skin mechanical properties as it is the outmost layer, interfacing with the external environment and influencing the skin conditions directly as it is affected more by exogenous factors, such as temperature, humidity, cosmetics and etc. A number of studies on investigating the effects of humidity and hydration on the elasticity of skin have been reported. Richard et al. (1971) found an initial decrease in the breaking strength of the stratum corneum as relative humidity rises from 1 to 100%. The elongation at fracture increased from 20% to 190%, however. A similar observation was also found by Wu et al. (2006) and Liang and Boppart (2010). The results in their experiments indicated that the Young's modulus is reduced with increasing hydration, which could be attributed to the hydrating process softening the

stratum corneum. In addition, Agache et al. (1980) also reported that the Young's modulus varies with respect to age, regions of body and individual.

The measurement of skin mechanical properties has been carried out using various methods *in-vivo* and *in-vitro,* which can be mainly classified into tensile tests (e.g. suction), compression tests (e.g. indentation) and torsion tests (see Table 2.1). The tensile test is a method for determining the behaviour of materials under axial tensile loading and can be performed on many materials including metals, plastics, rubbers, etc. In the studies of skin mechanical properties, most measurement techniques were designed based on the tensile deformation test. For example, suction test is commonly used to measure elastic and mechanical properties of the upper skin layer *in-vivo* (more details about the techniques are described in Chapter 3). Different from the tensile test, the compression test is method for determining the behaviour of materials under s compressive load. This test is generally used to measure elastic limit, yield strength, compressive strength, etc. Recently, some researchers have used this method to measure the elasticity of human skin (Bader & Bowker, 1983). The Young's modulus in a lateral direction was reported to be closely associated with the thickness of skin and stiffness in both tensile and compression tests (Park & Baddiel, 1972; Daly, 1982; Hendriks, 2005; Pailler-Mattei et al., 2008; Delalleau et al., 2008). The torsion test can provide global mechanical properties of human skin. For example, Escoffier et al. (1989) using a torsion device to investigate the Young's modulus on a participant's forearm. They found that the Young's modulus seemed not to be influenced by the hypodermis and underlying tissue of skin.

Not much information in connection to skin properties effects on skin friction is given in previous studies. The only work that has been done by Pailler-Matteri et al. (2007), suggested that the coefficient of friction increases due to skin adhesion force. It was also observed that both normal and lateral stiffness of skin were reduced by tape stripping, which was in good correlation with evolution of skin adhesion force; however, no evidence showed that there is a direct relationship between skin stiffness and the skin friction.

Table 2.1: *In-vivo* measurements of the modulus of elasticity for skin.

Authors	Skin region	Measurement technique	Young's Modulus (Elasticity)
Bader & Bowker (1983)	Forearm/Thigh	Indenter (20 *mm*)	11.1-2.0 kPa (whole skin)
Agache et al. (1980)	Forearm	Torsion (25 *mm*)	0.42 MPa (young skin) 0.85 MPa (aged skin)
Barel et al. (1995)	Back	Suction (2 *mm*)	2.1 MPa (stratum – corneum)
	Forearm		0.13-0.17 MPa
	Forehead		0.20-0.32 MPa
Diridollou et al. (2000)	Volar forearm	Suction (6 *mm*)	0.153 MPa
Hendriks et al. (2005)	Forearm	Suction (6 *mm*)	2.1 x 10^9 Pa (dermis)
Sanders (1973)	Doral side forearm	Torsion (8.7 *mm*)	0.02-0.1 MPa
Grahame (1969)	Forearm	Suction	18-57 MPa
Escoffier (1989)	Forearm, anterior part	Torsion	1.1-1.32 MPa
Alexander & Cook (1976)	Forearm, upper back	Suction	270-350 Pa
	Forearm, anterior part		270-800 Pa

2.3 Theoretical Background of Skin Friction

The frictional behaviour of skin is complex and involves different interactions between skin and substrates, which can be interpreted using the friction behaviour of rubber since skin shows similar viscoelastic properties as rubber. Those physical reactions are the results of many different mechanisms, such as interfacial shear, adhesion, capillary action and viscoelastic hysteresis (Derler et al., 2009; Tomlinson, 2009). A simple model (Amonton's law) cannot provide an accurate description for the skin friction. In dry sliding contacts, the skin friction is generally modelled as viscoelastic deformation forces of microscopical asperities in contact, (see Figure 2.3). Skin friction can be described to follow a classical two-term model; it is given by (Bowden & Tabor, 1954):

$$F = F_{ad} + F_{de} \tag{2.1}$$

where F_{ad} is the adhesion force of the interface, F_{de} is related to the incomplete recovery of the energy dissipated by skin deformation.

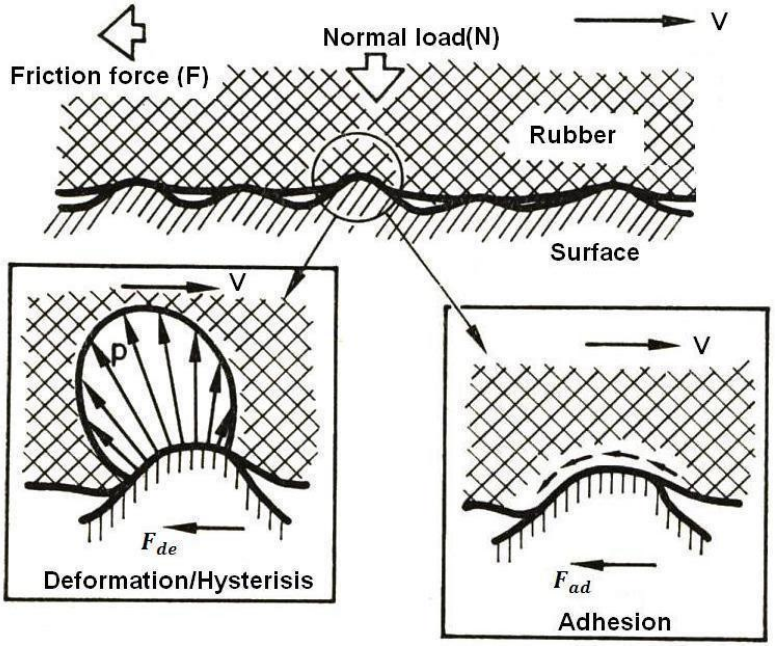

Figure 2.3: Principle components of elastomeric friction, modified from (Moore, 1971).

However, the friction of skin is assumed to be only associated with an adhesion mechanism, for dry and smooth surfaces, while the deformation is normally ignored (Wolfram, 1983; Johnson et al., 1993; Adams et al., 2007). Therefore, the friction force is expected to follow a linear relationship (Johnson, 1993; Han et al., 1996):

$$F = F_{ad} = \tau A_{re} \tag{2.2}$$

where τ is the interfacial shear stress and A_{re} is the real contact area. The adhesion force is determined by two factors: a) surface energetic of the counterfaces, i.e. the molecular nature of adhesive bonds-Van der Waals forces, electrostatics, hydrogen, hydrophobic, etc. and b) the area of contact over which such adhesive bonds are formed (Tomlinson, 2009; Mossel & Roosen, 1994; Tang et al., 2008). According to Herzian theory, the contact area is proportional to the 2/3 power of the load, in the case of a hemispherical probe sliding on deformable materials such as rubber or skin (Johnson, 1993; Adams et al., 2007).

$$A = \pi\left(\frac{9RN}{16E}\right)^{2/3} \tag{2.3}$$

where R is the radius of sphere, N is the applied normal load and E the reduced Young's modulus and given by the following expression:

$$E = \left(\frac{1-v_{skin}^2}{E_{skin}} + \frac{1-v_{sub}^2}{E_{sub}}\right)^{-1} \quad (2.4)$$

where v_{skin} and v_{sub} are the Poisson Ratios with respect to skin and a contacting substance, E_{skin} and $E_{sub}$are Young's modulus for skin and a contacting substance, respectively. In general, the reduced elastic modulus depends on the properties of skin due to $E_{sub} \gg E_{skin}$ and expressed as $E \approx E_{skin}/\ 1 - v_{skin}^2$, thus the contact area can be written as:

$$A = \pi\left[\frac{9RN}{16E_{skin}/\left(1-v_{skin}^2\right)}\right]^{2/3} \quad (2.5)$$

Combining the Equation (2.2), the friction coefficient can be expressed as:

$$\mu = \frac{\tau A_{re}}{N} = \tau\pi\left[\frac{9R}{16E_{skin}/\left(1-v_{skin}^2\right)}\right]^{2/3} N^{-1/3} \propto {E_{skin}}^{-2/3} N^{-1/3} \quad (2.6)$$

In the case of dry sliding friction on a surface with high roughness, skin friction is reported to depend on the adhesion mechanism and hysteresis. In contrast with smooth surfaces, the influence of hysteresis in the friction significantly increases, resulting from the deformation of skin due to the surface asperities sliding over the skin surface (Derler et al., 2009). The deformation force can be expressed as (Greenwood & Tabor, 1958),

$$F_{de} = \frac{3Na}{16R} \quad (2.7)$$

where a the radius of the circle of contact under a load of N and equal to $\left(\frac{3NR}{4}\frac{1-v_{skin}^2}{E_{skin}}\right)^{1/3}$. In moving forward a unit distance (D=1), the elastic work (W) done in horizontal direction is:

$$W = F_{de} = \left(\frac{3N}{16R}\right)\left(\frac{3NR}{4}\frac{1-v_{skin}^2}{E_{skin}}\right)^{1/3} \quad (2.8)$$

The work lost per unit distance of sliding is βW, thus the friction coefficient due to deformation can be expressed as:

$$\mu_{def} = \frac{\beta W}{N} = \left(\frac{9N}{64a}\right)\left(\frac{1-v_{skin}^2}{E_{skin}}\right)^{1/3} \propto N^{1/3} {E_{skin}}^{-1/3} \quad (2.9)$$

In a recent study, Tomlinson et al., (2011) has conducted experimental work on skin friction for human finger in contact with fine rough surfaces. They concluded that the skin friction force can be analysed in terms of an adhesion force (F_{ad}), a hysteresis mechanism (F_{hy}) and an interlocking mechanism (F_{int}), and can be expressed as:

$$F = F_{ad} + F_{hy} + F_{int} \tag{2.10}$$

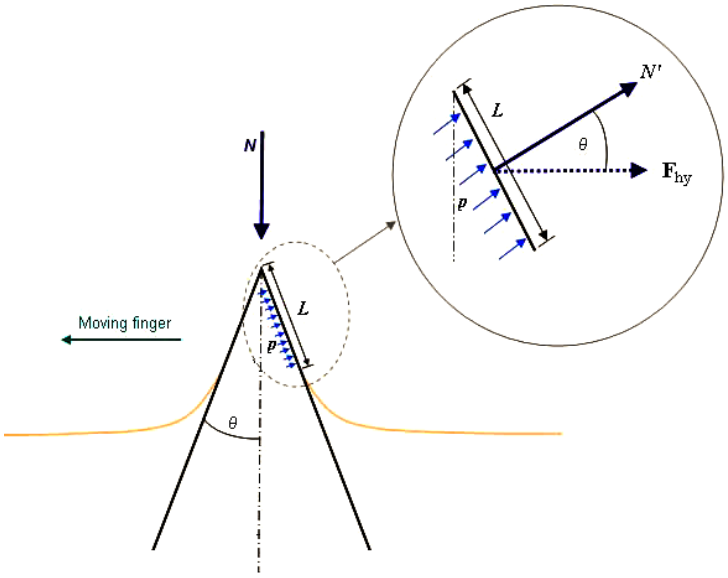

Figure 2.4: Human finger skin in contact with a single ridge. N is the applied normal load, θ is the angle of the ridge, p is the pressure along the contact area, L is the length of the contact area and N' is the resultant force due to the pressure of human skin against the ridge (Tomlinson et al., 2011).

The hysteresis friction is considered to be associated with hysteresis effects and ploughing of the finger skin by the contacting surface asperities in the case of a finger contacting a triangular ridged surface. As can be seen in Figure 2.4, the normal force is applied to the whole ridge; however, the skin is only displaced by the leading edge, therefore the deformation force is only along this side of the ridge. The deformation force can be calculated based on the numerical model derived by Greenwood and Tabor (1958), and the equation is given by the following form:

$$F_{hyst} = \frac{N}{2} \cdot \cot\theta \tag{2.11}$$

This model only works for the finger in contact with a single ridge, however, it cannot be used to fully describe the deformation force since the adjacent ridges restrict the finger from fully deforming. By considering this, Tomlinson et al. (2011) derived a new model for the case of the finger in contact with mutli-ridges (see figure 2.5). The model is expressed as:

$$F_{hy} = \begin{cases} \beta . n . \frac{N}{2.n} . \frac{\lambda . \cos\theta}{2.h_{ridge}} . \cot\theta & \frac{N}{n} < N_{max} \\ \beta . n . \frac{N_{max}}{2} . \cot\theta & \frac{N}{n} \geq N_{max} \end{cases} \quad (2.12)$$

where β is the viscoelastic hysteresis loss fraction, n is the number of ridges, λ is the distance between each ridge, h_{ridge} is the height of ridge and N_{max} is the normal load at which the deformation reaches a maximum. However, the above models are restricted to micro-scale deformation of skin (ridges height smaller than 42.5 μm).

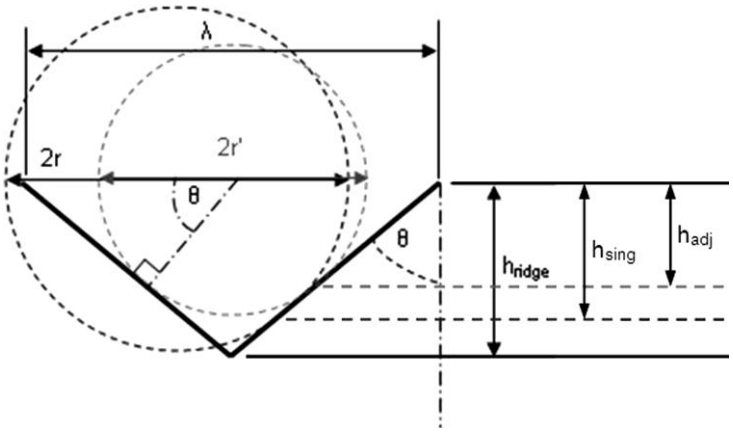

Figure 2.5: Schematic of circular representation of a finger deformation on a ridge. *r* is the radius of the circle without adjacent ridge and *r'* is the radius of circle with adjacent ridge (Tomlinson et al., 2011).

The interlocking mechanism refers to skin surface ridges moving over contacting surface asperities. Adams (1991) indicated that friction coefficient involves Coulmbic interlocking in the case that one spherical particle climbing over another spherical particle. The friction force was found to be equal to the tangent of the angle between the normal force and the vertical. This can be applied for the finger ridges 'climbing' over a ridge with the same result. Therefore, the mechanism of the interlocking friction can be described as:

$$F_{int} = N \cdot \cot\theta \quad (2.13)$$

There is another mechanism that is involved in skin friction when skin is saturated by water and excess water accumulates in the surface, is termed hydrodynamic lubrication. As shown in Figure 2.6, the hydrodynamic effect arises from the complete separation of the sliding surfaces by a liquid film, could replace the adhesion component of friction due to the viscous friction. An expression for the

friction coefficient with respect to hydrodynamic lubrication has been derived by Dowson (1997):

$$\mu_{viscous} = \eta\left(\frac{V}{h}\right).A_o N^{-1} = \eta\left(\frac{V}{h}\right).p^{-1} \quad (2.14)$$

where N is the normal load, η the viscosity of the fluid, V the sliding velocity, A_o the apparent contact area and p the contact pressure.

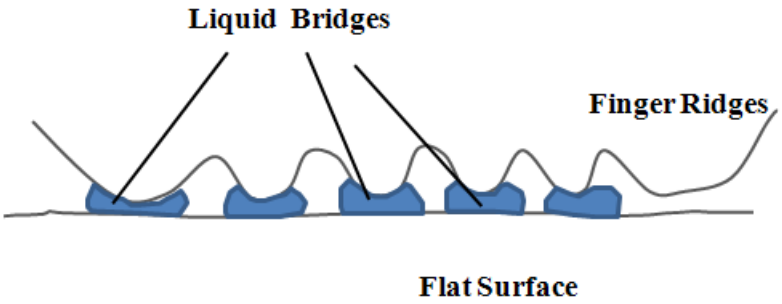

Figure 2.6: Liquid bridges formed at the interface between finger ridges and a flat surface, redrawn from (Dinc et al., 1991; Tomlinson et al., 2010).

2.4 Influence of Skin Properties on Skin Friction

2.4.1 Skin Roughness

As observed by naked eyes, the cutaneous surface is not smooth, but covered with hairy, sebum and series net-work of grooves. These patterns of ridges vary widely over the body. It is known as the "fingerprint" on hand fingers and feet soles and exhibits concentric ridges. On the dorsum (back) of the hand and forearm the skin surface in a grid-net pattern in that furrows intersect to enclose triangular and quadrilateral plateaus (Sarkany & Caron, 1965; Derler & Gerhardt, 2011).

In most studies, the skin surface topography was quantitatively recorded using profilometry methods and generally expressed as a mean roughness value of Ra. There are great variations in the mean value of roughness Ra according to anatomic regions of body and among different individuals, as shown in Table 2.2. By analysing those parameters in experiments, the roughness value was reported as high as 44 μm on the back of hand, while the forearm seems to be relatively smooth with a small value. In addition, Li et al. (2006) and Jacobi et al. (2004) found initially increases in the skin roughness of forearm and hand back with increased age.

So far, the study of skin texture has been widely investigated in the fields of cosmetics, medical diagnosis, and so on. For example, in cosmetics, characterising the skin surface texture is desirable for evaluating and improving the designed products. It seems little work has been done on the skin tribology correlation to skin roughness. Although many researchers found that the coefficient of friction varies with anatomic locations of body and is smaller for the forearm skin of an older person compared with that of the young (Zhang & Mak, 1999; Cua et al., 1990; Elsner et al., 1990; Asserin et al., 2000), none of them reveals this is due to the effect of the skin roughness, except Nakajima and Naraska (1993). They reported that the number of "domains" (i.e. areas enclosed by lines) has a big impact on the skin friction, particularly static friction. As the number of "domains" decreases, the static friction coefficient increases.

Table 2.2: Summary of skin roughness value-Ra for various anatomic locations of human body.

Author	**Age**	**Skin Region**	**Measurement Technique**	**Roughness Value (*μm*)**
Rohr&Schrader (1998)		Forearm	DermaTop	14.5
Rosén et al. (2005)	43	Forearm	GFM PRIMOS	17
Hof & Hopermann (2000)		Forearm	GFM PRIMOS	10.9
		Hand Back		27.3
Friedman et al. (2002)		Cheek	GFM PRIMOS	24.8
Jacobi et al. (2004)	25±2.5	Back	GFM PRIMOS	42.3
	27	Forearm		30.8
	41±2.7	Forearm		33.3
	65	Forearm		37.5
Derler et al. (2009)	23-45	Index finger	Perthometer M1	18.9~32.7
		Edge of hand		8.6~22.4
Lagarde et al. (2005)	25-65	Forearm	DermaTop	12-14
		Temple		12-15
Li et al. (2006)	20-29	Forearm	Dermsurf Image	16.92±3.37
		Hand back	System	23.24±4.22
	30-39	Forearm		20.01±6.22
		Hand back		27.98±10.47
	40-49	Forearm		21.99±8.51
		Hand back		32.85±13.71
	50-59	Forearm		21.76±4.99
		Hand back		34.91±10.93
	60-74	Forearm		28.50±6.78
		Hand back		43.93±14.91

2.4.2 Skin Hydration

The water content of human body takes 70% of total weight; there is abundant water in human skin that is stored in the epidermis, dermis and underlying tissues. It is fundamental to allow skin cells to work properly and maintain skin in a health condition. Adequate water gives you soft and smooth skin. The normal water content in healthy skin shows a high proportion in the dermis (around 70%), reducing to only 10% ~15% in the stratum corneum. As mentioned earlier, the stratum corneum layer plays a critical role in preventing excessive water loss through skin. The capability of water-holding relates to the unique intercellular lipids in the startum corneum that form a barrier to transepidermal water loss (TEWL), as well as other various compounds called the "natural moisturizing factor" (NMF), is skin's own self-moisturizing tool to help retain moisture level in the skin by attracting and retaining water. However, when the surface lipid or the level of NMF are reduced, the water content in the stratum corneum will decline resulting in skin becoming dry, scaling, rough and flaky (Verdier & Bonté, 2007; Fluhr et al., 2004). Since sweat is one of the main components of the surface film that helps maintain dampness (Wood & Bladon, 1985), studying the number of sweat glands may be a very useful way for investigation of the hydration of skin. The number of sweat glands in a finger tip was evaluated by Juniper et al. (1964). During the experiment, a finger was firstly stained by a solution of 3% iodine and 95% alcohol, second, a 1:1 starch-castor oil paste was massaged into the stain area when the iodine had dried, and fingertip was finally put under a 40-power pocket microscope with viewing field of 10 mm^2 to count the number of sweat glands. The results showed that the number of sweat glands ranging from 20 to 40 per 10 mm^2. There were significant changes in the number of sweat glands in both females and males with increasing age. Sweat glands, were found to have a trend of reducing in older age group people. In later studies, Dinc et al. (1991) used a high speed scanning optical coherence tomography (OCT) to help count the number of sweat glands. In the OCT images, dynamics of sweat ducts were captured and observed clearly as a bright thick broken line. It was found that the density of sweat glands was around 150 to 350 per square centimetre, the sweat glands had a diameter of approximately 5-20 μm (Nohara et al., 2005).

There are different biophysical techniques that can be used to measure skin hydration, which can be divided into two types according to the principle:

capacitance and conductance (André et al., 2008). Currently, devices available to measure the water content of the stratum corneum based on the measurement of electrical capacitance of the skin surface, include Corneometers, the Skicon, the MoistureMeter, and the Nova DPM 9003 (Cua et al., 1990; Tomlinson, 2009; Verdier & Bonté, 2007). The water content data is provided in arbitrary units (AU), ranging 0 to 120 AU for a "*corneometer*" and 0 to 100 AU for the "*moisturemeter*", respectively.

In addition to the above method, the measurement of skin hydration also can be achieved by monitoring the transepidermal water loss (TEWL) that is directly related to its barrier function. Under normal conditions, the rate of evaporation is very slow (approximate 3~5 g/hm^2 in forearm and back) (Cua et al., 1990). Treffel et al. (1994) have examined the skin hydration and TEWL in dominant and non-dominant forearms using an "*evaporimeter*" in their studies. They found that both skin hydration and TEWL show comparatively high values in a dominant forearm, which could be attributed to the larger muscle bulk and the increased metabolism of the dominant forearm. However, no work correlating to skin friction has been reported here. Lodén et al. (1992) pointed that there is a significant relationship between skin hydration and friction in normal skin. No correlation was found however, between TEWL and friction. The same conclusion was drawn by Cua et al. (1990) who suggested that skin friction strongly depends on skin hydration in most regions of body. The contribution of TEWL to skin friction was observed only in the palm and thigh. Moreover, those skin characteristics are known to be affected by endogenous and environmental factors, including aging, exposure to sunlight, chemicals, and mechanical damage; related work will be discussed in following sections.

2.4.3 Anatomic Region, Age, Gender and Ethnicity

There has been a large amount of work carried out on skin friction; however the different studies involve different subject groups and different test areas. With respect to anatomic site, the friction coefficient shows a huge variety, ranging from 0.12 on the abdomen to 1.4 on the finger pad or palm (Cua et al., 1990; Zhang & Mak, 1999; Derler et al., 2009; Hendriks & Franklin, 2010; Zhu et al., 2011; Veijgen et al., 2012). Ramalho et al., (2007) investigated the friction coefficient on the palm

and forearm and found that the palm had a higher value (1.2) than that of forearm (0.15~1). They assumed that the difference was related to skin thickness. In later studies, Zhang and Mak (1999) reasoned it was due to the fact that the palm is rarely sweat free, but the forearm is. Some authors reported that the friction coefficient is also dependent on the water content of skin and TEWL. For example, Cua et al. (1990) investigated skin frictional properties with respect to age, sex and anatomical regions using a frictionmeter. They observed that some regions (e.g. lower back, dorsal forearm) with higher capacitance, have lower friction coefficients. There was a correlation between the friction coefficient and TEWL found on the palm and thigh. They also found that the friction coefficient is independent of age at most of the anatomical regions. In the studies of Cole et al. (1999), who developed a grasping and lifting rig to exam the friction force on human finger-pads, it was indicated that the friction coefficient decreases with age. Recently, Zhu et al., (2011) conducted age-related tests in a large Chinese population using a Frictionmeter and a Corneometer. Their experimental results show that the skin friction coefficient on the dorsal hand skin gradually increases with age, up to 40 year old. Unfortunately no related details were given to explain the differences observed. With respect to gender, Cua et al. (1990) reported that the friction coefficient does not show significant difference between female and male. Similar conclusion was drawn by Zhu et al. (2011), who assessed the friction coefficient of skin on various anatomical regions. However, Veijgen et al. (2012) observed some significant differences on the dynamic friction coefficient at index finger-pads and dorsum of hands between men and women. Zhu et al. (2011) attributed the difference to the differences in skin hydration. The results of their studies show that there was no significant difference in friction coefficient on the forehead, however, on the canthus and the dorsal hand skin, the friction coefficients were showed to vary with gender. Sivamani et al. (2003) found no difference in the friction coefficient with regard to ethnicity.

2.5 Effect of Interface Materials on Skin Friction

In daily life human skin is in constant contact with various materials (e.g. textiles, rubber, metals), a good understanding the effect of materials on skin friction is generally believed to have potential benefits to the performance of conducting tasks, but also the prevention of pain and discomfort. For instance, a good understanding

of the mechanism between skin and various materials could help avoid the chance of getting blisters on the foot (Derler et al., 2009). Much of current knowledge focuses on characterising the effect of contact materials on the friction of skin since it is one of the important design parameters that has to be considered (Hendriks & Franklin, 2010, Kuilenburg et al., 2012). Numerous materials have been tested in previous studies, and it has been found that the coefficient of friction widely varies with materials.

In addition, it is generally agreed that the surface roughness of contacting materials is the other important factor affecting the skin friction. One study related to this was carried out by Derler et al. (2007, 2009), who assessed the friction coefficient between a finger and various textures. The results of those experiments showed that the smooth surfaces (R_a = 0.006~0.05 μm) have higher friction coefficients than those of rough surfaces (R_a = 11.94~45 μm) under dry conditions. A similar conclusion was drawn by Hendriks and Franklin (2010), they found that the friction coefficients of arm and cheek reduce with roughness following a power-law linear relation under both dry and humid condition. The average value of exponent *n* was equal to -0.4. They also reported that the amplitude of surface roughness has a significant impact on the friction coefficient, especially for surfaces with low R_a roughness values (i.e. <1 μm). In the studies of Van Kuilenburg et al. (2012), they indicated that the frictional behaviour of micro-scale textures is determined by the surface properties of human skin. However, in the case of very rough surfaces, some authors observed an increasing trend of friction coefficient with increasing material roughness (Cole et al., 1999; Tomlinson et al., 2009). For example, Tomlinson et al. (2009) found that as the roughness increases the friction coefficient increases when a finger was sliding against steel, up to a point (R_a= 26 μm). After that the friction coefficient researches a plateau. Tomlinson et al. (2009) have carried out a further study with respect to fine ridges and large rectangular ridges, respectively. On the surface with fine ridges, the main contributor to friction is the interlocking friction at heights greater than 42.5 μm, and hysteresis for ridges with height over 250 μm. In the case of large rectangular ridges, the increase of friction coefficient was attributed to the deformation of skin reducing with narrow ridges, leading the contribution of adhesion increasing.

2.6 Effect of Contact Conditions on Skin Friction

2.6.1 Load

According to Amontons' law of friction, the ratio of friction force to normal force is known as "friction coefficient", which was assumed to remain constant regardless of the applied normal load (Sivamani & Goodman, 2003). In most recent studies, it was concluded that the Amontons' law could not hold for human skin friction, as a result of human skin being a soft tissue. The friction behaviour of skin cannot be fully described by a simple linear model. From experiments performed by Comaish & Bottoms (1971) and Han et al. (1996) with various materials sliding against dorsum of a hand and abdominal skin using a simple linear rubbing technique, the static friction coefficient of skin was shown to decrease initially as the load increased and reach a plateau once the load was over a particular value (approximately 3 N). They reasoned that the decrease in friction coefficient was due to the viscoelastic properties of the skin allowing for a nonlinear deformation of the skin with increased normal load. A relatively complex model has been developed to express the relationship between the friction coefficient and loads: $\mu \propto N^{-n}$, where μ is the friction coefficient, N is the load and n is the exponent of load (a positive constant and less than 1). A suggested value of n for the skin is around 0.3 (Comaish & Bottoms, 1971; Asserin et al., 2000; Sivamani & Goodman, 2003). However, Tang et al. (2008) observed that increasing the load increased the friction coefficient when a polypropylene ball is sliding along the forearm. This could be due to the difference in testing materials, which was supported by Tomlinson (2009) in later studies, who investigated the friction coefficient for several materials under various load and found that all of materials show a decreasing trend with load, except polyprolene.

Tomlinson et al. (2009) have assessed the relationship of friction force to normal force with a finger sliding over different materials for both low load and high load conditions. For low load test (in the range of 0 to 10 N), a two part linear relationships was observed (see Figure 2.7). All data points between 0 N and 2 N seemed to show a linear relationship between friction force and normal force. Past the 2 N point there was still a linear relationship, but with a smaller gradient compared to that of the first line. A similar finding was also reported by Ramalho et al. (2007), who investigated the skin frictional behaviour at various anatomical sites

of body. They found a double stage Amontons-Coulomb linear model at the tested forearm.

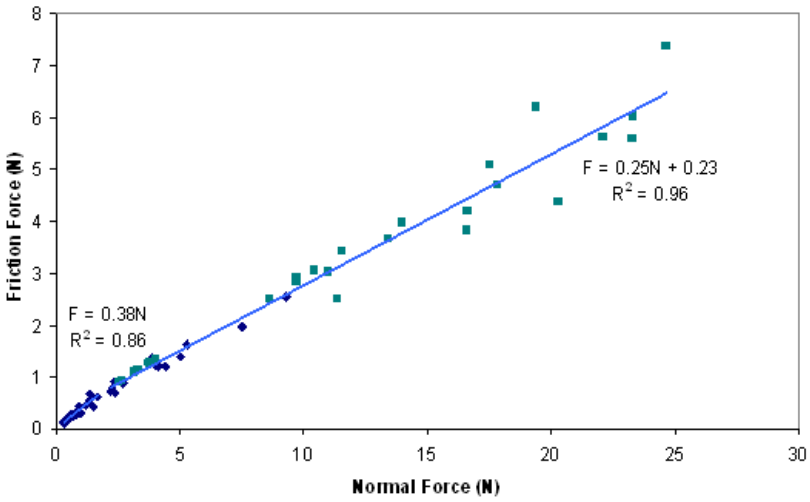

Figure 2.7: Two-part relationship between normal load and friction force (Tomlinson et al., 2009).

2.6.2 Contact Area

As stated earlier, the friction force of skin is dominated by the adhesion force for smooth surfaces at high load; the adhesion is found to be proportional to the real contact area. Therefore, examining the area of contact could provide a better understanding of the friction mechanism, and therefore how friction varies with load. According to Herzian theory, in the elastic phase, the contact area is proportional to the 2/3 power of the load, in the case of a hemispherical probe sliding on deformable materials such as rubber or skin. The equation is given by the expression: $= \pi(\frac{9RN}{16E})^{2/3}$, where R is the radius of sphere, N is the applied load and E is the reduced Young's modulus (Johnson, 1985; Adams et al., 2007). This model was accepted in most applications of skin friction using the probe method. However, this does not apply to the case of a finger sliding, because human fingers do not experience smooth spherical contact. In later studies, Han et al. (1996) indicated that the contact areas of human fingers were proportional to the normal force to the power of b. The equation is expressed as: $A = kN^b$, in which k and b are constants. The value of b was found to be in the range of 0.2 to 0.4 in their studies. Therefore the contact area would increase with normal load. In similar studies, Soneda and Nakano (2010) found that the value of k for apparent contact area was 0.54 and real

contact area was 0.66. However, someone argued that the normal load was not the key influencing factor on contact area as the contact area is also affected significantly by lots of parameters, such as the skin properties, size of contacting objects, environments conditions, etc. For instant, Warman and Ennos (2009) have conducted an experiment, where a finger was sliding along a perspex sheet attached on a force gauge; the results showed that the contact area of the finger pad was reduced by a power of 1/3 compare with flat skin. They also investigated the contact areas for fingers interacted with different sizes of objects. It was found that the larger size of object had a bigger contact area, which led to a higher friction force and hence the friction coefficient.

(a) (b)

Figure 2.8: (a) Finger pattern of a human finger in, (b) fingerprint created by finger ridge structure.

Measuring the contact area between the skin and objects is hard, especially the real contact area, though many researchers have been investigating it for years. A number of different techniques have been applied to analyse the contact area, such as an ink stamping method (Childs, 2006; Warman and Ennos, 2009; Tomlinson, 2009), optical methods (André et al., 2008; Tomlinson, 2009; Soneda & Nakano, 2010), electrical resistance (Tomlinson, 2009), etc. Ink stamping and optical methods were associated with the morphology of skin. For example, the portion of ridge on the skin surface showed as black regions when a finger was applied with ink and was stamped on a white paper (see Figure 2.8). Those white areas among black ink were assumed to be non-contact areas. Therefore the real area could be calculated by counting number of pixels. Tests were carried on the same finger under constant load; a high-speed video was also introduced in the testing for providing estimation

of nominal contact areas. Tomlinson (2009) found the percentage of ridges takes up approximately 50% of the total area of finger print. In Childs' (2006) work, when a 1.77 N load was applied on a finger, the contact area (apparent contact) was 11.50 mm^2; the percentage of real contact was 34%. However, Soneda and Nakano (2010) found that, in similar tests, the apparent contact area and real contact area were 99.4±14.8 mm^2 and 29.9 ± 7.0 mm^2, at the load applied was over 1 N, respectively. In this case, the percentage of real contact area accounted approximately 30% of apparent contact area. However, most of above methods described only allow static measurements. There are big errors in the measurements due to the drawbacks of ink spread, noise effects and threshold value setting in later image processing. Thus, exploring a new method is desired.

2.6.3 Hydration/Lubrication

Skin is hard to maintain in a "dry" condition. The state of the hand is easily changed with environmental factors. As well as perspiration secreted by sweat glands and external moisture, food and some cosmetics also influence the degree of hydration of the skin. So, in some research, hydration was considered as one of the most important areas in skin friction studies.

In general, dry skin has a lower coefficient of friction than that with hydration (Comaish & Bottoms, 1971; Yoshimune et al., 2009; Veijen et al., 2012). In these papers, a linear correlation between skin moisture and friction was reported. On the other hand, some authors observed a "bell curve" response in the friction coefficient when water was added to a dry contact, where the skin friction increased, up until a certain level of moisture and then decreased (Adams et al., 2007; Andre´ et al., 2009; Nonomura et al., 2009). For example, Adams et al. (2007) examined the friction of a hemi-spherical glass probe contacting the forearm; water was added to the forearm during the test. The coefficient of dynamic friction has a continuous increase as water is added at the beginning of a probe test, after it reaches a peak at 240 seconds, the coefficient of friction decreases as excess water is removed, (see Figure 2.9).

Three possible mechanisms were proposed for causing the friction increase: water absorption, viscous shearing of liquid bridges formed and capillary adhesion (Dinc et

al., 1991). With respect to the mechanism of water absorption, the contact area increases with hydration hence the friction coefficient (Adams et al., 2007; Gerhardt et al., 2008). The increase in viscous shearing of liquid bridges formed between the ridges on the finger surface and counterface could contribute to the increase in friction (Dinc et al., 1991). Capillary adhesion is the result of the surface is pulling together leading to a higher contact area (Persson, 2008; Deleau et al., 2009). Many experiments have been carried out with respect to each mechanism, individually. In particular, Tomlinson et al., (2010) have designed various tests to investigate the relative contribution of each mechanism on the skin friction in moist condition. After being fully examined, the water absorption was believed to be the major cause of the friction coefficient increase, followed by capillary adhesion. The viscous shear was found unlikely to affect friction.

Adams et al., (2007) and Gerhardt et al. (2008) found that the increase in the coefficient of friction resulted from the increase of real area of contact coupled with the effect of water plasticisation of the stratum corneum. Persson et al. (2008) suggested that the effect of capillary action is highly dependent upon the Young's modulus of the contacting zone. Values of the Young's modulus of the stratum corneum vary greatly, depending on the water content of the stratum corneum. On the basis of these findings, it can be concluded that friction coefficient is a function of skin mechanical properties. As part of work done by Hendriks et al. (2004) on the influence of hydration on mechanical properties of skin *in-vivo*, it was found that the skin mechanical properties vary with subjects. In three of thirteen subjects, the stiffness of the skin became less with hydration. An opposite phenomenon was found in other eight subjects, which shows an increase in the stiffness of the skin. Norlen et al. (1997) found that the area dimension of non-extracted stratum corneum is 8.4% ±1.4% bigger than its original size after incubation by distilled water for 90 minutes, as well as the thickness dimensions, the stratum corneum increased to $17.2 \pm 3.6\ \mu m$ from $13.6 \pm 3.5\ \mu m$.

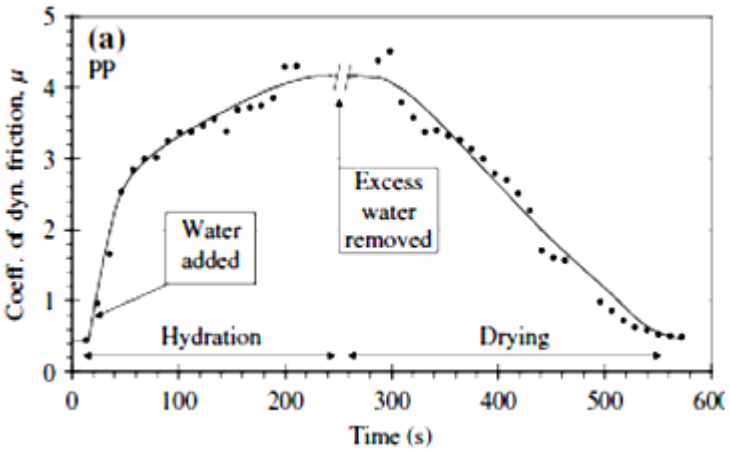

Figure 2.9: The dynamic coefficients of friction of skin for PP probe measured during hydration and drying (Adams et al., 2007).

2.6.4 Speed

Up to now, little work has been carried out on the influence of sliding speed on friction, Zhang and Mak (1999) found that the coefficient of friction had a slight change (7 ± 2%) as the rotation speed of a probe increased from 25 *rpm* to 62.5 *rpm*. Similar work by Tang et al. (2008), as shown in Figure 2.10, who observed an increase with rising sliding speed. The coefficient of friction rose up to 0.52 when increasing the sliding speed from 0.5 *mm/s* to 4 *mm/s*. They reasoned that when a probe slid on the skin, a phenomenon of "stick-slip" occurred between the skin and probe. In this case, the skin acted as an elastic material and was deformed into a stack as the probe contacted the skin, which would stand in the path way of a probe and held back the probe (as friction force). When the probe rotated at a fast speed, the deformed skin was not able to recover immediately, so more hysteresis energy was lost, for that the increasing hysteresis friction led to a higher coefficient of friction. In the case of a low speed sliding, skin had enough time to recover, little hysteresis friction was lost during sliding, therefore the friction force was smaller than with high speed (Zhang & Mak, 1999; Tang et al., 2008).

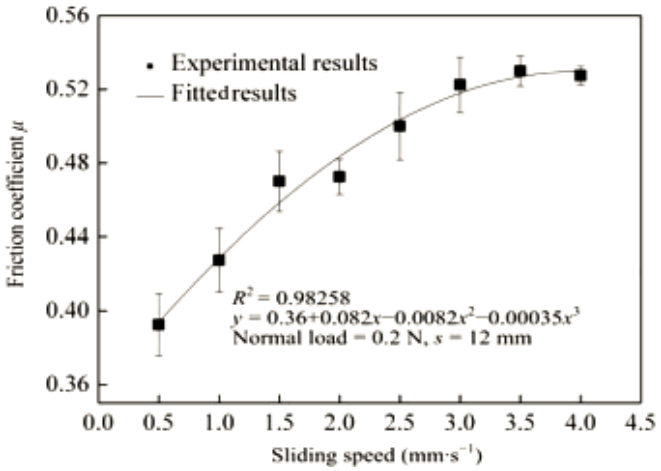

Figure 2.10: The coefficient of friction measured under various speeds (Tang et al., 2008).

2.7 Techniques for Measuring Skin Friction

The measurement of friction force has been carried out in many studies, and different machines have been specifically designed to measure skin friction. Those instruments are mainly classified into the probe method and the plate method. The basis of the probe method is the use of a spherical probe sliding on the surface of skin, e.g. the Tabor-Eldredge tribometer (Eldredge & Tabor, 1995; Sivamani & Goodman, 2003), as shown in Figure 2.11 (a). The design enables the probe to slide/roll at a constant speed with a constant contact load, which is of benefit to the accurate repeatability of testing. The probe method can also be grouped into two classes: 1) sliding type, 2) rolling type. In past studies, the probe method was widely used in measurement of dynamic skin friction in the forearm rather than the hand. The first design introduces a probe attached to a fixed weight sliding over the skin; therefore the dynamic skin friction is recorded. The rolling type has dominated in recent skin friction studies; the measurement apparatus of rolling type is similar as that of sliding type (see Figure 2.11 (b)). It relies on the torsion spring or light techniques to calculate the skin friction. These probe methods can be performed in various regions of the body. However, the disadvantage of those methods is that they are simulation tests, and are not representative of that which would be seen in real life.

Unlike the probe method, the plate method is specific for measuring the finger friction. A typical example is shown in Figure 2.11 (c). This device consists of two

load cells, one of them was placed at the front of the rig used to capture the lateral force, and the other one was placed under the flat plate for measuring the normal load when a finger runs along a surface (Eldredge & Tabor, 1995; Sivamani & Goodman, 2003; Tomlinson et al., 2007). The advantage of the plate method is that it can investigate the frictional behaviour of skin with various materials by using the actual move of the finger. However, this technique brings difficulties in controlling the load and speed applied since human controlled. Table 2.3 shows a summary of some of the tests carried out using different techniques. The coefficient of friction can be seen to vary substantially, but this is thought to be mainly due to the differences on test materials, methods (e.g. load applied, speed) as well as different fingers used.

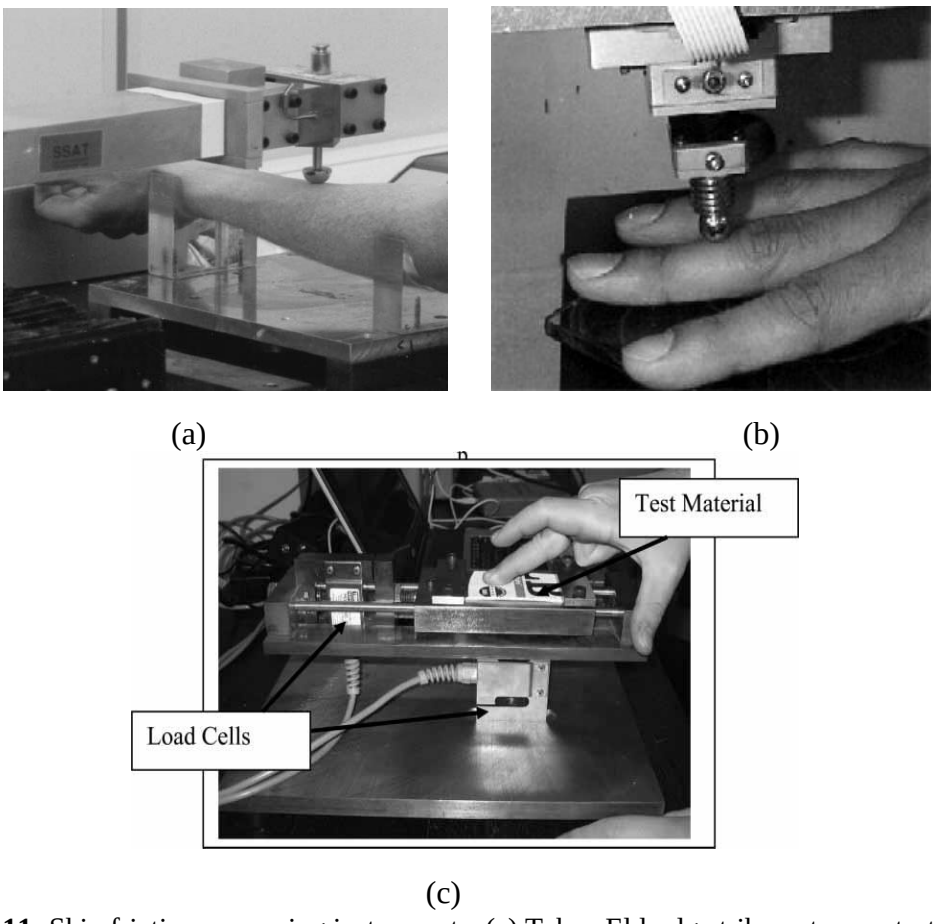

Figure 2.11: Skin friction measuring instruments: (a) Tabor-Eldredge tribometer run testing via probe sliding over skin, (b) UMT probe, provide translational, rotational and reciprocating motion for measuring important parameters of skin, (c) Finger friction rig for measuring finger skin friction, where finger moves along the plate (Eldredge & Tabor, 1995; Sivamani & Goodman, 2003; Tomlinson et al., 2007).

Table 2.3: Outline of *in-vivo* skin friction coefficient μ.

Authors	Measuring Region	Test Materials	Load (N)	Test Method	Friction Coefficient
Sivamani et al. (2003)	Finger	Steel	0.2	UMT probe rolling	0.33-0.55
Asserin et al. (2000)	Volar forearm	Ruby	0-0.3	Spherical indentor	0.7
Spurr (1976)	Fingertip	PE		Finger moving	0.42-0.55
Naylor (1955)	Tibia	PA	5.1	Probe sliding	0.5-0.6
Highley (1977)	Volar forearm		0.28	Wheel rotating	0.19-0.28
Adams et al. (2007)	Inner forearm	Glass/PP		Probe sliding	0.27-0.36
Koudine & Barquin (2000)	Dorsal forearm			Plate moving	0.24
	Volar forearm				0.64
Cua et al. (1990)	Forehead				0.34
	Volar forearm	Teflon	1.96	Probe rotating	0.26
	Palm				0.21
	Abdomen				0.12
	Upper back				0.25
Comaish et al. (1971)	Dorsum of hand			Linear moving	0.25-0.55 (static)
					0.2-0.48
Prall (1973)					0.4
Elsner et al. (1990)	Vulvar	Teflon	1.96	Disc rotating	0.66
	Forearm			Disc rotating	0.48
Tomlinson et al. (2007)	Finger	Glass/Steel	15-20	Finger moving	0.97-1.1
Bobjer et al. (1993)	Finger	Polycarbonate	1-20	Moving belt	0.7-1.4
Gee et al. (2005)	Finger	Rubber	11	Finger moving	0.6-1.75
Han et al. (1996)	Finger	Acrylic	0.5-6	Plate moving	0.4-1.5
Veijgen et al. (2012)	Forearm	Stainless steel	0.5-2	Cylinder rotating	0.53-1.78

2.8 Techniques for Measuring Skin Structure Parameters *in-vivo*

To gain insight to the internal structure of skin without biological biopsies, various non-invasive *in-vivo* skin image techniques have been developed and these include ultrasound, confocal microscopy, Magnetic Resonance Imaging (MRI), Optical Coherence Tomography (OCT), etc. These techniques are widely used in medical fields for examining eye health and diagnosing skin disease as they allow the

clinicians to visualize the structure and properties of skin through simple naked eye examination. Ultrasound can be used to image skin and measure the thickness of human body (up to 10 *cm*), however the resolution is too low for imaging the fine structure of skin. Confocal microscopy provides relative high resolution that enable to visualize details of skin structure at a cellular level. Unfortunately, it is limited to image only 0.35 *mm* depth of skin. The images made are parallel to the skin surface. Both MRI and OCT can produce high resolution images of the vertical section of the skin in short time. By considering the portability of the device, OCT system is commonly applied to investigate the properties of skin combined with other instruments (Hendriks, 2005; Wu, 2005).

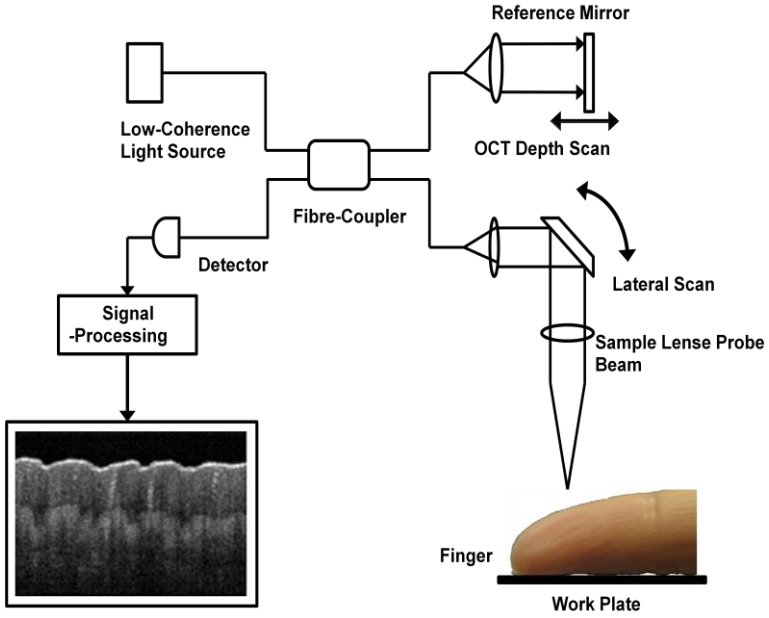

Figure 2.12: A modified set-up of OCT system.

Optical Coherence Tomography (OCT) has been developed as a non-invasive technique for investigating human skin by producing cross-section images of tissue (Huang et al., 1991), a typical example shown in Figure 2.12 (Fercher et al., 2003). This technique is widely used in the medical field for caring eye health and diagnosing skin disease. The principle of the OCT technique is dominated by interferometric methods. Infrared light split into two paths, one path launches into the sample and the other one goes to a reference mirror. The combination of lights scattering in the sample and the reference generates a two dimension as image (Welzel, 2008). Normally the OCT can image to a depth of 1~2 *mm* in a sample with

varying path length. With features of non-invasive, ability of penetrating into skin, and high resolution of *in-vivo* images, OCT is now mainly being applied in dermatology studies. Different information can be extracted by analysing skin images, such as number of sweat glands, thickness of stratum corneum, etc. Further detail will be described in the following Chapter 3.

2.9 Conclusions

This review summarises and highlights the work carried out in the field of human skin tribology as well as discussing the currently available technologies applied for measuring skin friction. Owing to its viscoelastic properties, human skin exhibits very complex frictional behaviour. In the literature, it can be seen that the skin friction coefficient widely varies within different ages and anatomical sites of body. Derler et al. (2009) indicated that the human skin friction is intimately associated with both skin properties and interplay materials. Understanding the contribution of the skin properties on the skin friction is desired. Thus, investigations of skin roughness, hydration and mechanical properties have also been reviewed. Currently, the mechanical properties of skin have been studied in the term of Young's modulus.

Different mechanisms of the skin friction have been proposed with respect to various contact conditions (e.g. load, sliding speed, contact area, etc). Under dry conditions, skin friction is generally considered to be dominated by adhesion and deformation mechanisms. It has been shown that the adhesion mechanism strongly depends on the real contact area between human skin and surfaces. The skin friction increases with increasing the contact area. Various methods have been applied to measure the contact area, includes a finger-print ink method, an optical method and an electrical resistance. However, most of these methods were restricted to the measurements of apparent contact area statically. There is a requirement to explore a new method to measure the real contact area.

In the case of wet conditions, it shows that the skin friction increases with increasing the moisture level of skin up to a certain level. Three different possible mechanisms have been suggested to explain this phenomenon. Compared to the mechanisms of water absorption and capillary adhesion, the effect of viscous shear seems limited. Many studies indicated that the mechanism of the water absorption is ascribed to the

increase in the contact area due to skin absorbs water and becomes smooth. However, no study has been conducted to investigate the skin properties related to water hydration. The mechanism of the capillary adhesion is highly dependent on the Young's modulus of the contacting zone (Persson et al., 2008). When skin is hydrated with water, the skin will become soft, leads surface ridges pulling together, hence increase the contact area. An investigation of the skin properties and how the Young's modulus of skin change related to water hydration is needed.

Chapter 3

Equipment and Testing Procedures

This chapter outlines all experiment-related instruments and testing procedures that have been used or developed in this research. Firstly, it introduces three different devices that have been applied to measure the frictional properties of human finger-pad skin, including a finger friction rig, a multi-axis force plate and a pinch grip rig. This is followed by standard testing procedures with respect to each method. This chapter then describes a medical optical system (Optical Coherence Tomography) used to investigate human skin structure, as well as the related image analysis technique for determining the thickness of stratum corneum (SC). The later part of this chapter describes a non-invasive "*cutometer*" MPA 580 and a simple indentation device used to assess the mechanical properties of human finger-pads. Finally, a brief description of the method of measuring human skin roughness is given.

3.1 Measurements of Frictional Properties

3.1.1 Finger Friction Rig

To measure the dynamic friction coefficient of human finger-pads, a finger friction rig has been designed and built at The University of Sheffield (see Figure 3.1). This rig originally consists of two strain gauge load cells, a work plate, an amplification unit, and a PC. The main frame of the rig is made of steel as well as the work plate. These two load cells used are s-shaped 50 kg rated load cells which are used to measure both the normal force and shear force in the range of 0.05 kg to 50 kg in 0.05 kg increments (for more details about the equipment, see Lewis et al. (2007) and Tomlinson et al. (2009)).

To simplify the data acquisition system and improve the efficiency of measurements, a *National Instruments data-acquisition* card (*DAQ:* NI USB-9237*)* was used to replace the amplification in the original design. The NI USB-9237 is a 4-channel analog input device and manufactured by National Instruments. The sample rates on four channels up 50 kS/s. The advantage of this new data acquisition card is that it is the combination of digital and analog filtering to remove the noise and optimize output signals.

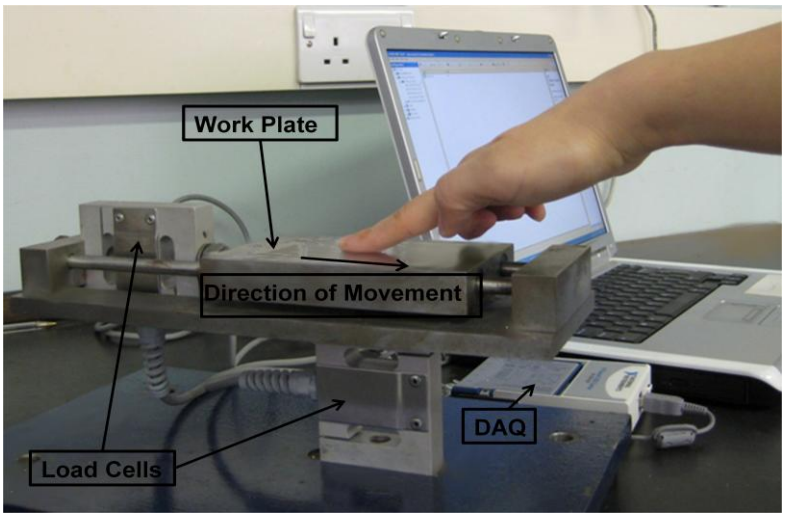

Figure 3.1: The experimental set-up of the friction measurement rig.

3.1.2 Multi-axis Force Plate

In this research, the friction experiments in the studies of contact area (Chapter 6), hydration (Chapter 7) and deformation (Chapter 8), in particular at low load conditions, were carried out using a multi-component force platform system (HE6X6) from Advanced Mechanical Technology Ltd; as shown in Figure 3.2. This set-up is mainly composed of a HE6X6 force plate, a PC, a PJB-101 interface box (AccuGait System posturographic plane) with a RJ cable and a RS-232 cable. This HE6X6 force plate is designed based on the strain gauge flexibility technique, which is able to provide three force components along the x, y, and z axes as well as their corresponding moments. These three force components are summed from the data of eight channels of ± 10 voltage. This device is ideal for quantifying low loads. The maximum load in the z axis is 44 N and 22 N for x and y axes. The working area on the top surface of the force plate is about 130 *mm* X 130 *mm*, which allows a finger to freely move around the plate and to attach test materials.

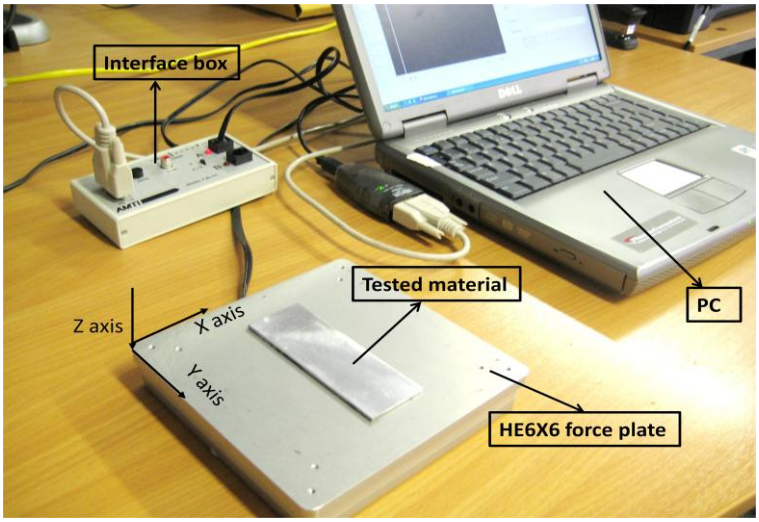

Figure 3.2: The set-up of the multi-component force platform system.

The software of *"NetForce"* is also provided with user interface and database functions (see Appendix B). It was used for controlling the platform and gathering all raw data from the force transducer. As can be seen in Appendix B, there are three real-time data displays in the window of *"NetForce"*. Both displays on the left side are data displays, in which 12 different channels (6 force data channels, 6 moment data channels) are used to monitor the outputs of force and moment. The one on the right side is real-time COP display (center of pressure), which can be used to plot the movement by detecting the data of COP. For instance, when a finger is moving on the top surface of the force plate, z axis always gives the normal force named F_z, x and y axes provide shear force in each orientation, named F_x and F_y respectively. To calculate the friction coefficient of the finger, F_z and F_x or F_y are selected to be assessed only according to Amonton's law.

3.1.3 Experimental Procedures

For the various techniques used to determine the friction coefficient of human finger-pads, there were different testing procedures developed. Since the finger friction rig and the multi-axis force plate are standard dynamic friction measurement devices, they used a similar testing procedure. There were some slightly differences in the details depending on the specific aims of tests.

In general, measurements were made by sliding fingers along the top surface of the work plates. The work plate of the finger friction rig was rigid ($Ra \approx 1.6\ \mu m$). The

tested fingers approached the top surface so that the largest area of the upper section (distal phalanx) of the finger was presented parallel to the surface. The angle between the surface and the fingers ranged between 25° and 35°. The fingers were then moved linearly towards the body. During experiments, subjects were requested to keep a constant speed for each test, counting slowly from 1 to 5 from start to finish of the slide (giving approximately 10-28 *mm/s*) (Tomlinson, 2009). To determine the friction coefficient of the tested fingers, subjects were also requested to repeat the test several times using the same method, but with different normal loads (> 2 N). Finally a demographic survey was completed, including age, gender and ethnicity (see Appendix C).

Figure 3.3 shows force data that was collected from friction experiments. Both the normal load and the friction force were plotted as a function of time as the tested fingers slide along the work plate. It can be seen that the normal load initially reaches a plateau and remains constant (at approximately 4 N) during finger movement. The friction force curve can be divided and analysed in two phases including "static" and dynamic movements. In the static movement, there was a movement at the finger-pad skin, and no relative sliding took place at the interface between the finger-pads and surfaces due to a high resisting force. As the normal load and the friction force were increased, the static friction increases until it reaches a maximum value. After that, the fingers break free and start to slide at a steady rate. To calculate the dynamic friction coefficient of the fingers, the force data taken from a relatively constant period in the dynamic movement were used. The ratio of the normal force to the friction force is generally considered to be the dynamic friction coefficient.

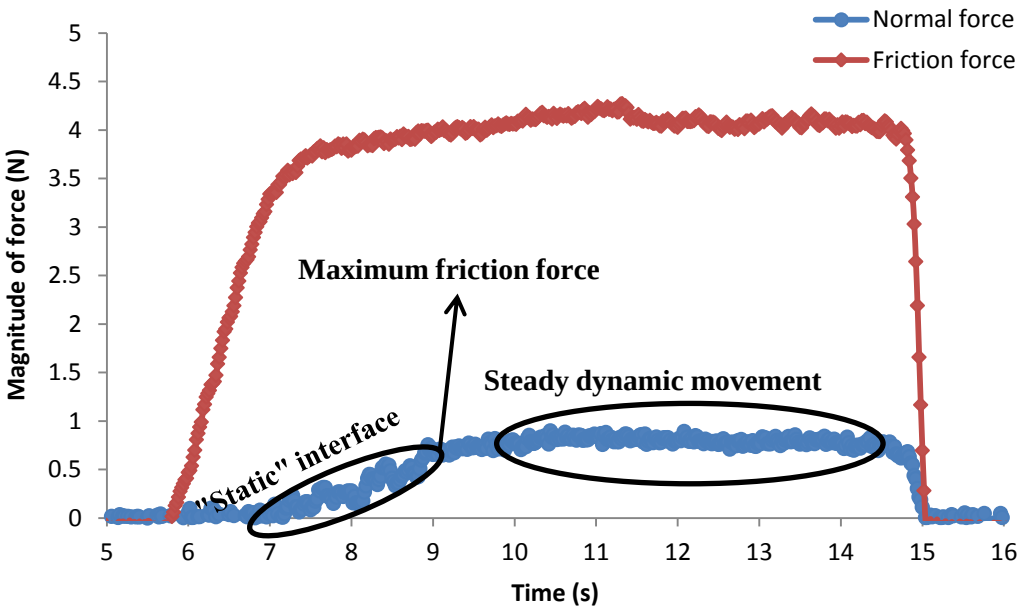

Figure 3.3: The normal load and the friction force plotted as a function of time.

3.1.4 Pinch Grip Rig

This pinch grip rig was designed by Peter Mylon (a PhD student at The University of Sheffield) with aims to assess human finger-grip ability. As shown in Figure 3.4, this experimental set-up consists of a pinch rig that is connected to a PC with a data acquisition unit (DAQ). This device shares a similar design with the above two rigs. The pinch grip forces and shear forces applied by subjects were measured directly with three load cells with capacities of 10 kg in the sides and 25 kg in the middle. These load cells (LCM703-100 universal link load cell, Omega) were attached to two aluminium discs (approximate 3 *cm* in diameter) that allow subjects to perform a pinch using their thumb and index finger. Various tested materials can be easily attached to the surfaces of discs by adhesive tape. This means that this rig could also be used to investigate the effect of different materials on finger-grip ability. The friction force can be altered by adding dead weights to the metal rod that was inserted into the centre of the rig. Finally, all obtained force data is recorded by a computer using a Labview data acquisition programme (see Appendix D).

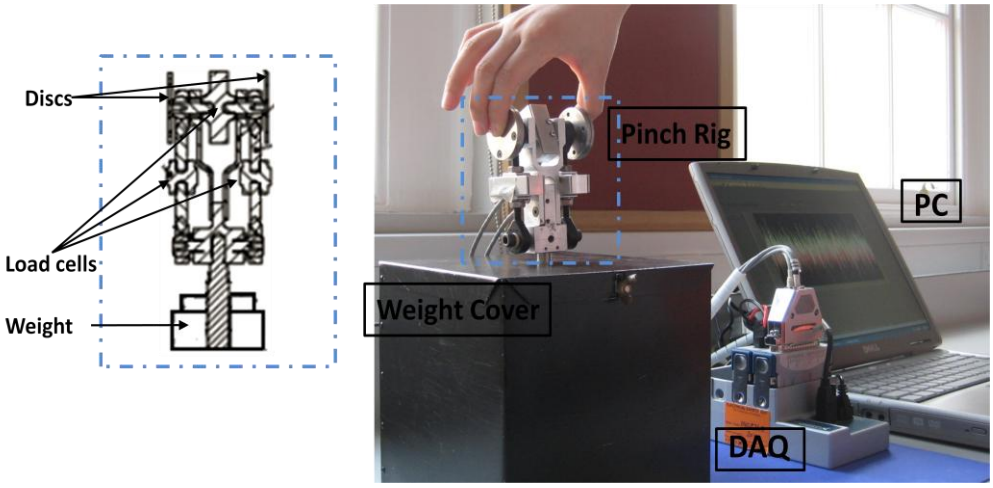

Figure 3.4: The experimental set-up of the pinch grip rig.

3.1.5 Experimental Procedure for the Pinch Grip Rig

Experiments were generally performed by a thumb and an index finger of a subject following verbal instructions. The subject was asked to conduct the thumb-index grip and lift the rig at the "START" instruction; keep it about this position until the "DROP" instruction was given; at the "DROP" instruction, the subject was requested to move the thumb and the index finger apart slowly to allow the rig to drop. Each test was repeated several times. In order to avoid the effect of gripping time on the output data, experiments performed should not run too fast or too slow.

An example of the force data acquired from the friction measurements using the pinch grip rig is displayed in Figure 3.5. According to previous studies (Johansson & Westling, 1984; Kinoshita & Francis, 1996; Bleenerhassett et al., 2006), this data can be divided into five phases referring to the performance of the thumb-index grip, including preload, loading, lift-off, unloading and slipping. To calculate the static friction coefficient, both the normal force (pinch force) and the friction force (i.e. a combined lift force) exerted by the thumb and index finger are needed at the moment when the rig starts to slip. The tangential forces recorded are strongly dependent on dead weights, and appear as constant values in the phase of lift-off. Lift force 1 was recorded from the tested thumb and lift force 2 for the tested index finger. At the moment of the beginning slip, it can be seen that there are some sudden decreases on the tangential forces (at around 15.7 *s*). Therefore, the tangential forces at that point are considered as the slip forces. The corresponding normal force could also be determined according to the signal of the tangential forces. In addition, it is observed

that lift forces are non-zero when the pinch force is zero. This could be attributed to the fact that the two load cells at the sides of the pinch grip rig are relatively sensitive compared to the load cell in the middle, which causes the outputs of the friction force to be easily impacted by vibration of the two discs. It can also be observed that it generally takes about 0.2 seconds for the system to settle down as all signals finally return to zero with time (from 15.8 s to 16 s) after the rig impacts with surface (see figure 3.5).

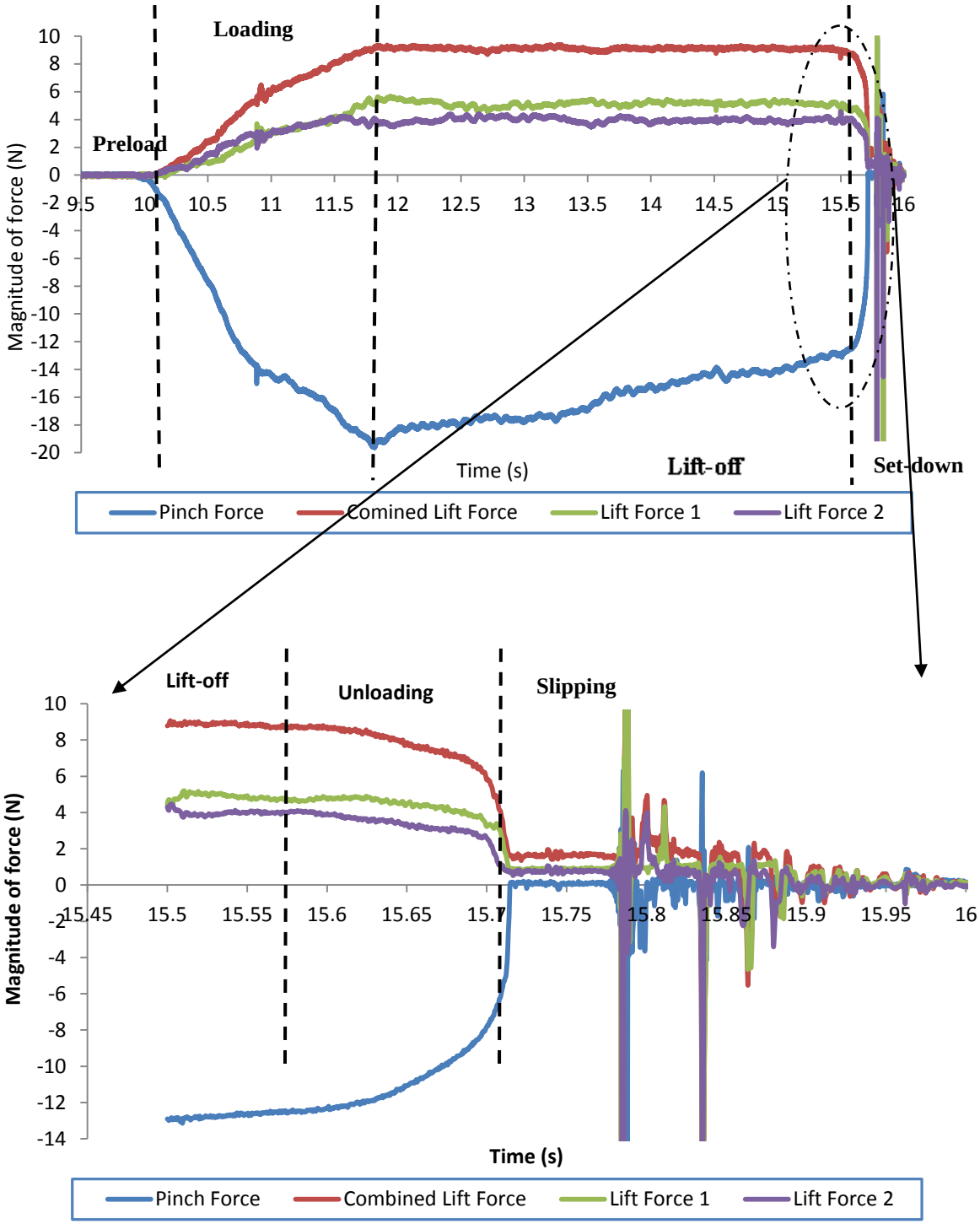

Figure 3.5: The normal load and the friction force obtained from the pinch grip rig are plotted as a function of time (lift force 1 is the friction force acquired from the thumb, lift force 2 is the friction force acquired from the index finger and combination lift force is the sum of lift force 1 and 2).

3.2 Investigations of Skin Structure

3.2.1 Optical Coherence Tomography

Optical Coherence Tomography (OCT) has been developed as a non-invasive imaging technique that allows for cross-section images of biological tissues. This technique is widely used in the medical fields for assessing eye health and diagnosing skin disease. The principle of the OCT technique is dominated by the interferometric method. The infrared light is split into two paths, one path launches into the sample where it is scattered (sample arm) and the other one goes to a reference mirror (reference arm). These two beams of light signals reflected from the sample and the mirror arms, respectively, are overlayed then. A constructive interference takes place only when signals in both arms are equal. The combination and subsequent inference of these two light paths generates a two dimensional image. In biological materials, the optical properties (light scattering and reflectance) vary widely with different tissues or cells. The internal structure of the tested sample is displayed with different grey-levels in OCT images. The penetration depth of the light signal in samples is limited to few millimeters by the power of the light source used and its wavelength. The axial resolution depends on the bandwidth of the light source. Measurements at different depths in tissues can be achieved by changing the length of the reference arm. The lateral scans (B-scan) are determined by the mechanical movement of the probe beam, composed of single line images (A-scan). The lateral resolution is independent of bandwidth of light source, determined only by the numerical aperture of the lens of the OCT system. For a 3D volumetric image, a combination multiple lateral scans is required (Fercher et al., 2003; Welzel, 2008).

In the current research, the studies of human skin structure were carried out using a commercial Optical Coherence Tomography system (Michelson Diagnostic Ltd), see Figure 3.6 (Fercher et al., 2003). This system uses a light source with a centre wavelength of 1300 *nm* and 110 *nm* FWHM bandwidth (Santec Limited). A two dimensional image has a lateral dimension of 4 *mm* (up to 6 *mm*) and a penetration depth of 2 *mm*. The resolution of the image is 10 μm (axis) x 15 μm (lateral). The step size was approximate 4 μm in both axis (x) and lateral (z) directions. In the case of multi-slice scanning, the interval between slides in the y direction was set to be 0.04 *mm*. The average refractive index of the sample medium is assumed to be 1.44

(Lu et al., 2011). The system is capable of producing a few slices for each measurement in a second. The disadvantage of the system is that the resolution in the axial and lateral directions is relatively low to observe fine details of skin (skin cells).

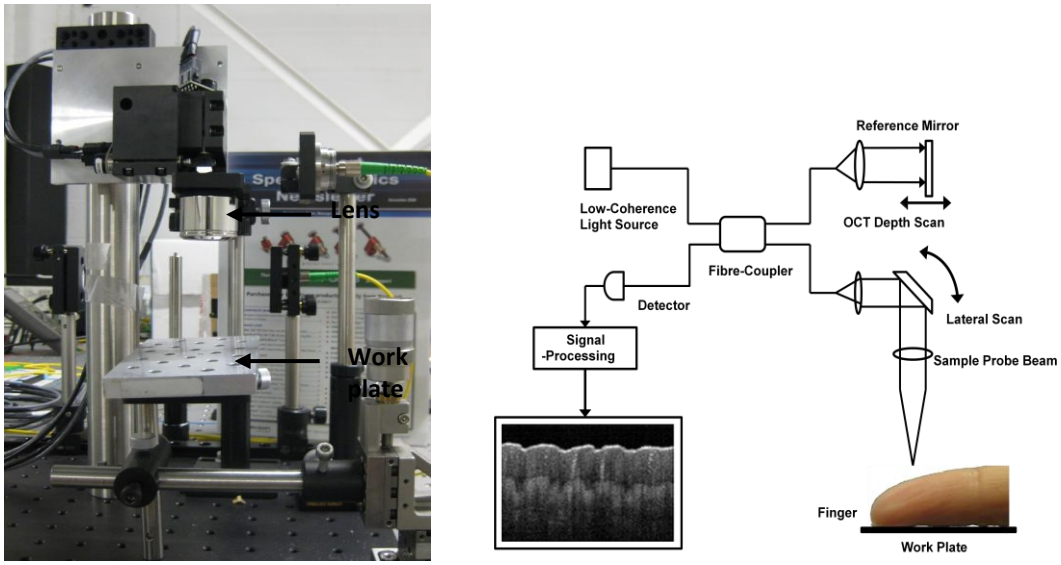

Figure 3.6: A typical set-up of an OCT system.

3.2.2 Image Analysis

In a 2D image of skin, the skin structure was clear according to the distribution of the intensities of the signal. Each layer of the skin displays different light refractance properties and produces peaks on the linear profile of light intensity in the vertical depth (Bagei et al., 2008). As seen in Figure 3.7(a), the skin surface is defined as a bright line at the top surface of the cross-sectional image of the skin, which corresponds to the refractance intensity reaching its first peak in Figure 3.7(c). This may be attributed to those dead cells and/or lipid film on the surface of the skin that give strong light reflection. Beneath the skin surface is a thick homogenous band containing some bright spiral lines (Gambichler et al., 2011). This layer is generally considered as the cornified layer of the skin (i.e. stratum corneum and stratum lucidum), which is confirmed by the histological image of thick skin (see Figure 3.7(b)) (taken from Burkitt et al. (1993)). The layer of the stratum lucidum is a relative thin layer located under the stratum corneum and gives less dense of light refractance in OCT images. Hence, the border between the stratum corneum and the stratum lucidum cannot be clearly detected in OCT images. Therefore, the thickness of the stratum corneum is generally estimated from the thickness of the whole

cornified layer in OCT images of the skin. The living epidermis is observed as a more signal dense layer with waves of papillary ridges (Welzel et al., 1997; Fruhstorfer et al., 2000). In contrast to the living epidermis, the layer of the dermis is usually less dense. There is no distinct boundary between the layer of the living epidermis and the layer of the dermis. In addition, some sweat ducts were captured and observed as bright thick broken lines in the cornified layer of the skin in OCT images. Therefore, the measurement of number of sweat ducts was mainly dependent on a manual count of the spiral lines in the images.

The thickness of the stratum corneum was easily determined by measuring the distance between the skin surface (first peak in Figure 3.7(c)) and the border between the cornified and living epidermis (the trough before the second peak in Figure 3.7(c)). 16 single frames were collected from each participant; frame Nos. 1, 5, 10, 15 were selected to be assessed individually. For each frame, ten predefined measurement points in the OCT images of skin were used for determining the thickness of the stratum corneum. The measurements were performed manually using the "image tools" (ruler) in "Matlab". The average data of ten predefined points for four frames was calculated (in pixels) to give the thickness of the stratum cornuem. All of measurements were done in pixels unit and then converted to SI units (e.g. 512 pixels in 2 *mm*).

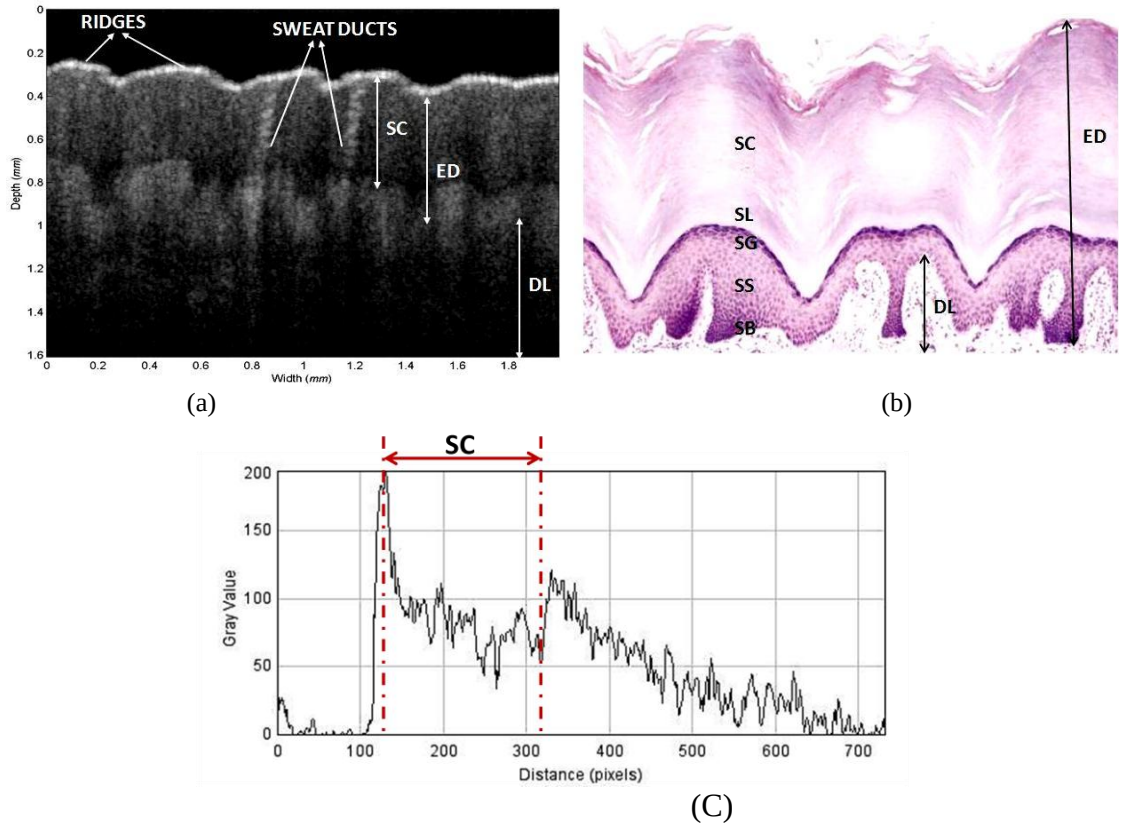

Figure 3.7: (a) Optical coherence tomography images of the skin of the left middle finger, (b) Tissue histology of the thick human skin tissue (Burkitt et al., 1993); no scale on original source found, here this is used only for indentifying various layers of skin. (c) Intensity profile of the OCT image (A-scan).

3.2.3 Experimental Procedures

During image scanning, volunteers were guided to place their fingers on the work plate and facing the lens of OCT. The work plate was attached to mechanical stages for adjusting the distance between fingers and lens. In order to obtain the average value of the thickness of the stratum corneum, the examined finger pads have to be fixed in position to ensure images are taken in the same position.

3.3. Measurements of Mechanical Properties

3.3.1 Cutometer MPA 580 used at Philips Applied Technologies

A non-invasive "*cutometer*" MPA 580 based on the suction method was used to characterise the biomechanical properties of human skin, via measuring the vertical deformation of the skin surface with response to the negative pressure. As seen in Figure 3.8, the device consists of a handheld probe with a distinctive central suction head (2, 4, 6 and 8 *mm* in diameter), attached to the main unit with an air and an

electric cable. The main unit includes a vacuum pump that can generate constant pressure up to 500 mbar and evaluation electronics. This device provides two modes: a stress-strain mode and a strain-time mode. With respect to the stress-strain mode, it is mostly used for studying the elastic properties of skin; the deformation of the skin is displayed as a function of stress. The strain-time mode refers to the measurement of the viscoelastic properties of skin. It was used with a 5-second application followed by a 5-second relaxation under a constant negative pressure.

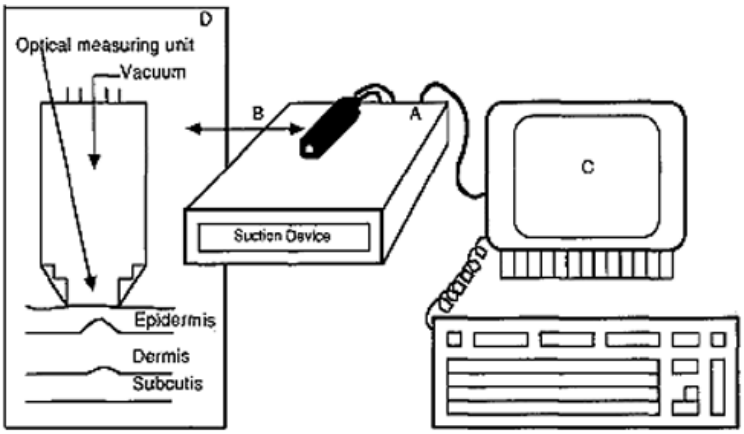

Figure 3.8: A modified schematic diagram of the cutometer (Cua et al., 1990).

A typical strain-time curve for human skin is illustrated in Figure 3.9. The following deformation parameters used to describe the curve were proposed by Agache et al., (1980): immediate distension-skin extensibility (U_e); delayed distension reflecting the viscoelastic contribution of the skin (U_v); immediate retraction (U_r); final skin deformation-skin distensibility (U_f); total recovery of skin after remove vacuume (U_a); gross elasticity of the skin, including viscous deformation (U_a/ U_f); net elasticity of the skin without viscous deformation (U_r/ U_e); the portion of the viscoelasticity on elastic segment of the curve (U_v/ U_e); biological elasticity (U_r/ U_f) (Barel et al., 2004; Cua et al., 1990). Apart from those biomechanical parameters that can be directly read from the device, it also permits determination of the normal contact stiffness of skin since the normal force and the corresponding deformation of the skin are known. The normal stiffness of the skin (S) is given by:

$$S = \frac{dN}{d\delta} \tag{3.1}$$

where N is the applied normal load to the skin and δ is the vertical deformation of the skin. The normal force to the skin is defined as the applied pressure p (approximate value of 500 mbar) multiplied by the area of the probe A_P (the diameter of probe used is equal to 2 *mm*) that is attached to the main apparatus.

$$N = p \times A_P \tag{3.2}$$

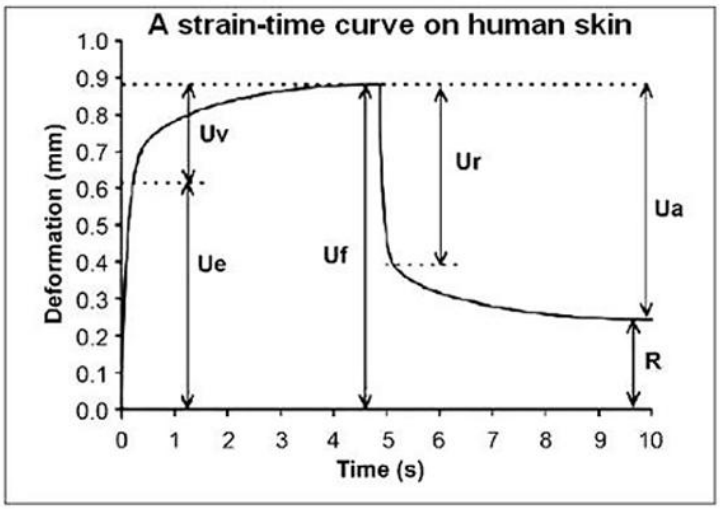

Figure 3.9: A strain-time curve of the cutometer on human skin (Cua et al., 1990).

3.3.2 Experimental Procedure

The measurements were performed using the time-strain mode that can be used to estimate the viscoelastic properties of the skin. The tested region of the human body was requested not to be treated by any chemical or cosmetic products in the 12 hours prior to the measurement. A 2 *mm* diameter measuring probe was used, which applied a constant pressure of 500 mbar to the skin.

3.3.3 Indentation Tests

A purpose built indentation device has been developed at The University of Sheffield to measure the stiffness of soft elastic objects (e.g. rubber, human skin). This device consists of a force gauge (940-233E, Mitutoyo) with a 5.5 *mm* diameter spherical tip, a digital scale (Absolute, Mitutoyo) and a manual test stand (shown in Figure 3.10). It is able to measure the penetration depth in the tested objects as function of the applied load during loading. Measurements were performed in controlled applied load mode. The applied load was controlled manually by the hand-wheel of the test

stand (out of the picture). In order to measure the penetration depth, the tip of the digital scale was placed in contact with a flat metal strip that was attached to the extend rod of the force gauge. The tested samples were required to be fixed in a position in order to reduce the impact associated with sample movement through the tests. Prior to loading, the tip of the force gauge was initially positioned as it just touched the tested samples, for this case, we assume that there was no load applied to the sample. The maximum load applied to the tested samples ranged from 0.5 to 10 N with an increment of 0.5 N.

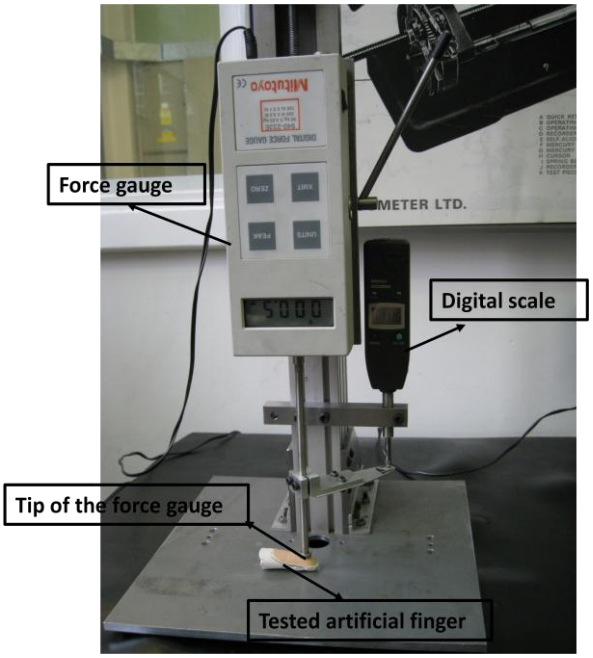

Figure 3.10: A photograph of the indentation device to determine the stiffness of samples.

A representative load-displacement curve from the indentation tests of artificial fingers (results in Chapter 4) is shown in Figure 3.11. A second order polynomial model is applied to describe the curve behaviour, is given as:

$$N = B\delta^2 + U\delta + H \tag{3.3}$$

where N is the load applied, B, U and H are constant and δ is the penetration depth. Therefore, according to Equation (3.1) the stiffness of the artificial fingers can be calculated as:

$$S = \frac{dN}{d\delta} = 2B\delta + U \tag{3.4}$$

This load-displacement sensing indentation test could also be used to estimate the Young's modulus of the tested samples. For example, Oliver and Pharr (1992) have proposed a simple model which was used to determine the Young's modulus of skin based on the indentation tests. This model is expressed as:

$$E_{skin} = S\sqrt{\pi}\Big/_{2\sqrt{A}} \tag{3.5}$$

where A is the projected contact area.

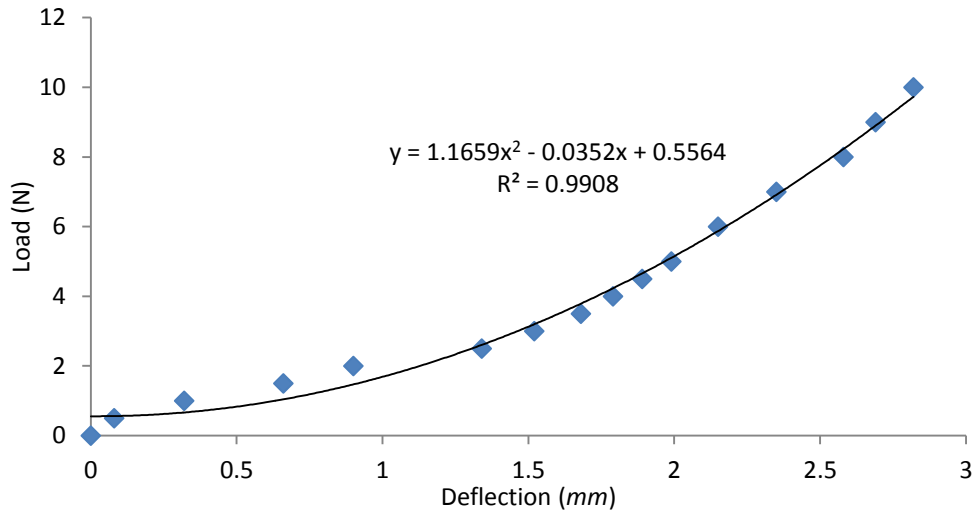

Figure 3.11: An example of the load-deflection data.

3.4 Measurement of Skin Roughness

For measurements of skin roughness on human finger-pads, an indirect approach using a surface profilometer (MitutoyoSurftest SV-600) has been introduced. Since finger-pads skin is a non-flat and soft material, it is not possible to conduct measurements on finger-pads directly, for this case, a polymer replica of the hand skin has been made. Human skin texture can be moulded on the polymer replicas, so that the roughness of human skin can be quantified as the profilometer stylus moving over the casts (see Appendix E). In this research, measurements were carried out exactly following Tomlinson's roughness procedure (2009), in which the stylus was moved 2 *mm* along in the same direction as the finger-pad or the palm in the friction tests, with a speed of 0.1 *mm/s*. In order to gain reliable data of roughness, each measurement needs to be repeated at 3 different positions on the tested region and average values calculated.

3.5 Conclusions

This chapter gives an overview of all required equipments and testing procedures that have been used to collect the data presented within this thesis. The skin friction on human finger-pads was measured by using different friction rigs. The OCT system enables charactersion of the skin structural properties. The use of "*cutometer*" MPA 580 and an indentation device make it possible to have comprehensive assessments of the skin mechanical properties. In the next chapter, the investigation of the skin frictional properties on human finger-pads is conducted.

Chapter 4

Investigations of the Skin Frictional Properties of Human Finger-pads

From the literature review, it was found that the frictional behaviour of human skin is unique and does not obey the traditional friction law of Amontons-Coulomb. For a better understanding of skin frictional properties, a few series of friction tests were conducted in this chapter. Firstly, an experimental comparison of three different techniques has been made in order to select the most suitable device for measuring the skin friction coefficient. A pilot study to investigate the relationship between the friction coefficient and the normal load was also carried out. Finally, this chapter describes how the skin friction coefficient varies with age, gender and ethnicity in participants.

4.1 Experiment 1: Comparison of Different Techniques for Measuring Finger-pad Skin Friction

4.1.1 Introduction

Various instruments (discussed in Chapter 2) have been applied to measure skin friction, which can be classified into two classes of techniques. The first technique is the rolling method, which allows apparatus to roll against the examined skin tissue. This method provides high accuracy, repeatability for tests, and could be performed in most anatomical sites of human body. The second technique is based on the sliding method which allows apparatus to slide along the examined skin tissue. The advantage of this technique is that it can investigate the frictional behaviour of skin with various materials during the actual movement. It is believed that the sliding method is more suitable for measuring the frictional properties of fingers. In the

current studies, three different finger-specific devices based on the sliding method, including a purpose built finger friction rig, a multi-axis force plate and a pinch grip rig were used to measure the skin friction coefficient of finger-pads (more details about these devices have been discussed in Chapter 3).

4.1.2 Experimental Procedure

Experiments were carried out under normal laboratory conditions. The temperature was in the range of 20˚C and 26˚C and the humidity was around 58% RH. In order to avoid the effects of different materials and roughness conditions on the friction measurements, a smooth aluminium strip ($R_a \approx 0.2\ \mu m$) was attached to the work plates of the finger friction rig and the multi-axis force plate, on which the tested finger could be positioned to perform the slide movement. The discs of the pinch grip rig are made of aluminium and have a similar roughness of 0.5 μm. A 25-year-old female was invited to carry out all experiments in this study. In the measurements using the finger friction rig and the multi-axis force plate, the subject was requested to drag her dominant index finger along the aluminium strip with various loads (in the range of 0.2 N to 12 N). Similarly, six different dead weights were added to the pinch grip rig for gaining different shear force.

4.1.3 Results and Discussion

Figure 4.1 shows a plot of the log friction forces against the log normal forces. It is observed that, for all three different techniques used, the log friction force rose with the log normal force in a function of $log(F) = Blog\ (N) + U$, where B is the slope of the linear relationship, U is a constant. With regard to the investigation of the relationship between the friction force and normal force, it will be discussed in Section 4.2. It is found that the value of B (Table 4.1) relating to the multi-axis force plate is greater than those of finger friction rig and pinch grip rig. On the other hand, there is no significant difference observed in the y-intercept (B) between the finger friction rig and the multi-axis force plate (equal to -0.5), while the value of U for the pinch grip rig was zero.

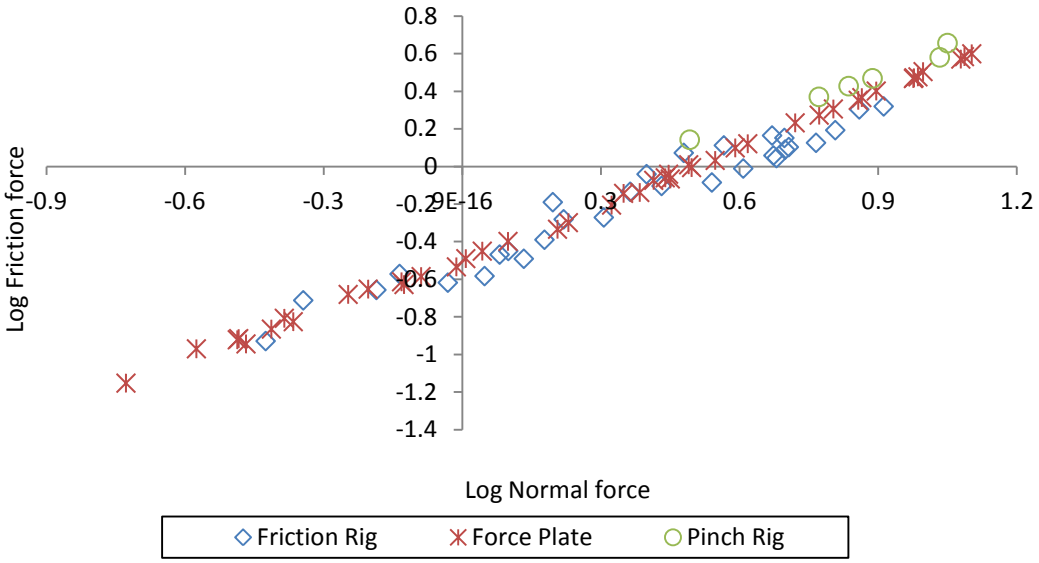

Figure 4.1: Log normal force against Log friction force using all three different techniques.

Table 4.1: Some parameters of the linear relationships between log normal force and log friction force.

Methods	$log\,(F) = Blog(N) + U$			
	B	U	R^2	t
Finger Friction Rig	0.90	-0.50	0.96	0.07
Multi-axis Force Plate	0.96	-0.48	1.00	0.02
Pinch Grip Rig	0.87	-0.30	0.99	0.02

The results of the above experiments show that the log friction force is linearly proportional to the log normal load for all three devices used. There is no significant difference observed in the slope (B) of the linear relationship between the finger friction rig and the multi-axis force plate. This is reasonable as these two devices are very similar in apparatus and operation. The parameter of R squared as well as the parameter of t (Table 4.1) is considered one of the most important parameters for comparing three different equipments in the current study. R^2 is the square of the correlation coefficient as an indicator for measuring how well the real data fits the regression line. The closer the R^2 is equal to one, the stronger relationship between variables that could be used to predict the trend. It can be clearly seen that R^2 relating to the multi-axis force plate presents a maximum value of 1, followed by those

relating to the pinch grip rig and the finger friction rig. The parameter *t* is the estimated standard deviation of the residuals (standard error of the regression). The value of *t* will be equal to zero if there is a perfect prediction. By analysing these parameters obtained relating to three different techniques, it is suggested that the multi-axis force plate is the most accurate device to measure the skin friction coefficient.

Although, the results gained from the finger friction rig also suggests a linear relationship for the log normal load and the log friction force, the standard error is twice large as those of the other two techniques. This could be attributed to the low sensitivity in the measurements using the finger force rig. According to Chapter 2, the finger friction rig has a large measuring range (between 0.2 and 500 N). However, those forces applied by a finger (up to 30 N) seem too small to be detected, thus big errors could result in the data collection. On the other hand, the multi-axis force plate is specifically designed for qualifying low loads. This technique allows the measurements of forces in Z direction up to 44 N (with resolution of 0.02 N), 22 N for X and Y directions (with resolution of 0.01 N), which enables it to detect even tiny changes in the force applied due to its high sensitivity. Therefore, the correlation related to the finger force plate is relatively weak compared to that using the multi-axis force plate.

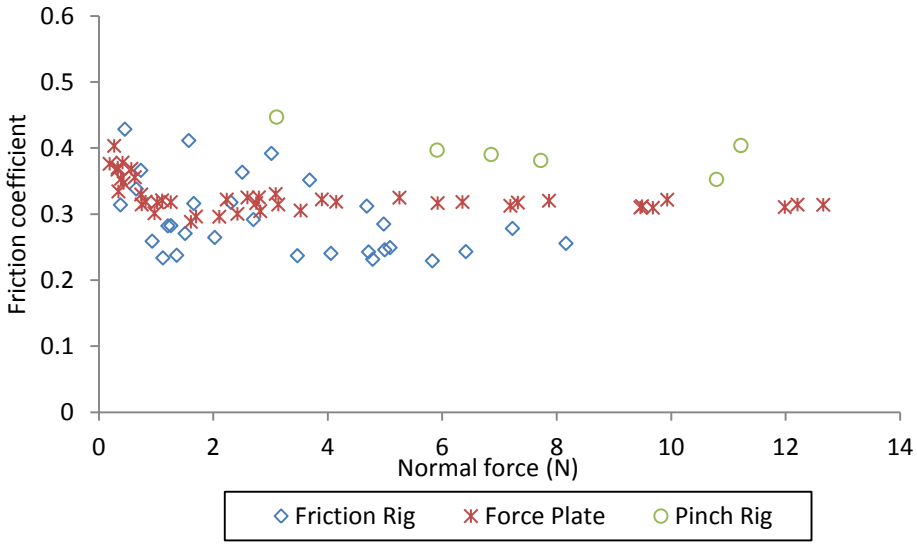

Figure 4.2: Data of the friction coefficient with different normal forces obtained using three different techniques.

Figure 4.2 shows the variation of the friction coefficient for the finger with different loads and different devices. It can be seen that both the finger friction rig and the multi-axis force plate show similar trends in friction coefficient, which is around 0.4 for 0.3 N and is reduced to 0.3 when load is greater than 2 N. While, the pinch grip rig displayed relative constant values of friction coefficient with load.

The pinch grip rig provides a simple way to assess human gripping ability as measurements of normal force (i.e. the force is applied by human finger) and tangential force (i.e. shear force from dead weight load). In this study, it was used a method for measuring the skin friction coefficient (discussed in Chapter 3). The friction coefficients obtained by the pinch grip appear to slightly higher than those obtained using the other two techniques (Figure 4.2). This could be caused by the fact that the different methods tested different fingers. In the above two experiments using finger sliding, only one finger of the subject (the right index finger) was examined, the friction coefficient obtained could be considered as the friction coefficient of the right index finger. However, this experiment was performed by both the right index finger and the right thumb finger, so the results of the pinch grip rig were the average values of the friction coefficients obtained from both fingers. It is impossible for this technique to characterise the frictional properties on a single finger. The other disadvantage is that this technique is limited to those tests with small load ($\leq$ 3 N) as the mass of the rig is 300 g. Moreover, the most challenging thing about using this pinch grip rig is the difficulty of identifying the point of "slip initiation" in the display of data for the measurements of dynamic friction coefficient. The determination could also be affected by subject biases. The same problem was also reported by Savescu et al. (2008), who indicated that the measurements of finger friction were likely influenced by some subjective errors.

It can be concluded that the multi-axis force plate is the best device for the measurement of the skin friction coefficient of fingers for this research. The finger friction rig could also be a good option for the tests under high load conditions. Due to the wide variability in the identification of the "slip initiation" point, the pinch grip rig was not considered for use in this study. In addition, although the multi-axis force plate could perform relatively accurate measurements, there are still some

disadvantages. For example, it is difficult to manage the applied load and speed since they are manually controlled by the subject.

4.2 Experiment 2: Investigation of the Relationship between the Normal Force and the Friction Force

4.2.1 Introduction

According to Amontons-Coulomb's laws of friction, the friction coefficient is considered to be independent of the load applied. However, in most recent studies, it was found that this conclusion does not hold for soft viscoelastic materials (e.g. rubber, skin). A number of studies have been done on investigating the effect of load on the friction coefficient of skin as well as the relationship between the normal force and the friction force. In the case that a spherical probe was used for investigating the frictional behaviour of human skin, the friction coefficient of skin was generally reported to decrease with loads following the relationship of $\mu \propto N^{-n}$, where n is the exponent of the linear regression and suggested to be around 0.3 for human skin. For example, Koudine et al. (2000) found that the dynamic friction coefficient of skin decreases with increasing the normal load to the power of -0.28. The corresponding value of n was reported to be -0.32 in the studies of Sivamani et al. (2003). Some other authors looked at the relationship between the normal force and the friction force instead of the relationship between the friction coefficient and the normal force. A simple power relationship has been developed by Asserin et al. (2000) to estimate how friction force is altered with loads, $F = \mu N^n$, where μ is friction coefficient, F is the friction force, N is the normal force and n is friction factor (a constant). However, the results of the studies of Tomlinson et al. (2009) did not follow this trend. They attempted to explain the relationship between the normal force and the friction force in terms of skin elastic properties. A two-part relationship was used to characterise the skin friction behaviour referring to the level of load applied. For a finger-pad contacting a smooth flat surface with loads greater than 1 N, the frictional force appeared to follow a linear relationship. There was a different relationship between the normal force and the friction force at the low load condition. Derler et al. (2009) have investigated the relationship between the pressure and the friction coefficient of skin in order to characterise the load dependence of the friction coefficient. The results of their experiments demonstrated that the friction coefficient

can be expressed as a function of pressure: $\mu = B \times p^{n-1}$, where B is a constant, p is the contact pressure and $n-1$ is the exponent of linear regression. The exponent $n-1$ was found to be ranged from -0.26 to -0.15 when a dry finger was sliding against a smooth glass using a pushing motion, ranged from -0.96 to -0.79 for a pulling motion. In summary, the frictional properties of human skin are very complex and a deep understanding of how friction coefficient varies with load is required.

4.2.2 Experimental Procedure

The findings from section 4.1 suggested that the multi-axis force plate is best device that could be used to measure the skin friction coefficient of fingers. Therefore, all experiments were carried out to test the right index finger of a female (aged 26) using the multi-axis force plate system under normal laboratory conditions. The subject was asked to slide her index finger on a smooth optical glass window (*Quartz Glass*) ($Ra \leq 0.01$ μm) and a relatively smooth aluminium strip ($Ra \approx 0.5$ μm) that were attached to the force plate individually, under various loads. The materials were cleaned using a cleaning wet wipe every three runs to avoid the effect of the superficial sebum and/or the sweat across the skin surface on the friction force.

4.2.3 Results and Discussion

The friction coefficient shows a non-linear decreasing trend with increasing normal load for glass and aluminium, as shown in Figure 4.3. There is initially a rapid decrease in the friction coefficient for low loads (≤ 2.5 N) and it reaches a plateau after the initial stage. This phenomenon indicates that Amontons law is not applicable for human skin. In order to further investigate the relationship between these two variables, all the data were plotted in a log-log form. As seen in Figure 4.4, the log friction coefficient shows a linear dependence on the log normal load, for both materials. The slopes of the log-linear relationships were -0.22 for glass (R^2 = 0.91), -0.16 for aluminium (R^2 = 0.87).

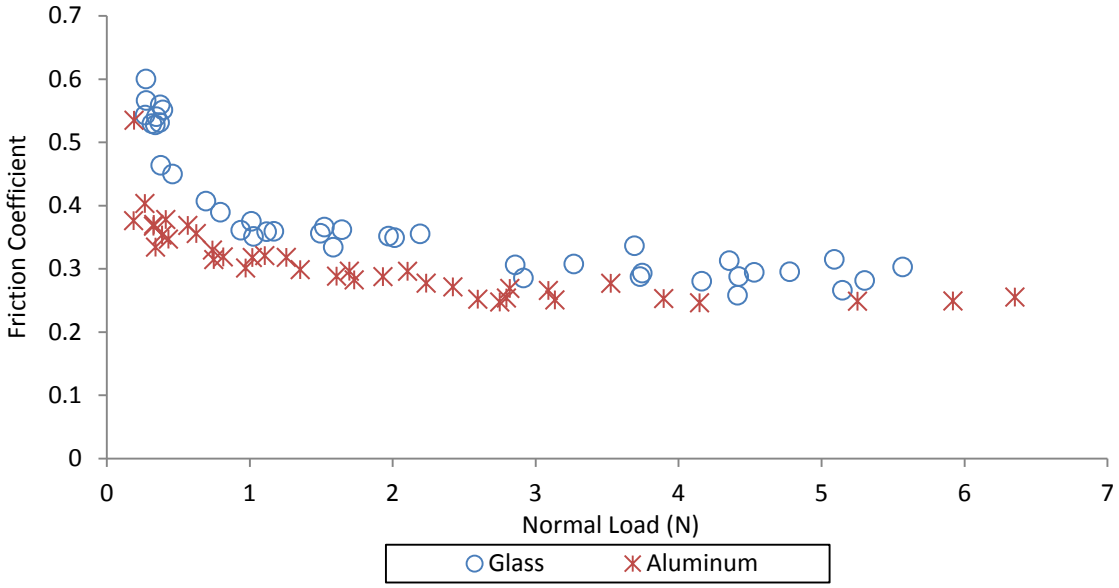

Figure 4.3: Plot of the friction coefficient against the normal force for glass and aluminium.

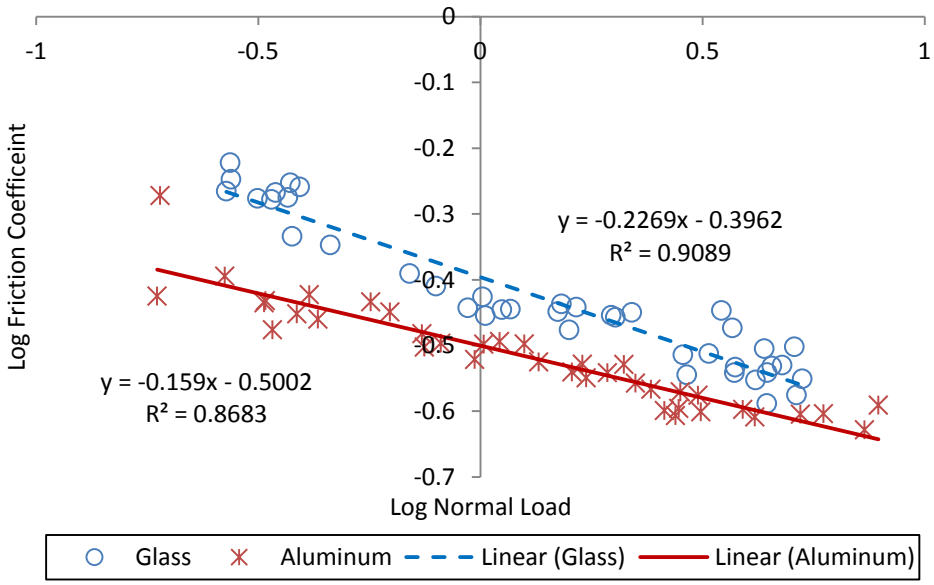

Figure 4.4: Plot of log normal load against log friction coefficient for glass and aluminium.

Figure 4.5 displays the output of the indentation test on the right index finger of the participant. Two possible relationships between the normal load and the deflection are plotted on the graph. The point of intersection of these two lines is near 2.5 N (2 *mm*). At low load conditions (≤ 2.5 N), the skin on finger-pads becomes stiff with increasing the load as the deflection of skin increases from 0.38 *mm* to 1.88 *mm*. After that, there is a relatively slight rise in the stiffness when the applied load ranges from 2.5 N to 6 N.

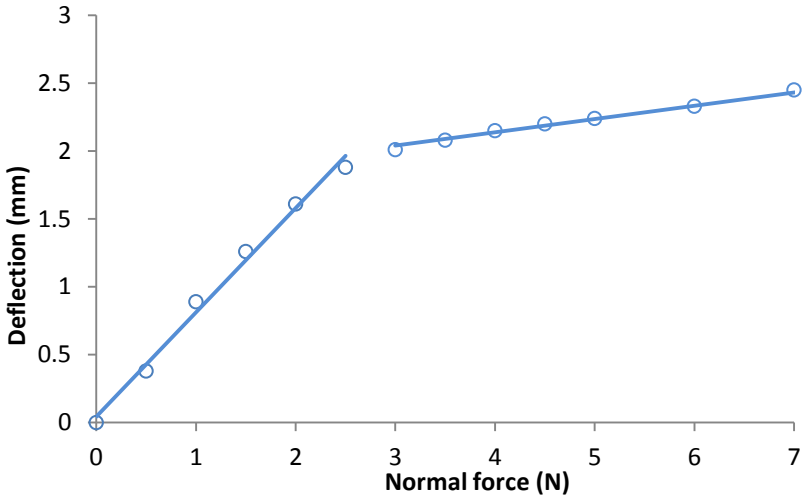

Figure 4.5: Plot of deflection against normal load for human finger.

As discussed above, the relationship between the friction coefficient and the normal load could be split into two parts, so they will be assessed separately referring to the mechanical properties of human skin. Figure 4.6 (a) shows the relationship between the friction coefficient and the normal load in the condition of low load, its log-log form is plotted in Figure 4.6 (b). It can be observed that the slopes of the linear regressions are slightly higher than those in Figure 4.4, for both materials. The correlations of determination are also very high. In contrast to those results at low load condition, the correlation between the friction coefficient and the normal load for high loads (>2.5 N) is weak as the value of R^2 is smaller than 0.75 (0.25 for the glass and 0.33 for the aluminium).

Figure 4.7 shows the difference in the friction coefficient between the glass and the aluminium tested at the same loads, where the corresponding data of skin deflection at the tested finger-pad is also plotted. It can be seen that the magnitude of difference shows a decreasing trend as increasing the normal load.

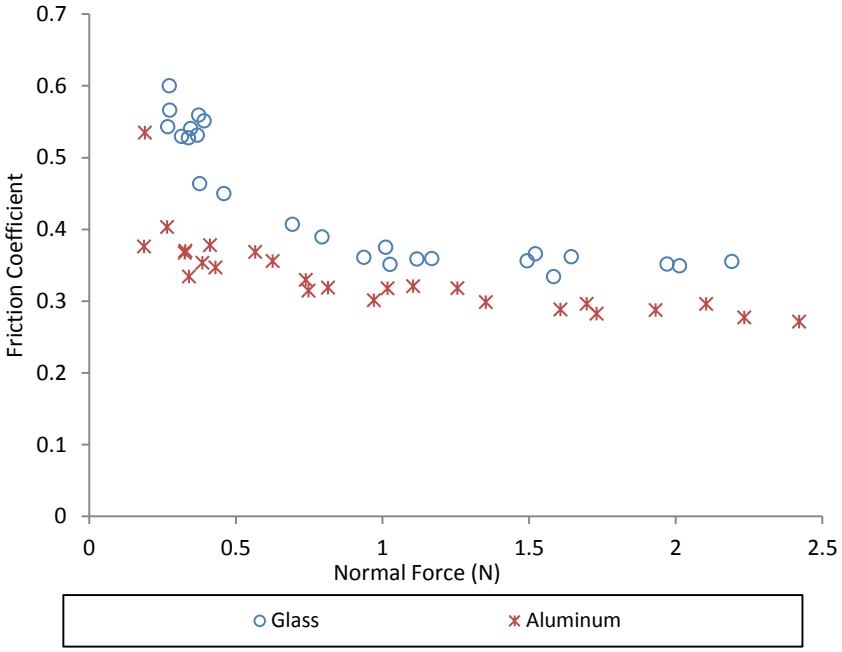
Friction Coefficient
0.7
0.6
0.5
0.4
0.3
0.2
0.1
0
0
0.5
1
1.5
2
2.5
Normal Force (N)
Glass
Aluminum

(a)

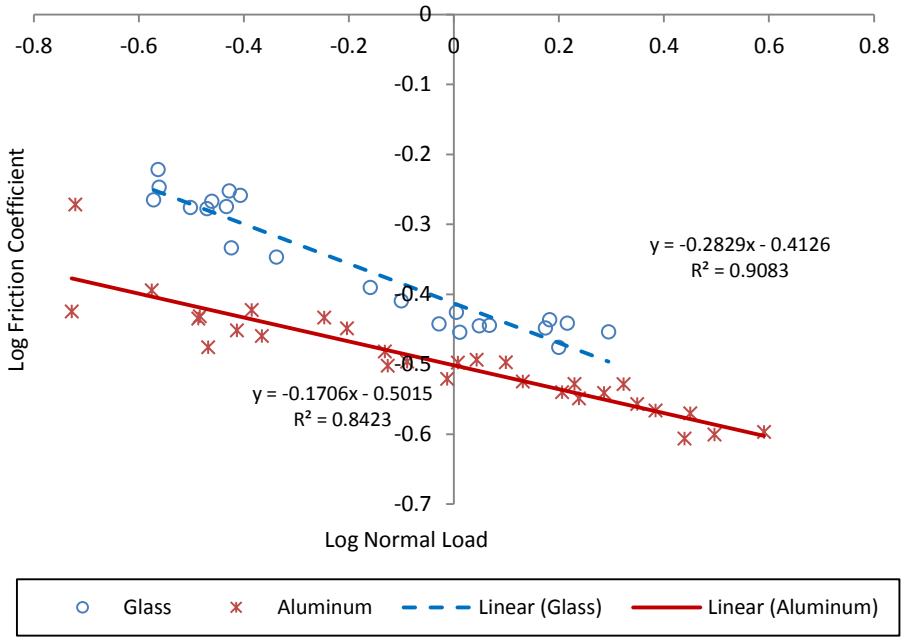
Log Friction Coefficient
-0.8
-0.6
-0.4
-0.2
0
0.2
0.4
0.6
0.8
-0.1
-0.2
-0.3
-0.4
-0.5
-0.6
-0.7
y = -0.2829x - 0.4126
R² = 0.9083
y = -0.1706x - 0.5015
R² = 0.8423
Log Normal Load
Glass
Aluminum
Linear (Glass)
Linear (Aluminum)

(b)

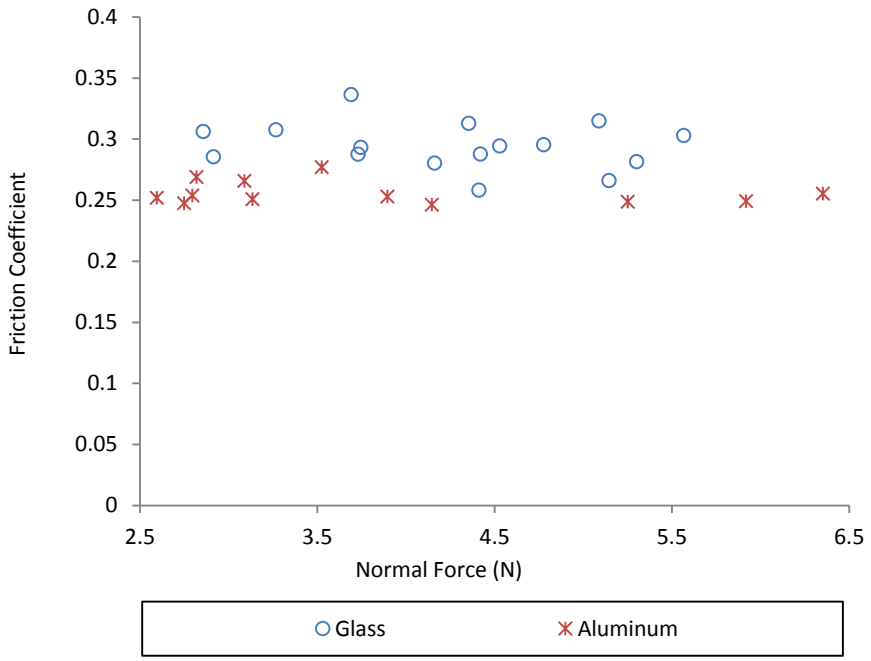

(c)

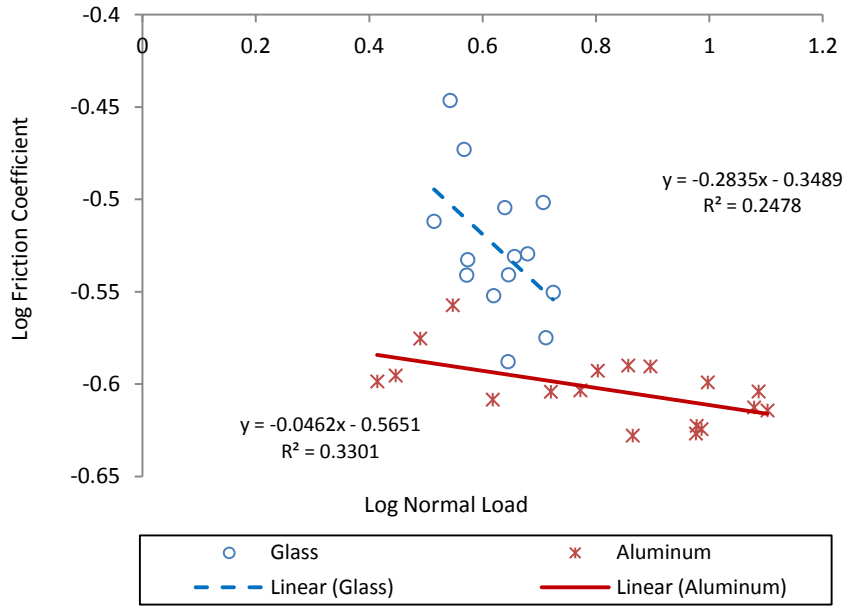

(d)

Figure 4.6: Plots of friction coefficient against normal load on normal and logarithmic graphs: (a) and (b) for low loads, (c) and (d) for high loads.

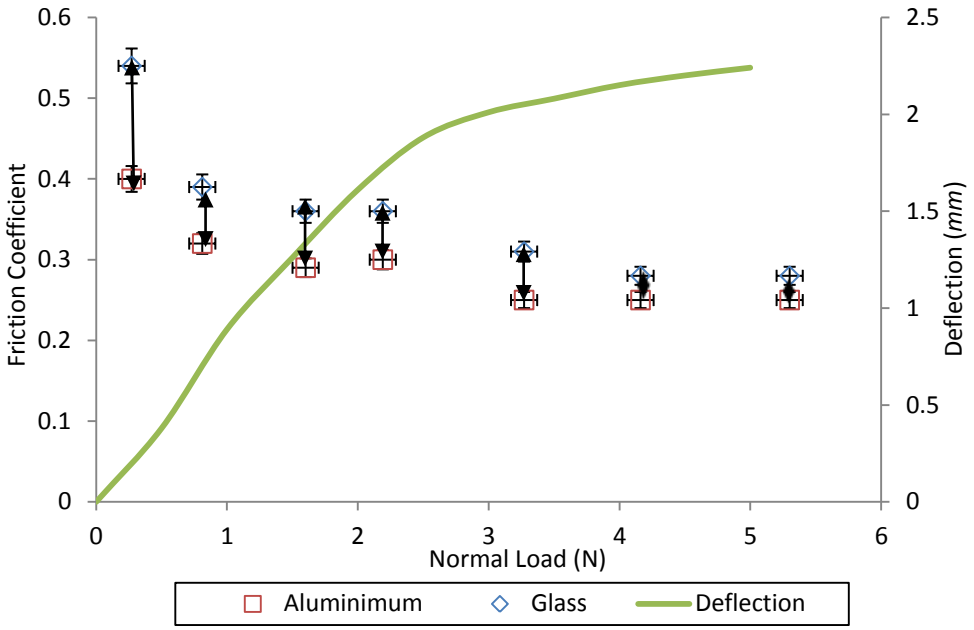

Figure 4.7: Difference in the skin friction coefficient between the glass and the aluminium samples and corresponding deflection of the tested finger as a function of the normal load (error ± 0.1 N).

The above study shows that the friction coefficient of skin decreases non-linearly with increasing normal load, which verifies that Amontons law could not characterise the skin frictional behaviour of human fingers. Furthermore, the skin friction coefficient of fingers was found to be associated with its Young's modulus in vertical direction and can be described as a two-part relationship (see Figure 4.7). A similar phenomenon was also found by Tomlinson et al. (2009), who looked at the relationship between the friction force and the normal load, instead of the friction coefficient and the normal load. They suggested a linear relationship for high loads (> 1 N) for the case that a dry human finger was sliding along a smooth surface. However, in the current study, the cut-off points for both the friction tests and the stiffness measurements were found to be around 2.5 N. The difference could be attributed to different fingers being used, where the mechanical properties of the skin on various fingers are obviously different. In this study, the friction coefficient appears to be proportional to the normal load, at low load conditions (≤ 2.5 N), in accordance with the model of $\mu \propto N^{-n}$. The value of n is found to be 0.28 for glass and 0.17 for aluminium. This finding could be explained by the mechanical properties of skin in combination with friction mechanisms. The skin friction is considered to be associated with both deformation and adhesion mechanisms when a

low load is applied on the skin. The skin exhibits different types of deformation with various loads, which causes the mechanical properties of the skin to alter with load, thus the skin behaves as different materials and gives different coefficients of friction. When skin is suffering heavy loads (> 2.5 N), it stiffens at high strain and acts as a material with steady mechanical properties (see Figure 4.5). In this case, the friction of skin is considered to rely on adhesion force, and the deformation factor is normally ignored (Greenwood & Tabor, 1958; Wolfram, 1983). Thus, we can assume that the coefficient of friction is a constant and independent on the load under the condition of the applied load that reaches a certain level. This could be the reason why there was no or weak correlation observed between the log friction coefficient and the log normal load in Figure 4.6 (d).

This research also provides an interesting result for comparing the friction coefficients between the employed glass and aluminium under the same load conditions. It can be observed that the magnitude of the difference tends to be gradually reduced with increasing the normal load. There were big differences in friction coefficient between the glass and the aluminium at low loads. This could be attributed to the fact that the surface properties of the tested materials have significant impacts on the skin friction, where the skin on finger-pads does not fully contact surfaces. In this case, there are many contributions to the skin friction force, including molecular forces, electrostatic forces, chemical hydrogen bonds and capillary forces (Scherge & Georb, 2001). The friction force is considered to be dominated by the mechanical properties of the skin when the skin experiences high loads, because the influence of surface properties of materials to the skin friction at high load conditions is relatively small compared to that at low load conditions.

4.3 Experiment 3: The Frictional Properties of Artificial Fingers

4.3.1 Experimental Materials and Methods

In order to investigate the effect of skin elastic properties on the skin friction coefficient of fingers, some artificial fingers with different stiffness and sizes were made. These artificial fingers mainly consist of two parts, bones and finger-pads. The bones were made from the casting plaster. The soft finger-pads were developed using the Room Temperature Vulcanizing (RTV) silicone rubber (base and catalyst with

ratio 1:1). In order to simulate the feel of human skin, a deadener was added to the silicone fluid to soften the RTV silicone rubber. To give different stiffness, the proportions of the deadener in the silicone fluid were: 30%, 25%, 20%, 15% and 10%. Then the mixture was poured into spherical shape molds with three different dimensions of 8 *mm*, 6 *mm* and 4 *mm*. Finally, all samples were coated with astringent powder to provide dry and no-sticky surfaces. The stiffness of the samples was determined using a simple indentation device (see Chapter 3) to obtain measurements of the force applied and the deflection from the initial position, expressed as:

$$S = {}^{dN}/_{d\delta} \tag{4.1}$$

where N is the force applied to sample, δ is the penetration depth. Measurements of the friction coefficient of artificial skin were carried out on the aluminium strip using the multi-axis force plate following the standard testing procedure (see Chapter 3). The normal load applied was 1 N.

4.3.2 Results and Discussion

Figure 4.8 shows five artificial fingers with the same thickness of 8mm, but different stiffness; in which the sample S1 is the most stiff one (5% deadener) and the sample S5 is the least stiff one (35% deadener). The normal load against the deflection for both artificial samples and a human index finger are plotted in Figure 4.9. In this figure, it can be observed that the human finger exhibits unique properties from those artificial ones. However, the trends of variety for samples S3 are similar to that of the human finger within the force range of 0 to 2 N. Thus, the sample S3 sample is considered the best simulation model for human fingers at low loads.

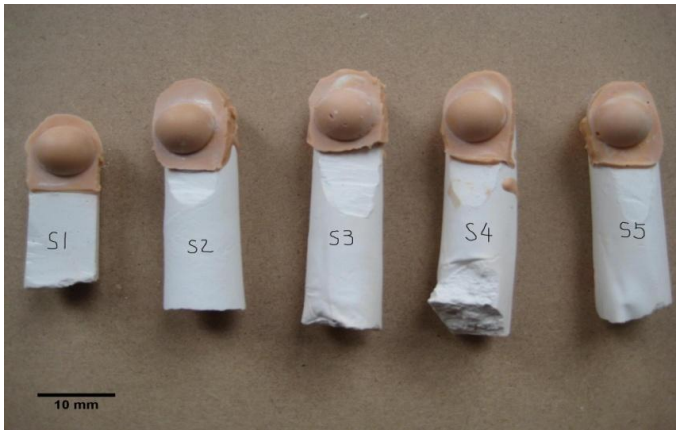

Figure 4.8: Five samples of artificial fingers with depth of 8mm, but different stiffness.

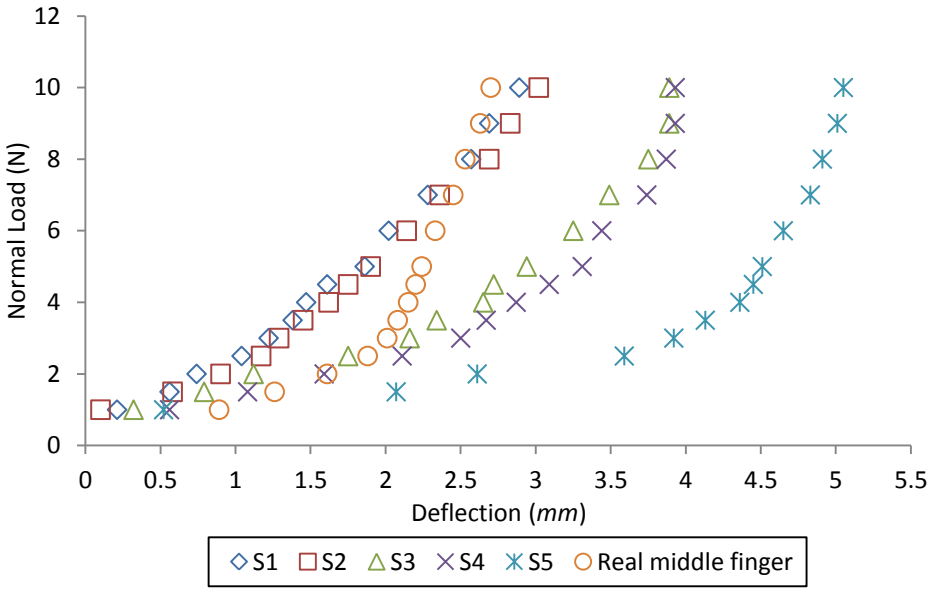

Figure 4.9: Plot of deflection against normal load for all five artificial fingers with depth of 8 *mm*.

Three different thicknesses of Sample S3 were developed and assessed. The corresponding normal load against the deflection is shown in Figure 4.10. A 2nd order polynomial model is suggested to describe the relationship between the normal load and the deflection as it is the best fitting line to all the data points. The values of *B* and *C* in polynomial functions for all the artificial samples and the human finger are given in Table 4.2, as well as the magnitude of stiffness with a deflection of 2 *mm*. The stiffness could be qualified using Equation (1). The stiffness of the artificial fingers was found to be 4 N/*mm* for 8 *mm* thick sample (S_8), 9 N/*mm* for 6 *mm* thick one (S_6) and 15.5 N/*mm* for 4 *mm* thick one (S_4), respectively. It is noted that

decreasing the thickness of finger-pads from 8 *mm* to 4 *mm* results in an increase of two orders of magnitude in the stiffness.

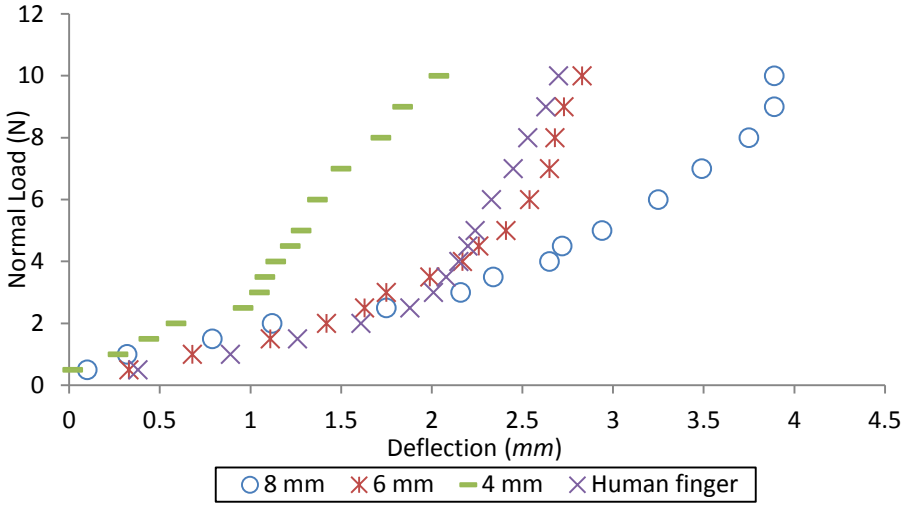

Figure 4.10: Plot of deflection against normal load for Sample S3 with the thickness of 4 *mm*, 6 *mm* and 8 *mm*.

Table 4.2: Parameters of polynomial relationships for all artificial fingers (8 *mm*) and a human finger.

	$F = B\delta^2 + U\delta + H$			
Samples S3	B	U	H	$S = {dN}/{d\delta}$ $(\delta = 2\ mm)$
8 *mm*	0.74	-0.98	1.68	1.98
6 *mm*	1.92	-2.93	1.86	4.74
4 *mm*	1.97	0.88	0.52	8.76
Human finger	3.02	-5.78	3.01	6.31

Figure 4.11 shows the friction coefficient data for all Sample S3 specimens and the human finger under a normal load of 1 N. As expected, the friction coefficient shows a slight decrease from 0.75 to 0.6 in response to the decrease in the thickness of finger-pads. It proves that there is a significant relationship between the thickness of finger-pads and the friction coefficient. The skin friction coefficient of the human finger appears to be relatively small compared to those artificial fingers.

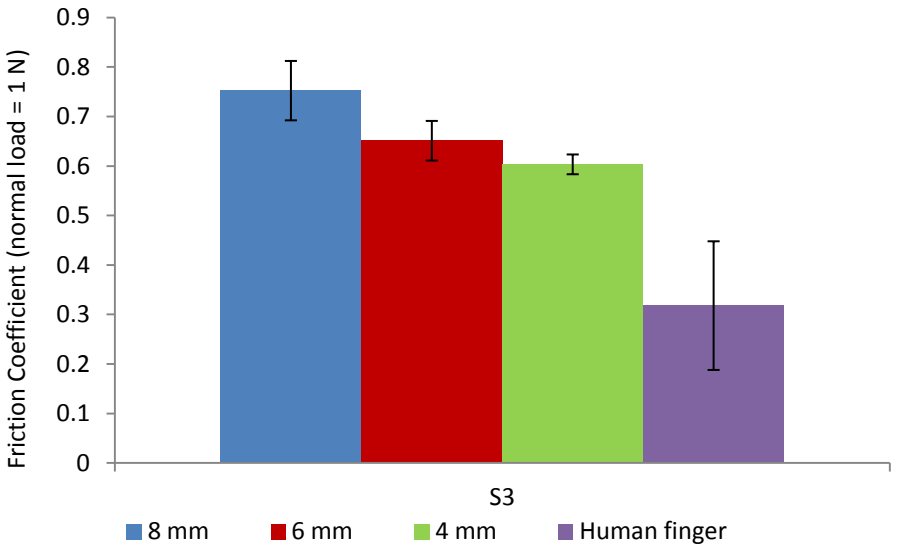

Figure 4.11: (a) Stiffness for Sample S3 with three different depths (8 *mm*, 6 *mm* and 4 *mm*) and (b) corresponding friction coefficient data for all three samples.

According to previous studies, it was accepted that the thickness of different skin layers is one of the key factors affecting the skin mechanical properties (Grahame, 1969; Sander, 1973; Agache, 1980; Bader & Bowker, 1983; Escoffier, 1989; Barel, 1995; Diridollar, 2000; Hendriks, 2005; Geerligs et al., 2011). The human skin is a multi-layer tissue consisting of epidermis and dermis, each of which is endowed with different mechanical properties. When subjected to an external force, the skin generally works as a whole (2009). However, due to the technical limitation in this study, it only possible to develop the finger-pad models with a single layer. Therefore, this study concentrated on the influence of the depth of skin on skin friction with consideration of the related change in the global Young's modulus.

In earlier studies of skin friction, it was indicated that the friction of skin in a dry state involves two mechanisms of interfacial shear force and deformation. The equation was given by Adams et al. (2007), as follows:

$$F = F_{ad} + F_{de} \tag{4.2}$$

where F_{ad} is the interfacial shear force, F_{de} is the deformation force. However, the friction of skin is assumed to be only associated with adhesion mechanism, for dry and smooth surfaces, while the deformation is normally ignored (Wolfram, 1983; Johnson et al., 1993; Adams et al., 2007). In the case of a hemispherical probe

sliding on deformable materials such as rubber or skin, the friction force can be expressed as:

$$F_{ad} = \tau A_{re} = \tau\pi({}^{9RN}/_{16E})^{2/3} \propto E^{-2/3}N^{2/3} \quad (4.3)$$

where τ is the shear strength, A_{re} is the real area of contact, R is the radius of probe and N is the applied load. E is the reduced Young's modulus and is defined as ${}^{1}/_{E} = (1 - {}^{v_{skin}{}^2}/_{E_{skin}}) + (1 - {}^{v_{sub}{}^2}/_{E_{sub}})$, where E_{skin}, v_{skin} and E_{sub}, v_{sub} are the Young's modulus and Poisson's ratio for the contact surface and the human skin respectively. Due to $E_{sub} >> E_{skin}$, the reduced Young's modulus is considered to be associated with the Young's modulus of the human skin (Johnson et al., 1993; Adams et al., 2007). With respect to the contribution of skin deformation to the skin friction, Greenwood and Tabor (Greenwood & Tabor, 1958) developed a model to estimate the friction force that arises from energy dissipated. The expression of deformation force is written in the following form:

$$F_{de} = \beta({}^{9}/_{128R})^{2/3}E^{-1/3}N^{4/3} \propto E^{-1/3}N^{4/3} \quad (4.4)$$

where β is the viscoelastic hysteresis loss fraction (Greenwood & Tabor, 1958; Adams et al., 2007). Combing the equations (4.2) and (4.3), the friction coefficient could be expressed as:

$$\mu \propto \begin{cases} E^{-\frac{2}{3}}N^{\frac{2}{3}} & \text{adhesion mechansim} \\ E^{-\frac{1}{3}}N^{\frac{4}{3}} & \text{deformation mechansim} \end{cases} \quad (4.5)$$

The friction coefficient is inversely proportional to the Young's modulus of the skin.

To measure the Young's modulus of skin, there are a number of tests that have been carried out *in-vivo* and *in-vitro*, which can be mainly classified into tensile tests, torsion tests, indentation and suction tests (Grahame, 1969; Sander, 1973; Agache, 1980; Bader & Bowker, 1983; Escoffier, 1989; Barel, 1995; Diridollar, 2000; Hendriks, 2005; Geerligs et al., 2011). For example, Oliver & Pharr (1992) proposed a method to investigate the global Young's modulus of skin using load-displacement sensing indentation tests. The global Young's modulus of skin can be calculated by the following equation:

$$E_{skin} = S\sqrt{\pi}\Big/_{2\sqrt{A}} \tag{4.6}$$

where A is the projected contact area. According to the equation (4.6), the corresponding Young's modulus is expected to increase with increasing stiffness. Some experiments were carried out by Geerligs et al. (2011) with a sapphire sphere with a radius of 500 μm at various thicknesses of the silicon rubber (in the range of 50 μm ~ 2 mm) under various loads. The experimental results show that the normal stiffness of the rubber decreases as the thickness of the rubber decreases. However, the Young's modulus was found to rise from 1.69 MPa to 3.67 MPa, which is not in accordance with Oliver & Pharr's model (1992). They explained that the difference between the experimental findings and theoretical prediction maybe because the artificial samples examined were too thin. In the current study, the skin thickness is shown to have an influence on the skin friction measured (see Figure 4.11). It can be clearly seen that the decrease in the thickness of samples decreases the corresponding friction coefficient. It was also found that the stiffness value reduces with increasing the thickness of the sample (see Table 4.2). These experimental results are in good agreement with the prediction of Equations (4.5) and (4.6). A stiffness of 6.31 N/mm was provided by the human finger which is larger than those of 8 mm and 6 mm thick artificial samples, hence a relatively larger value of friction coefficient is expected for the human finger. However, the corresponding data of friction coefficient measured for the human finger provided a minimum value. This could be due to the fact that the surfaces of these artificial fingers are smooth and cause larger contact areas than that of the human finger covered with ridges. Another possible reason for this, though, is the relatively strong adhesion on the surface of finger-pads contributing to the friction coefficient.

4.4 Experiment 4: Effects of Gender, Age and Ethnicity on Friction of Human Finger

4.4.1 Introduction

From previous studies on the skin friction coefficient, it is known that the friction coefficient varies with anatomical regions of a human body. It is generally considered that the skin friction coefficient on hands, forearms and feet are higher than those on the abdomen, legs and back (Cua et al., 1990; Zhang & Mak, 1999;

Sivamani et al., 2003; Derler et al., 2009; Hendriks & Franklin, 2010; Zhu et al., 2011). The skin friction coefficient also appears to be associated with gender, age and ethnicity. For example, Zhu et al. (2011) reported that the skin friction coefficient varies with gender as some differences in the friction coefficient were found on the canthus and the dorsal hand between females and males. For the influence of age on the skin friction coefficient, Elsner et al. (1999) observed that the friction coefficients on the forearm (or volar) for younger women was higher compared to that for old women. Numerous studies related to gender, age and ethnicity on skin friction coefficient have been conducted, however, few studies have addressed human fingers particularly. For a better understanding towards the frictional behaviour of human fingers, this section studies how the friction coefficient of human fingers is altered with gender, age and ethnicity.

4.4.2 Experimental Procedure

Twenty-one Asian volunteers (16 females and 5 males) and thirty-one western volunteers (16 females and 15 males) were invited to participate in this study, aged between 19 to 80 years. The tests were performed on the index fingers of their dominant hands using the multi-axis force plate. Each volunteer was requested to apply 5 different normal loads (in the range of 2 to 25 N) in order to allow calculation of the friction coefficient (from the gradient). Finally a demographic survey was completed, including age, gender and ethnicity.

4.4.3 Results and Discussion

Table 4.3 summarises the friction coefficient data that was collected from the dominant index fingers of volunteers. The friction measurement results were assessed with respect to gender, age and ethnicity, individually. Figure 4.12 shows a scatter plot of the friction coefficient for all participants aged between 19-24 years. The analysis of data was divided into parts, gender and ethnicity. There is no significant difference found in the friction coefficient with regard to gender for both Asian and Westerns. The friction coefficient is also unlikely to be affected by ethnicity. The investigation of the effect of age on the skin friction coefficient for fingers was done on western males. As shown in Figure 4.13, the skin friction

coefficient increases with age up to 40 years. There is a big reduction in the skin friction coefficient for volunteers over 60 years of age.

Table 4.3 Friction coefficient data for the index fingers of all participants.

	Asian				Western			
Age	**Female**	**SD**	**Male**	**SD**	**Female**	**SD**	**Male**	**SD**
19-24	0.70	0.43	0.76	0.36	0.76	0.58	0.65	0.21
25-30	0.67	0.74					1.63	0.50
30-40			1.57				1.72	0.93
60+					0.40	0.17	0.57	0.26

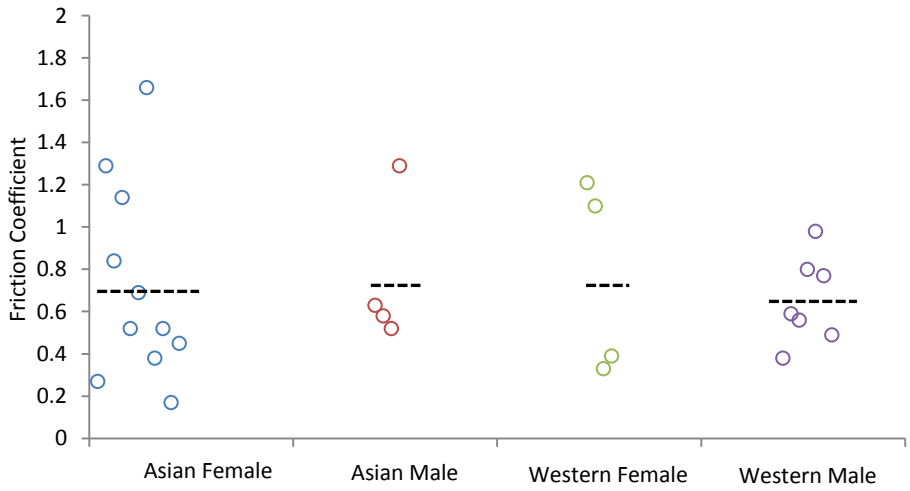

Figure 4.12: A scatter plot shows the friction coefficient for all participants aged between 19-24 years, the means for each group are indicated by horizontal lines (find the values and SD in Table 4.3)

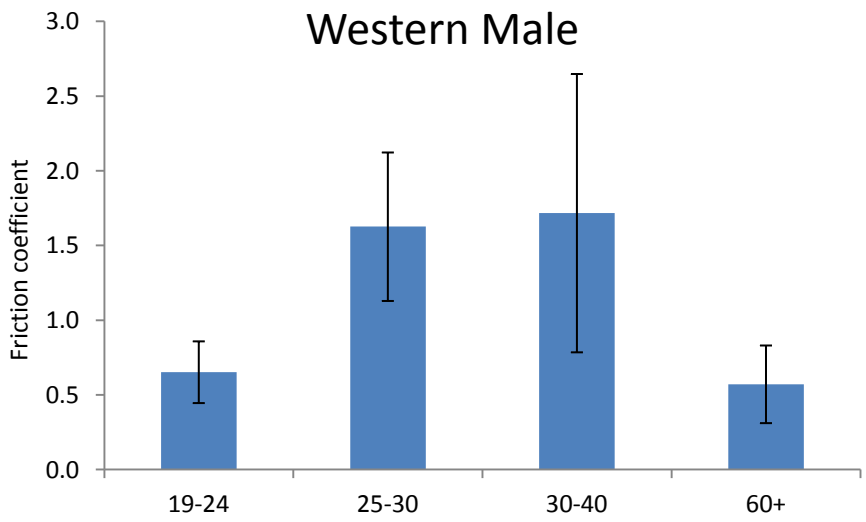

Figure 4.13: The effect of age on the friction coefficient for western male volunteers.

The results of above experiments indicate that skin friction coefficient is independent of ethnicity and gender. A similar conclusion was also drawn by Sivamani et al. (2003) who examined the influences of age, gender and ethnicity on the skin friction at volar foearm using a UMT Series Micro-Tribometer (UMT). In addition, Cua et al. (1990) reported no significant gender-related difference in skin friction for various anatomical regions of the body. However, Tomlinson, et al. (2009) observed a different phenomenon. In their studies, the average friction coefficient in 32 volunteers with three different materials were measured and compared. In the case of glass and rugby ball rubber, they found that the skin friction coefficients in males were slightly higher than in age-matched females. However, there was no reason given to explain the difference. In recent studies, Zhu et al. (2011) conducted a study of characterization of skin frictional properties in a normal Chinese population. Experimental results of comparison of skin friction coefficient between males and females indicated that females aged 31-40 years have relatively high values of the skin friction coefficient than that of age-matched males. They attributed this difference to the fact that females have higher estrogen levels since estrogen replacement can change skin biophysical properties in female aged around 30 years (Hall & Phillips, 2005, Man et al., 2009, Xin et al., 2010). Furthermore, there are many other possibilities that could cause the difference. For example, in general, it is believed that a male's hand has thick stratum corneum and is relatively stiffer than that of female. Therefore, it can be assumed that the male's skin has a high Young's modulus according to the model of Equation (4.6). A lower friction coefficient is expected for a skin with a higher Young's modulus. The other possible reason could be attributed to the different size of finger-pads and skin moisture level difference.

As expected, the effect of age on the skin friction coefficient for human fingers is significant. It is observed that the skin friction coefficient for fingers in males increases from 0.65 to 1.72 as the age increases from 19~24 years to 30~40 years. For the group of 60+ years, the skin friction coefficient reduced to be only one third of those aged 30~40 years. A similar conclusion was also drawn by Zhu et al. (2011), who investigated the skin friction coefficient at three different anatomical sites of body using a large Chinese sampling population. The results of their experiments show that the skin friction coefficient for a dorsal hand shows a gradually increasing trend with age increase from 0 to 40 years in males. Moreover, there are maximum

friction coefficients observed on the canthus and the forehead of females around 40 years old. These observations are reasonable because the skin friction coefficient is strongly associated with skin structure.

With increasing age, the mount of collagen in skin gradually reduces, which results in a decrease in the thickness of skin (Shuster et al., 1975). This observation agrees with other studies (Escoffier et al., 1980; Takema et al., 1994; Gniadecka & Jemec, 1998). In the recent studies on skin dynamic properties, the results of indentation tests show that the elasticity of skin was 10.7 ± 2.64 kPa for the youngest group, which is relatively high than those in the oldest group (7.17 ± 2.06 kPa) (Zahouani et al., 2011). However, a different phenomenon was reported by Diridollou et al. (2001), who found the thickness of skin on the forearm increases as a function of age up to 60 years. There was a significant decrease after 60 years. In their studies, a suction technique has been applied to measure the Young's modulus of skin. The experimental results showed that the Young's modulus of skin in older groups is higher than young groups. These differences between the above studies may be attributed to the difference in the anatomical sites and measuring techniques used. Consequently, we could predict that the corresponding Young's modulus of skin would increase with increasing age leading to a relatively high value of skin friction coefficient in old subjects according to Equation (4.6). However, the assumption is not applicable for those subjects aged over 60 year. For the 60+ group, it is limited to use the thickness of skin as a guide to the change in the friction coefficient since there are some other factors involved. Cua et al. (1990, 1995) indicated that low levels of the capacitance, trans-epidermal water loss and lipid content contribute to a low friction coefficient in elderly people (aged between 72 and 77 years) compared to that in young people (aged between 23 and 29 years). Additionally, these changes in the Young's modulus of skin are unlikely in accordance with the model of Oliver & Pharr (1992). This might be due to that the standard Oliver and Pharr's model is limited for soft materials with viscoelastic behaviour (i.e. human skin).

4.5 Conclusions

The studies conducted in this chapter revealed that the multi-axis force plate is the most suitable device for the measurement of the skin friction coefficient in our research. The relationship between the skin friction coefficient and the normal load

was also initially assessed. It was found that, under the high load conditions (>2.5 N), the skin friction coefficient tends to be independent on the normal load, as a constant. On the other hand, a power-law relationship was suggested to describe the skin frictional behaviour of fingers at low load conditions. The friction tests using artificial fingers simulated potential correlation between the skin friction coefficient and the mechanical properties of skin. In the end, the skin friction coefficient was shown to vary with gender, age and ethnicity. More details about the mechanisms behind the phenomena observed will be further discussed in Chapter 5.

Chapter 5

The Contribution of Skin Structure to Skin Friction

The frictional behaviour of human skin is not only determined by the complex interplay of materials, but also the properties of skin (Derler et al., 2009). The current knowledge on the tribology of the skin mainly focuses on skin in touch with various materials, however, little is known about the effect of skin properties on friction. It is important to characterise this, as it may help explain the wide spread of friction data among test candidates (see Chapter 4) under nominally similar test conditions. This chapter focuses on the investigation of skin structure on skin friction. To achieve it, an AMTI multi-axis force plate combined with an Optical Coherence Tomography (OCT) system were used in experiments. In this chapter, the friction behaviour has been assessed via the following work: firstly, investigating the potential relationship between skin structural properties (i.e. the thickness of stratum corneum and the number of sweat glands) and skin friction using the OCT system; secondly, measuring skin physical parameters using the "*cutometer*" MPA 580 and studying how the friction coefficient was altered by these parameters.

5.1 Experiment 1: Evaluating the Impact of Various Skin Properties on Skin Friction

5.1.1 Introduction

The aim of this test was to explain the wide spread of the friction data among test candidates by investigating some structure parameters of the skin on their dominant index fingers, such as the thickness of the stratum corneum (SC), skin hydration and number of sweat ducts (related OCT image analysis has been discussed in Chapter 3). The measurements were carried out under normal laboratory conditions and at a

room temperature of 24°C and a relative humidity of 58%. Seven white male volunteers were invited to participate in this study, aged between 22 to 29 years. Volunteers were requested to wash their hands and dry them using a paper towel, prior to the test. The tests were performed on the index fingers of their dominant hands. Firstly images of their fingers were taken using the OCT system. During image scanning, volunteers were guided to place their fingers on a work plate and facing the lens of OCT. The work plate was attached to mechanical stages for adjusting the distance between fingers and lens. In order to obtain the average value of the thickness of the stratum corneum, the examined finger pads have to be fixed in position to ensure images were taken in the same position. The levels of moisture in the skin were recorded in "arbitrary units" (AU) using a "Moist Sense" Device (Moritex USA).

5.1.2 Results and Discussion

The skin and friction related parameters, including the mean value of dynamic friction coefficient, number of sweat ducts (SD) in an area of 1 cm^2, the stratum corneum (SC) thickness from all seven participants are shown in Table 5.1. It is observed that the number of sweat ducts varies widely between participants. Similarly, the measurement of stratum corneum thickness shows a variation between participants. The values of friction coefficient ranging from 0.2 to 0.58 were obtained in the friction measurements for all participants. There is no significant difference in moisture level of skin from participant 1 to participant 5; participants 6 and 7 show relatively low values.

Table 5.1 Skin and friction data for seven human participants.

Participant	**Age**	**Sweat ducts (in cm^2)**	**Moisture level (± 2 AU)**	**Thickness of SC (μm)**	**Speed (mm/s)**	**Friction Coefficient (> 2 N)**
1	23	940	90	370	12.8	0.38
2	24	470	89	640	24.8	0.59
3	25	310	94	440	27.9	1.25
4	26	470	96	210	16.0	1.44
5	29	780	95	320	23.6	2.19
6	24	470	60	320	19.7	0.56
7	22	1090	72	530	10.1	0.80

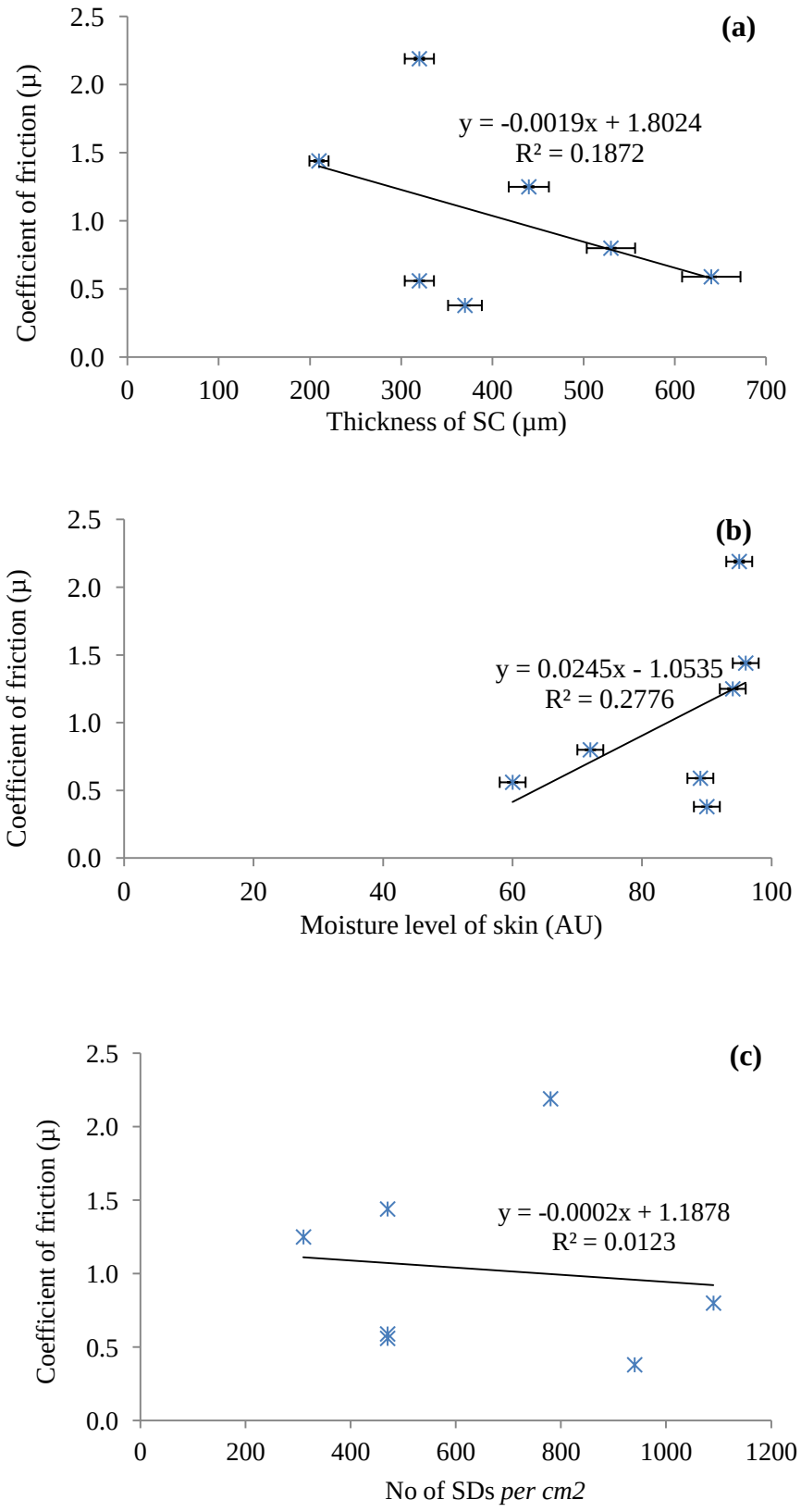

Figure 5.1: The relations between (a) the thickness of the stratum corneum and the corresponding coefficient of friction measured, (b) the coefficient of friction and the moisture level of the skin and (c) the coefficient of friction and the number of sweat glands in a cm^2 area (moisture level of skin error ± 2 au (Tomlinson et al., 2010), friction coefficient error 0.4% and thickness of stratum corneum SD 6%).

Based on previous studies, it was expected that the thickness of the different skin layers could be one of the key factors affecting the skin mechanical properties (Hendriks, 2005; Geerligs et al., 2011; Agache et al., 1980; Alexander & Cook, 1976; Bader & Bowker, 1983; Barel et al., 1995; Diridollou et al., 2000; Escoffier et al., 1989; Grahame, 1969; Sanders, 1973). The human skin is a multi-layer tissue consisting of epidermis and dermis, each of which is endowed with different mechanical properties. When subjected to an external force, the skin generally works as a whole (Tomlinson et al., 2009). However, in this study, concentration was placed on the influence of the stratum corneum on skin friction with consideration of the related changes in the Young's modulus.

Pailler-Mattei et al. (2007) found that the normal stiffness of the skin and the global Young's modulus seem not to be affected by the reduction of the stratum corneum thickness. This could be explained by the fact that the thickness of the stratum corneum removed was too small (up to 6 μm). However, the lateral stiffness of the skin was found to be reduced when the thickness of the stratum corneum was reduced by tape stripping. The friction coefficient decreased as a function of the thickness of the stratum corneum, which matched well to that of the lateral stiffness with respect to the removal of the thickness of the stratum corneum when the first micron of stratum corneum was removed. However, no details were given to explain what exactly was causing the effect. The research performed by Geerligs et al. (2011) with a sapphire sphere on various thicknesses of the silicon rubber, revealed that normal stiffness of the silicon rubber reduces with increasing the thickness of the silicon rubber from 50 μm to 2 mm. The Young's modulus of the silicon rubber was shown to decrease with increasing the thickness of the silicon rubber respectively, which indicates that the friction coefficient of the silicon rubber should increase with the silicon rubber thickness. On the basis of this experimental finding, it can be assumed that the both normal and lateral stiffness of the thick stratum corneum are smaller than those of the relatively thin stratum corneum. Therefore, the Young's modulus of the skin is expected to decrease with increasing the thickness of the stratum corneum, leading to a corresponding increase in the friction coefficient of the skin. However, Figure 5.1(a) shows a different phenomenon that was not expected, where no direct relationship is found between the friction coefficient and the thickness of stratum corneum. This phenomenon may be due to the fact that there are

too many factors influencing the measurement of skin friction such as skin moisture level, participants' age, gender and sliding speed, etc., the influence of the thickness of the stratum corneum on skin friction is difficult to be analysed individually.

Naturally, human skin has an adhesive behaviour due to the hydrolipidic film produced by the sebaceous glands present on the skin surface (Pailler-Mattei et al., 2004). This secretion is not only to destroy bacteria on skin, but also to help maintain skin hydration. For dry and smooth surfaces, the friction force of skin was considered to be dominated by the adhesion force, so the moisture level of skin is another factor needed to be assessed. In Figure 5.1(b), the coefficient of friction shows an increasing trend when the moisture level increases, in which the peak value of friction coefficient found is around 95 AU. Similar research has been done by Tomlinson et al. (2010), who carried out a survey to look at how moisture varied between people. They found that the moisture level of the skin varies from person to person (in the range of 40 to 99 + AU) and is very sensitive to the environmental conditions. However, due to the limitation of their study, the friction coefficient of the skin versus natural moisture level was not investigated. The results of their further research indicated that the friction coefficient of skin increased significantly when artificially increasing the moisture level by wetting the fingers (Tomlinson et al., 2010).

Since sweat is one of the main components of the surface film that helps skin maintain dampness (Wood & Bladon, 1985), studying the number of sweat glands may be a very useful way for predicting the hydration of the skin. In this study, the number of sweat glands per cm^2 was found to be between 300 and 1000, which were slightly higher compared with those results from Juniper & Dykman (1967) and Dinc et al. (1991). The number of sweat glands was evaluated by Juniper, et al. using a microscope and ranged from 200 to 400 per cm^2 (Juniper & Dykman, 1967). In the study of Dinc et al. (1991), he used the same OCT method as that described here to help count the number of sweat glands. The density of sweat glands was around 150 to 350 per cm^2. Therefore, the result in the study was considered as reliable data, in a reasonable range for participants with varying age, sex and ethnicity. However, the contribution of the number of sweat glands to the moisture level is not significant since no correlation is found between them, (see Table 5.1). This is due to the fact

that the skin hydration level is determined by not only the perspiration of the skin, but also the hydration level of the skin layer. The number of sweat glands seems to have little effect on the skin moisture level in its natural state. The inter-individual differences of the 7 volunteers could be another possibility for what causes the phenomenon. In the case that skin is being hydrated with perspiration, this assumption will no longer hold since much sweat is secreted by sweat glands and acts as a lubrication layer on the surface of skin. It could be assumed that the magnitude of friction coefficient of skin will reduce as the number of sweat glands increases, during significant perspiration. Additionally, the measurement of skin hydration also can be achieved by monitoring the transepidermal water loss (TEWL) that is directly related to its barrier function. Cua et al. (1990) suggested that the skin friction strongly depends on skin hydration in most regions of the body. The contribution of TEWL to skin friction was observed only in the palm and tight. The results of the study by LodeÂn et al. (1992) indicated that the TWEL tends to increase with increasing the capacitance in some area of normal skin. However, there was no correlation between the TEWL and the friction in both atopic and control group.

5.2 Experiment 2: Detailed Analysis of the Influence of Mechanical and Structural Properties on Skin Friction

5.2.1 Introduction

As observed above, the skin friction coefficient widely varies from person to person, which could be attributed to various skin parameters as well as some human factors. It brings challenge to investigating the relationship between each individual structural parameter (e.g. the thickness of the SC, the moisture level of skin) and skin friction. In order to avoid the influences of human factors on skin friction, such as, age, sex, etc., and mainly focusing on one structural parameter, this test was designed based on one participant. The measurements of skin mechanical properties using the "*cutometer*" MPA 580 were carried out by a PhD student (Daniel Gad) at Philips Applied Technologies, under my supervision.

5.2.2 Experimental Procedures

Measuring Skin Physical Parameters and Friction

Studies of how the skin friction coefficient differs with various regions of body were done by two series of tests. The first series of tests looked at the mechanical properties of the skin. This test was done with the right hand of participant 1 in a normal lab condition, where all five fingers and palm were examined. The hand was not treated by any chemical or cosmetic products in the 12 hours prior to the measurement. The measurements were performed using the time-strain mode that can be used to estimate the viscoelastic properties of the skin. A 2 *mm* diameter measuring probe was used, which applied a constant pressure of 500 mbar to the skin.

In the second series of tests the friction coefficient and some physical parameters of the skin were measured on the right hand of participant 2, with the same positions as examined in above mechanical tests. With respect to the friction test, the top of the force plate was covered with a 5 *mm* wide acetal bar that is less than a finger-pad width, so that all fingers can experience the same contact area under a certain load, since the contact area is one of the key factors influencing the skin friction. As observed in Chapter 4, when a low load (< 2 N) was applied to the skin, the surface properties of the skin dominate the skin friction. Therefore, this test was done in both low load (< 2 N) and high load (> 2 N) conditions to examine the effect of the skin mechanical properties on the skin friction, individually.

The Effect of the Superficial Sebum/Sweat on Skin Friction

As discussed earlier, a thin hydrolipid film covers the surface of skin, which not only helps maintain the skin in good condition, but also influences some of its physic-chemical properties. To investigate the influence of the hydrolipid film on skin friction, a simple test was designed, named the tape stripping test. This test was carried out on the left index fingers of two participants. An adhesive tape was adhered to the finger-pad and peeled off after a few seconds. After that, images of the finger-pad using the OCT system were taken and then begin the friction measurements were carried out using the force plate.

The Effect of the Thickness of Stratum Corneum on Skin Friction

The aim of this test was to examine the effect of the SC thickness on skin friction, since the skin thickness was found to be associated with some mechanical properties of the skin (e.g. distensibility). To do this a simple rubbing test was designed and carried out on the right middle finger of the two participants. A sheet of fine grade sandpaper was used to rub the surface of finger-pads, causing some skin tissue to be removed and hence reduce the thickness of the SC. OCT was used to take images of the finger-pads to determine startum corneum thickness.

5.2.3 Results

Measuring Skin Physical Parameters and Friction

The cutometer and OCT results for the first series of tests are given in Table 5.2, which shows some deformation parameters (e.g. skin distensibility, elasticity, viscosity) with respect to the examined regions of hand, as well as the thickness of the SC from OCT. The distensibility of the skin (*R0*) was found to be strongly dependent on the thickness of the skin. There were no significant relationships found between the thickness of the SC and other biological ratios, however.

Table 5.2 Cutometer deformation parameters and the thickness of stratum corneum for different regions of hand.

Region of Hand	***R0* (±SD)**	***R2* (±SD)**	***R5* (±SD)**	***R7*(±SD)**	**Thickness of SC (*mm*)**
Thumb-pad	0.166±0.012	0.727±0.070	0.375±0.085	0.235±0.032	0.21
Index Finger-pad	0.157±0.008	0.748±0.040	0.368±0.033	0.248±0.027	0.20
Middle Finger-pad	0.165±0.011	0.697±0.042	0.360±0.074	0.246±0.043	0.20
Ring Finger-pad	0.149±0.007	0.705±0.047	0.390±0.024	0.254±0.015	0.18
Little Finger-pad	0.142±0.012	0.691±0.023	0.439±0.083	0.281±0.032	0.16
Palm	0.078±0.002	0.725±0.049	0.696±0.073	0.336±0.037	0.13

R0: the skin distensibility (U_f), R2: gross elasticity of the skin (U_a/ U_f), R5: pure elasticity of the skin (U_r/ U_e) and R7: biological elasticity of the skin (U_r/ U_f).

Table 5.3 displays some corresponding data of physical parameters measured from all five finger-pads and the palm, as well as the friction coefficients at different load conditions. The moisture levels among all positions examined were very similar in the range of 39~42 AU, except for the ring finger which had a slightly higher reading. This was expected since all fingers and palm examined were taken from in the same hand of one participant, so they should have similar temperature and moisture levels under the same body conditions. It was also observed that the thickness of the SC varies among fingers. The thumb and index finger have relatively thick SC compared with other regions which are twice as thick as those of the palm. This difference may be due to these fingers being nvolved in human daily activities frequently, thick SC could help prevent skin from damage or injury.

The measurable roughness of the skin was reported to range from 7 to 30 with respect to different regions of the hand. As expected, there was no significant difference among them except for the thumb which compared well with the data in Childs et al. (2006). Most tested regions of the hand have similar frictional behaviours, particularly when they experienced high loads (> 2 N). In this case, except the thumb and the ring finger, the magnitudes of the friction coefficient are around 0.34. At the low load condition, the friction coefficient showed a higher variability among those tested regions compared with that at high load condition, ranging from 0.30 for the palm to 0.42 for the ring finger.

Table 5.3 Skin surface properties and friction coefficients for different regions of hand.

Region of Hand	**Moistsense (± 2 AU)**	**Thickness of SC (*mm*)**	**Roughness (*μm*)**	**CoF (*N* = 1 N)**	**CoF (*N* > 2 N)**
Thumb-pad	40	0.61	10-30	0.37	0.40
Index Finger-pad	42	0.63	9.5-16	0.32	0.34
Middle Finger-pad	41	0.54	10-16.5	0.35	0.35
Ring Finger-pad	44	0.45	7-13.4	0.42	0.43
Little Finger-pad	39	0.48	8-15	0.33	0.35
Palm	42	0.27	7-14	0.30	0.34

The Effect of Superficial Sebum/Sweat on Skin Friction

Figure 5.2 (I) shows OCT images obtained from the tested finger-pad of participant 1 after the tape stripping. The corresponding changes in the structural properties were quantified and plotted as described in Figure 5.2 (II), (III) and (IV). As can be seen in Figure 5.2 (II), there was a slight reduction on the thickness of the stratum corneum (approximate 10 μm) in the first 5 tape strippings, resulting from some dead cells (horny substance) and sebum film/sweat being removed. After that, the thickness of the SC finally reached a plateau for the rest of the stripping. Unfortunately, those changes were too small to be viewed by naked eyes in the obtained OCT images. Figure 5.2 (III) shows some corresponding changes occurred on the moisture level of the skin after remove of the sebum film on the skin surface. This phenomenon displays as a curve and could be explained using two phases. In the first phase, the "moistsense" reading was found to drop slightly within the first 6 strippings, after that it increases to reach a constant value (65 AU) in the second phase. Figure 5.2 (IV) displays the friction force against the number of strippings, in which the friction force was observed to dramatically increase when 10 μm of the SC was removed, see figure 5.2 (V).

In the case of the female, similar phenomena were found in the thickness of the stratum corneum, moisture level of the skin (see Figure 5.3), which helped to confirm the assumption that only surface sebum and little dead cells were being removed by tape stripping. The corresponding results of the friction force shown in Figure 5.3 (IV) present a different trend compared to the case of the participant 1 though. There was a slight drop of 2% in the friction force with 8 tape strippings, after that, the friction force was found to rise to 0.36. Moreover, it can be seen that the moisture level of participant 2 was relatively low compared in participant 1. This may be why the changes in the friction force was not significant in participant 2. A linear relationship between the friction force and skin moisture level was also observed in participant 2 (Figure 5.3 (V)).

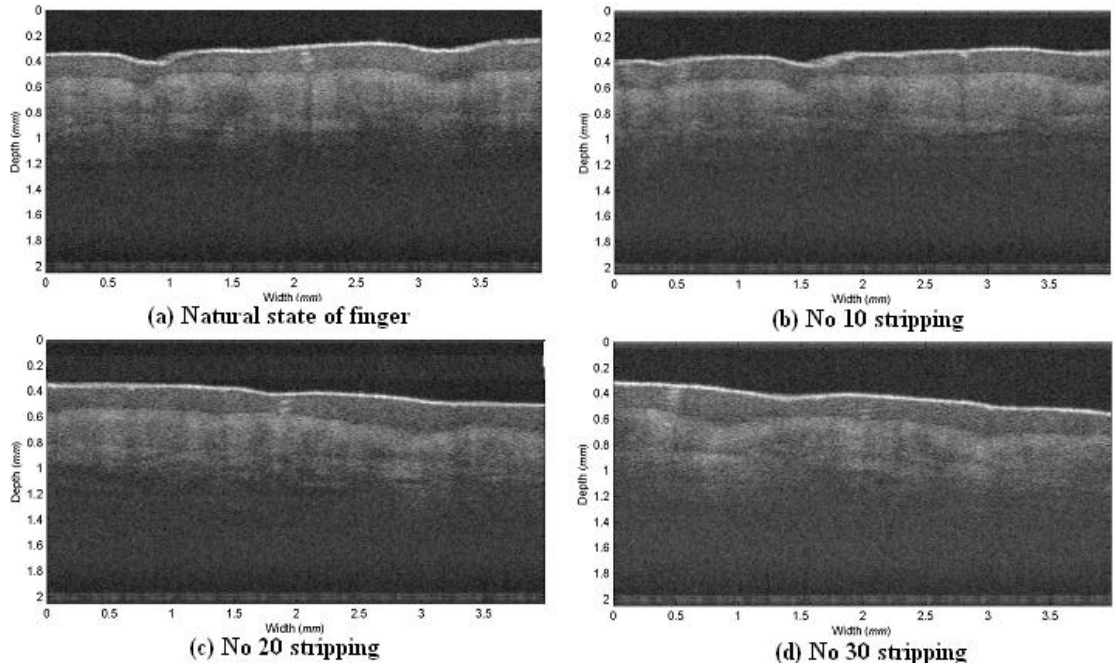

(I)

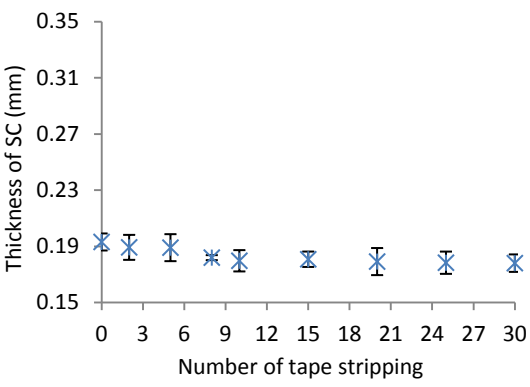

(II)

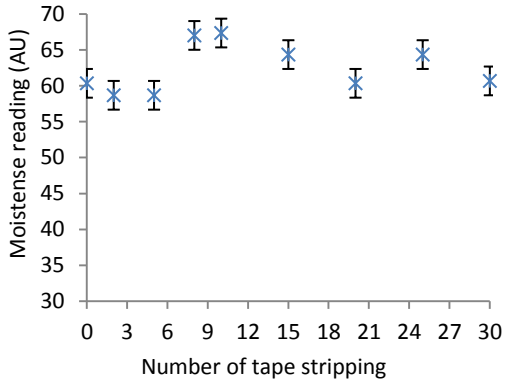

(III)

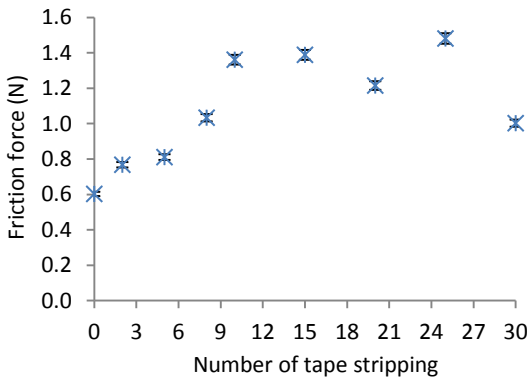

(IV)

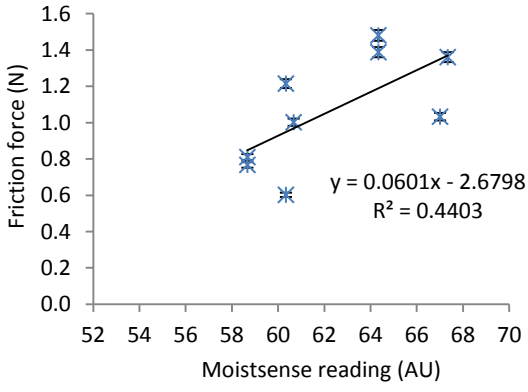

(V)

Figure 5.2: (I) OCT images of the skin of the index finger-pad of participant 1 were taken with various numbers of tape stripping; plots of the corresponding changes in the thickness of the stratun corneum (II), moistsense reading (III) and friction force (IV), as well as the relationship between the friction force and the moistsense reading (V).

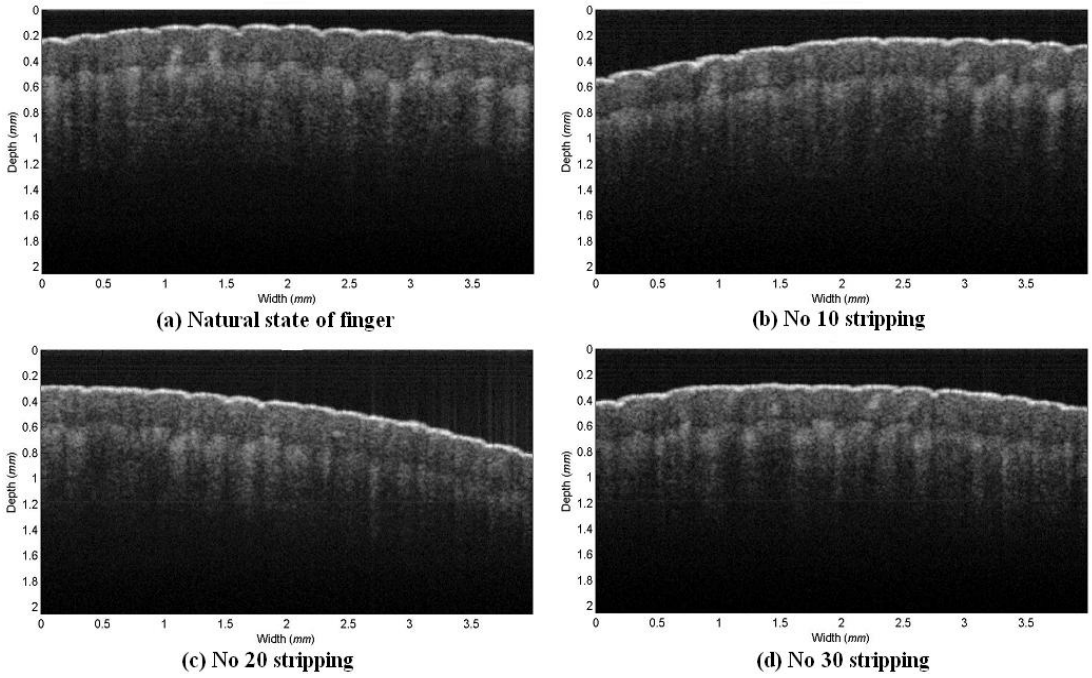

(I)

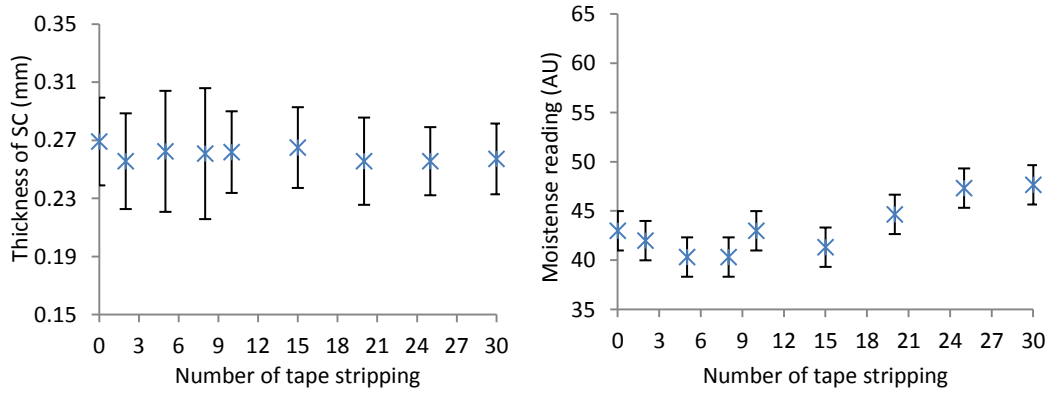

(II) **(III)**

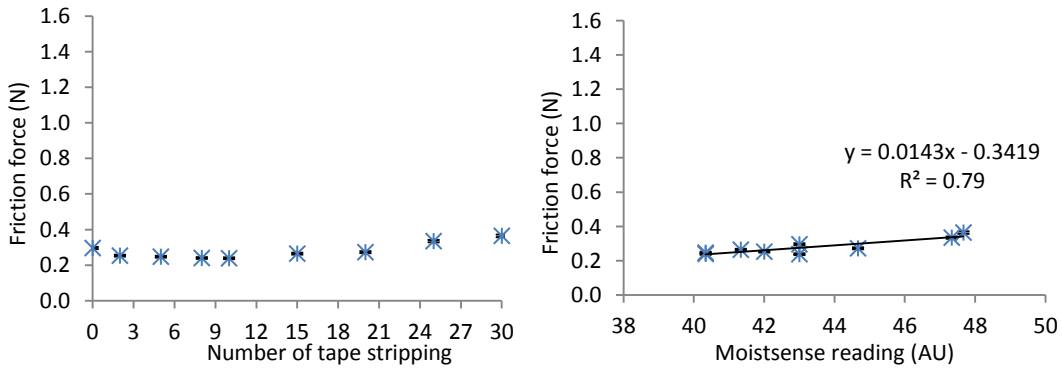

(V) **(IV)**

Figure 5.3: (I) OCT images of the skin of the index finger-pad of participant 2 were taken with various numbers of tape stripping; plots of the corresponding changes in the thickness of the stratun corneum (II), moistsense reading (III) and friction force (IV), as well as the relationship between the friction force and the moistsense reading (V).

Figure 5.4 (a) shows that for the measurements of elasticity of the skin in participant 1, as seen in results, there is no significant change in the elasticity of the skin with the tape stripping, as well as the normal stiffness of the skin (Figure 5.4 (b)). The general trends in both figures appear to be approximately constant when considering the error bar for each point; consequently, it can be assumed that the change of skin surface properties related to the tape stripping do not affect its elasticity and normal stiffness.

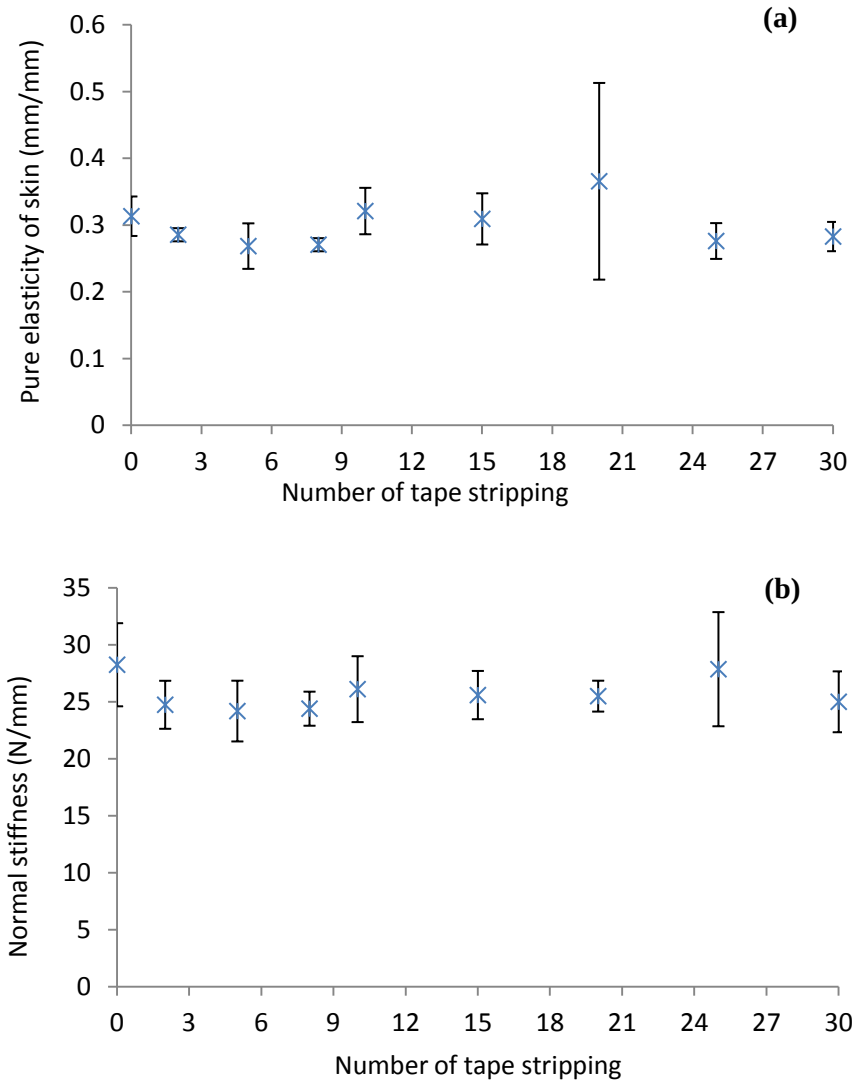

Figure 5.4: Changes in pure elasticity and normal stiffness of the skin at the finger-pad of participant 1 for various numbers of tape strippings.

The Effect of the Thickness of Stratum Corneum on Skin Friction

The results refering to the influence of the skin rubbing on the thickness of the stratum corneum, the "moistsense" reading and the friction force are summarized in Figure 5.5 (participant 1) and 5.6 (participant 2). It is clear to see that the thickness of the SC significantly decreases (approximate 0.03 *mm* in the male and 0.06 *mm* in the female) when the finger-pad is rubbed by sand paper, particularly in first 6 skin rubbings (see Figure 5.5 (II) and Figure 5.6 (II)). There was no further decrease with increasing the number of skin rubbings from 8 to 12, the reason may lie in the fact that the sandpaper was fully covered with skin tissue after being used for a period of time and relatively less tissue was removed. In the OCT images (Figure 5.5 (I) and Figure 5.6 (I)), the layer of the SC is clearly showed and corresponding changes in the thickness with various numbers of rubbings is easily observed by naked eyes, which will help validate the data obtained. While it was also found that the skin in both subjects gradually becomes relatively smooth. This was attributed to the fact that the ridges on the skin surface were worn down by the sand paper. The moisture level of the natural skin in participant 2 (approximate 36 AU) was lower than half of the moisture level in participant 1 (approximate 91 AU). Furthermore, Figure 5.5 (III) shows that the "moistsense" reading in the male decreases slightly in the beginning, after that it gives a successive increase (from 90 AU to 94 AU) with skin rubbing. However, the corresponding results in the female were found to not follow the same trend. As increasing the number of skin rubbings, the "moistsense" reading increased from 36 AU to 47 AU and decreased to 44 AU. In the friction measurements, the friction forces were displayed as a function of the number of skin rubbings, which are very similar with those of the skin thickness. The friction force was observed to drop by 29% in participant 1 and 34% in participant 2, respectively. For example, as can be seen in Figure 5.5 (III), the friction force was 3.5 N for the natural skin and reduced to 2.3 N after 6 rubbings with the same normal load applied to the skin. The investigations of the relationship between friction force and thickness of the stratum cornem indicate that the friction force was dependent on the thickness of the stratum cornem as all data points were fitted into linear regression lines (see Figure 5.3 (V) and Figure 5.4 (V)). However, the normal stiffness of the skin seems not to be effected by the number of skin rubbings according to the results in Figure 5.7.

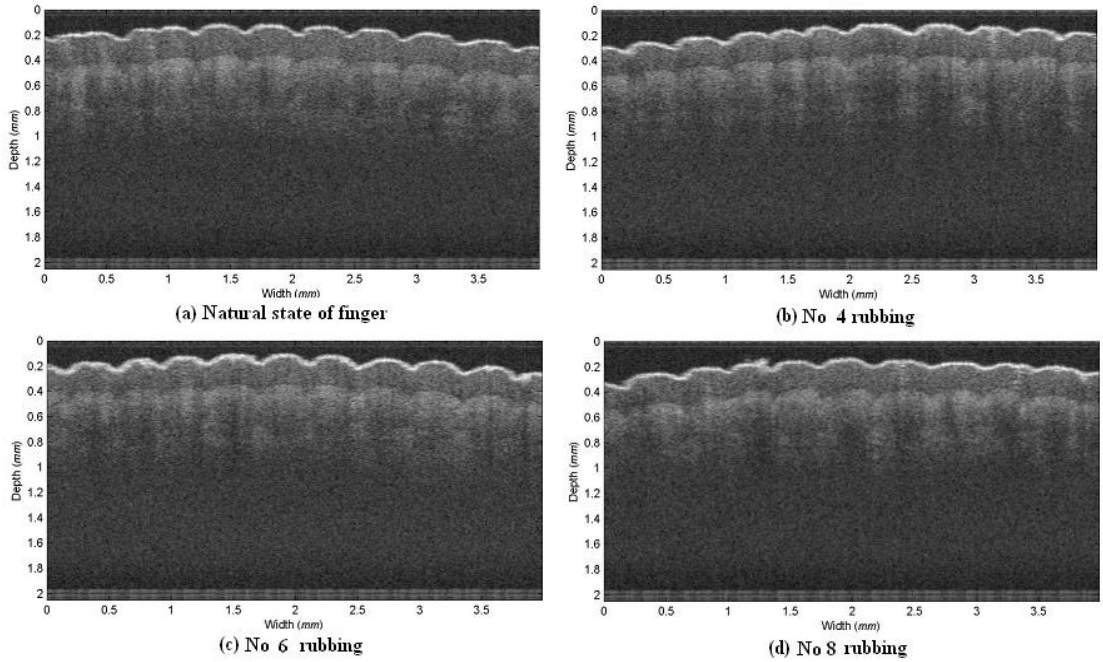

(I)

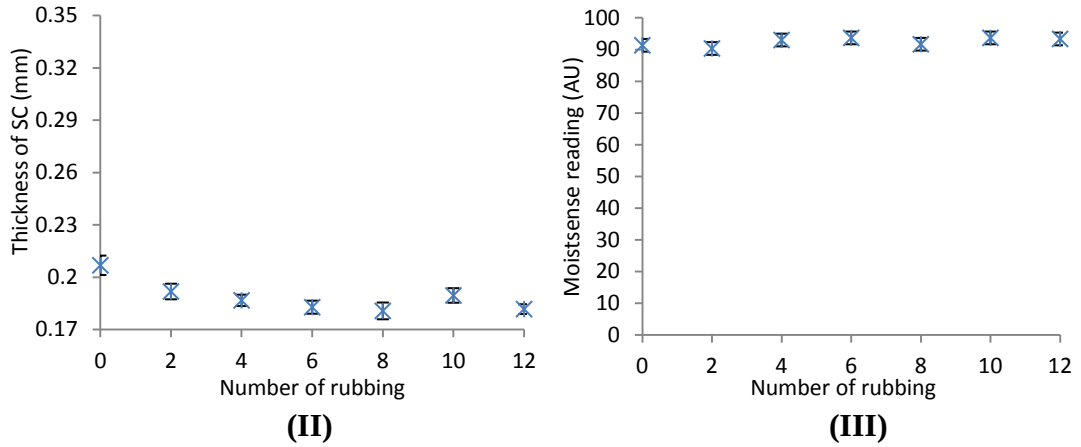

(II) **(III)**

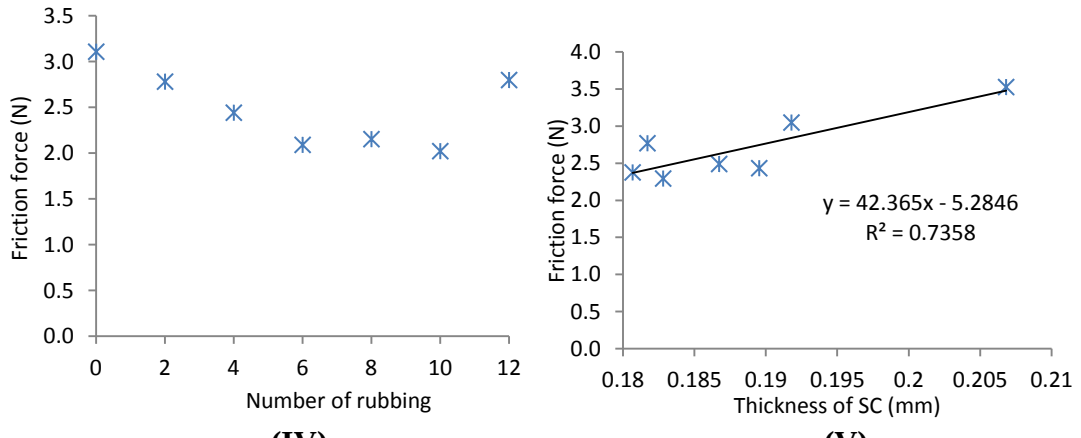

(IV) **(V)**

Figure 5.5: (I) OCT images of the skin of the middle finger-pad of participant 1 were taken with various numbers of skin rubbing; plots of the corresponding changes in the thickness of the stratun corneum (II), moistsense reading (III) and friction force (IV), as well as the relationship between the friction force and the moistsense reading (V).

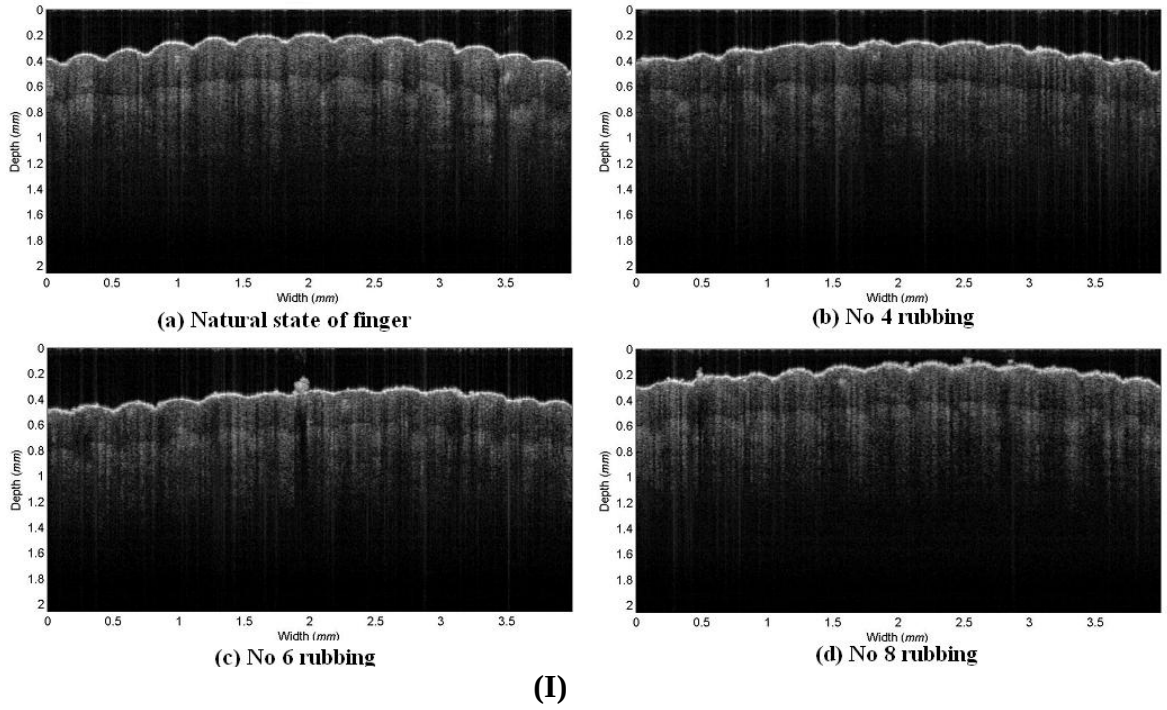

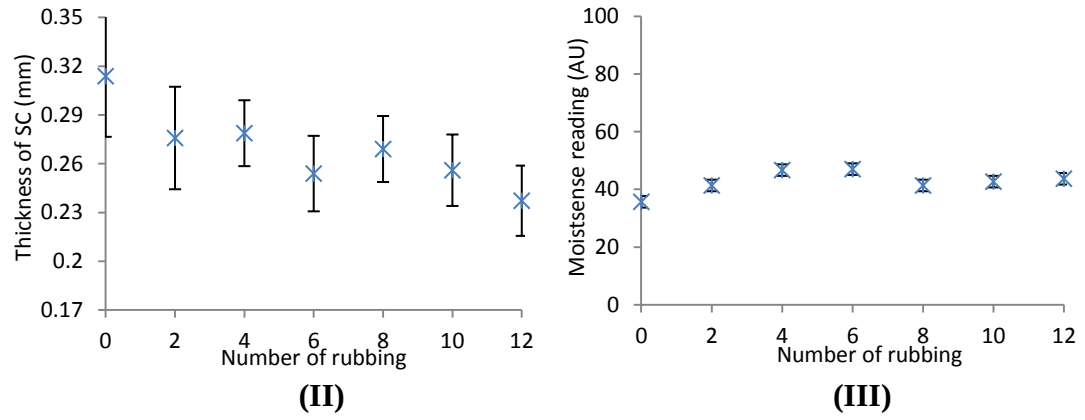

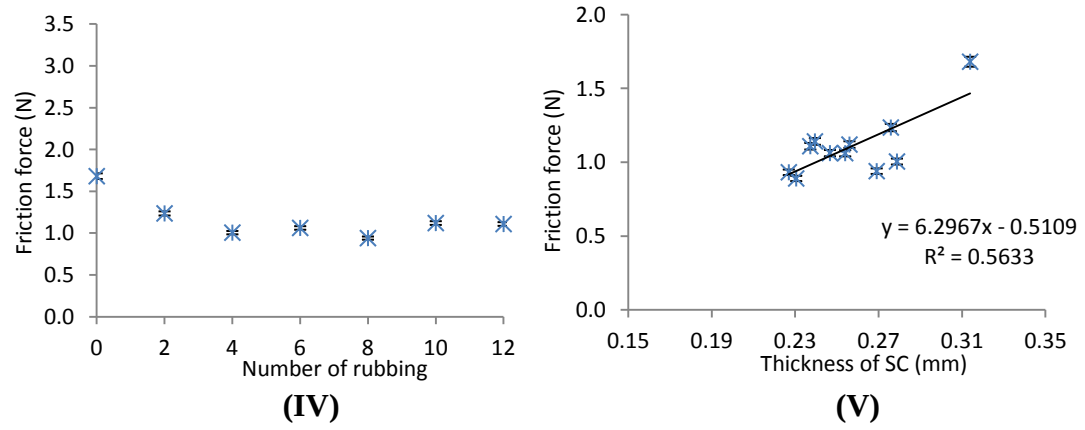

Figure 5.6: (I) OCT images of the skin of the middle finger-pad of participant 2 were taken with various numbers of skin rubbing; plots of the corresponding changes in the thickness of the stratun corneum (II), moistsense reading (III) and friction force (IV), as well as the relationship between the friction force and the moistsense reading (V).

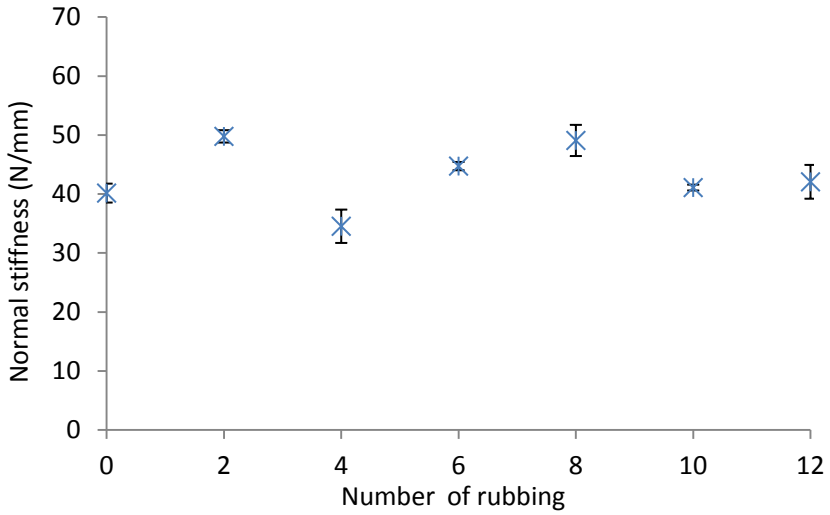

Figure 5.7: The change in normal stiffness of the skin at the finger-pad of Participant 1 with skin rubbing.

5.2.4 Discussion

Scherge & Gorb (2001) suggested that the impact of surface properties dominates their friction forces at low force condition (< 1 N). In order to understand how skin friction alters with its surface properties, some parameters of the skin properties have been assessed in this study, including skin roughness, skin hydration, the thickness of the SC. As can be seen in Table 5.3, the skin friction widely varied between anatomic regions tested with low load, compared with that at high load condition. This could be explained by the fact that, under low load condition, almost all skin parameters make contributions to the skin friction and lead to a large variety. However, only few factors affect the skin friction under the higher load conditions. By analysing all parameters, it was found that the skin hydration makes a great impact on the skin friction at low and high load conditions. For example, by comparing the friction coefficient between the ring finger and the little finger, it was noticed that the ring finger has a higher value than that of the little finger, due to both of them have similar thickness of the SC and surface roughness, therefore it can be assumed that there is a potential relationship between the moisture level of the skin and the skin friction.

In both tape stripping and skin rubbing tests, the "moistsense" readings of the skin show an initial decrease and then increase with removal of the superficial serum and the skin tissue. Leveque (2005) and Pailler Matteri et al. (2007) reported that human

skin has a gradient of material properties across different layers. A water gradient exists through skin layers, which can be attributed to the capabilities of water diffusion in internal layers and water evaporation at the skin surface. The changes that occurred in the moisture level seem to be related to water gradient in skin layers. In the first 5 peelings of tape stripping test, it was assumed that only the serum film at the surface of the skin was removed, as no changes occurred on the skin structure. Skin becomes drier with the number of tape strippings, so the "moistsense" reading obtained from the surface reduced. An increasing trend of the "moistsense" reading was found in further stripping (ranging from 8 to 10) and may be due to that the numerous extractions of the serum film resulting in a reduction of the thickness of the SC when the serum film was cleared way. As skin cell layers were removed, those cells beneath the removed cells were exposed and formed a new skin surface. Those new cells have relative high water content because they are close to living layers, hydrated by water diffusing longer and faster compared with the outmost skin cells (Philip & Bozena, 2005). Therefore the "moistsense" reading was found to increase as more skin cells removed. This explanation also holds for the case of skin rubbing test. Finally, the "moistsense" reading and the friction force reach a plateau in both experiments as no more skin tissue was removed.

A significant increase was found in the friction force with tape stripping, particularly in the first 10 strippings (Figure 5.2 (III)). As discussed earlier, the frictional behaviour of the skin involves an adhesion mechanism and deformation mechanism under low load conditions (< 2 N). The deformation mechanism refers to the deformation of asperities on the skin surface. However, no significant morphological change was found on the skin with the tape stripping except the thickness of the SC (see Figure 5.3 (I)). Therefore, it can be assumed that the component of deformation mechanism can be neglected and the friction force is only dominated by the adhesion mechanism. According to previous research, the biological adhesion between living tissues and substrates is considered to be associated with their structures and chemical properties (Pailler-Mattei & Zahouani, 2004). Marti et al. (1988) and Erlanson et al. (1988) indicated that the adhesion force in most cases can be expressed as a combination of electronsatic forces, van der Waals forces, capillary forces and forces due to chemical bonds or acid-base interactions. In later studies, Scherge & Gorb (2001) found that there are four main contributions to the adhesion

force for a silicon model in the micro-range. This observation is applicable for the study of the skin frictional behaviour, since both of them appear to behave similarly with respect to the friction. Those four contributors to the adhesion force of skin are molecular forces, electrostatic forces, capillary forces and forces due to excess charge. However, in ambient environments, it is believed that only the molecular forces (van der Waals forces) and electrostatic forces play important roles for governing the adhesion force, as well as chemical hydrogen bonds. Consequently, in this study, the total changes of the friction force can be calculated following the equation of Maksić & Thomas (1999), Scherge & Gorb (2001) and Butt et al. (2005):

$$\Delta F = \Delta F_{vdW} + \Delta F_{el} + \Delta F_{chem} \tag{5.3}$$

where ΔF_{vdW} is the change of van der Waals force, ΔF_{el} is the electrostatic force and ΔF_{chem} is the force due to chemical bonds or acid-base interactions. The van der Waals force is attributed to a repulsive and/or an attractive interaction between molecules. For two flat surfaces, the van der Waals force follows the law of Butt et al. (2005):

$$\Delta F_{vdW} = \frac{\Delta G}{d} = -\frac{A_H}{6\pi d^3} \tag{5.4}$$

where ΔG is the van der Waals energy, d is the distance and A_H is the Hamaker constant (equal to $\pi^2 C \rho_1 \rho_2 \approx 10^{-19} J$, C is the constant in the atom-atom potential, ρ_1 and ρ_2 are the numbers of atoms per unit volume). However, the van der Waals force is generally considered as a relatively small force compared with other factors in most cases, because the spacing between the solids is not able to be reduced to 10 *nm*, because of their rough surfaces (Scherge & Gorb, 2001). According to Equation (5.4), there was no significant change on the van der Waals force since the Hamaker constant and the distance were not altered with tape stripping. Therefore, it can be assumed that the influence of the van der Waals force on the adhesion force can be neglected. The electrostatic forces and the force due to chemical bond are the main contributors to the change of the adhesion force.

Landau and Lifshits (1960) have proposed a model for measuring the electrostatic energy between two different dielectrics (respective dielectric constant ε_1 for medium dielectric and ε_{skin} for skin). In accordance with this model, the electrostatic

force correspond to a electronic charge Q, at a distance of D to the interface, is given by

$$\Delta F_{el} = \frac{\Delta E_{el}}{d} = \frac{-Q^2}{4d(4\pi\varepsilon_0\varepsilon_1)D}\left(\frac{\varepsilon_{skin}-\varepsilon_1}{\varepsilon_{skin}+\varepsilon_1}\right) \quad (5.5)$$

where ε_0 is the dielectric constant of the air (see Figure 5.8). It shows that the electrostatic force is proportional to the electronic charge of the dielectrics tested.

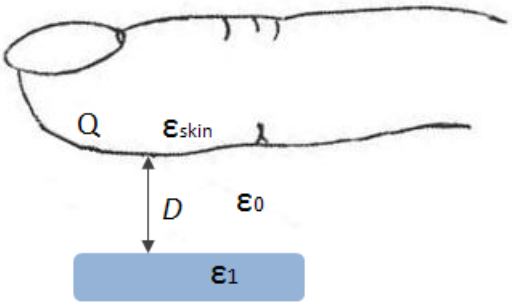

Figure 5.8: Schematic of the measurement of the electrostatic force.

The electronic charge Q on the stripped skin can be calculated with "moistsense" reading. The measuring principle of skin "moistsense" reading is one of capacitance, with non-electric contact with the skin (Fluhr et al., 1994; Tomlinson et al., 2009).

$$Read\ out\ (\text{AU}) = B \times C = B \times \frac{\varepsilon \times s}{d_p}(F) \quad (5.6)$$

where B is the arbitrary constant, C is the capacitance, ε is the difference of dielectric constant between skin and contacting dielectric $\varepsilon \approx \varepsilon_{skin}$, s is the size of sensor surface and d_p is the distance between negative and positive poles. Since the value of B, the contact area (A) and the distance (d_p) are constant, the "$Read\ out$" highly depends on the capacitance, thus the dielectric constant of the skin. The surface electrical charge, is defined as $Q = C \times H$, where H is the potential difference (a constant).

$$Q = \frac{\varepsilon_{skin} \times s}{d_p} \times H \propto Read\ out\ (\text{AU}) \quad (5.7)$$

By replacing the term of electronic charge Q in Equation (5.5), the model of the electrostatic force is given by the following equation:

$$\Delta F_{el} = \frac{-(\varepsilon_{skin} \times s \times H/d_p)^2}{4d(4\pi\varepsilon_0\varepsilon_1)D}\left(\frac{\varepsilon_{skin}-\varepsilon_1}{\varepsilon_{skin}+\varepsilon_1}\right) \propto -{\varepsilon_{skin}}^2\left(\frac{\varepsilon_{skin}-\varepsilon_1}{\varepsilon_{skin}+\varepsilon_1}\right) \propto Read\ out\ (\text{AU}) \quad (5.8)$$

Therefore, it can be assumed that the absolute value of the electrostatic force would increase when the electronic charge increases due to the increase of the dielectric constant of skin. This assumption was verified by the results in Figure 5.2 (V) and 5.3 (V), where the friction force shows an increasing trend as the "moistsense" reading increases from 59 AU to 68 AU. This conclusion was also drawn by Guerret-Piécourt et al. (2003), who assessed the influence of the electrical charges on the friction coefficient of insulating materials using a scanning electron microscope mirror method (SEMM). In their experiments, they found that the sapphire's ability for trapping electrons was improved after it was irradiated by UV, leading to more electrons being trapped, hence increasing the adhesion force.

In recent studies, Pailler-Mattei et al. (2007) conducted similar tape stripping tests on the inner forearm. The results of their experiments show that the adhesion force rapidly increases for the first tape stripping, which is in good accordance with data presented here. They reasoned that it may be caused by the electrical phenomenon at the interface between skin and a probe. In a later study, they used a "fieldmeter" device to measure and compare the electric charge on the surface of skin before and after tape stripping (Pailler-Mattei et al., 2011). Unfortunately, they did not observe any significant change on the electric charge, as well as the physico-chemical properties. This could be explained by the fact that unlike human fingers which have hydrophilic skin (sebum-rich), the forearm is considered to be hydrophobic skin (sebum-poor). There is little sebum or no found at the surface of the forearm. Thus the change of the adhesion force seems to be mainly attributable to the removal of the SC. Therefore, it is not surprising no correlation was found between the superficial sebum and the adhesion force in their studies. However, in the current test, corresponding changes on the moisture level of the skin with respect to the numbers of tape strippings can be directly observed.

According to Butt et al. (2005), the force due to chemical bonds or acid-base interactions formed at the jump-off-contact can be measured by a simple model. It is assumed that the chemical bond form randomly and have all the same value of force (F_i). The total force (ΔF_{chem}) for *n* chemical bonds formed is obtained as follows:

$$\Delta F_{chem} = nF_i + F_0 \tag{5.9}$$

where F_0 is a non-specific interaction, depending on the chemical components of the interfaces. Elkhyat et al. (2004) have investigated the effect of the hydrophilic/hydrophobic balance for both slider surfaces and sliding materials on friction coefficient. The results from their tests indicated that friction coefficient for the hydrophobic/hydrophobic tribo-pair is relatively lower than those for hydrophilic/hydrophobic and hydrophilic/hydrophilic tribo-pairs. For example, under similar conditions, the forearm skin (serum-poor) was considered as a medium level of hydrophobic surface and exhibits a lower friction coefficient compared with other low-level hydrophobic surfaces. However, in the current study, those physico-chemical properties of the skin (hydrophilicity) and their effects on the skin friction related to the tape stripping test cannot be assessed due to limited techniques.

In contrast to the tape stripping tests, the results of the rubbing tests showed that the friction force is reduced significantly with skin rubbing, see Figure 5.5 (IV) and 5.6 (IV). This may be caused by the morphological and structural changes of the stratum conreum with skin rubbing (e.g. skin ridges, moisture level and thickness of SC). For example, in Figure 5.5 (I), it was found that the ridges at the surface of the skin shrink after skin rubbing, which contributes to a relative flat surface of the skin. Meanwhile, the thickness of the SC was found to gradually diminish after a few skin rubbings, which is validated by the experimental data in Figure 5.5 (II). In general, it is believed that the mechanical properties of the stratum corneum cannot influence the global mechanical properties of the skin (Pailler-Mattei et al. 2007, 2011). This could explain why the mechanical parameters of the skin are independent on the thickness of the SC in the "*cutometer*" measurement except the distensability of the skin (see Table 5.2). As mentioned above, the frictional interaction between human skin and contacting surfaces is complicated, and involves various mechanisms. The skin would experience two different deformations with respect to the normal load and shear force respectively when it was sliding against a flat surface. For a better understanding of the skin frictional behaviour, deformations in both vertical and horizontal directions were analysed and represented by two parameters, the normal stiffness (S_v) and the lateral stiffness (S_l). They can be used to determine the Young's modulus of skin in both directions according to the following relationship (Pailler-Mattei et al., 2007; Geerligs et al., 2011):

$$\begin{cases} E_v = \frac{2\sqrt{A}}{S_v\sqrt{\pi}} & Young's\ modulus\ in\ vertical\ direction \\ E_l = \frac{2\sqrt{A}}{S_l\sqrt{\pi}} & Young's\ modulus\ in\ lateral\ direction \end{cases} \quad (5.10)$$

Wolfman (1983) derived a relationship between the adhesion component of the friction coefficient and the Young's modulus, the equation is given as follows:

$$\mu_{ad} \propto N^{-1/3}E^{-2/3} \quad (5.11)$$

where N is the normal load, E is the reduced Young's modulus and μ_{ad} is the adhesion component of friction coefficient. As a consequence, the adhesion friction can be written as a function of stiffness, as

$$F_{ad} \propto {S_{v/l}}^{2/3} \quad (5.12)$$

However, in the current test, there was no significant change in the normal stiffness after skin rubbing, even though the thickness of the SC was reduced by 25 μm, which confirms that the change of the thickness of the SC is too small to affect the global mechanical properties of the skin (Figure 5.7). Due to the limitation of techniques, particularly the lateral stiffness of the skin was not investigated here. In similar studies, Pailler-Mattei et al. (2007) found that both the normal stiffness and the lateral stiffness appear to decrease as a function of the stratum corneum removed, however. The thickness of the SC had a drop of 6 μm after 30 tape strippings, the corresponding adhesion force was observed to slightly decrease as well, expect for the first tape stripping, which is in a good agreement with Equation (5.6). As a consequence, those observations reveal that the reduction of friction force after skin rubbing may be attributed to the reduction of the lateral stiffness of the skin with respect to the removal of the SC.

The morphological change of the SC is other reason to for friction force reduction in the skin rubbing test. As can be seen in Figure 5.5 (I), those ridges on the surface shrink with skin rubbing, thus, the skin becomes more flat, and hence increases the contact area between the finger skin and a surface. In fact, this hypothesis was not hold for all subjects as the skin surface became rougher instead. Under a normal condition, after the outmost layer of skin is rubbed by sandpaper, it becomes brittle and scaly, which can be directly observed by the naked eye, particularly in subject 2 (see Figure 5.6 (I)). Therefore, the contact area should decrease after skin rubbing.

Those influences on the friction force with respect to the physico-chemical properties of the skin should not be considered, such as chemical bonds, electronstatic forces, because it was assumed the superfacial sebum was removed by hand wash prior the rubbing test.

5.3 Conclusions

This chapter introduces a commercial OCT system combined with a "*cutometer*" MPA 580 device to investigate skin properties and related influences on skin frictional behaviour. In the first series of tests, it looked at the potential relationships between various structural parameters and skin friction. Results showed there was no significant relationship between the natural thickness of stratum corneum and skin friction, which could be attributed to the fact that there were too many factors influencing the measurement of skin friction. The friction coefficient increased slightly with increasing moisture level of the skin, however, the moisture level was not likely affected by the number of sweat ducts in skin. In the second series of tests, a skin rubbing test and a tape stripping test were developed to evaluate the effects of skin surface properties on skin friction. In the case of the tape stripping tests, no significant change was observed on the thickness of the stratum corneum. It was also found that the skin friction coefficient initially increases and then reaches a plateau with increasing the number of tape stripping. The moisture level of the skin had a significant effect on the friction force as a linear relationship found between the friction force and the "moistsense" reading. In the case of the skin rubbing tests, the skin friction coefficient was found to have a significant drop with skin rubbing. Two different possibilities have been proposed to explain the change: (a) skin became smooth as the ridges on the skin surface shrink with skin rubbing and hence increased the friction force, (b) the thickness of the stratum corneum was reduced, which decreased the lateral Young's modulus of skin and decreased the friction force.

Chapter 6

Measurements of the Contact Area between Finger-pads and Flat Surfaces

From Chapters 4 and 5, it was found that skin friction is not only determined by the mechanical properties of finger-pad skin and the applied load, but also strongly depends on the contact area (or contact pressure) between finger-pads and contact surfaces. Similar conclusions were also suggested by other authors (Bowden & Tabor, 1964; Loden et al., 1992; Gulati & Srinivasan, 1995; Han et al., 1996; Sivamani et al., 2003; Derler et al., 2009). For example, Bowden & Tabor (1964) investigated the effect of load on the friction of polymers, and indicated that the contact area is the major factor affecting the friction. They also concluded that the friction of visco-elastic materials is ascribed to the adhesion mechanism in the case that the tested materials experience slow movements. Furthermore, they derived a simple model to explain the relationship between the friction force and the contact area, expressed as: $F = \tau \times A_{re}$, where τ is the shear strength, A_{re} is the real area of contact. The contact area was shown to be proportional to the normal load applied. This observation is in good agreement with the results in other studies (Derler et al., 2009; Childs, 2006; Warman & Ennos, 2009; Tomlinson, 2009; Soneda & Nakano, 2010).

For those samples with ridges of hemispherical shape, there are two different deformations, i.e. pure plastic deformation and pure elastic deformation, which are considered to be involved in the contact area (Archard, 1957; Moore, 1972). The real contact area is expected to be directly proportional to the normal load in the case of pure plastic contact. Different from the plastic contact, the real contact area is proportional to the normal load to the power of 2/3 in the case of pure elastic contact,

which is in accordance with the Hertz's equation. El-shimi (1977) suggested that the contact area for visco-elastic materials is likely to be dependent on the elastic deformation rather than the plastic deformation. However, Han et al. (1996) indicated that the Hertz's model is only applicable for the case of a hemispherical probe sliding on deformable materials. As human fingers do not experience smooth spherical contact, Hertz's model cannot be used to accurately estimate the contact area between finger-pads and contact surfaces. They also suggested that the change in the contact area with loads follows a power-law relationship.

Although, the investigation of the contact area between finger-pad skin and object interfaces is critical for characterising the frictional behaviour of skin, it is difficult to measure the real contact area due to the limited techniques available, however. As discussed in Chapter 2, human finger-pad skin is not smooth and is covered with a pattern of ridges. These ridges do not permit skin to contact surfaces completely, even at high load (see Figure 6.1). The objective of this chapter is to experimentally investigate both static and dynamic contact areas (macro- and micro- scales) between human finger-pads and smooth glass surfaces using various methods, including a fingerprint stamping method, an Optical Coherence Tomography (OCT) method and a Digital Image Correlation (DIC) method. Since the contact area alters with different fingers as well as different contact angles between the finger-pads and contact surfaces (Warman & Ennos, 2009; Tomlinson et al., 2007), experiments to study the effects of finger angle and different fingers on the skin friction were also conducted in this study.

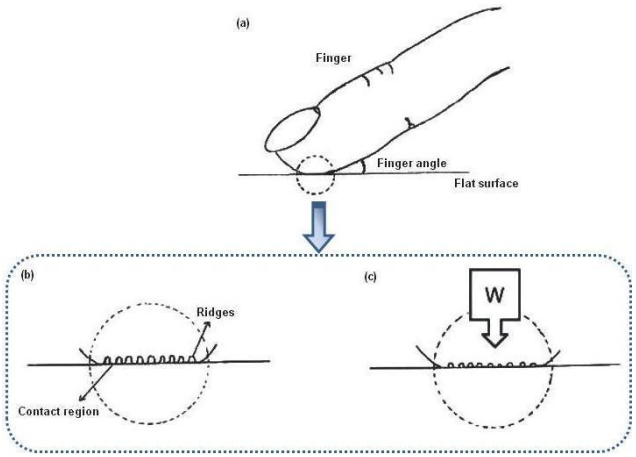

Figure 6.1: (a) the macro-scale of a finger-pad in contact with a flat surface, (b) the micro-scale of the contact region without load, and (c) the micro-scale of the contact region with a load (W) applied.

6.1 Measurements of Static Contact Area

To calculate the static contact area of finger-pads in contact with glass surfaces, the fingerprint ink method and the OCT method were employed in this study. Four separate sets of tests have been carried out: (a) to investigate the effect of the normal load on the contact area, (b) to investigate the effect of the finger angle on the skin friction, (c) to measure the contact area at different fingers, (d) to compare the fingerprint ink method with the OCT method.

6.1.1 Methods

6.1.1.1 Finger-print Ink Method

Experimental Set-up

As discussed in previous literature (Chapter 2), the fingerprint ink method is one of the most common methods that has been used for calculating the contact area of finger-pads in contact with flat surfaces. In the current study, measurements were performed on the multi-axis force plate (see Chapter 3 for more details). A white paper sheet was attached on the top surface of the force plate, which allowed participants to record their fingerprints by pressing down stained finger-pads.

Experimental Procedure

To investigate the effect of the normal load on the contact area, the right index finger-pad of a 25 year old female was used. Firstly, the finger-pad was pressed onto an ink sponge so that a thin film of ink covered the surface of the skin. The stained finger-pad was then pressed onto a white paper sheet at an angle of 25° ~ 40° with various loads (in the range of 0.5 ~ 24.5 N) to produce fingerprints. In order to avoid ink drying and image blurring, the participant was requested to conduct the test quickly. The time delay between finger-pad staining and the contact area measurement was approximately 2 ~ 5 seconds. To investigate the effect of the contact angles on the contact area, the participant was also asked to repeat the test under the condition of various angles, including 15°, 30°, 45° and 60°. Finally, the test was repeated by all 5 fingers of the right hand at a 40° angle. All fingerprints produced were recorded using a digital camera.

Image Analysis

All fingerprints obtained were recorded using a digital camera and then transferred to a PC, and then were analysed using a "Matlab" programme. The total apparent and real contact areas were measured respectively, samples of which is shown in Figure 6.2. The shape of the index fingerprint at angles between 15° and 45° could be assumed as an ellipse, in this case, the apparent contact area could be determined using the equation: $A = \pi ig$, where i is the length of the semi-major axis and g is the length of the semi-minor axis (Figure 6.2(a)). To calculate the real contact area, the images of fingerprints were converted to binary black-white images, in which the non-contact region is presented as white and the real contact area refers to the inked area (Figure 6.2(b)). The threshold of the image binarization was determined such that the boundaries of fingerprints before and after binarization were similar. The real contact area was calculated using the sum of the number of black pixels inside the outline of the contact zone in binary images (Derler et al., 2009; Soneda & Nakano, 2010).

(a) (b)

Figure 6.2: Images of a fingerprint. (a) made by staining a fingerprint and press it onto a white paper sheet, where i and g is length semi-major and minor axis respectively, (b) a binary image of (a).

6.1.1.2 OCT Method

Experimental Set-up

The Optical Coherence Tomography system provides a new and effective method to calculate the actual contact area. A force plate with a glass insert was built to allow a

finger press force to be recorded while OCT images were collected (Figure 6.3). The glass window is made of optical glass (*Quartz Glass*) with thickness 1 mm. It is transparent, smooth (Ra ≤ 0.01 μm) and relatively stiff (Young's modulus ≈ 73 GPa). In order to reduce the light reflectance from the top surface of the glass window and improve the clarity of OCT images, the top surface of the glass plate was angled so as not to be perpendicular to the axis of the camera. 2D cross-section OCT images of human skin are generally used to study the sub-facial structure of the skin. In the current studies, in order to gain contact area data, the multi-slice OCT system that can provide 16 slices was applied. In the case of multi-slice scanning, the interval between slides in the Y direction was set at 0.05 mm.

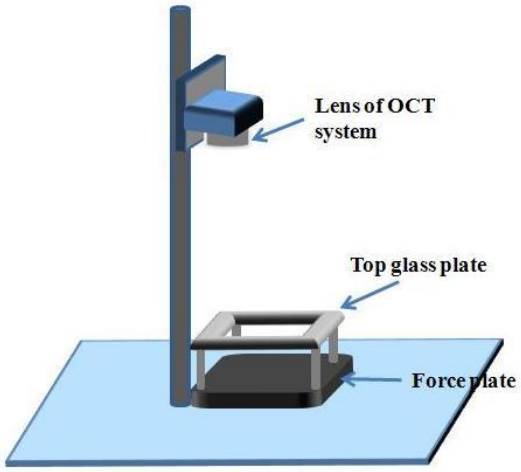

Figure 6.3: The OCT system used for producing skin images.

Experimental Procedure

The experiments were done using the same finger used in the fingerprint stamping method. Due to the fact that the OCT system is limited to imaging a 4 ~ 6 *mm* wide rectangle of human skin, four different regions of the finger-pad were selected to estimate the real contact area between the finger-pad and contacting surfaces (see Figure 6.4). The participant was requested to wash her hands and dry them using a paper towel, prior to the test. The participant was then guided to press her index finger-pad against the glass window with the various loads. The angle between the finger-pad and the glass window was controlled to be between 25° and 40°. During the process, the index finger was fixed and not allowed to move away from the glass, which helped to ensure that the images of finger pad skin were scanned from the

same position. In order to compare these two different methods, the corresponding data with respect to the same tested positions on the finger-pad were also measured using the fingerprint stamping method.

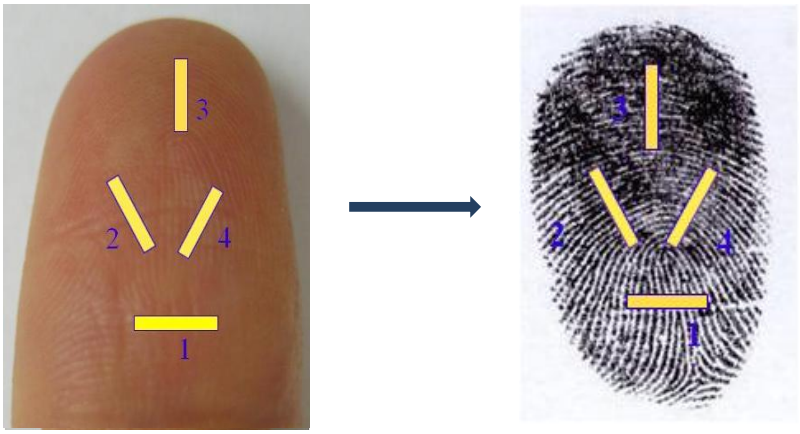

(a) (b)

Figure 6.4: (a) Four different regions of the right index finger-pad were selected for comparing the OCT method, and (b) the fingerprint stamping method.

Image Analysis

An example is given to explain how to determine the real contact length from a 2D OCT skin image. As seen in Figure 6.5(a), an OCT image of a finger-pad was taken from an unloaded index finger, in which the ridges were clearly observed at the surface of skin. The finger-pad was then loaded against the glass insert, the grooves between the ridges on the surface shrank and the surface of the finger-pad became smoother. These flat portions caused by the deformation of skin ridges were considered to be the contacting region (see Figure 6.5(b)). The measurement of the real contact length in the 2D image of skin was in accordance with the sum of lengths of flat regions in ridges, $L_{re} \approx \sum_{j=o}^{n} d_j < L_{ap}$, where L_{re} is the real contact length, L_{ap} is the total contact length and d_j is the contact length for individual ridge, as shown in Figure 6.6. The measurements were conducted using the ruler in the image tools of "Matlab". In the case of multi-slice images of skin, the sample interval was set 0.05 mm between each slice. Therefore, the real contact area for a single slice could be estimated by multiplying the real contact length (L_{re}) by the sample interval. The total real contact area was in accordance with the sum of real contact areas from all slices, $A_{re} = \sum_{j=0}^{n} 0.05 L_{re\,j}$.

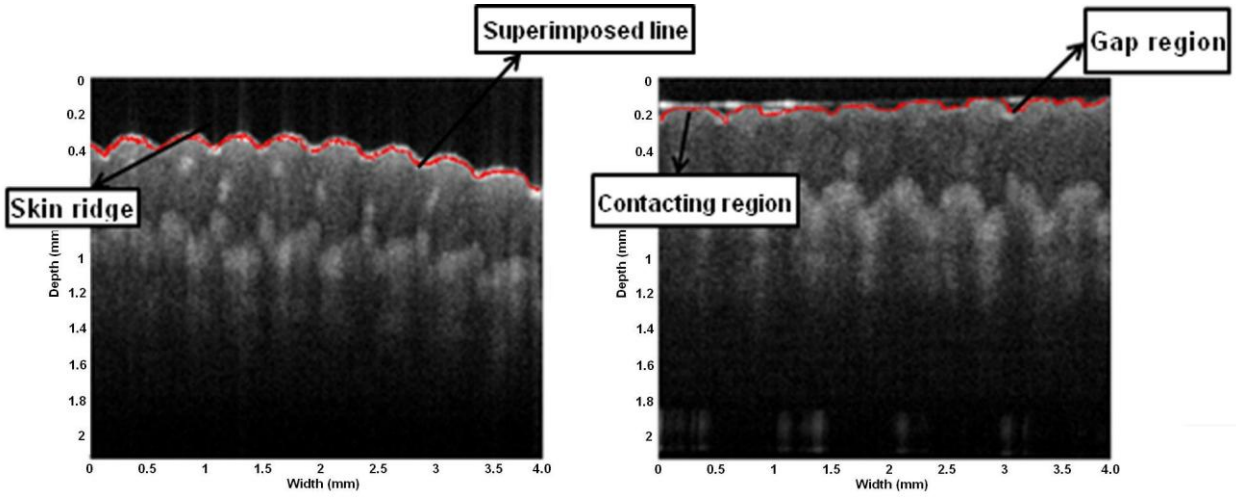

Figure 6.5: 2D OCT images of a finger, (a) in nature state (no load applied), (b) in contact with a glass plate (0.2 N load applied).

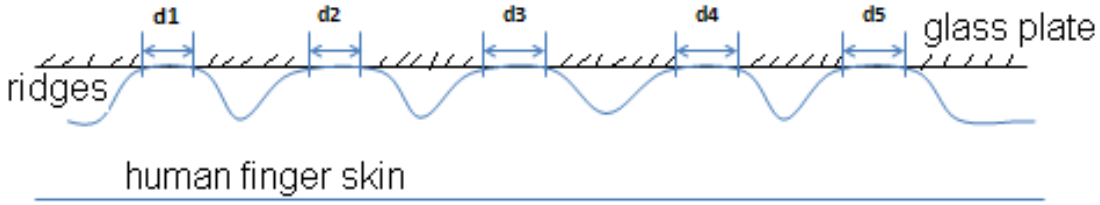

Figure 6.6: Schematic diagram of finger-pad loaded against a glass insert.

6.1.2 Results and Discussion

6.1.2.1 The Effect of the Normal Load on the Contact Area

Figure 6.7 shows some images of fingerprints that were taken from the same index finger-pad under different loads. In this study, the apparent contact area of a finger-pad refers to the size of the fingerprint, and the real contact area depends on the mount of black ink. By comparing these eight images, it can be found that the apparent contact area has an increasing trend with increasing load, particularly in the first four images (from Figure 6.7(a) to 6.7(d)). These changes in the contact area (i.e., apparent and real contact areas) have been quantified and plotted in Figure 6.8. In order to study the effect of the normal load on the contact area in detail, these fingerprint images were divided into two groups considering the level of load applied, which is also believed to be helpful for explaining the two-part relationship of skin friction obtained (see Chapter 4).

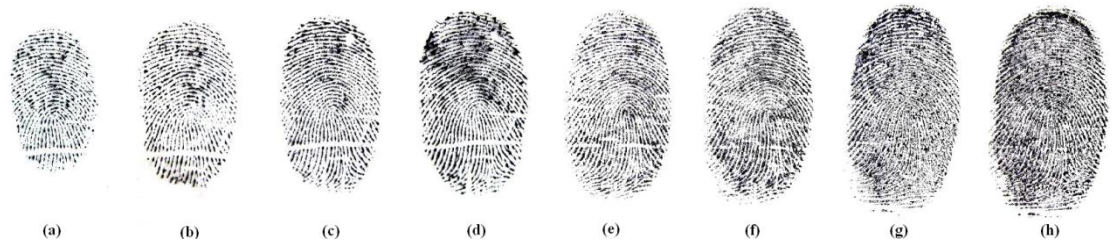

Figure 6.7: Binary images of fingerprints varying with loads, (a) 0.47 N, (b) 0.66 N, (c) 1.02 N, (d) 1.50 N, (e) 2.82 N, (f) 6.07 N, (g) 12.81N and (h) 24.46 N.

Four different relationships between the contact areas and the normal load were plotted in Figure 6.8 (a) and (b) (i.e. apparent and real contact area at "low" and "high" load conditions). With respect to the low load condition (< 2 N), as increasing the normal load, the results showed a 68% increase (from 78 mm^2 to 130 mm^2) in the apparent contact area and a 156% increase in the real contact area (from 16 mm^2 to 39 mm^2). As expected, the change in the apparent contact area at the high load condition is relatively smaller (a 30% increase) compared to that at the low load condition. The power-law line regression of the real contact area seems not to be affected by the normal load due to no significant difference being found for both low and high load conditions. The increasing trends for all contact areas were found to obey the power law:

$$A \propto N^c \tag{6.1}$$

where N is the normal load and c is the exponent of N (constant). As suggested by the equation, at the low load condition, the real contact area was found to depend on the normal load to the power of 0.66, while the apparent contact area was found to depend on the load to the power of 0.41. The corresponding data were found to be 0.41 for the real contact area and 0.11 for the apparent contact area. A power law dependence between the real contact pressure (was calculated by dividing normal loads by real contact areas) and the normal load with an exponent of 0.66 was also found in Figure 6.9. The coefficient of determination (R^2) is around 0.96.

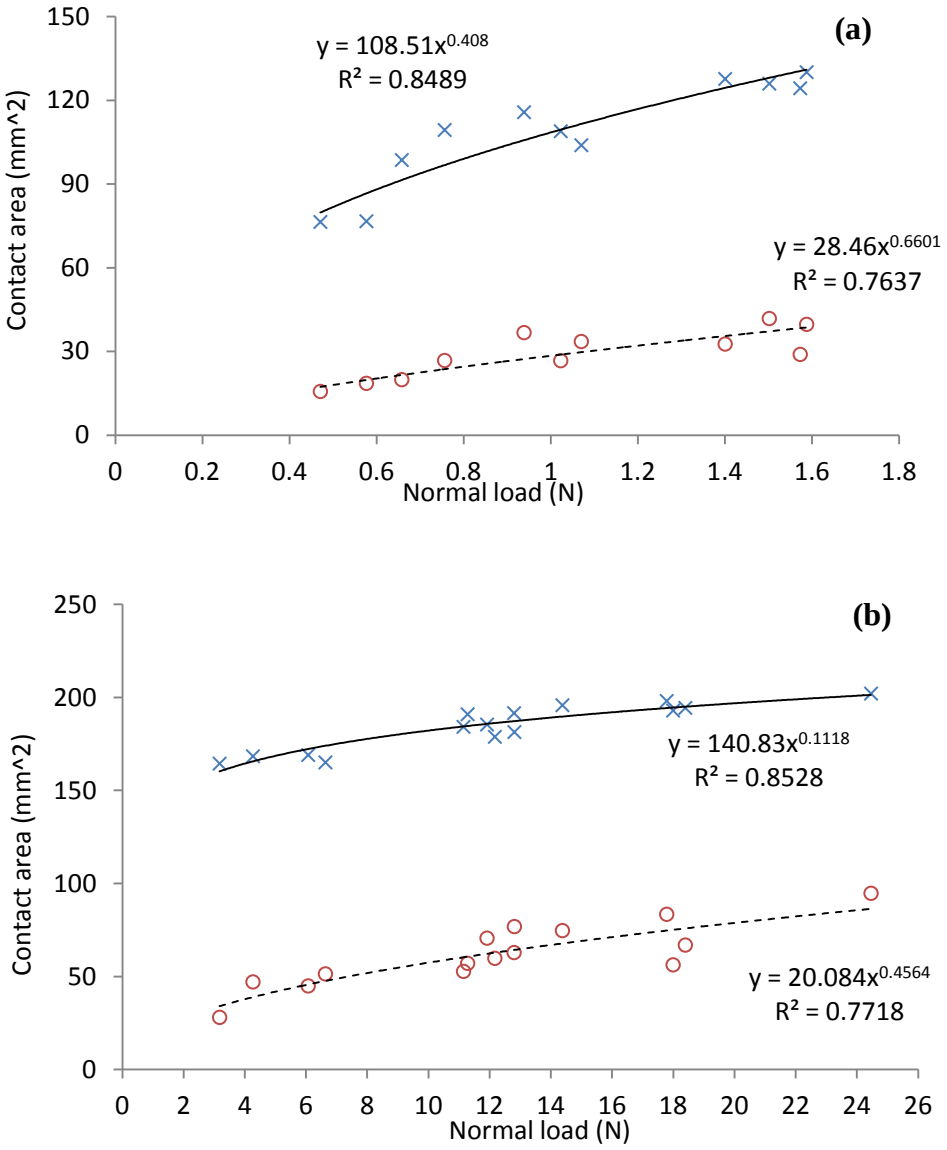

Figure 6.8: Both the apparent (blue cross) and the real contact area (red circle) between the finger-pad and paper sheets measured as a function of the normal load: (a) under "low load" conditions (< 2 N), (b) under "high load" conditions (> 3 N).

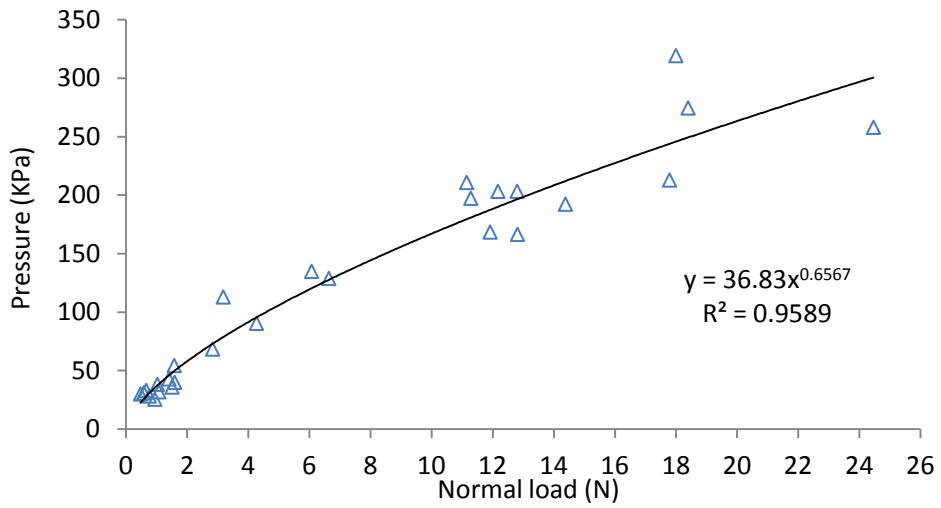

Figure 6.9: Variation of the real contact pressure with normal loads.

As discussed earlier, human skin is a heterogeneous, anisotropic and a non-linear viscoelastic material. Owing to these unique properties, it allows more skin tissue to come into direct contact with a surface and hence the apparent contact area increases with increasing load. Figure 6.8 shows that the apparent contact area has a rapid increase at the low load condition and it reaches a plateau (approximately 200 mm^2) at the high load condition. This observation could be explained by the stress-strain behaviour of the skin (see Figure 6.10). In the case that low magnitude loads are applied to human skin (phase II), the collagen fibres in the skin will be straightened, and result in large deformations, which is reflected on the steep increase of the apparent contact area. When the external load goes up to a certain level, the stress-strain relationship tends to be linear due to the fact that skin gradually approaches its maximum capability of extension, becomes stiff, and leads to small deformations (phase III). Therefore, there was no significant change observed in the apparent contact at the high load condition. The real contact areas obtained in both cases show different phenomenon compared to those of the apparent contact areas. Due to the fact that the real contact area is related to the junctions of the skin asperities and a surface, the real contact area will keep increasing because of the deformation of asperities on skin surface, though the apparent contact area no longer changes under the condition of a certain load.

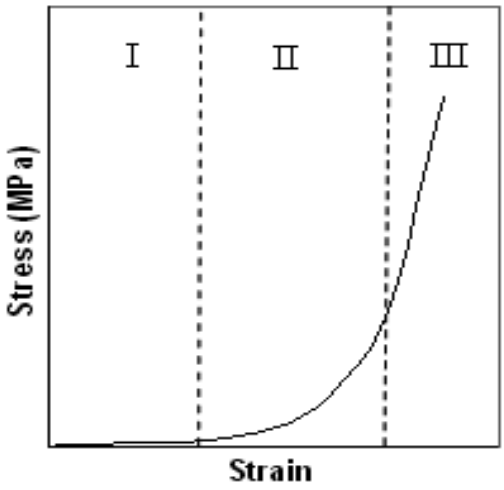

Figure 6.10: Stress-strain curve for human skin (Tomlinson et al., 2007).

As suggested by Hertz (1882), the contact area for no-linear elastic materials would be expected to increase with the normal load to the power of 2/3, and is given by the expression:

$$A = \pi \left(\frac{9NR}{16E}\right)^{2/3} \tag{6.2}$$

where *R* is the radius of the sphere and *E* is the reduced Young's modulus. In general, it is believed that human skin exhibits similar mechanical properties to those of the rubber. Therefore, the Hertz theory has been widely used to estimate the contact mechanism of human skin. For example, Tomlinson (2009) modified the Hertz contact model in order to determine the contact area between human fingers and a flat surface. With respect to her new model, *R* was assumed to be the radius of the finger, *E* was the reduced Young's modulus $= \frac{(1-{v_{skin}}^2)}{E_{skin}}$, E_{skin} is the Young's modulus of human skin (approximately 0.49 MPa) and v_{skin} is the Poisson's ratio of human skin (approximately 0.5). A similar model was also proposed by van Kuilenburg et al. (2012), they found that the apparent contact area depends on the normal load to the power of 0.36. In the current study, a comparison between the estimated contact areas calculated using different Hertz models and the experimental data obtained in this study has been made (see Figure 6.11). In the case of constant Young's modulus, it can be seen that the results of Tomlinson and van Kuilenburg show a similar linear behaviour. The value of the exponent for the current experimental data (0.22) is much smaller than 2/3, which is in a good agreement with the experimental results of Han et al. (1996). They have investigated the contact area

between human fingers and a transparent acrylic board using a CCD camera and found that the corresponding exponent value ranged from 0.2 to 0.4. They reasoned the Hertzian contact theory is not suitable to calculate the contact area as human fingers do not experience spherical contact. This assumption was evidenced by Figure 6.8 in the current study. In the study of Xydas & Kao (1999), they found that the corresponding exponent values of their experiments were found to be 0.55 for rubber fingers, 0.51 for silicon fingers and 0.09 for real fingers. Moreover, they indicated that the Hertz model is a linear elastic model and since human skin exhibits as a non-linear elastic material involving large deformations, the Hertz model with constant Young's modulus could not be used to describe the contact mechanism of human fingers. A similar conclusion was also drawn by Tomlinson (2009), they found that the area of contact calculated using vary Young's modulus and their experimental data show similar change trend with some minor difference.

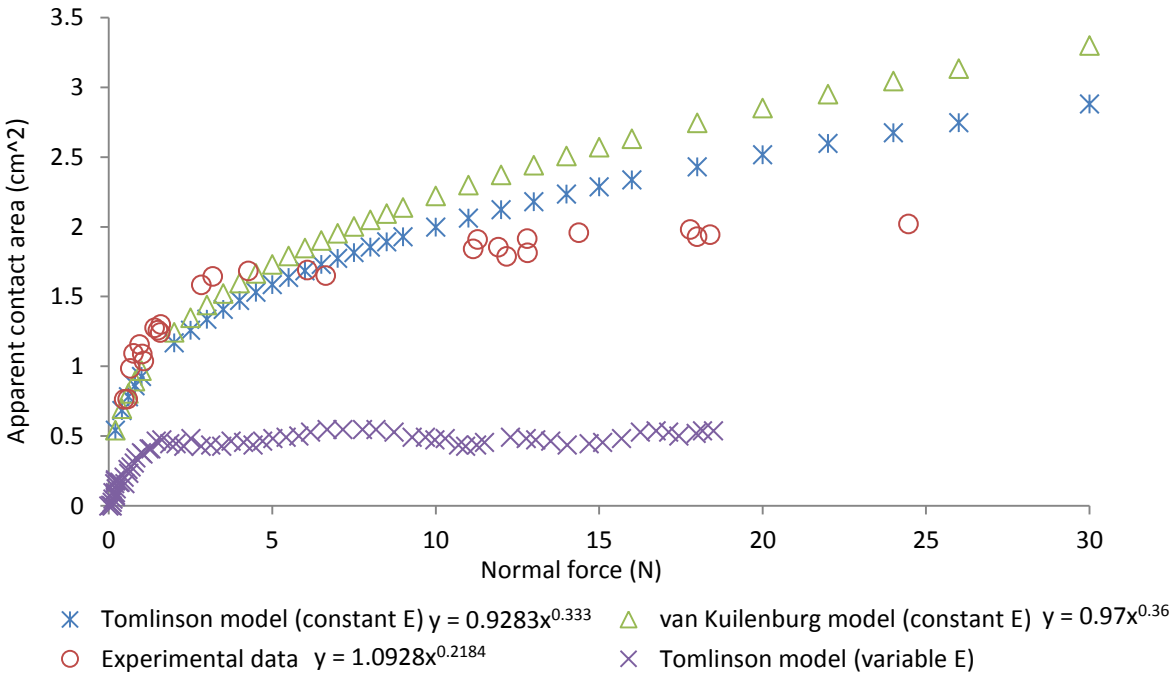

Figure 6.11: Variation of the relationships between the apparent contact area and the normal load for different methods.

Soneda and Nakano (2010) have conducted a similar study of contact area using the optical method. They found that both the apparent and real contact areas increased following the power law (Equation 6.1) when the load increased. The dependence of the apparent contact area (A_o) was 0.52 ± 0.06 and the real contact area (A_{re}) was 0.68 ± 0.09 for load between 0.1 N and 5 N. A similar observation was also reported

by Warman and Ennos (2009), who indicated that the apparent contact area rose with the normal load to power between 0.54 and 0.85 for all five fingers under the condition of a load less than 2 N and the real contact area was about 66.7% of the total perimeter area. These results appear large in contrast with the results of the current study. In the current study, under the low load condition, the corresponding exponent of A_o was 0.41 and the exponent of A_{re} was 0.66. Increasing the normal force, the exponent of A_o reduced to 0.11 and 0.46 for the exponent of A_{re}. These wide variation ranges in the exponents for both A_o and A_{re} among the above studies could be attributed to several possibilities. The first possibility is that the results in the experiments of the fingerprint ink method were inaccurate due to these drawbacks of ink spread, noise effect, threshold setting, etc. The second possibility may lie in the difference among various tested subjects and finger-pads. Environmental conditions, such as temperature and humidity, test materials, and performing angle will also influence the results.

In the recent study carried out by Derler et al. (2009), who looked at the effect of the normal load on the apparent contact areas for both the edge of hand and a finger using a CCD camera. The experimental data points for each anatomical site were fitted into a polynomial equation: $(N) = B + U.N^{1/4} + H.N$, where B, U, and H were constant. They found that there are steep initial increases on the apparent contact area with load for both anatomical sites (between 1 N and 8 N). After that, the apparent contact area reached a plateau with maximum value of about 4 cm^2 on the index finger and 15 cm^2 on the edge of the hand, respectively. Although they applied a polynomial model to describe the relationship between the apparent contact area and the normal load, rather than a power-law model, their trends of changes are consistent with the results of the current study. In addition, the maximum apparent contact for the finger was found to be slightly larger than the results obtained (ranged from 1.3 cm^2 to 2.9 cm^2 with respect to different fingers) in the current study (see Figure 6.11). This difference could be attributed to the fact different finger-pads were examined in these two tests.

6.1.2.2 The Effect of the Finger Angle on the Contact Area and Skin Friction

Figure 6.12 shows four fingerprints of an index finger that were taken at four different angles (i.e. 15°, 30°, 45° and 60°), where the fingerprints at the angles of 15° and 30° appear to be elliptical shape and gradually turn to round shape when the angle increases to 45° and 60°. Moreover, it was also found that, under the same load conditions, the apparent contact area of the fingerprint reduces when increasing the finger angle.

Figure 6.13 displays the relationships between the friction force and the normal force with respect to all four angles, which are presented by the linear law: $F = mN + e$, where m and e are constant. The values of R^2 were in the range of 0.93 and 0.98. According to the findings in Chapter 4, it is known that the skin friction obeys a linear regression model at the high load condition, thus the slope of m was assumed to be the friction coefficient. The magnitude of the slope (m) shows a slight decrease when increasing the contact angle from 15° to 45°. The minimum value of friction coefficient was found at the angle of 60°.

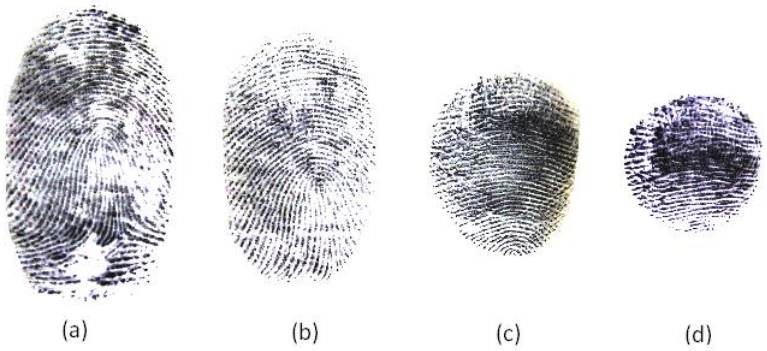

Figure 6.12: Index fingerprints obtained at different angles, (a) 15 degree, (b) 30 degree, (c) 45 degree and (d) 60 degree.

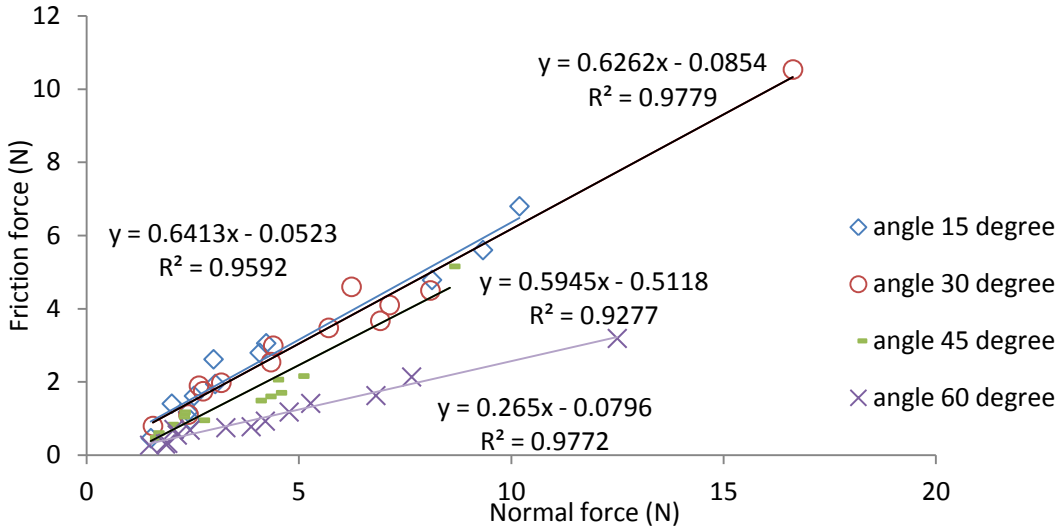

Figure 6.13: The relationship between the normal force and the friction force for four different finger angles.

As observed in Figure 6.12, the magnitude of the slope (m) has the highest value (0.64) at the angle of 15° and decreases to 0.27 when the angle rises to 60°, which is in good agreement with expectation that the increase in the angle between a finger pad and an object can reduce the friction coefficient. The friction coefficient is intimately associated with the contact pressure as expressed: $\mu \propto p^n$, in which n was -0.67 (Derler et al, 2008). As the finger angle is increased by the uplift of a finger and the contact region (apparent contact area) is reduced due to less and less tissue coming in contact with objects. The decreased contact areas result in an increase in the contact pressure under the same condition of load, so that the coefficient of friction increases. The other possibility is that the front part of the finger-pad is stiffer with less tissue. As increasing the finger angle, the finger-pad involved in contact became stiffer, and resulted in high Young's modulus and low skin friction coefficient. Han et al. (1999) have investigated the friction behaviour of skin under various conditions. They found that the exponent of the contact area equation ranges between 0.2 and 0.4 for three different angles (30°, 45° and 60°). The exponent value showed a decreasing trend when the finger angle increased from 30° to 60°, a similar phenomenon was also found for the coefficient of friction. The results relating to friction coefficient in both studies were very similar. Han et al. (1999) indicated that the relationship between the contact pressure and the dynamic friction coefficient is a continued decreasing curve line. However, due to the technical restriction in the

current study, the dynamic friction coefficient could not be measured with the contact area at the same time.

6.1.2.3 Contact Areas for Different Fingers

Table 6.1 shows the experimental results of the maximum normal load, the related apparent contact area and the coefficient of skin friction at 45 degree for all fingers. It can be observed that the thumb has the largest value of the apparent contact area, and its corresponding load to achieve the maximum apparent contact area is also largest compared with other fingers. The minimum apparent contact area was found in the little finger. The maximum skin friction coefficient was found in the thumb, followed by the ring finger, the middle index finger and the little finger, which is exactly the same as the order of the apparent contact area, except the ring finger. The normal load applied in the measurement of skin friction ranged from 3 to 12 N.

Figure 6.14 displays how the apparent contact area changes with the normal load for all five fingers. It can be seen that the apparent contact area is unlikely to be affected by the load at the high load condition, which matches well to the observations in Figure 6.8.

Table 6.1: Experimental results of 5 fingers using the ink printing method.

Fingers	Mean Apparent Contact Area (cm^2)	Normal Force for Maximum Apparent Contact Area (N)	Coefficient of Friction (μ) (load > 3 N)
Thumb-pad	2.88	15.2	0.47
Index Finger-pad	1.35	3.1	0.36
Middle Finger-pad	1.97	11.9	0.41
Ring Finger-pad	1.71	3.6	0.44
Little Finger-pad	1.27	3.4	0.34

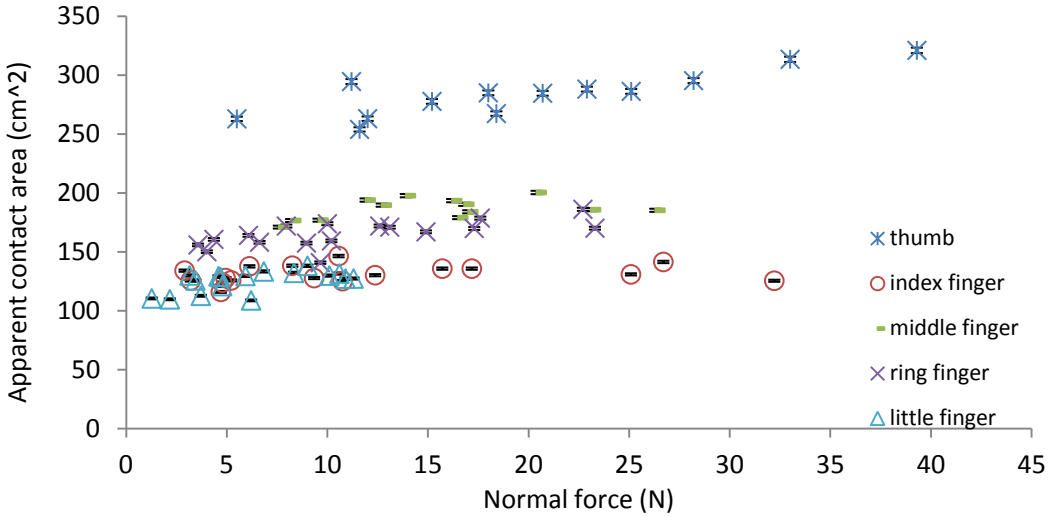

Figure 6.14: The data of the apparent contact area obtained from all five fingers with various loads.

As discussed above, the contact area between human skin and contacting surfaces is considered closely associated with the fingers' physiological structures. In general, thumb has the largest finger-pad and is followed by middle finger; no significant difference exists between index finger and ring finger, and little finger has the smallest finger-pad. Therefore, it is not surprised to observe a similar trend of change in the apparent contact areas (Figure 6.14). By analysing the data in Table 6.1, it was also found that the skin friction coefficient varies from finger to finger in the same hand, which follows the same order of the apparent contact area related, except the ring finger. From the findings in Chapter 5, it is known that the skin moisture level in the ring finger is relatively higher compared to other fingers. This is the reason why the ring finger, with a smaller contact area, presents a larger skin friction coefficient than that of the middle finger with a relatively larger contact area. The above observations reveal that the skin friction of fingers strongly depends on the contact area. However, different results were reported by Warman & Ennos (2009) in similar studies. The results of their tests seem not to agree with the conclusion that the friction coefficient of a human finger-pad is mainly determined by the contact area. They found that the largest friction coefficient was found in little finger followed by thumb, index finger, middle finger and ring finger; the maximum contact area was found in the index finger, however. Unfortunately, no detailed analysis was given to explain this phenomenon.

6.1.2.4 Comparison of Different Methods

The OCT images of the finger skin in Figure 6.15 show that the flattening of the finger ridges as increasing levels of pressure were applied. Therefore, the real contact area would be expected to rise as the load increase due to more and more skin tissue coming into contact with the glass.

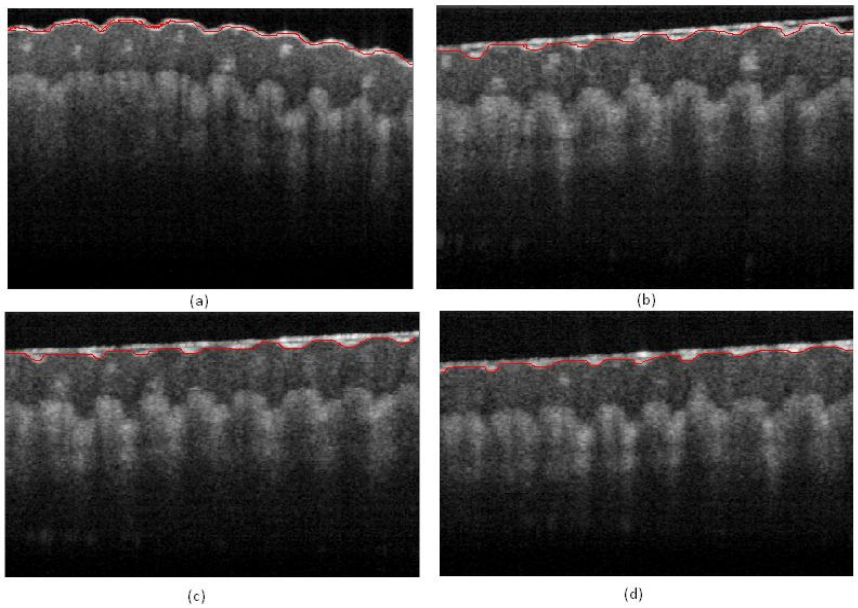

Figure 6.15: 2D images of finger skin with different levels of pressure applied on: (a) 0 N, (b) 0.7N (c) 3N and (d) 10N.

A power-law relationship was applied to describe the ratio of the real contact area to the apparent contact area as a function of the normal load, with the coefficient of determination (Figure 6.16). Figure 6.16 displays the experimental results that were measured in four different positions on the examined finger-pad, in which, with increasing normal load, the ratio of the real contact area to the apparent one was found to increase by approximately 20% for the OCT method, and 10% for the fingerprint stamping method.

Table 6.2 shows some parameters of the power-law relationship between the ratio of the real contact area to the apparent one and the normal load obtained from both methods. The exponent k was found to range from 0.12 to 0.20 for the OCT method and from 0.40 to 0.66 for the fingerprint stamping method depending on different positions. With respect to the coefficient of determination, the OCT method presents a high correlation between the ratio of the real against apparent contact area due to

the values of (R^2) varying between 0.8 and 1 for all different positions. In contrast to the OCT method, the corresponding values of (R^2) obtained from the fingerprint stamping method are relatively small, thus a weak correlation between these two variables would be expected.

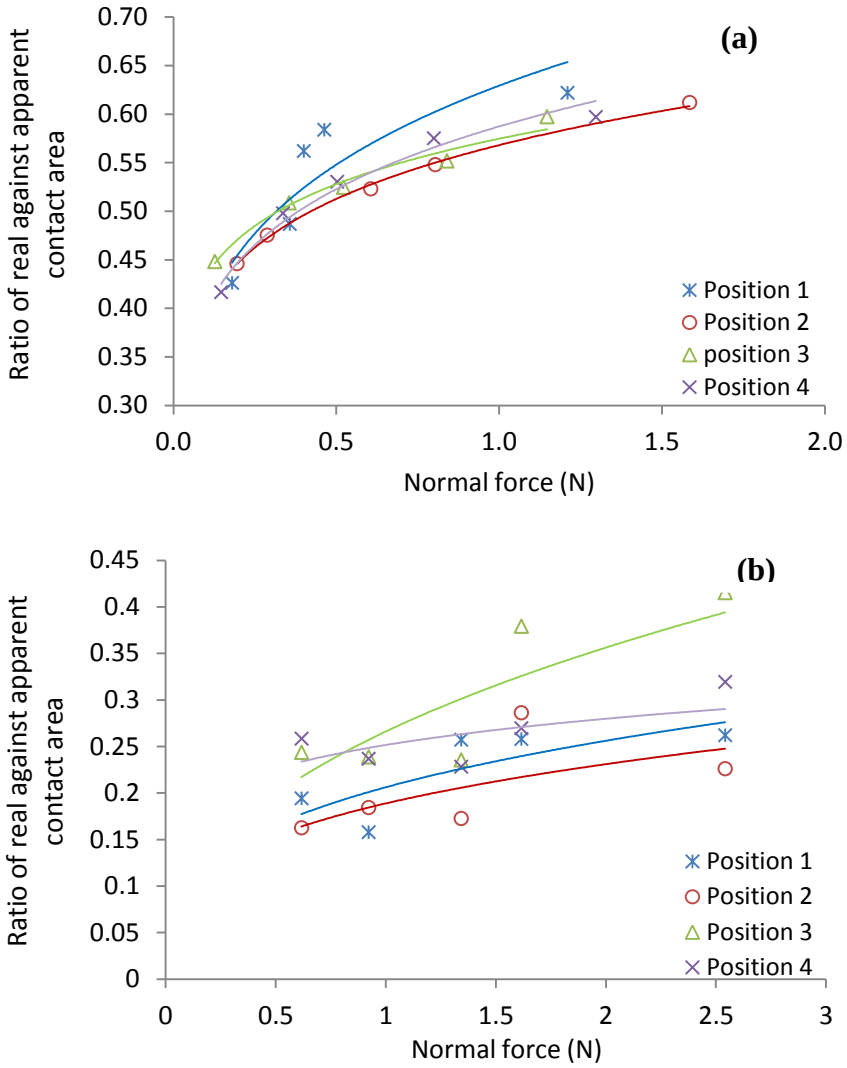

Figure 6.16: Ratio of the real contact area against the apparent contact area with load at four different positions: (a) OCT method and (b) fingerprint stamping method.

Table 6.2: Some parameters of the power-law relationships between the ratio of the real contact area against the apparent contact area and the normal load obtained from both methods.

position	OCT method			Fingerprint stamping method		
	constant (e)	exponent (c)	coefficient of determination (R^2)	constant (e)	exponent (c)	coefficient of determination (R^2)
position 1	0.6293	0.1997	0.8022	0.2062	0.3132	0.555
position 2	0.5681	0.1481	0.9973	0.1888	0.2911	0.4608
position 3	0.5747	0.1225	0.9774	0.2661	0.4211	0.6629
position 4	0.5873	0.1681	0.976	0.2516	0.1533	0.3953

There have been several studies measuring the real contact area of finger skin in contact with objects and involved different techniques such as the fingerprint ink method (Childs & Henson, 2006; Warman & Ennos, 2009; Tomlinson, 2009), the electrical resistance method (Tomlinson, 2009), optical methods (André et al., 2008; Tomlinson, 2009; Soneda & Nakano, 2010), etc. The fingerprint ink method is the most common method used at the moment. Tomlinson (2009) conducted investigations of contact area for fingers interacting with various materials using three different methods. In the experiment of the fingerprint ink method, the contact area of the examined finger was reported to increase with load following a linear relationship, and the ratio of the ridges area to the total area was between 0.38 and 0.5. In the similar studies of Childs & Henson's (2006), they found that the apparent contact area increases with load (up to 2 N) to the power of 0.2. The percentage of the real contact area to the apparent contact area was found to increase with load as well. The ratio was 12% at the load of 0.41 N, increased to 34% when the load rose to 1.77 N. These results are very similar to the results in the current study. As can be seen in Figure 6.16 (b), the results of the ratio were fitted into a curve regression. The percentages of the real contact area to the apparent contact area were found to be around 0.15 for 0.5 N, and 0.3 for 2 N. These results were also in good agreement with the experimental results from the experiments of Soneda & Nakano (2010), who developed a device based on light reflection for investigating the contact mechanism of human fingers. The principle of the measurements of the apparent contact area and

the real contact area relates the morphology of the finger skin. They found that the mean value of $\frac{A_{re}}{A_o}$ was 0.3 at a contact of 1 N.

In contrast to the above results, the OCT method shows a relatively higher percentage, about 0.45 for 0.2 N and 0.60 for 1.2 N. This difference is probably due to the over-estimated real contact length measured between finger skin and the glass window in the OCT tests. In the OCT tests, the measurement of the real contact area was done by manual observation. Due to the fact that there was strong light reflectance on the superficial of the stratum corneum considerable affect the measurement results, the experimental results measured were considered inaccurate. As discussed above, there are many disadvantages to apply the fingerprint ink method for measuring the contact areas of fingers, including ink spread, noise effects and threshold value setting. It can be assumed that the area of ink coverage would increase due to ink spread, and can result in a large real contact are. On the other hand, some amount of ink coverage might be lost due to inappropriate choice of threshold value setting in image processing. This might account for the reason why the ratios of the real contact area to the apparent contact area are smaller for the fingerprint ink method than those of optical experiments.

The limitation of the OCT technique related to the measurement of contact area is that the scanned area of the finger-pad (4 *mm* × 0.8 *mm*) was so small that it cannot be used to estimate the contact areas of whole finger-pad. However, in contrast to other methods, the OCT technique provides an accurate method for examining the internal micro-structure of skin that could help to predict the changing trend in the real contact area of finger-pads. In this study, we have compared the OCT method and the fingerprint ink method (see Figure 6.16). In the OCT tests, the experimental results show the linear regression models with respect to four different positions perform higher similarities than those in the fingerprint ink tests. Additionally, it was noted that the corresponding coefficient of determination (R^2) related to these linear regression models obtained are ranged from 0.8 to 1 for the OCT tests, 0.40 to 0.66 for the fingerprint tests. These strong correlation relationships between variables in Table 6.2 reveal that the OCT method provides more accurate experimental results than use of the fingerprint ink method.

6.2 Measurements of Dynamic Contact Area

The work outlined in the above sections described various methods for measuring the contact area (i.e. the apparent contact area and the real contact area) statically. However, all experimental results are static state data that were measured for fingers held against surfaces. These data are limited in terms of characterising the dynamic frictional behaviour of human fingers. This section introduces two different approaches to measure the dynamic contact area between fingers and contacting surfaces. Furthermore, the relationship between the dynamic contact area and friction coefficient will also be analysed.

6.2.1 Experimental Details

6.2.1.1 OCT Tests

The *in-vivo* experiments were conducted on the right middle finger of a 25 year old female using the OCT system (details have been discussed in Section 6.1.1.2) and the multi-axis force plate combined with a linear positioning stage (Reliance Precision Mechatronics) (see Figure 6.17). Measurements of dynamic contact were carried out by sliding the multi-axis force plate with a glass plate insert against the finger. During the measurements, the subject was requested to hold the tested finger against the glass plate and face up to the lens of the OCT system. The finger was not allowed to move away from the glass plate. The frame rate of the OCT system was about 2.5 slices per second.

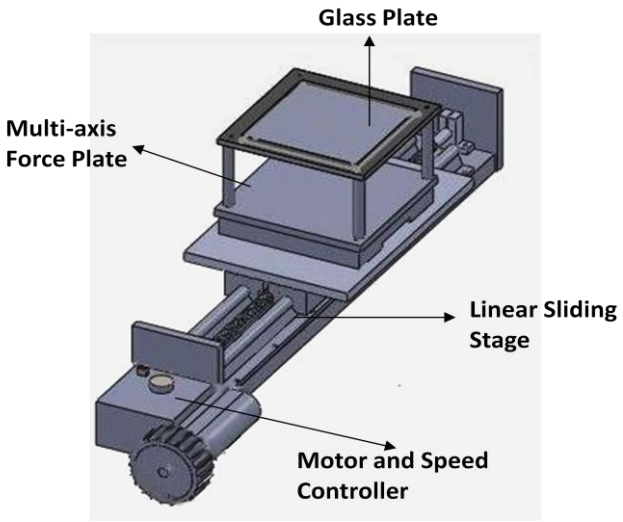

Figure 6.17: Schematic representation of the linear stage combined with the multi-axis force plate.

6.2.1.2 DIC Tests

A Digital Image Correlation system (DIC) (for more details, see Chapter 8) based on the principle of light reflection was also introduced to measure the dynamic contact area. The experiments were carried out with the same finger as in the OCT tests. The tested finger was stained with random back-spots on its surface; in this case, the contact condition between the finger-pad and the glass window could change. In the current study, the effect of the painted spots on measurements is considered to be relatively small and can therefore be neglected. The left image (Figure 6.18) is a reference image that is generally used for calibration. The middle DIC image was recorded for the middle finger in contact with the glass window. It can be clearly seen that there is a bright ellipse region on the finger-pad, which is considered as the contact region between the finger-pad and the glass window. This bright region might appear because pressing fingers onto objects hard causes the blood flow in the finger-pad to be cut so, the skin on the contact region of the finger-pad becomes relatively pale compared to other normal anatomical sites. In order to quantify the size of the bright ellipse region, the image is modified by enhancing the contrast. In the enhanced image, the contact area can be easily traced by a yellow line (Figure 6.16 (c)). The results of the contact area measured are in pixels, therefore, they need to be converted to mm^2 (1 pixel = $2.5X10^{-3}$ mm^2).

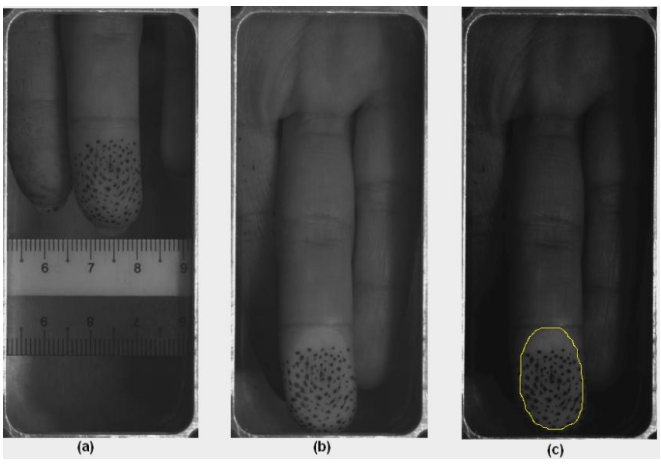

Figure 6.18: DIC images of the middle finger-pad: (a) a reference image, (b) an image for the finger pressing against the glass window and (c) an enhanced image of (b).

6.2.2 Results and Discussion

6.2.2.1 OCT Tests

Figure 6.19 shows two OCT images of the finger in contact with the glass under different contact conditions. During the preloading phase (static phase), the finger ridges came into contact with the glass surface, as shown in Figure 6.19 (a). It can be seen that the skin does not completely contact with the glass plate as some gaps were found between the skin and the glass plate. As the finger started to move against the glass plate, a friction force that rose from the relative motion and acted a surface drag. The friction force resulted in a large real contact area between the skin ridges and the glass as the finger ridges were diminished and the skin became smooth (see Figure 6.19 (b)).

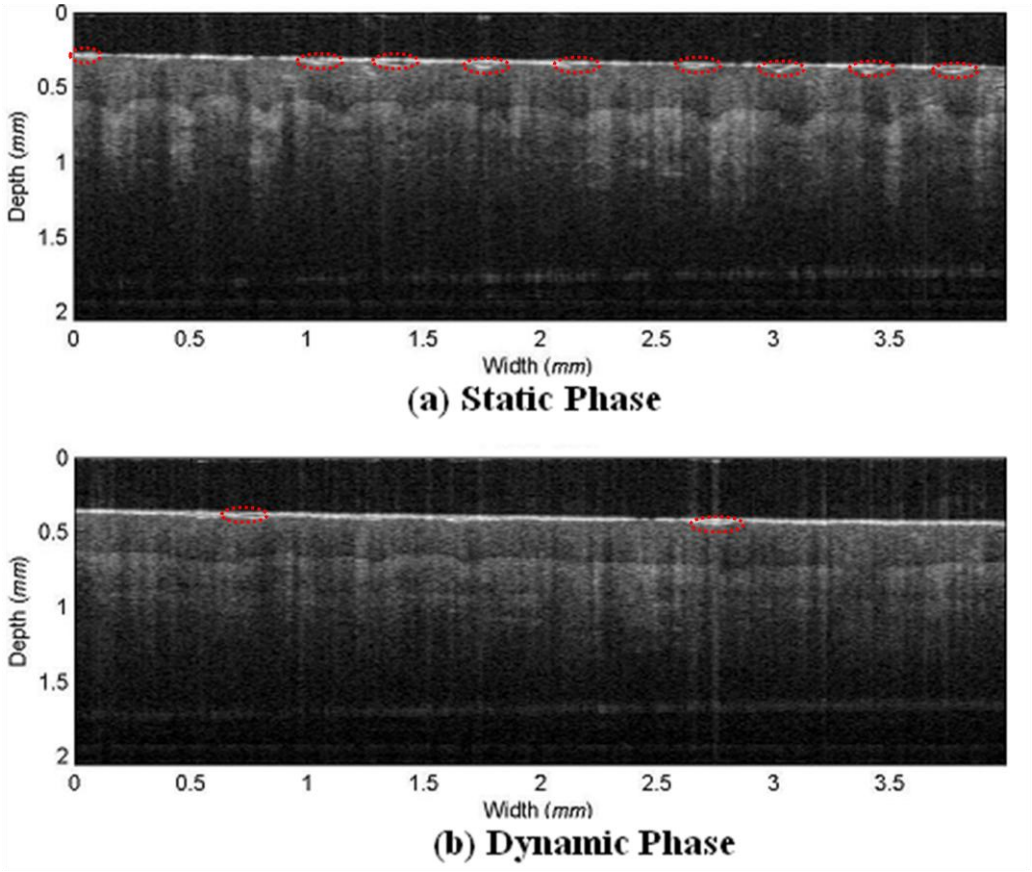

Figure 6.19: OCT images of finger skin in contact with the glass (gap between the skin and the glass plate was marked by red circle), which were obtained from (a) static phase and (b) dynamic phase.

6.2.2.2 DIC Tests

Figure 6.20 shows a schematic diagram of a finger moving along a glass plate. DIC images of the tested finger-pad were collected at different positions. Figure 6.21 displays the corresponding plot of the friction force and the normal force obtained from the multi-axis force plate during finger sliding, as well as some correlated DIC images of the finger-pad. In these DIC images, the direction of finger movement across the glass window is shown by a blue arrow. Meanwhile, the contact regions on the finger-pads were also traced by dashed lines with respect to different stages of movement.

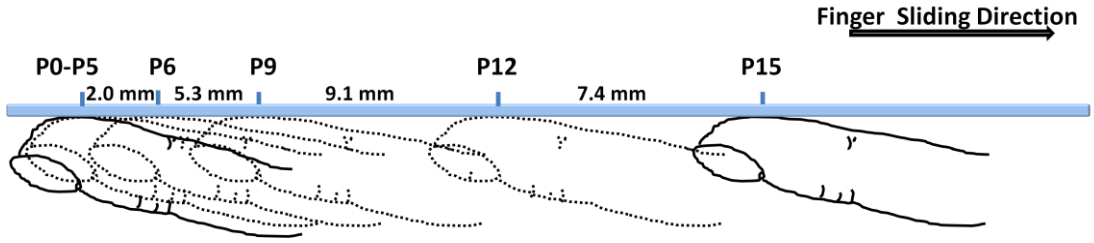

Figure 6.20: A schematic diagram showing that DIC images of a finger-pad (from P0 to P15) were taken from different positions when the finger moving along a glass plate: P0-P5 were collected from the pre-movement period, P6 was taken from the point that the finger started to move, and P9-P15 were taken from the movement period.

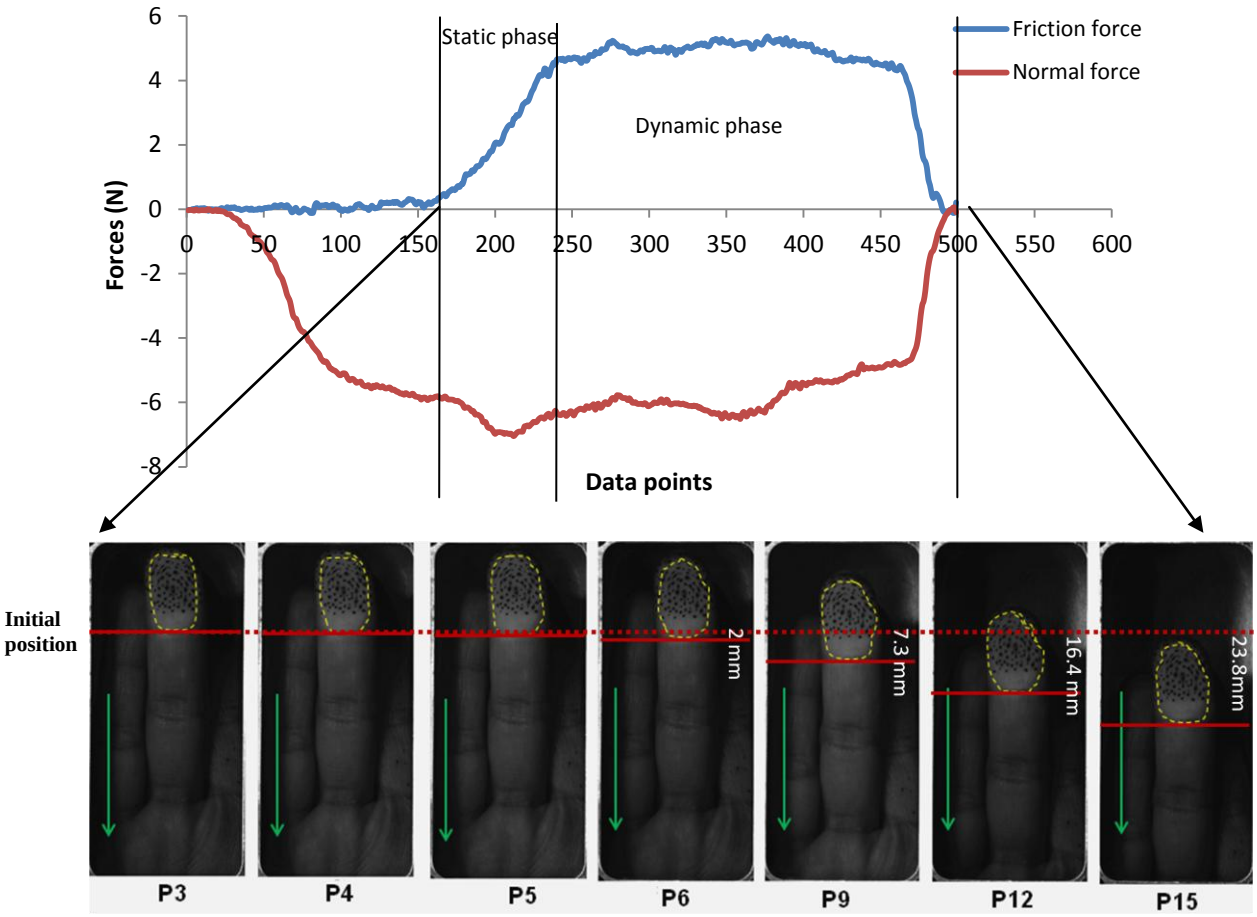

Figure 6.21: Graph showing the data of the friction force and the normal force, as well as the correlated finger-pad images from the DIC system.

These experimental results and images were divided into a static phase (adhesion) and a dynamic (slip) phase (Figures 6.22 and 23). Each phase has been assessed individually. Figure 6.22 shows the experimental results of the apparent contact area as a function of time for the finger sliding over the glass window at a constant normal force 6 ± 0.5 N. In the static phase, the contact area is found to decrease from 230 mm^2 to 214 mm^2. However, there was no significant change observed in the contact area with time in the dynamic phase. Figure 6.23 shows the time-dependent evolution of the friction force during the same period of Figure 6.22. The friction force was found to gradually increase before sliding began at around 4.9 *s*. After that, the finger started to slip with a constant friction force of about 4.8 ± 0.2 N.

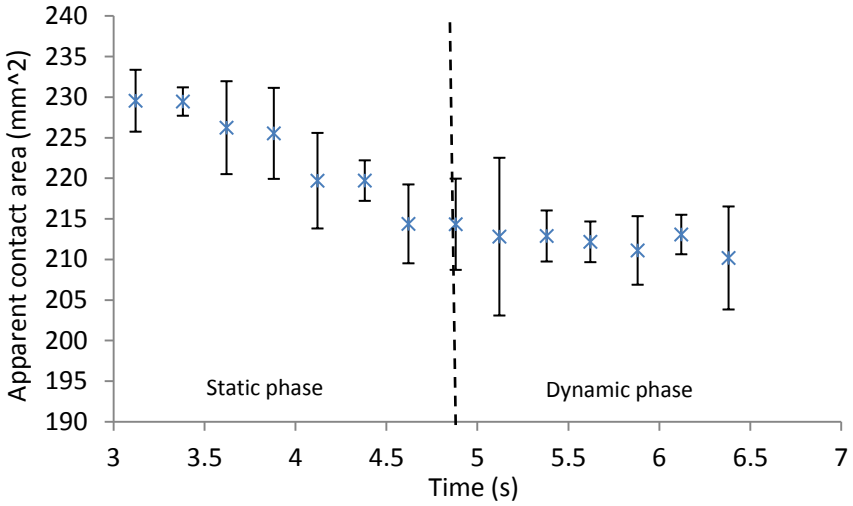

Figure 6.22: The apparent contact area as a function of time for an middle finger sliding along a glass window (mean values ± SD).

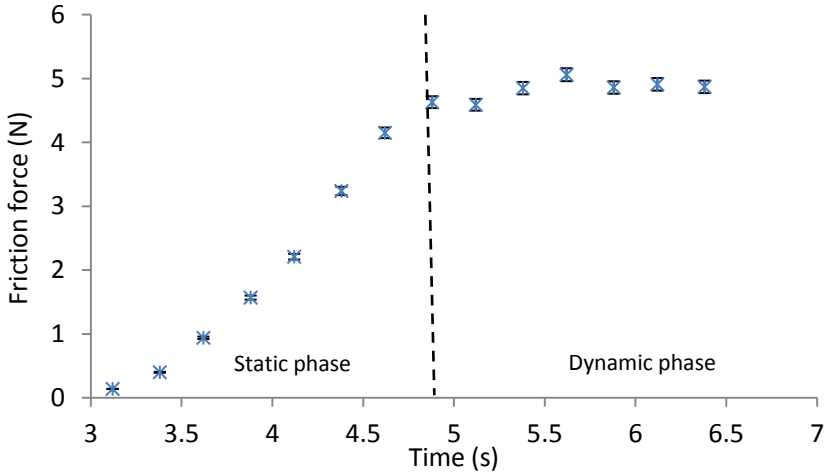

Figure 6.23: The friction force as a function of time for an middle finger sliding along a glass window (mean values ± SD).

Recently, André et al. (2008) conducted some experiments to investigate the contact mechanism of human fingers in contact with a smooth glass surface during the transition from the stuck contact to full slip, under dry and wet conditions. These experiments were performed using an optical fingerprint recording system combined with a force sensor, in which the areas of contact regions on finger-pads were present as ellipses. The experimental results showed that the normalized contact area between the examined fingertip and the prism varies with subjects. As the normal load was increased from 0.2 N to 10 N, the normalized contact area was increased by a factor of three. They also found that there is 12.5% decrease in the horizontal ellipse axis with time at a constant normal force of 5 N, which revealed that the

normalized contact area was decreased by 6.25. They suggested that the decrease in the normalized contact area during preloading may be due to the initial deformation of skin. These observations are in good agreement with the results of our studies. Figure 6.22 shows that the apparent contact area has a decrease of 7% when the middle finger moves along the glass window during the transition from the static phase to the dynamic phase. Owing to the increase in the friction force due to adhesion, the skin on the surface of finger-pads was stretched in the same direction of finger movement (lateral direction), which results in a decrease in the dimension of the contact region in the horizontal direction. However, no significant change occurred in the lateral dimension of the contact regions. With respect to more information about the deformation on skin surface of finger-pads responded to friction force, it will be discussed in Chapter 8.

From previous studies, it is noted that the friction of skin is assumed to be only associated with an adhesion mechanism in the case of fingers in contact with dry and smooth surfaces, while the deformation is normally ignored (Wolfram, 1983; Johnson et al., 1993; Adams et al., 2007). The friction force is generally reported to be proportional to the real contact area. Therefore, we can assume that as the real contact area on fingers decrease, the friction force of skin will decrease. However, in the current study, the experimental results obtained are the apparent area of contact between human finger-pads and surfaces, which could not be used to estimate the friction force based on the above theory. Terekhov & Hayward (2011) have developed a simple numerical model to characterise the friction force between a fingertip and a flat surface in the stick-slip transition. This model is given by:

$$F = \pi i g {r_s}^2 q_{stick} + \mu W (1 - {r_s}^2)^2 \quad (6.3)$$

where ${r_s}^2$ is the stick ratio of the struck region area to the total contact area (between 1 and 0); μ is the dynamic friction coefficient; and q_{stick} is the traction in the stuck area and is given by:

$$q_{stick} = (\frac{2\mu_s N}{\pi i g})(1 - {r_s}^2) \quad (6.4)$$

where μ_s is the static friction coefficient. By adding Equation (6.4) to Equation (6.3), the model could be simplified as:

$$F = 2\mu_s N (1 - {r_s}^2){r_s}^2 + \mu N (1 - {r_s}^2)^2 \quad (6.5)$$

From Figure 6.18, it can be seen that the maximum value of the static friction force is similar to the average dynamic friction force at a constant normal load of 6 N. Therefore, we can tell that the static friction coefficient (μ_s) is the same as the dynamic friction coefficient (μ) in the case of fingers in contact with dry and smooth glass surfaces. Therefore, Equation (6.5) can be expressed as:

$$F = \mu N[2(1 - {r_s}^2){r_s}^2 + (1 - {r_s}^2)^2] \quad (6.6)$$

Since the dynamic friction coefficient and the normal load are constant, it can be seen that the friction force is strongly dependent on the stick ratio (${r_s}^2$). Terekhov & Hayward (2011) indicated that the stuck contact area reduces with increasing friction force. However, this conclusion is only valid if the dynamic friction coefficient is larger than the static friction coefficient. For the case that the dynamic friction coefficient is equal or smaller than the static friction coefficient, no related discussion was given in their study. A similar conclusion was also drawn by André et al. (2008), they found that both the stick area and the total contact area decrease over time when fingers sliding along a flat surface. As the friction force increased, the stick area had a significant decrease compared to the total contact area, hence the stick ratio was shown to gradually decrease from 1 to 0. On the basis of above findings, we can suggest that the stick ratio of the stuck area to the total contact area decreases in the transition from a stuck state to full slip, and results in an increase in the friction force.

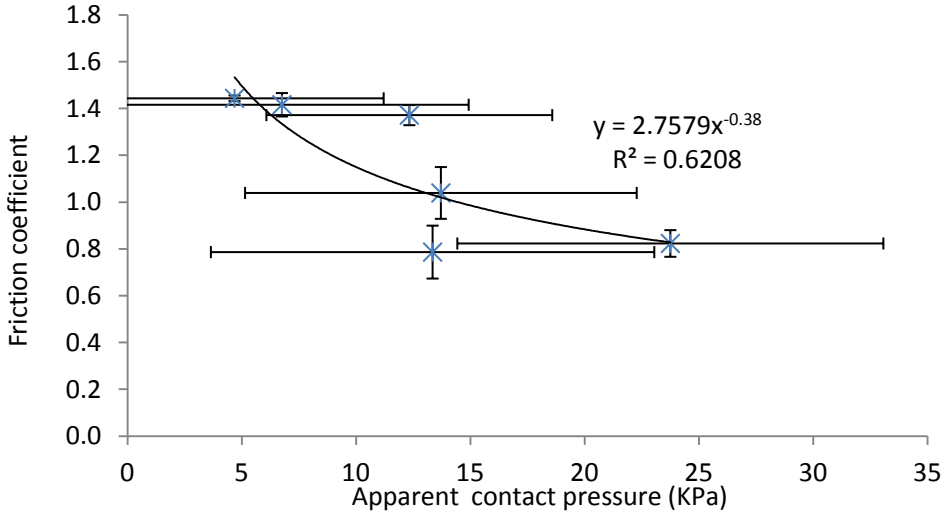

Figure 6.24: Dynamic friction coefficient measured as a function of the contact pressure applied (mean values ± SD).

From the above findings, it has been shown that the apparent contact area and the friction force vary with time in the static phase, and both of them reach steady-state in the dynamic phase. In this section, in order to gain accurate results of the contact areas and the friction coefficients, at least two DIC images with related friction data obtained from a point in the steady-state phase were analysed. Figure 6.24 shows the skin friction coefficient plotted as a function of the apparent contact pressure. These experimental data points can be fitted by a curve and described by a power-law model with the exponent of -0.38, as expected. The coefficient of determination was around 0.62. Furthermore, the skin friction coefficient was found to decrease by 42% when the apparent contact pressure increased from 4.7 kPa to 23.8 kPa.

In order to investigate the effect of the contact pressure on skin friction, Adam et al. (2007) derived an expression based on the adhesion mechanism dominating the skin friction in the case that skin is in contact with a smooth glass surface under dry conditions. This simple model is given as:

$$\mu = \frac{F}{N} = \frac{\tau_0 A_{re}}{N} + \alpha \tag{6.7}$$

where τ_0 is the intrinsic interfacial shear strength ($\tau = \tau_0 + f\frac{N}{A_{re}}$), and f is a pressure coefficient.

Figure 6.8 (a) and (b) suggest that the real contact area between human fingers and flat surfaces can be written as: $A_{re} = \rho N^c$, where ρ is a constant. Adding it to Equation (6.7), we obtain:

$$\mu = (\frac{\tau_0 \rho N^{\,c}}{N} + f) \propto N^{c-1} \tag{6.8}$$

The real contact pressure was found to increase with the normal load following a power-law model (Figure 6.9), and is given as:

$$p = kN^b \tag{6.9}$$

where *k* is a constant. Therefore, the relationship between the skin friction coefficient and the real contact pressure could be described as follows:

$$\mu \propto p^{(\frac{c-1}{b})} \tag{6.10}$$

According to the results in Figure 6.8, the exponent *c* related to the real contact area is found to be 0.66 at load between 0.4 N and 1.8 N, and 0.46 at load between 3 N

and 24 N. The value of the exponent b is 0.66. The exponent of P in Equation (6.10) is calculated to be -0.51 at the low load condition, and -0.83 at the high load condition. Compared to the results measured directly from the DIC tests, the value of the exponent p obtained from Equation (6.10) is relatively large. This observation could be explained by the fact that the values of these parameters used in Equation (6.10) were derived from the measurements of static contact areas, which are different from those in the DIC tests. As suggested by Figure 6.22, the dynamic areas of apparent contact are always smaller than the static areas of apparent contact. A similar phenomenon should be expected in the real contact area. These differences in the real contact area between the static and dynamic movements contribute to different values for the exponents b and c, thus result in different exponents of p.

Soneda & Nakano (2010) also used a similar model $\mu \propto p^{-(\frac{1-n_{ap}}{1-n_{re}})}$ (where n_{ap} is the exponent related to the static area of apparent contact and n_{re} is the exponent related to the static area of real contact) to analyse the relationship between the skin friction coefficient and the contact pressure. For loads between 0.1 N and 10 N, the exponent of p was calculated to be -0.67, which was within the range of our results in the current study. A similar study was also carried out by Derler et al. (2008), in which subjects rubbed their index fingers and the edges of hands against smooth glass and rough glass with loads up to 50 N, under dry and wet conditions. They found that the skin friction coefficients for both anatomical sites decrease with increasing the contact pressure in accordance with the model of $\mu \propto p^{c-1}$. The exponent $c-1$ was found to be ranged from -0.79 to -0.96 for the case that dry fingers were dragged along a smooth glass. The corresponding value of exponent $c-1$ was between -1.05 and -1.42 under wet sliding conditions. It is interesting to note that these results related to dry sliding condition are close to these calculated results in this section. Additionally, it can be seen that Derler's model is slightly different from the model in the current study, because the model derived by Derler et al. (2008) was under the assumption that the contact pressure is independent on the normal load. However, in the current study, it is shown that the contact pressure is strongly associated with the normal force in a relationship represented by a power function rather than a linear function (Figure 6.9).

6.3 Conclusions

In this chapter, three different techniques have been introduced to investigate the contact area between finger-pads and smooth glass surfaces. With respect to the fingerprint ink method, the experimental results suggested that the data points of the real contact area and the apparent area are in good agreement with power-law relationship under both low and high load conditions. The corresponding exponent values of c were smaller than 2/3 suggested in Hertzian theory. In the case of investigating the effect of the finger angle on the skin friction, it was found that as increasing the finger angle from 15˚ to 60˚ the skin friction coefficient decreased by 42%. It has also been shown that the OCT method is an effective way for measuring the real contact area between these asperities on skin surface and objects. The final part of this study has assessed the dynamic contact area using the DIC technique, as well as the pressure dependence of skin friction coefficient. The dynamic contact area was found to reduce with time in the transition from the static phase to the dynamic phase. As expected, the pressure dependence of skin friction coefficient was in accordance with a power-law expression with an exponent of -0.38.

Chapter 7

Investigation of Water Hydration on the Skin Friction of Finger-pads

As previously discussed, human skin is sensitive to environmental conditions and hard to maintain in a "dry" condition. It is found that the skin friction varies with different moisture levels of skin. Three different relationships (i.e. a linear, a power-law, and a bell-curved relationship) have been generally proposed to describe the hydration dependence of the skin friction coefficient (Cua et al., 1990; Sivamani et al., 2003; Adams et al., 2007; Gerhardt et al., 2008; André et al., 2009; Tomlinson et al., 2010; Hendriks & Franklin, 2010). For example, Cua et al. (1990) found a significant linear relationship between the skin hydration and the skin friction coefficient for both young and old groups. Sivamani et al. (2003) reported that the dynamic friction coefficient for the hydrated abdomen skin gradually decreases from 0.35 to 0.2 (pre-hydration value) after water exposure. Adams et al. (2007) and Tomlinson et al. (2010) observed a "bell curve" response in the friction coefficient with respect to different contacting materials and hydrated fingers. The experimental results showed an initial increase in the skin friction with increasing soaking time and then a decrease once the skin reaches its maximum hydration balance. Three possible mechanisms have been proposed for the friction increase: water absorption, viscous shearing of liquid bridges and capillary adhesion (Dinc et al., 1991). Tomlinson et al. (2010) carried out various tests on investigating the effect of the skin moisture on the skin friction with respect to each mechanism. After being fully analysed, water absorption was the main contributor of the change on the skin friction coefficient. In the case that fingers were soaked in water, there would be some changes to the skin mechanical parameters (e.g. stiffness, Young's modulus) and contact parameters (e.g. contact area, applied load) caused by water being

absorbed into the skin, which could impact the skin friction coefficient. They also proposed that, when water was added to skin, the skin would swell and became soft and smooth, leading the stiffness and/or roughness of the skin to decrease, hence increasing the area of contact. However, there seems to be little work carried out on the skin structure-related changes.

The aim of this chapter is to extend further understanding of the effect of the skin hydration on the skin frictional behavior by investigating some related changes of the skin structure and the mechanical properties. Firstly, measurements of the thickness of the stratum corneum in combination with skin friction tests were carried out. Experiments were then conducted to assess the effect of the skin hydration on skin mechanical properties using a "*cutometer*" device. A further study was carried out to investigate how the contact area between finger-pads and contact surfaces is altered with skin hydration.

7.1 Experimental Materials and Methods

7.1.1 Measurements of Skin Friction Coefficient and Stratum Corneum Thickness

These experiments were carried out on the index fingers of the dominant hands of two healthy subjects. The tested hands were washed with soap and dried in air for 30 minutes before the test. The subjects were required to soak their index fingers in tap water for various periods of time, up to 3 minutes, and then to dry off any surface water using paper towels. In order to avoid water evaporating, these tested fingers were then immediately moved to the work plate and scanned by the OCT system. Finally, the corresponding friction coefficient was measured using the multi-axis force plate (discussed in Chapter 3). Measurements were made at a normal load of 1.5 N ± 0.2. The moisture level of skin with respect to different periods of hydration was also recorded using a "Moistsense" (Tomlinson, 2009), prior to the friction measurement. The time delay between skin hydration and friction measurement was approximately 15 s ~ 30 s.

7.1.2 Measurements of Skin Mechanical Properties

To investigate the effect of skin hydration on the mechanical properties of finger-pad skin, the right index finger of participant 1 was investigated using a non-invasive

"*cutometer*" MPA 580 (details have been described in Chapter 3). The subject was requested to prepare the finger tested following the same procedure as that of the friction measurement.

7.1.3 Measurements of Contact Area

The measurement of contact area was also carried out on the index finger of participant 1 using the OCT system. More details about the set-up of the system and image analysis have been given in Chapter 6. In the tests, the subject's finger was soaked in tap water and then dried off skin surface water with paper towels. The measurements of the contact area were taken by pressing the dried and soaked finger against the glass window of the multi-axis force plate. The normal force applied was 1 ± 0.1 N.

7.2 Results

7.2.1 Measurements of Skin Friction Coefficient and Stratum Corneum Thickness

Figure 7.1 shows four OCT images of skin that were collected from the right index finger of participant 2 relating to different periods of time soaked in water (i.e. dry, 20 s, 120 s and 400 s). In each image, the stratum corneum layer is identified by vertical arrows, which enable the change in thickness of stratum corneum to be observed.

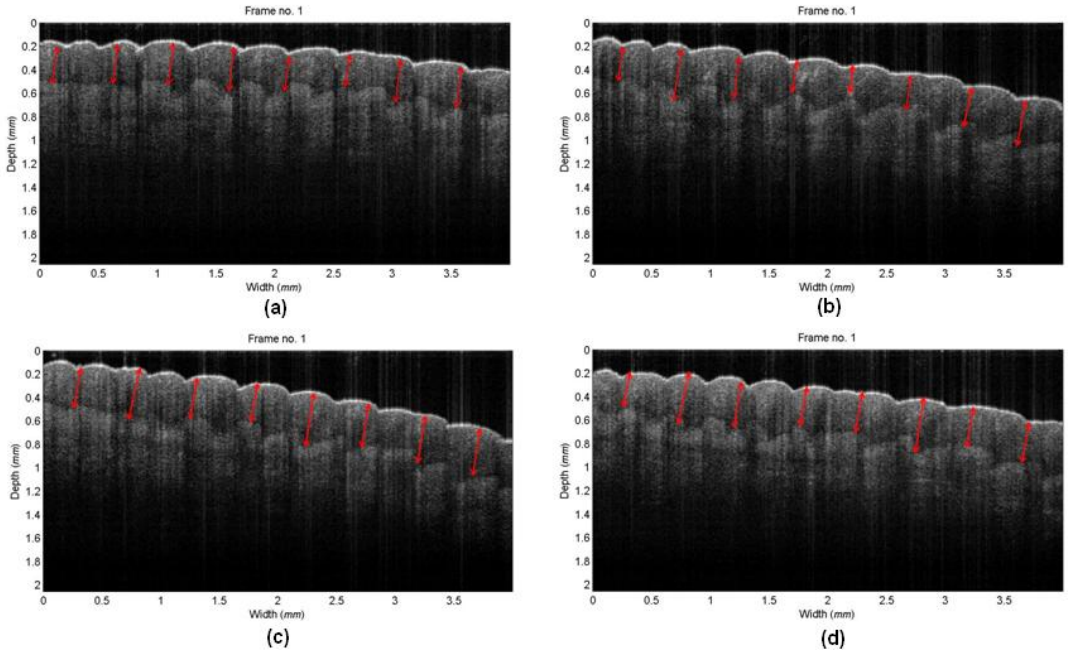

Figure 7.1: Skin OCT images for a finger of participant 2 after being soaked in water for different periods of time: (a) dry skin, (b) 20 seconds, (c) 160 seconds and (d) 400 seconds.

These changes in the thickness of the stratum corneum with respect to the soaking time were quantified and plotted in Figure 7.2(a). It was found that the thickness of the stratum corneum is increased by 16 ± 1% when increasing the soaking time for both subjects as expected. In the natural state, the thickness of the stratum corneum was found to be 0.2 *mm* in the male and 0.32 *mm* in participant 2 and it rose to 0.234 *mm* in the male and 0.37 *mm* in the female after being soaked for 400 seconds. The skin seems to become saturated after 120 seconds of hydration as no significant change was observed in the thickness of the stratum cornuem for both subjects. Furthermore, the surface texture on the skin is unlikely to be affected by the absorption of water as no significant change was observed on the surface ridges.

Figure 7.2 (b) shows plots of the moisture level of skin as a function of hydration time for both subjects respectively, in which two non-linear relationships are observed. In the natural skin conditions, participant 1 has a higher moisture level of skin (70 AU) than that of participant 2 (40 AU). The moisture level of skin is increased by 10% in participant 1 and 80% in participant 2 after 80 s of hydration. In the test done by the female, the result shows that the moisture level of skin has a rapid increase at the beginning, and then levels off at around 70 AU with soaking time. This could be due to the keratinocytes in the upper layer of skin (stratum

corneum) reaching a hydration-balance and being unable absorb more water, thereby the moisture level remains constant between 80 s and 160 s. After that, the skin may become over-hydrated and begin to reduce the capacity of water-binding, which will cause the moisture level to slightly drop and reach a plateau. A similar phenomenon was also found in the case of the male. However, the corresponding moisture level of skin was found to decrease from 70 AU to 50 AU when the tested finger was initially soaked in water for 5 seconds.

The corresponding changes in the skin friction coefficient for the fingers soaked in water are presented in Figure 7.2(c). It can be seen that both figures are very similar to those of the skin moisture (Figure 7.2(b)), i.e. there is an initial decrease in the skin friction coefficient for the male, which corresponds to these starting points in Figure 7.2(b). After then, the friction coefficient starts to increase and then decrease and reaches a plateau related to the moisture level of the skin. By analysing the figures of the friction coefficient, it was noted that there is 25% increase in participant 1, 35% in participant 2 when the tested fingers were saturated, which indicates that the frictional properties of the finger-pad skin appear to be more easily influenced by water in the female. In addition, the friction coefficient for participant 1 is approximately three times higher than that of participant 2 under both natural and wet skin conditions.

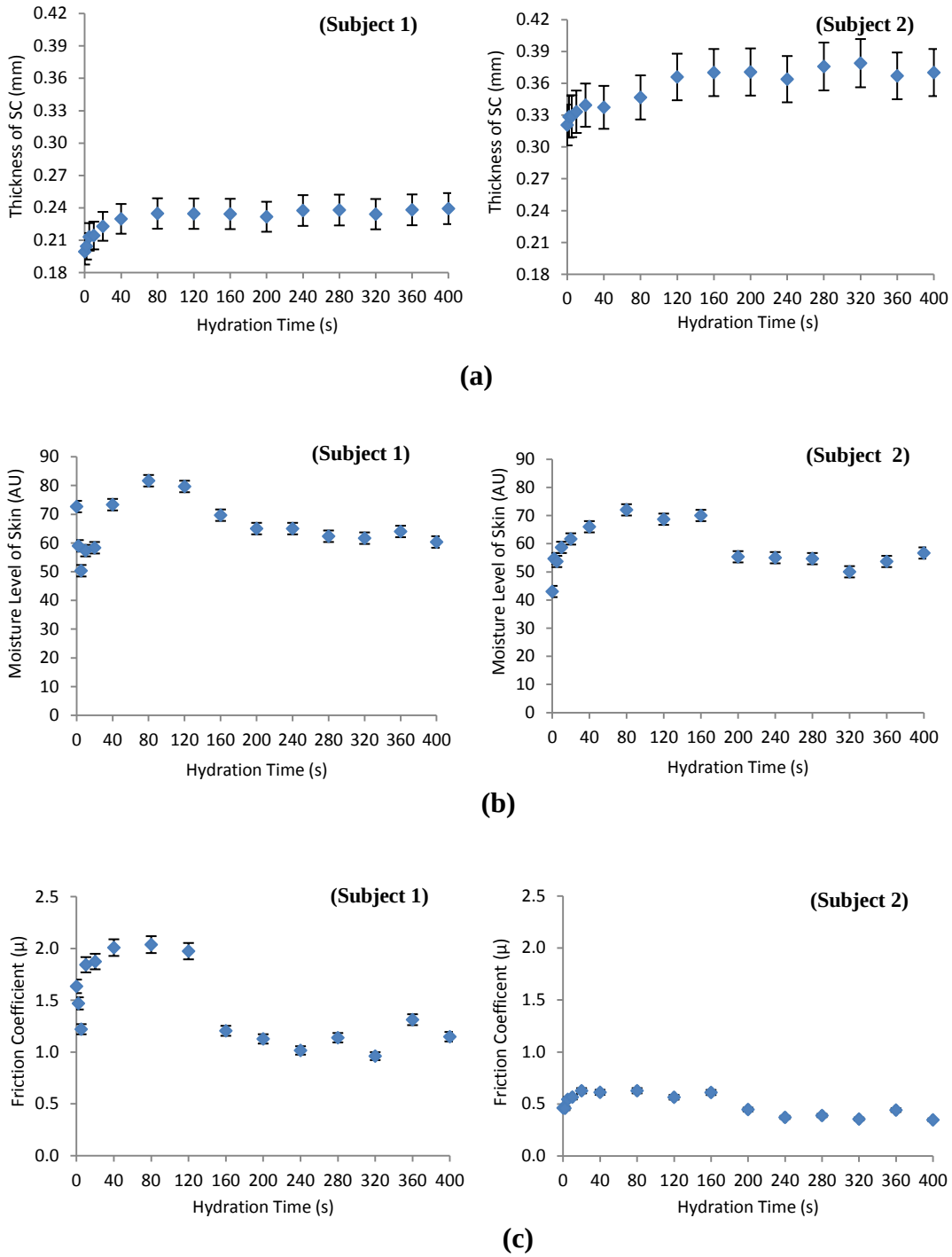

Figure 7.2: Relationships between (a) the change of the thickness of the SC and hydration time, (b) the moisture level of skin and hydration time, and (c) the friction coefficient of skin and hydration time.

7.2.2 Measurement of Skin Mechanical Properties

To investigate the effect of skin hydration on the mechanical properties of finger-pad skin, some cutometer-specific parameters relating to the skin deformation, elasticity

and viscoelastic properties (i.e. U_f, U_r/ U_e, U_a/ U_f, U_v/ U_e and U_r/ U_f) were analysed, as shown in Figure 7.3. The total skin deformation (U_f) was found to decrease from 0.15 *mm* to 0.11 *mm* when increasing the hydration time. After being hydrated for 120 seconds, the deformation of skin gradually returned to the initial value. There was an opposite phenomenon found in the global elasticity of skin (U_r/ U_e), in which the global elasticity initially increases to a peak of 0.7 between 120 s and 160 s, after that it starts to decrease down to 0.5 with hydration time (Figure 3 (b)). Figure 7.3 (c) shows that the net elasticity (U_a/ U_f) is unlikely affected by water hydration. The ratio of the viscoelastic to the elastic distension (U_v/ U_e) was found to be independent on the epidermal water content. It can also be seen that there is a significant decrease on the parameter of U_v/ U_e with hydration time in Figure 7.3 (d). With respect to the biological elasticity of skin (U_r/ U_f), it was found that the value of U_r/ U_f slightly increases from 0.17 to 0.22 after application of water.

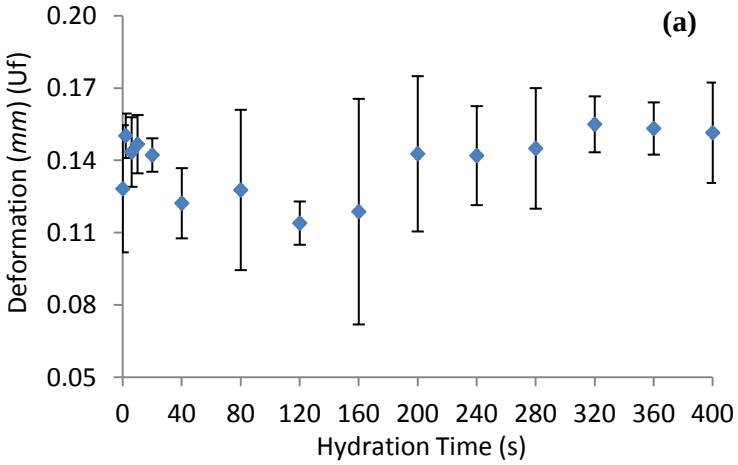

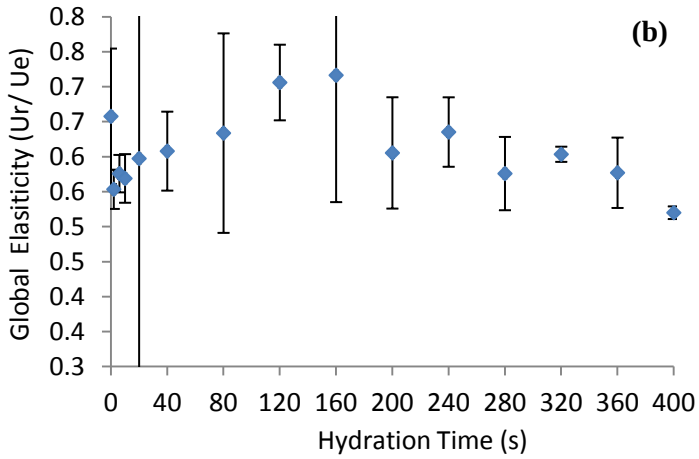

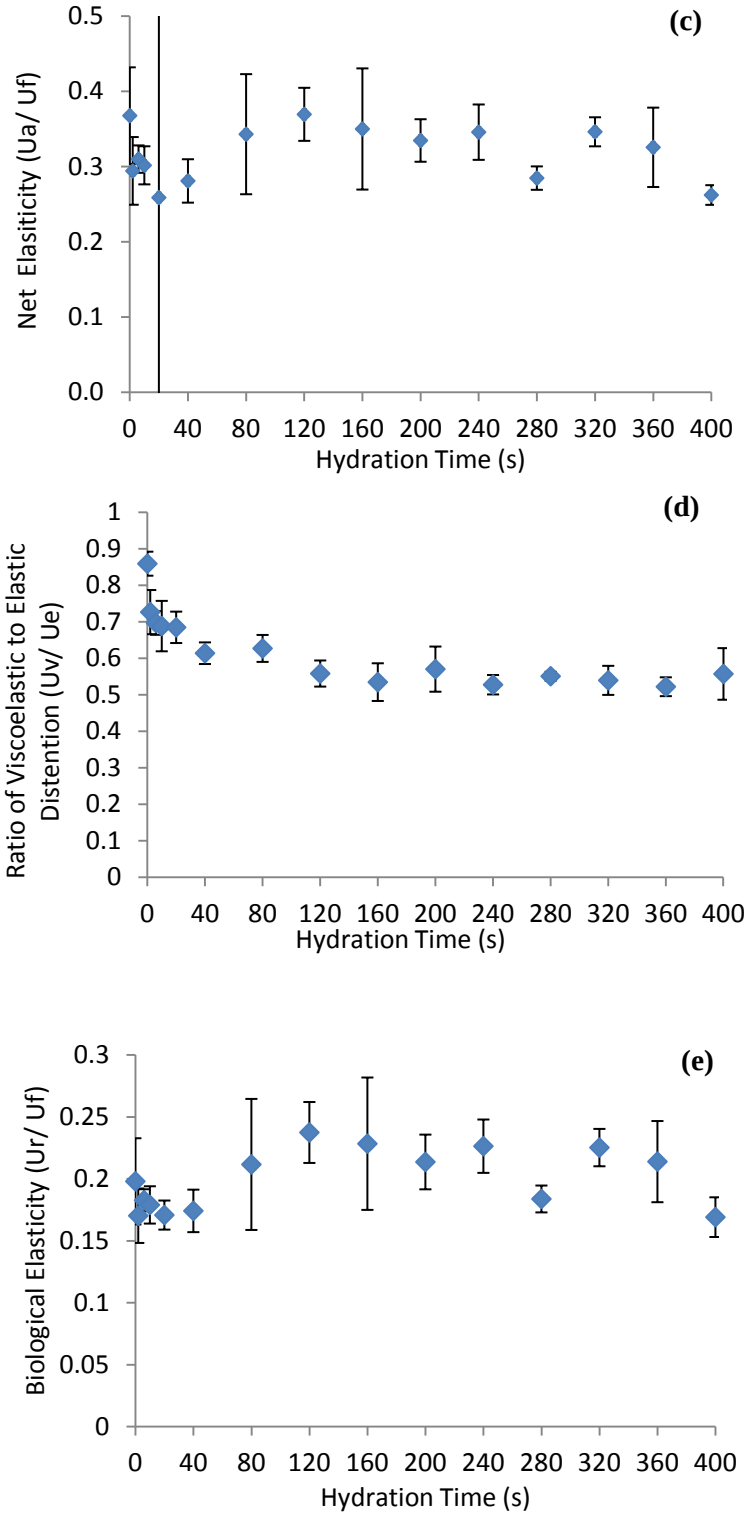

Figure 7.3: Some cutometer-specific parameters versus hydration time for a finger-pad was soaked in water.

7.2.3 Measurements of Contact Area

Figure 7.4 shows four OCT skin images of a finger-pad in contact with a glass window (0.2 N load applied) with respect to different periods of hydration time; the

top superimposed line represents the ridge boundary at skin surface, and the bottom one within the living epidermis is the papillary layer. When increasing the hydration time, more and more skin tissue will be expected to be involved in contact with the glass plate, which will result in an increase in the contact length between the finger skin and the glass surface. This assumption is proved to be true by the results of experiments in the current study. As can be seen in Figure 4.5, the ratio of the real contact area against the nominal contact area is around 0.4 for the natural finger. When the finger was soaked in water, the corresponding ratio was found to increase to 0.5 for 20 s hydration, 0.57 for 80 s and 0.64 for 400 s hydration, respectively.

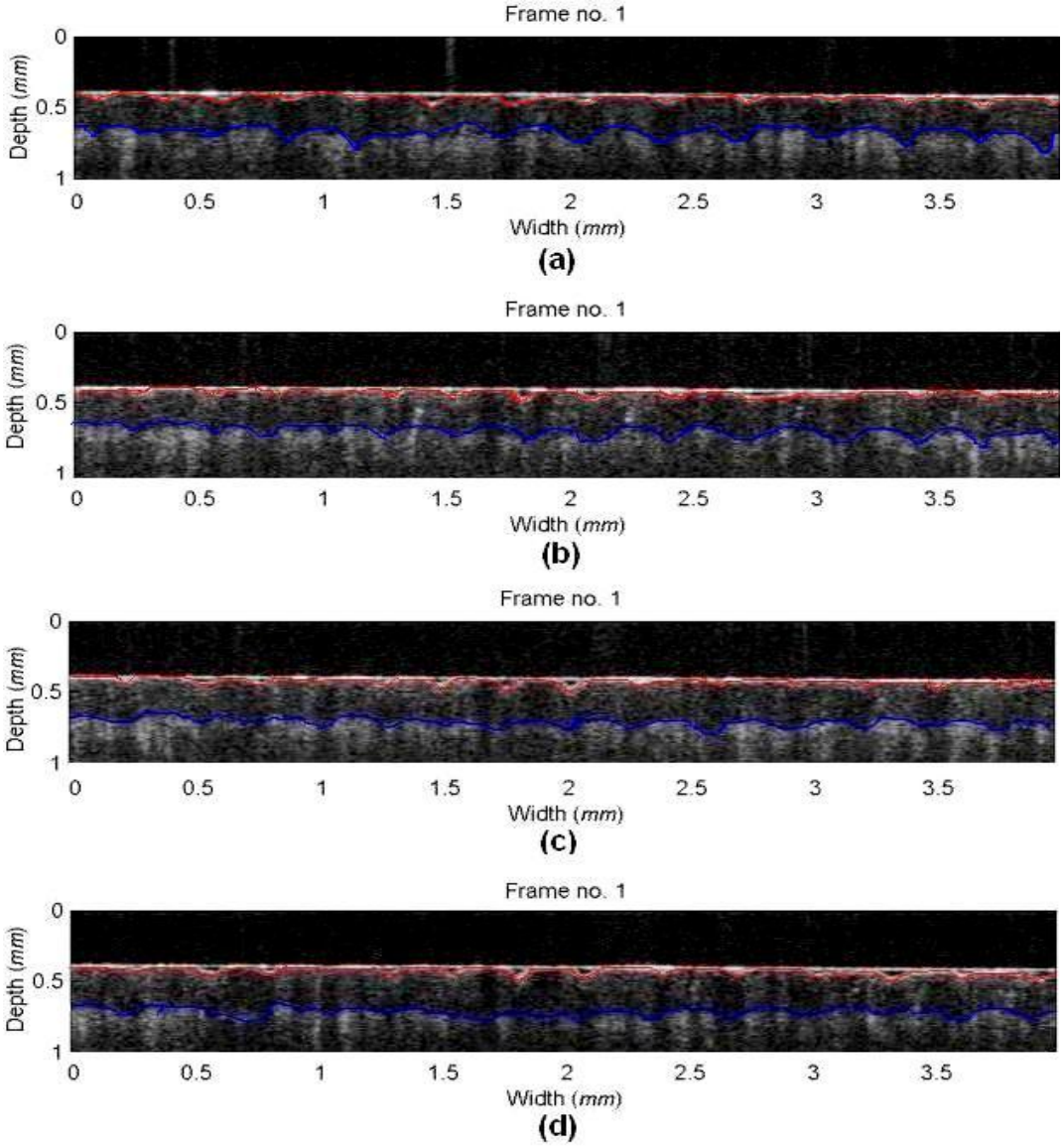

Figure 7.4: The OCT images for a dried and hydrated finger in contact with a glass plate (0.2 N load applied) with respect to different periods of hydration time: (a) dry skin, (b) 20 seconds, (c) 80 seconds and (d) 400 seconds.

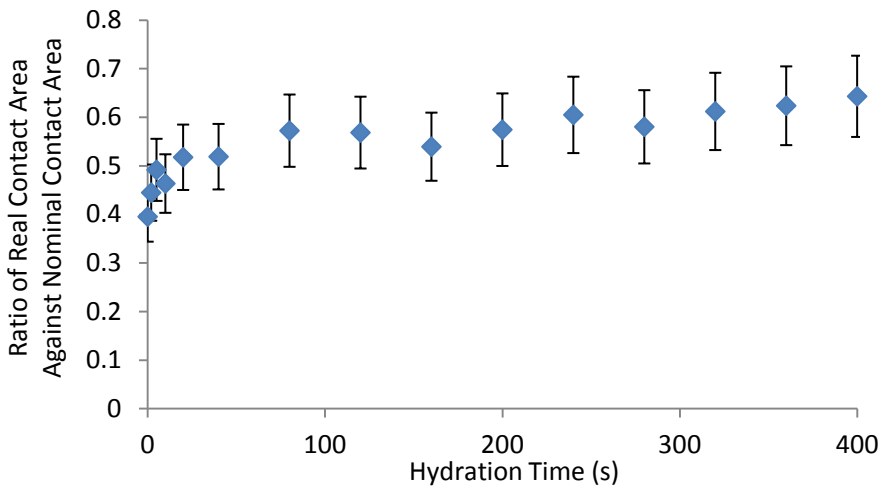

Figure 7.5: The plot of the ratio of real contact area to nominal contact area with hydration time.

7.3 Discussion

7.3.1 The Effect of Skin Hydration on the Skin Friction Coefficient

The results of the friction measurements show that there is a curved relationship between the skin friction coefficient and the hydration time for both participants (Figure 7.2 (c)). In a similar study of Tomlinson et al. (2010), a finger examined was soaked in tap water for different times and dried with paper towels prior the friction tests. The results of their experiments indicated that the skin friction coefficient has an initial increase with hydration time and reaches a plateau after 30 s, which is in good agreement with the corresponding results of the current studies. However, the corresponding skin friction coefficient with long period hydration (over 3 minutes) was not tested. This could be the reason why no bell curve response is found in their study. Additionally, the friction coefficient reported in the current study is relatively smaller than that in the study of Tomlinson et al. (2010), particularly for participant 2. This difference in the skin friction coefficient could be attributed to different fingers, as well as different experimental conditions (e.g. load applied, hydrating time and participants).

This curved relationship between the skin friction coefficient and the hydration time in the current study was found to be in accordance with the "bell-shape" distribution reported by Adams et al. (2007), who investigated the skin frictional behaviour for a polypropylene probe sliding against human forearms. They found that the skin

friction coefficient increased from 0.2 to 4.2 when demineralised water was directly applied to the inner forearm using syringe, and returns to the value for dried skin as water removed from the skin. It is surprising to observe a similar frictional behaviour response to skin hydration using different experimental methodologies. In the current study and Tomlinson et al. (2010), skin friction experiments were designed on the basis of water absorption being the only possible cause of the skin friction increase as most surface moisture was removed using towel drying. In the studies of Adams et al. (2007), however, there were several mechanisms that could possibly influence the experimental results. As adding water directly to the examined skin surface during sliding movement, the skin became soft due to a part of the water being absorbed by the human skin, and thereby contributing to the increase in the contact area and the skin friction coefficient. With respect to the water that had not permeated into the skin, it forms "liquid bridges" between the finger ridges and the contacting surface, which may make some contributions to the increase of the friction coefficient due to the viscous shear stress being increased. The contact area in this case might increase and cause the increase of the capillary adhesion as well. Consequently, several different physical mechanisms have been assumed to be able to contribute to the changes in the friction coefficient, the similarity of results obtained from these two different experiments reveals the hypothesis that water absorption has a large impact on the skin friction is true.

Other authors (Gerhardt et al., 2008; Tomlinson et al., 2010; André et al., 2009) investigated the relationship between skin moisture and skin friction, rather than that between the hydration time and the skin friction. For example, Gerhardt et al. (2008) conducted a study on investigating the effect of epidermis moisture on the skin friction against a hospital textile. They found a highly positive linear correlation between the skin hydration and friction coefficient for all participants. Hendricks & Franklin (2010) have examined the effect of climate conditions on the skin friction coefficient. They suggested a power-law relationship between the skin friction coefficient and the skin moisture level at the forearms of participants, and a linear relationship at the anatomical site of cheeks. However, these observations are not consistent with the findings in the study of Tomlinson et al. (2010), who examined how the skin friction coefficient is altered with different levels of skin moisture in the case that fingers were brought into contact with various materials. The results of

their experiments show that the skin friction coefficients increase and reach a peak at around 90 AU, after that they start to decrease. While, it is interesting to observe that the decreasing trend in those data points beyond the moisture of 90 au is linear which matches up well to those in other studies (Gerhardt et al., 2008; Hendricks & Franklin, 2010). Unfortunately, no mechanism was given to explain this effect. In the current studies, it is believed that the investigation of the skin moisture level is difficult to predict the frictional behaviour of skin. As can be seen in Figure 7.2 (b), for the male, the skin moisture obtained (approximately 70 AU) at the hydration point of 40 s is the same as that of 160 s. However, the corresponding skin friction coefficients at these two points are different, which could be attributed to the differences on the skin structure and/or the skin mechanical properties with respect to different hydration time.

7.3.2 Morphology and Mechanical Properties of Skin

Owing to the plasticizing effect of water, the human skin surface is expected to become smoother under water treatment, thereby generating a larger contact area and skin friction. However, information on human skin structure related to water hydration is not generally available. Sato et al. (2000) have analysed the effect of water hydration on the skin texture of a rat. They observed a reduction in the roughness of the rat skin when it was immersed in distilled water. In this study, these changes on skin structure in OCT images caused by the hydration are visible to the naked eyes (see Figure 7.1). However, no significant changes were observed on the skin surface texture as expected, but in the thickness of the stratum corneum. When a finger is exposed to water, the keratinocytes of stratum corneum absorb water and swell, which leads the stratum corneum to become thicker as well as the moisture level increase (Tomlinson et al., 2010). These surface ridges, as they are known, form corresponding to the pattern of the papillary layer (Wood & Bladon, 1985). However, due to the fact that the time scale of water hydration was not sufficient, it is believed that no (or less) water has been transmitted into the layers of living epidermis and/or dermis and alter the appearance of the skin surface. This assumption was evidenced by the findings of Bouwstra et al. (2003), who found that the swelling of cells mainly occurs in the vertical direction of the human abdomen skin. 57% and 87% water content was present in the middle cell layers of stratum corneum followed by superfacial cell layers, no swelling was observed in the deeper

cell layers. The thickness of cells was found to increase linearly as a function of hydration time. The average cell thickness in the stratum corneum was 360 ± 27 *nm* at nature state and increased to 2970 ± 260 *nm* when fully hydrated. In recent studies, Egawa et al. (2007) measured the thickness of the stratum corneum from the water concentration profile of skin using a confocal Raman spectrometer. When hydrating the skin of volar forearm for 15, 50 and 90 min, the thickness of stratum corneum was found to increase by 3%, 40% and 96%, respectively. It is reasonable to observe that the thickness of SC varies in different studies due to the skin thickness varying from person to person. These experimental findings also strongly support that the results obtained using OCT system are reliable (see Figure 7.2 (a)). Based on the above findings, it is noted that the effect of skin morphology on skin friction can be neglected in the current study since no significant changes took place on the skin surface in the short soaking time used.

Hendricks & Franklin (2010) indicated that moisture reduces the skin stiffness by at least an order of magnitude in the stratum corneum of finger-pads under humidity conditions, which leads to more skin being deformed, and therefore the contact area increases. A similar conclusion was drawn by Yuan & Verma (2006), who found the Young's modulus of wet skin is one order of magnitude smaller than that of dry skin. In the study of Adams et al. (2007), it was found that water absorption causes the skin to swell and reduces the Young's modulus, and therefore the contact area increases. Consequently, we can assume that those changes in the skin structure are due to water absorption, which has potential influences on the skin friction coefficient according to those observations in Chapters 4 and 5. Furthermore, the results in Chapter 4 indicate that both the Young's modulus and the stiffness of artificial fingers reduce when increasing their thicknesses. Therefore, in this study, a decrease in the Young's modulus of the finger-pad skin would be expected due to water absorption increasing the thickness of the stratum corneum. However, in the measurements of skin mechanical properties (Figure 7.3), where various mechanical parameters were assessed with respect to different periods of hydration, the experimental results indicate that neither the net nor the biological elasticity of skin is likely to be affected by water absorption. This could be explained by the fact that the "*cutometer*" MPA580 device allows us to measure the elasticity of the whole skin rather than individual layers of skin. It is generally believed that the dermis layer of

skin dominates the global elasticity of skin. As discussed early in this chapter, the effect of water hydration on the skin structure only occurred in the epidermis since no-water is transmitted into the dermis, therefore it is not surprised to observe no significant change on the skin elasticity in Figure 7.3.

7.3.3 Measurements of Contact Area

In previous studies, many authors indicated that the increase of skin friction is ascribed to an increase in the contact area between skin and surfaces due to skin's Young's modulus reducing with water hydration (Adams et al., 2007; Gerhardt et al., 2008; André et al., 2008; Tomlinson et al., 2010; Hendricks & Franklin, 2010; Pasumarty et al., 2011). However, there is little work that has been done at the moment. The only related work was reported by André et al. (2011), who studied the ratio of the stuck skin area to the total contact area using an optical system during a finger sliding along a glass surface under dry and wet conditions. They found that the ratio of the stuck skin area to the total contact area is strongly associated with skin friction force (discussed in Chapter 6). This ratio was found to be higher for the wet skin than that for the dry skin. Moreover, the ratio of the friction force (TF) against its ultimate value (TF during slip) was shown to reduce as a function of the hydration. However, there was no work done on the skin friction coefficient related to the skin hydration.

In the current study, we introduced an OCT system to quantify the change of the real contact area between a finger and a glass surface with respect to different periods of water hydration. Due to the fact that within the OCT system it is impossible to monitor the whole finger-pad, a small area (3.2 mm^2) on the finger-pad was selected to predict the tendency of the contact area related to skin hydration. The real contact area was determined by a reference to the contact length between the finger surface ridges and the glass window (for more details, see Chapter 6). It can be seen in Figure 7.5, the ratio of the real contact area to the apparent contact area between the finger and the glass surface increases by about 60% with hydration time, particularly in the first 80 s. Meanwhile, it is also noted that both the real contact area and the thickness of the stratum corneum experienced the same trend, which reveals that the increase of contact area could be ascribed to the decrease in the skin stiffness due to skin swell.

Since these experiments were designed based on the mechanism of water absorption, and the adhesion force was thought to dominate the skin friction, it would be expected to see that the skin friction coefficient is strongly dependent on the contact area. However, the figure (Figure 7.2 (c)) of the friction coefficient against water hydration presents a different tendency compared to that of the contact area (Figure 5), which reveals that there were other mechanisms enhancing the skin friction besides the water absorption. Masen (2011) suggested that the increase of friction coefficient of the skin related to hydration could be attributed to the increase in both adhesion and deformation. When skin is hydrated with water, it softens skin and causes the folding of the skin around the contact surface ridges, resulting in the real area of contact increasing, hence the adhesion increasing. Meanwhile, the deformation of skin will have a corresponding increase due to the further increase of area of contact associated with the adhesion (Masen, 2011).

In addition to above, Pailler-Mattei et al. (2007) suggested that the skin friction coefficient increases with removal of the thickness of the stratum corneum and they believed that the increase of the friction coefficient is associated with those changes in the physico-chemical properties of skin due to tape stripping. We can assume that there may be some physico-chemical properties of skin that are altered by water absorption, which results in some changes occurring in the skin friction. However, the measurement of changes in the physico-chemical properties of skin corresponding to water hydration is restricted due to current limited techniques.

7.4 Conclusions

This chapter presents the work on investigating the effect of skin hydration on the skin friction coefficient based on the mechanism of water absorption. The results of experiments show that the skin friction coefficient increases with hydration time (up to 400 seconds) following a “bell-shape” curve behavior. It was also found that the increase in the ratio of the real contact area to the apparent contact area is likely due to the skin swell. Under water treatment, the stratum corneum will become thick, which will lead decreases in the stiffness and the young’s modulus of the skin. It has also been shown, in addition to the mechanism of water absorption, there may be other mechanisms contributing to the skin friction.

Chapter 8

A Pilot Study to Investigate the in-plane Deformation of Finger-pad Skin in-vivo using a Digital Image Correlation System

From the findings in previous chapters and other related studies (Johnson et al., 1993; Adams et al., 2007; Pailler-Mattei et al., 2007; Kwiatkowsa et al., 2009), human skin friction is found to be associated with its deformation and mechanical properties. A number of experiments related to human skin deformation and mechanical properties have been conducted *in-vitro* and *in-vivo*. With respect to the mechanical properties, there are different techniques that have been reported to measure skin's Young's modulus and stiffness. For example, Oliver and Pharr (1992) proposed a method to investigate global Young's modulus of skin using the load-displacement sensing indentation tests. A simple model has been developed to determine the Young's modulus and was given as: $E_{skin} = {S\sqrt{\pi}}/{2\sqrt{A}}$, where S is the stiffness of skin based on a normally loaded finger-pad and A is the projected contact area. On the basis of this model, Pailler-Mattei et al. (2007) and Yuan & Verma (2006) reported that the elastic modulus of a dry stratum corneum was approximately 1 GPa using an Atomic Force Microscope (AFM) indentation. They also found that the elastic modulus of the isolated stratum corneum varies with indentation depth. Experiments performed by Barel et al. (1995) and Diridollou et al. (2000) with a suction device on a subject's volar forearm revealed that the Young's modulus of skin was equal to 130 kPa and 150 kPa, respectively. In the study of Escoffier et al. (1989), a torsion method has been applied to measure the Young's modulus of skin. They concluded that the Young's modulus is unlikely to be influenced by hypodermis and underlying tissue of skin. It is noted that most of these

experiments were limited to the investigation of the *in-vivo* normal mechanical response of skin, which cannot be used to accurately describe human skin's anisotropic characteristics.

In addition, Johnson et al. (1993) and Pailler-Mattei et al. (2007) concluded that the shear modulus of human skin (e.g. tangential stiffness and interfacial shear strength) plays a crucial role in determining its frictional behaviour. In the case of investigating the transverse mechanical properties (Young's modulus) of skin, an *in-vitro* tension test has been widely used. However, due to the difficulty of preparing human skin samples, in general, this technique uses animal skin to help estimate the transverse mechanical properties of human skin. Recently, a new non-invasive method, Digital Image Correlation (DIC), has been proposed to characterise skin transverse mechanical properties from tensile tests. The DIC system was developed from a speckle photography technique, and originally used to provide strain and displacement fields of solids, in particular metals. This technique provides the opportunity for measurements to be carried out on real human body part, without the need for strain gauging or application of needles etc. Owing to these advantages, the DIC system is gradually becoming a common method for determining the *in-vivo* mechanical response of human skin. For example, Hendriks (2005) used a 3D-DIC system combined with a purpose built tensile device to measure the *in-vivo* sub-surface deformation in human forearm. Experimental results showed that both the in-plane strain and deformation of the surface of skin decreases with increasing suction depth (out of plane). A similar study was also carried out by Evans & Holt (2009), in which adhesive tape was used to connect the tested skin surface of the tested forearm and a load cell. Skin images were acquired in all three directions when a load of 1 N was applied on the surface of the skin in a transverse direction. The corresponding maximum displacement in the loading direction was found to be 8.48 *mm*.

Though the mechanical properties of human skin have been investigated extensively, there is little work that has been reported on *in-vivo* surface deformation at human finger tissue during dynamic movements. Therefore, in this chapter, a 2D-DIC system coupled with a multi-axis force plate has been used to determine the deformation behaviour of finger-pad skin with respect to different stages of

movement when the finger slides along a glass plate. Work on the effect of load on the deformation behaviour of the skin has also been done.

8.1 Materials and Methods

8.1.1 Digital Image Correlation

Digital Image Correlation is an optical technique which can provide non-contact full-field displacement/strain measurements of the surfaces of specimens. The fundamental principle of the 2D-DIC technique is to track and match the same points in two images recorded before and after deformation based on the grey intensity variance (Sutton et al., 1983). This technique is only applicable on flat specimens with random speckle pattern on their surfaces. These patterns produce unique contrast distributions on the surfaces of specimens that can be used to evaluate the correlation between the undeformed and deformed images. Due to the difficulties that arise from the matching procedure using a single pixel or whole image to determine the correlation, the reference image is divided into a mesh of subsets (see Figure 8.1) (Hendriks, 2005; Yoneyama & Murasawa, 2011). The full-field displacement field with respect to external forces can be determined by computing the displacement of each subset.

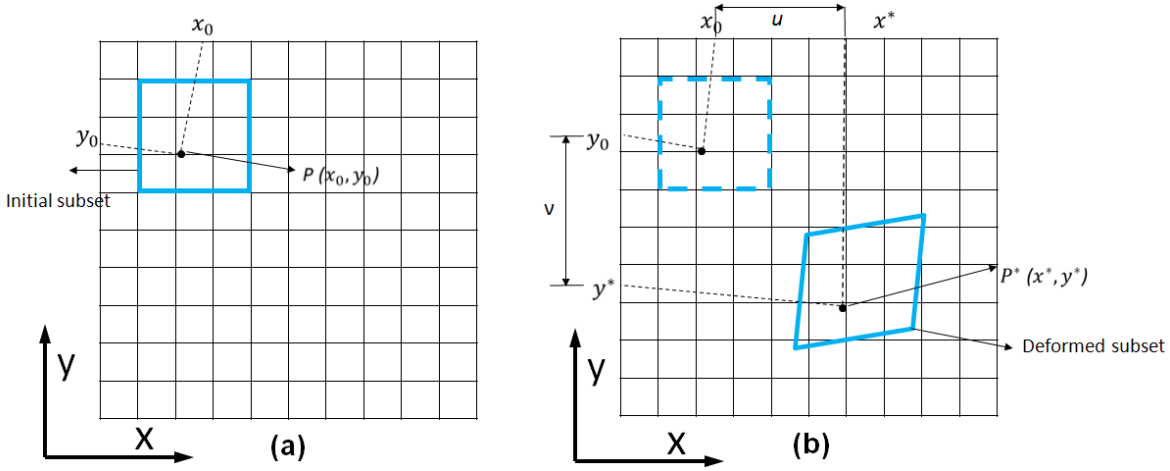

Figure 8.1: Basic Principle of 2D digital image correlation (Sutton et al., 1983).

As shown in Figure 8.1(a), a coordinate $P\ (x_0, y_0)$ is plotted in the selected subset in the initial reference image, which can be mapped to the coordinate $P^*(x^*, y^*)$ after deformation (Figure 8.1(b)). The displacement mapping function between these two coordinates is expressed as:

$$P^*(x^*, y^*) = P\ (x_0 + v(x, y),\ \ y_0 + \ u(x, y)) \tag{8.1}$$

where v and u represent two components of the displacement field. The displacement field for each subset in DIC image is assumed to be homogenous and bilinear in *x* and *y* directions (Marcellier et al., 2001; Jacquemoud et al., 2007):

$$v(x\ , y) = a_v u + b_v v + c_v uv + d_v \tag{8.2}$$

$$u(x\ , y) = a_u u + b_u v + c_u uv + d_u \tag{8.3}$$

where a_v, a_u, b_v and $b_u$are elongation terms, c_v and c_u are shearing terms and $d_v$and d_u are translation terms. The coordinate $P^*(x^*, y^*)$ can be defined using the first-order Taylor expansion:

$$x^* = x_0 + v + \frac{\partial v}{\partial x}\Delta x + \frac{\partial v}{\partial y}\Delta y \tag{8.4}$$

$$y^* = y_0 + u + \frac{\partial u}{\partial x}\Delta x + \frac{\partial u}{\partial y}\Delta y \tag{8.5}$$

where $\frac{\partial v}{\partial x}$, $\frac{\partial v}{\partial y}$, $\frac{\partial u}{\partial x}$ and $\frac{\partial u}{\partial y}$ are displacement gradients. Δx and Δy are the distances between the centre of the subset and the coordinate $P\ (x_0, y_0)$ along *x* and *y* axes respectively, which are given by:

$$\Delta x = x_0 - x \tag{8.6}$$

$$\Delta y = y_0 - y \tag{8.7}$$

The deformation of the subset-image can also be computed using the relationship between the reference image and the deformed image. The normalised correlation coefficient is expressed as (Tung & Sui, 2010):

$$NCOR = \frac{\sum g_{ij}\tilde{g}_{\bar{\imath}\bar{\jmath}}}{\sqrt{\sum {g_{ij}}^2 \sum {\tilde{g}_{\bar{\imath}\bar{\jmath}}}^2}} \tag{8.8}$$

where g_{ij} and $\tilde{g}_{\bar{\imath}\bar{\jmath}}$ are the greyscale of a reference subset-image on the coordinate (i , j) and a deformed subset-image on the coordinate ($\bar{\imath}$, $\bar{\jmath}$), respectively. There will be a perfect correlation between these two coordinates when the correlation coefficient value is equal to 1. The corresponding strain field (Green-Lagrange strain tensor E') can be expressed as a function of deformation tensor F' of displacement field:

$$E' = \frac{1}{2}(F^T \times F' - I) \tag{8.9}$$

where *I* is the unit tensor. Chu et al. (1985) derived a new model of the strain tensor *E'* related to the displacement field as follows:

$$E_{ij} = \frac{1}{2}\left(u_{i,j} + u_{j,i}\right) + \frac{1}{2}u_{k,i}u_{k.j} \tag{8.10}$$

where *i, j* and *k* ϵ(*x* , *y*) and $u_{i,j} = \frac{\partial u_i}{\partial j}$. The strain value with respect to different directions can be determined using the following equations:

$$E_{xx} = \frac{\partial u_x}{\partial x} + \frac{1}{2}\left[\left(\frac{\partial u_x}{\partial x}\right)^2 + \left(\frac{\partial u_y}{\partial x}\right)^2\right] \tag{8.11}$$

$$E_{yy} = \frac{\partial u_y}{\partial y} + \frac{1}{2}\left[\left(\frac{\partial u_y}{\partial y}\right)^2 + \left(\frac{\partial u_x}{\partial y}\right)^2\right. \tag{8.12}$$

$$E_{xy} = \frac{1}{2}\left(\frac{\partial u_x}{\partial y} + \frac{\partial u_y}{\partial x}\right) + \frac{1}{2}\left[\frac{\partial u_x}{\partial x} \times \frac{\partial u_x}{\partial y} + \frac{\partial u_y}{\partial x} \times \frac{\partial u_y}{\partial y}\right] \tag{8.13}$$

8.1.2 Experimental Set-up

In the experiments, images and force data during finger movements were recorded separately using two standard measurement systems (Figure 8.2). A 2D DIC system was used to record the images of finger-pad skin throughout the tests. The 2D DIC system consists of a 5MP AVT Pike camera (2452 X 2054 pixels), a computer and two white-light sources (one white-light source is out of the picture). The Pike camera is capable of high speed flash synchronization at full resolution. In the current study, the frame rate applied was set to be 6.7 frame/s. All required images were analysed using a commercial DIC software package (Vic-2D, 2007, Correlated Solutions, Inc). A multi-axis force plate combined with a metal frame and a glass insert used to measure the forces applied (details have been discussed in Chapter 6).

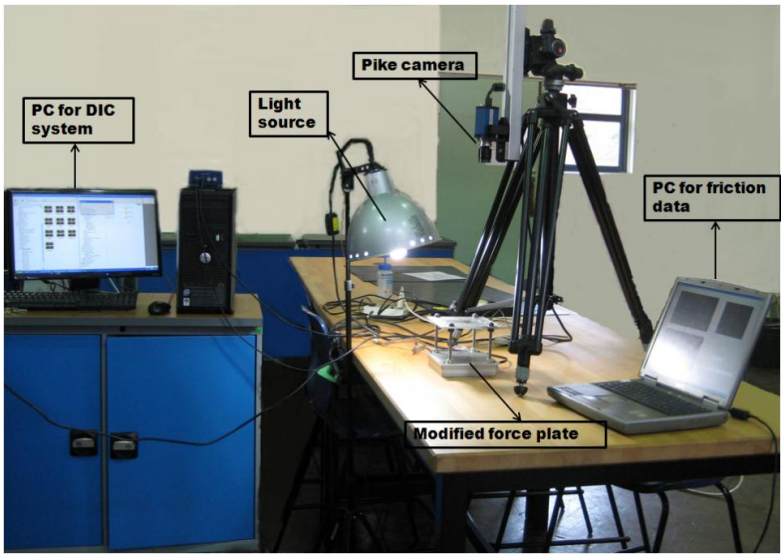

Figure 8.2: Experimental set-up of a 2D optical image acquisition system.

8.1.3 Experimental Procedure

Experiments were carried out on the right middle finger of a 26 year-old female. Prior to the tests, the tested finger-pad was requested to be cleaned and random black-dots were applied, as seen in Figure 8.3 (a). In order to image deformations occurring on the finger-pad skin at various stages of movement, the subject was requested to press her finger against the bottom of the glass window and face up to the camera. To assess the effect of normal load on the deformation behaviour of skin, this experiment was also repeated under different loads. All measurements were conducted at a constant speed around 10 ± 2 *mm/s*.

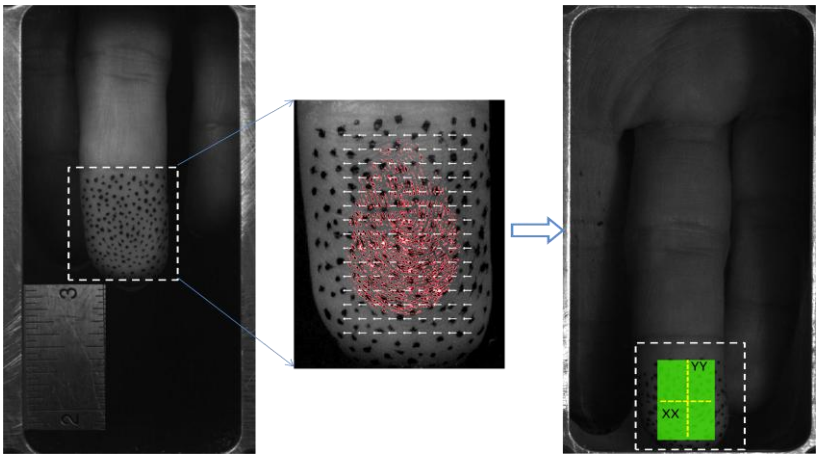

(a) (b) (c)

Figure 8.3: DIC images of the middle finger-pad: (a) a reference image, (b) area of analysis on the finger-pad (red region represents the initial area of contact) and (c) two centre lines were plotted along XX and YY axes.

In later image analysis, as can be seen in Figure 8.3 (b), there was an initial contact between the finger-pad and the glass plate when the finger came into contact with the glass (approximately 133.5 mm^2 at 0.2 N). A rectangular region on the finger-pad for all images was selected and analysed (10 X 17 mm^2). Furthermore, this window was divided into a mesh of subsets (40 X 40 pixels) in order to gain the correlation between the images acquired before and after deformation. To quantify the deformation behaviour of finger-pad skin at each stage during sliding movement, two lines across the centre of the finger-pad were drawn (XX (horizontal direction) and YY (the direction of finger movement)), see Figure 8.3 (c). With respect to each centre line, there were 100 points were selected along the line for analysis. Due to the fact that the initial area of contact was about 80% of the selected rectangular region, the measurement of strain data took place mainly between point 10 and 90 in both centre lines.

8.2 Results and Discussion

In the current study, all experiments have been performed on a "dotted" finger-pad that was sliding along a smooth and transparent glass plate. Figure 8.4 shows three vector displacement maps of the examined region on the finger-pad along XY axis, with respect to different stages of finger movement. The initial image (Figure 8.4(a)) was taken when the finger was flattening with glass (at 0.2 N), in which minor deformation was observed on the finger-pad skin. When the finger came into contact with the glass window (static phase) and started to move (dynamic phase), the patterns on the skin moved over the imaging area, which resulted in some distortions in both XX and YY directions (see Figure 8.4 (b) and (c)). These distortions can be used to estimate the motion of the finger-pad skin regarding to finger movements, i.e. it can be seen that there is a significant motion in the XX direction in the displacement map (Figure 8.4 (b)) of the finger-pad corresponding to the static phase by comparing to the initial one. This means that localized deformations mainly occur in the XX direction on the finger-pad skin when a finger only experiences a normal force. While in the case that the finger is sliding over a surface, a friction force between the finger skin and the surface emerged that led to some distortions in the YY direction on the skin.

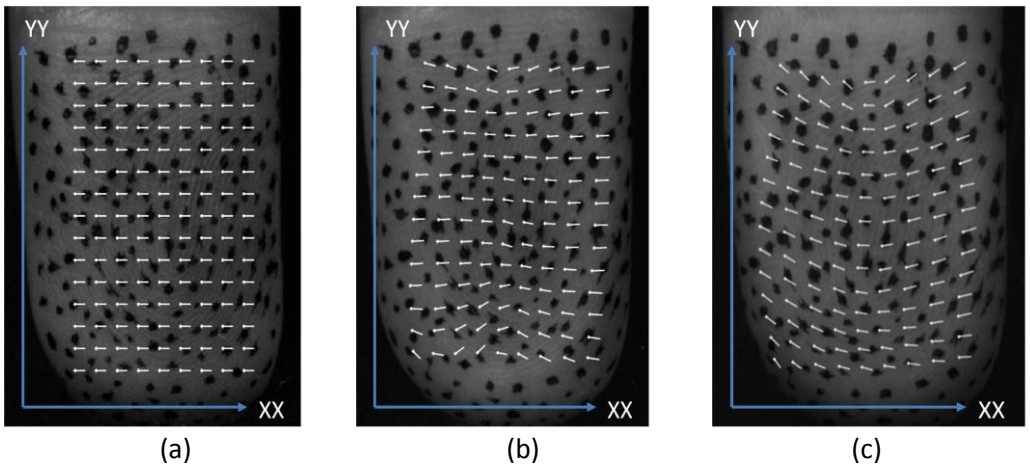

Figure 8.4: Displacement field of a finger in XY axes corresponding to: (a) finger is flattening with glass with minor deformation, (b) finger in contact with glass without movement between interfaces (static phase), and (c) dynamic movement.

Figure 8.5 shows a schematic diagram of a finger moving along a glass plate, in which DIC images of the tested finger-pad were identified at different positions. Image P0 to P15 were collected from the pre-movement period, P16 was taken from the point that the finger started to move, and P17 to P56 corresponds to a dynamic movement.

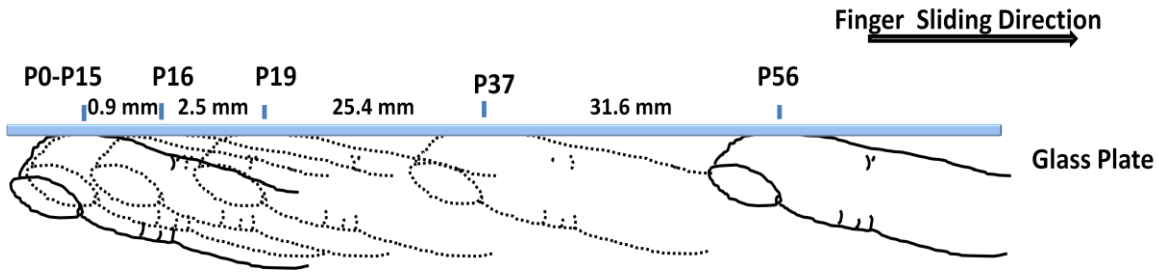

Figure 8.5: A schematic diagram shows that DIC images of a finger-pad (from P0 to P56) were taken from different positions when the finger moving along a glass plate: P0-P15 were collected from the pre-movement period, P16 was taken from the point that the finger started to move, and P17-P56 were taken from the movement period.

Skin mechanical properties corresponding to those planar skin deformations on skin surface can be quantified using full-field strain maps. Figure 8.6 illustrates the results of the strain data that were obtained from the measurement conducted along the horizontal direction on the tested finger-pad skin under different load condition, where a horizontal line across the middle of the imaging region was drawn to help measure the change of strain value on the skin. These corresponding strain data

produce a wave-shape line, which means skin stretches mainly exist around the left and right edge regions in the imaging window. The local highest strain value can reach around 22% when a low force (approximately 1 N) is loaded on the texted skin. The centre region of the finger-pad skin with strains around 2.5 % is rarely influenced by external forces. It was also found that the values of the strain across the finger-pad skin increase when the normal load increases.

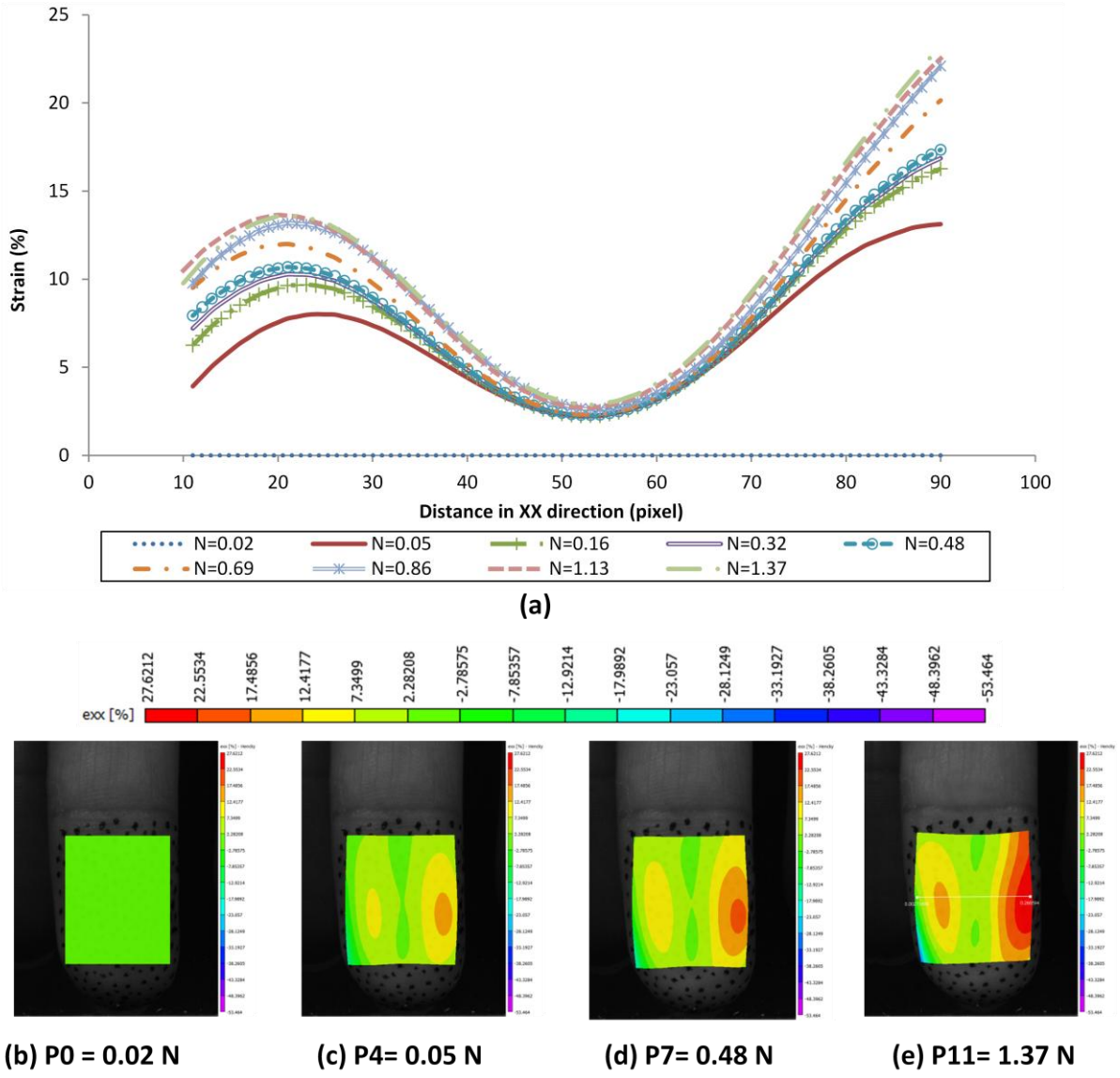

Figure 8.6: (a) The plot of strain data along the centre line in XX direction (measurement started from the left edge of the imaging window to the right edge) on a finger-pad skin under different loads, (b) four examples of corresponding DIC images of the skin.

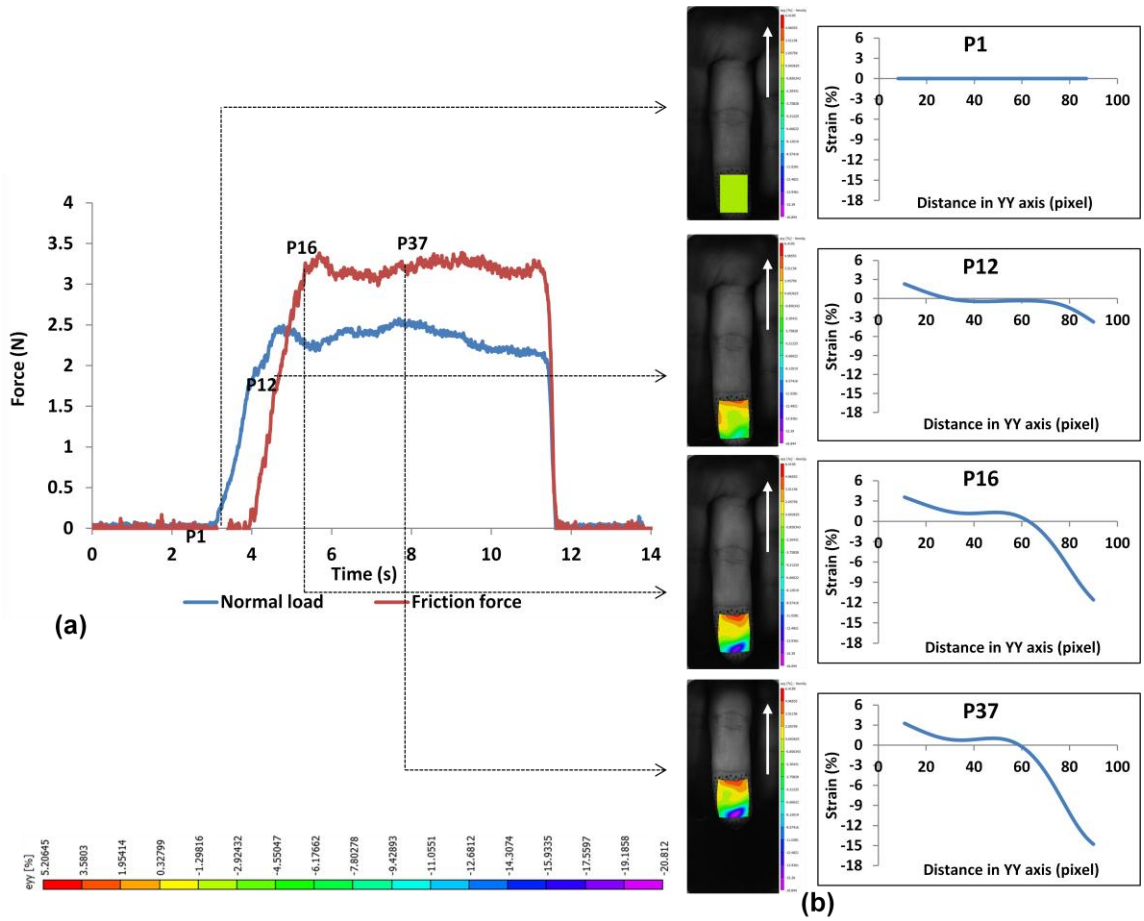

Figure 8.7: Four different data points in a figure of friction and normal forces as a function of time were selected and analysed using strain fields, i.e. P1 was collected from the natural state; P12 was taken from the static phase (no movement occurred in the interface between the finger-pad and the glass); P16 was the point that the finger broke free and started to move and P37 was taken from the dynamic phase.

Figure 8.7 displays a view of the local shear strain on the finger-pad skin surface corresponding to the friction force during the finger sliding. Calculations of the strain value started from the end closest to the distal interphalangeal joint on the front fingertip. Four different points in the time history curves (Figure 8.7 (a)) of the normal force and the friction force were taken and analysed. Point P1 was located at the point where no or less external forces were applied to the skin, and acts as a reference point, thus its corresponding strain values were found to be equal to zero along the vertical line in YY axis. After the finger was placed onto the glass surface, the normal load initially reached a plateau (approximately 2.5 N) at around 4 *s*; meanwhile the friction force was continually increasing. At this moment there was no relative moment between the finger-pad and the glass, Point P12 was chosen at

the point when the normal force reached its maximum value. It can be seen that the skin was stretched at the front fingertip with a strain value of 2.3%, and squeezed at around the distal interphalangeal joint with a strain value of -3.2%. Point P16 was referred to as the transition point between the static stage and dynamic motion of the finger. At Point P16 the shear strain value of the skin was found to increase to 3.6% at the front fingertip, and decrease to -11.2% at around the distal interphalangeal joint. Point P37 was taken from the point where finger was sliding along the glass steadily. Due to the fact that both the normal and friction force remained unchanged when the finger moved from P16 to P37, it is reasonable to observe that P37 gives a similar plot of the strain data along the vertical line (in YY direction) on the skin.

In addition, the strain values in the centre region of the vertical line (in YY direction) on the skin (ranged from 30 pixels (5 *mm*) to 60 pixels (10 *mm*)) were found relatively small compared to other regions for all tested positions. This observation confirms the previous finding that skin deformation only exists in specific areas on skin. It can be seen that the middle region of the finger-pad was unlikely to be influenced by external forces in the preloading phase during finger movement over a dry and smooth surface. The value of the strain rose to about 1% in the dynamic phase.

By analysing the DIC images, it was found that, as the finger started to contact with the glass surface, there was an initial contact area between the centre of finger-pad skin and the glass plate. The centre skin was sticking to the glass plate while the surrounding skin moved with the finger. In this case, the initial contact area can be referred to as the "stick" region. The trailing edge in the imaged region of the skin performed some large deformations when the finger overcame the interface resistance and started to move, which can be defined as the "slip" region. As the finger sliding along the glass plate, the stuck region gradually evolved to a slip region and then remained unchanged. The current finding is in good agreement with previous observations reported by Tada et al. (2005). Tada et al. (2005) used a tactile imaging system (includes a light source, CCD camera, etc.) and a force sensor to investigate the contact interface between a finger-pad and a transparent indenter under different contact conditions. They reported that the full stick region gradually

transformed into full slip region during finger sliding. The skin was being stuck for a longer period in the case of low speed and high load.

Recently, similar studies were also reported by André et al. (2008) and Terekhov & Hayward (2011). In their studies, an optical flow technique based on the light reflection has been employed to investigate the contact area of a finger in contact with a planar surface. The principle of the optical flow technique was to use a matching algorithm to detect the motion of the tested object. They observed that a round stick region (black region) existing on the middle of the contact area, is enclosed by slip region (grey region), as seen in Figure 8.8. At a constant normal load of 5 N, the stick ratio (stick area against the contact area) was found to decrease from 0.6 to 0 with increasing the friction force due to the stick area diminished continuously in the preloading phase. In the current study, the stick ratio can also be quantified by analysing the strain data with respect to different phases of finger movement. As shown in Figure 8.7, at Point P1, the strain was found to equal to zero along the YY axis, thus the ratio should be equal to 1. As the friction force increased to 1.79 N (at Point P12), the stick ratio was found to be reduced to 0.48. Since the middle region of the contact area evolved to a slip region during dynamic movement, the corresponding values of the stick ratio were equal to zero for Point P16 and P37.

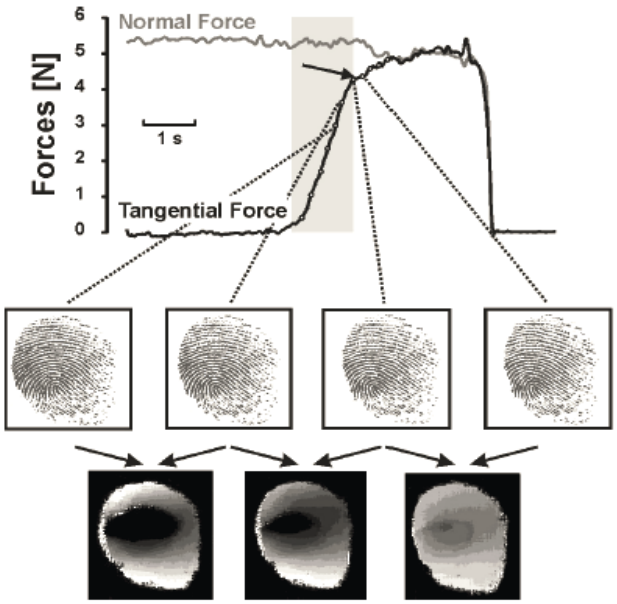

Figure 8.8: Experimental results of the studies conducted by André (2011).

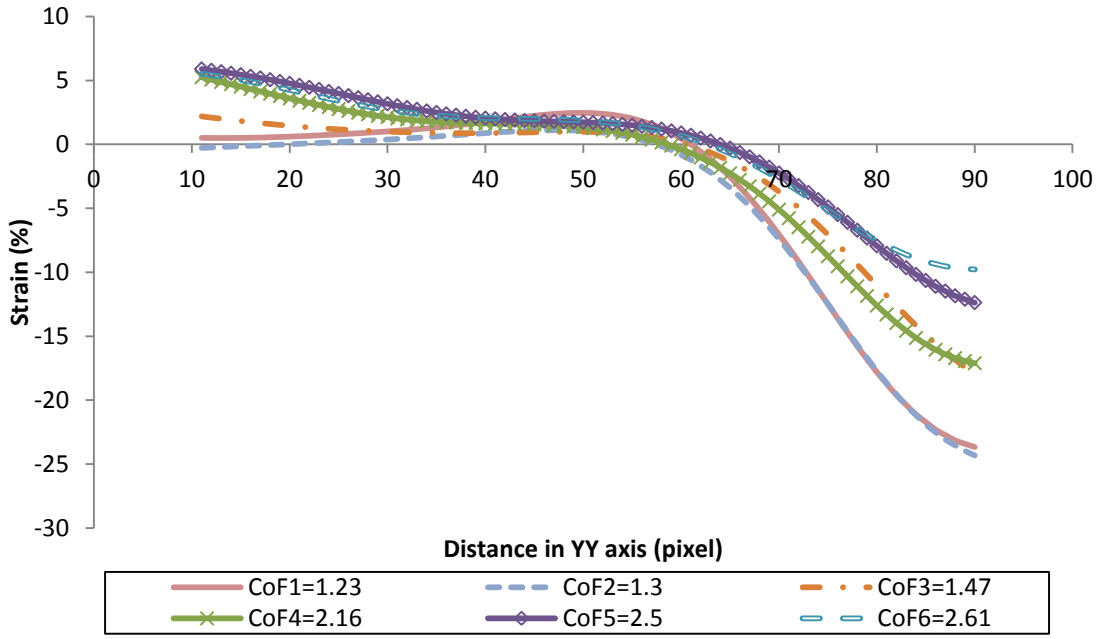

Figure 8.9: The plot of shear strain data along the vertical line in YY axis (obtained from position P37) with respect to different skin dynamic friction coefficients.

Figure 8.9 shows a plot of the shear strain data obtained from Point P37 as a function of the distance along the vertical line corresponding to different dynamic friction coefficients. As the value of the dynamic friction coefficient decreased, the corresponding shear strain data was found to gradually reduce from 5% to 0 at the fingertip, and -10% to -24% at the region around the distal interphalangeal joint. Interestingly, it can be seen that there was a small difference in the shear strain value for the regions of skin stretch (at the fingertip) and squeeze (at the region closest to the distal interphalangeal joint) in the case of the highest dynamic friction coefficients. The difference between the absolute values of the shear strain between these two different regions became bigger as the value of the dynamic friction coefficient reduced.

This phenomenon could be attributed to the differences in the friction force corresponding to different dynamic friction coefficient. In general, under same contact conditions, skin dynamic friction coefficient reduces as the normal load increased. Thus, it can be assumed that a high value of friction coefficient has a relatively small normal load compared to that of a low friction coefficient. Although, the increasing rate of friction force reduces with increasing the normal load, the friction force is still relatively high for a high normal load compared to that of a low

normal load. Increasing friction force caused large deformations occurred in the transverse direction of skin, hence increasing the value of strain. Therefore it is not surprising to observe a large value of strain for a high dynamic friction coefficient. This hypothesis seems be supported by the observations of Tada et al. (2005). They indicated that increasing the normal load would lead to larger stuck region of contact area, resulted in a large stuck area. It is reasonable to observe that the strain value increased with increasing the friction force due to the fact that the friction force is proportional to the contact area.

8.4 Conclusions

This chapter describes a pilot study to investigate the in-plane deformation on finger-pad skin *in-vivo* using a 2D Digital Image Correlation system. This technique can provide full fields of the displacement map and strain distribution on the finger-pad skin corresponding to both static and dynamic movement. By analysing these displacement maps or strain distribution on the skin, it is possible to determine the transverse mechanical properties of the finger-pad skin. Results of this study demonstrated that, in the case of static movement, the skin in the horizontal direction (XX axis) performed some relatively large deformations when a normal load was applied on the skin. For a finger moving over a glass surface, the friction force between the finger and the glass has a significant impact on the skin in the direction of finger movement (YY axis). All the above findings can be used as the basis for assessing the contribution of skin properties on skin friction. In further studies, it would be expected that this technique could also be extended to other aspects in the research field of skin tribology and improve the understanding of the complex skin frictional behaviour on human finger-pads.

Chapter 9

Conclusions and Future Work

In this final chapter the main results and findings from the *thesis* work are summarised and evaluated. Some possibilities for further research into the topic of skin friction of human finger-pads are also outlined.

The thesis aims to gain a better understanding of the human skin frictional properties at finger-pads. From literature, the frictional behaviour of human skin is found to be determined by the complex interplay of materials and surface properties of skin. However, the current knowledge on tribology of skin mainly relates to skin in touch with various materials, and little is known for the effect of properties of skin on friction. Therefore, comprehensive studies to understand how the skin properties affect the friction of human finger-pads are required. In this thesis, the skin frictional properties of human finger-pads have been assessed by combing skin friction measurements using different finger friction rigs with the investigation of skin structural properties using an Optical Coherence Tomography. Firstly, various tests have been carried out to examine the influence of different factors (e.g. load, ages, gender, ethnicity, etc.) on skin friction. Secondly, the OCT technique has been applied to image the sub-surface skin structure, so as to measure the thickness of stratum corneum, the number of sweat ducts and the surface properties of skin, from which the potential relationships between skin structure and its mechanical properties have been assessed. Then, this technique has been extended to measure both the static and dynamic contact areas of finger-pads in contact with a flat surface, which is considered to provide an accurate method for predicting the real contact area compared to the finger-print ink method. Then, the effect of water hydration/lubrication on skin friction based on the mechanism of water absorption has also been investigated. Finally, a pilot study has been conducted using a 2D DIC

system to characterise the lateral skin properties, as the lateral deformation or mechanical properties of skin are believed to have important roles in determining skin friction.

9.1 Conclusions

Investigation of the skin frictional properties

This thesis has presented a general investigation into the frictional properties of human finger-pads in contact with smooth surfaces under dry conditions (Chapter 4). It starts with an evaluation of three different techniques available in The University of Sheffield for measuring the skin friction coefficient at human finger-pads, including a finger friction rig, a multi-axis force plate and a pinch grip rig. The results of the comparison suggested that the multi-axis force plate was the most suitable device for use in this study. The finger friction rig was only considered for use in the case of high load tests due to its low sensitivity in measurements. It also indicated that the pinch grip rig was not applicable for measuring finger friction in this study.

Human skin has a complex frictional behaviour. In this study, the investigation of the skin friction of human fingers indicated that skin friction coefficient varies with loads following a two-term relationship. The first term of the two-term relationship was a power function obtained from low load tests ($\leq$ 2.5 N). The skin friction coefficient was shown to continuously decrease with increasing normal load. In this case, it was assumed that skin friction is associated with both deformation and adhesion mechanisms. When low loads were applied on finger-pad skin, the skin exhibited different types of deformation with different loads, which resulted in different mechanical properties of skin and skin friction coefficient. Increasing the normal load up to certain level, skin became stiff and behaved as a material with steady mechanical properties. The skin friction was considered to be only dominated by the adhesion mechanism. Therefore, it was not surprising to observe a linear regression between the skin friction coefficient and the normal load under high load conditions.

The contribution of skin structure to skin friction

In order to explain the wide spread of friction data obtained among participants in previous work, it would be helpful to investigate the effects of skin properties on its friction and mechanical properties, respectively. Chapter 5 describes some experimental works conducted using a commercial OCT system combined with a "*cutometer*" MPA 580 device. The findings in these studies suggested that the moisture level of skin, skin thickness, and physic-chemical properties play important roles in determining skin friction. The skin friction coefficient was found to increase as a function of the moisture level of skin, which was in good agreement with the experimental observations in the study of Tomlinson et al. (2010) and others (Dinc et al., 1991; Adams et al., 2007; Gerhardt et al., 2008; Hendricks & Franklin, 2010).

Furthermore, a skin rubbing test and a tape stripping test were developed to evaluate if there are potential relationships between skin structural properties and skin friction coefficient. Experimental results of the skin rubbing test showed that the skin friction coefficient has a significant drop with skin rubbing. One of the possibilities for the change in the skin friction coefficient is that skin becomes smooth as the ridges on the skin surface shrink with skin rubbing. The other possibility could be attributed to the decrease in the lateral Young's modulus of skin with respect to the removal of the stratum corneum. In the case of the tape stripping test, it was found that the skin friction coefficient initially increases and then reaches a plateau when increasing the number of tape strips. This phenomenon was ascribed to the changes of adhesion force related to tape stripping. In the current study, the adhesion force was then well studied by investigating van der Waals forces, electrostatic forces, and chemical hydration bonds. Experimental results suggested that the electrostatic forces and the force due to chemical bond are the main contributors to the change of the adhesion force. However, due to the current limited techniques in this study, it won not possible to measure the changes in the electrostatic forces and the chemical bonds.

Measurements of contact area

In Chapter 6, different experimental tests were carried out to determine both static and dynamic contact area between human finger-pads and flat surfaces. The measurements of the static contact area measured using a finger-print ink method and an OCT method were strongly associated with the morphological properties of

finger-pads skin. Both the apparent and real contact area were found to increase as increasing applied normal load, which were in good agreement with a power law relationship of $A \propto W^c$. Comparing the OCT method and the finger-print ink method, indicated that the OCT method provides more accurate experimental results than use of the finger-print ink method. In addition, the investigations of the effect of contact angle and different fingers on skin friction showed that the skin friction was reduced by 42% when the contact angle increased from 15° to 60°. The findings also confirmed that the skin frictional properties of fingers strongly depended on the contact area. However, the results of static measurements were restricted in term of characterising the dynamic frictional behaviour of fingers.

In order to measure dynamic contact area during finger sliding, a DIC method was introduced into this study. As the tested finger was moving along a glass surface, the apparent contact area between the finger-pad and the glass was found to reduce with time, particularly in the static phase. The skin friction was assessed in terms of applied contact pressure. The pressure dependence of the skin friction coefficient was in accordance with a power-law expression. Moreover, the OCT method was also applied in the measurement of the dynamic contact area. However, due to the limitation of imaging area on the skin, the OCT method was more useful for monitoring how skin structural properties change during finger sliding.

The effect of hydration on skin friction

As suggested by previous studies on the effect of water hydration or lubrication on skin friction, the mechanism of water absorption was considered to be the main contributor to the change of skin friction. Therefore, in the current study, the investigation into the influence of hydration or lubrication on skin friction focused on investigating skin structural, mechanical properties and contact area due to water absorption of the skin (Chapter 7). In the measurements of skin structural properties, the thickness of the stratum corneum was assessed as a predictor of changes in the skin physical structure. When a finger was soaked in water for 400 s, its stratum corneum thickness was found to increase by 16%. No significant change was observed on the surface ridges of the skin. As expected, a “bell” curve line was found between the moisture level of skin and hydration time, which was very similar to that of the skin friction. According to previous findings (Chapter 4), skin mechanical

properties are closely associated with its thickness. Therefore, a decrease in the Young's modulus of the finger-pad skin was expected due to water absorption increasing the thickness of the stratum corneum. However, the corresponding experimental results showed that skin mechanical properties were unlikely to be affected by water absorption. These phenomena evidenced that skin moisture level plays a crucial role in determining the skin friction of finger-pads. Furthermore, the effect of water absorption on the contact area between finger-pads and a flat surface was also conducted using the OCT system. In measurements, changes in the ratio of the real contact area against the apparent contact area related to water absorption have been measured. A 60% rise was found in the ratio with hydration time, which could be attributed to the decrease in the skin stiffness due to skin swell. In addition, there may other mechanisms that could enhance the skin friction. Therefore, further studies on these mechanisms behind this phenomenon are needed.

In-plane deformation of finger-pad skin in-vivo

From the knowledge gathered from previous studies and Chapter 4, there was a gap in the lateral deformation/mechanical properties of skin in the studies of human skin friction. Chapter 8 presents a pilot study of using a Digital Image Correlation system to characterise the in-plane deformation properties of finger-pad skin *in vivo*. These studies have been achieved via analysis of displacement maps and strain distributions obtained on the skin surface. When a finger was brought into contact with a flat surface, there were some distortions observed in the horizontal direction on the finger-pad. When the finger overcame the interface resistance and started to move, deformations in the direction of finger sliding on the skin gradually became significant. These observations can be used as the basis for assessing the contribution of skin properties on skin friction.

9.2 Future Work

The work presented in this thesis has involved a detailed study of several aspects of finger friction with the aim to close the gaps in the current knowledge on the skin friction of human finger-pads. A number of questions have arisen during this research, which suggest a variety of research directions that need to be pursued. Each

aspect below contains a list of suggestions that could be undertaken in further research.

Skin frictional properties

- All experiments conducted in the current study were based on the hypothesis that skin friction was only associated with the adhesion mechanism in the case when a finger was sliding a smooth surface under dry conditions. In real daily life, human finger could not be always in contact with flat surfaces. There is a need for detailed studies to be performed on other mechanisms (e.g. deformation mechanisms and interlocking) related to rough contact between finger-pads and surfaces.

- Due to the current limited techniques, most measurements of skin friction were restricted to between 1 N and 10 N (defined as the macroscopic level). Theoretical concepts of skin friction in the microscale (< 1 N) are widely unknown. Knowledge of the microtribology would allow a detailed investigation of the deformation mechanism in connection with skin structural properties, and improve the knowledge of tactile perception and haptics necessary for the developments of artificial devices.

Human skin properties

- It is general considered that skin friction is highly dependent on the global Young's modulus of skin rather than the layer of the stratum corneum. The global Young's modulus of skin is ascribed to the contribution of the dermis. The OCT system applied in this study is ideal for investigating skin surface properties. Measurements of the thickness of dermis can accurately characterise the relationship between skin structural properties and skin friction, which could be achieved using some medical instruments with ability that can image a fewer millimetre depth in skin, such as advanced OCT system, MRI and ultrasound.

- Findings in Chapter 5 provide evidence that the physico-chemical properties of skin have enormous influences on the skin friction force. However, these

physio-chemical properties involving various mechanisms are poorly understood, therefore, related studies will be required in future research.

Contact conditions

- The importance of the contact area between finger-pads and surfaces on skin friction has been emphasised. However, in the current study, measurements using the OCT (in micro-scale) and the DIC systems (in macro-scale) were only applicable for fingers are contacting with flat and transparent materials. A new method needs to be developed. It should be able to investigate of the contact area between finger-pads and various rough and non-transparent surfaces.

- So far, the study of the effect of hydration on skin friction is focused on the mechanism of water absorption, as well as some related changed in skin structural properties and contact area. Knowledge of the capillary adhesion and viscous shearing of liquid bridges in relation to skin friction is still not clear. Further studies are required to identify their roles in the frictional properties of hydrated skin with respect to each mechanism.

References

Adams, M. J, “Friction of granular non-metals”, in *Fundamentals of friction: Macroscopic and microscopic processes*, Singer, I.L. and Pollock, H.M., Eds., Kluwer Academic, Dordrecht; 183–209, 1991.

Adams, M. J., Briscoe, B. J. and Johnson, S. A., “Friction and lubrication of human skin”, *Tribology Letter* ; 26; 3, 2007.

Agache, P. G, Monneur, C., Lévèque , J. L. and Rigal, J., “Mechanical properties and Young's modulus of human skin in vivo”, *Archives in Dermatological Research*; 269: 221-232, 1980.

Alexander, H., Cook, T. H., “Variations with age in the mechanical properties of human skin in vivo. In: Kennedi RM, ed. Bedsore. *Biomechanics”, Bath: McMillan Press*; 109–118, 1976.

André, T. M., Wan, D., Lefe`vre, P. and Thonnard, J. L., “Moisture Evaluator: a direct measure of fingertip skin hydration during object manipulation”, *Skin Research and Technology*; 14: 385–389, 2008.

André, T. M., Lefe`vre, P. and Thonnard, J. L., “A continuous measure of fingertip friction during precision grip”, *J. Neurosci. Methods*; 179: 224–229, 2009.

André, T. M., Wan, D., Lefe`vre, P. and Thonnard, J. L., “Effect of skin hydration on the dynamics of fingertip gripping contact”, *Journal of the Royal Society Interface*; 8: 1574-1583, 2011.

Archard, J. F., “Elastic deformation and the laws of friction, Proceedings of the Royal Society of London”, Series A, Mathematical and Physical Sciences; 243(1233): 190-205, 1957.

Asserin, J., Zahouani, H., Humbert, P. h., Couturaud, V. and Mougin, D., “Measurement of the friction coefficient of the human skin in vivo. Quantification of the cutaneous smoothness”, *Colloids and Surfaces B: Biointerfaces* ;19: 1-12, 2000.

Bader, D. and Bowker, P., “Mechanical characteristics of skin and underlying tissues *in-vivo*”, *Biomaterials*; 4: 305-308, 1983.

Bagci, A. M, Shahidi, M., Ansari, R., Blair, M., Blair, N. P. and Zelkha, R., “Thickness profiles of retinal layers by optical coherence tomography image segmentation”, *Am. J. Ophthalmol*; 146: 679 -87, 2008.

Barel, A. O., Courage, W. and Clarys, P., “*Suction method for measurement of skin mechanical: the Cutometer*”, In: Serup, J. and Jemec, G.B.E. (eds.) Handbook of Non-Invasive Methods and the skin. Boca Raton, CRC Press; 335-340, 1995.

Blennerhassett, J. M., Carey, L. M. and Matyas, T. A., "Grip force regulation during pinch grip lifts under somatosensory guidance: Comparison between people with stroke and healthy controls", *Archives of Physical Medicine and Rehabilitation; 87*(3): 418-429, 2006.

Bobjer, O., Johansson, S. E. and Piguet, S., "Friction between hand and handle. Effects of oil and lard on textured and non textured surfaces; perception of discomfort", *Appl. Ergon*; 24:190–202, 1993.

Bouwstra, J. A., de Graaff, A., Gooris, G. S., Nijsse, J., Wiechers, J. W. and van Aelst, A. C., "Water distribution and related morphology in human stratum corneum at different hydration levels", *J. Invest. Dermatol*: 120: 750–758, 2003.

Bowden, F. P. and Tabor, D., *Friction and Lubrication of Solids*, Oxford University Press, London, 1954.

Butt, H. J., Cappella, B. and Kappl, M., "Force measurements with the atomic force microscope:Technique, interpretation and applications", *Surface Science Reports*; 59: 1–152, 2005.

Burkitt, H. G., Young, B. and Heath, J. W., *Wheater's Functional Histology: A Text and Colour Atlas*, 3rd ed. New York: Churchill Livingstone, 154, 1993.

Childs, T. H. C., "Human tactile perception of screen printed surfaces: self-report and contact mechanics experiments", *Proc. IMechE; 221: Part J:J, Engineering Tribology*; 427-441, 2006.

Chu, T. C., Ranson, W. F., Sutton, M. A. and Peters, W. H., "Application of digital-image-correlation techniques to experimental mechanics", *Experimental Mech*; 25: 232–244, 1985.

Cole, K. J., Rotella, D. L. and Harper, J. G., "Mechanisms for Age-Related Changes of Fingertip Forces during Precision Gripping and Lifting in Adults", *The Journal of Neuroscience*; 19: 3238–3247, 1999.

Comaish, S. and Bottoms, E., "The skin and friction: deviations from Amonton's laws, and the effects of hydration and lubrication", *Br. J. Derm*; 84: 37, 1971.

Cua, A., Wileherim, k. P., and Maiback, H. I., "Frictional properties of human skin: relation to age, sex, and anatomical region, stratum corneum hydration and transepidermal water loss", *Br. J. Dermatol*; 123: 473-9, 1990.

Cua, A., Wileherim, k. P., and Maiback, H. I., "Elastic properties of human skin: relation to age, sex, and anatomical region", *Arch Dermatol Res*; 282: 283-288, 1990.

Cua, A. B., Wilhelm, K. P. and Maibach, H. I., "Skin surface lipid and skin friction: relation to age, sex and anatomical region", *Skin Pharmacol; 8:246–251, 1995.*

Daly, C., "Biomechanical properties of dermi", The Journal of Investigative Dermatology; 79: 17-20, 1982.

Davim, J. P., *Biotribology*, Wiley-ISTE. London, 2010.

Delalleau, A., Josse, G. Lagarde, J. M. Zahouani, H. and Bergheau, J. M., "A nonlinear elastic behavior to identify the mechanical parameters of human skin in vivo", *Skin Research and Technology*; 14: 152, 2008.

Deleau, F., Mazuyer, D. and Koenen, A., "Sliding friction at elastomer/ glass contact: Influence of the wetting conditions and instability analysis", *Tribol. Int*; 42:149–159, 2009.

Derler, S., Schrade, G.U. and Gerhardt, L.C., "Tribology of human skin and mechanical skin equivalents in contact with textiles", *Wear*; 263: 1112-1116, 2007.

Derler, S., Gerhardt, L. C., Lenz, A., Bertaux, E. and Hada, M., "Friction of human skin against smooth and rough glass as a function of the contact pressure", *Tribology International*; 42: 1565–1574, 2009.

Derler, S. and Gerhardt, L. C, "Tribology of skin: review and analysis of experimental results for friction coefficient of human skin", *Tribol Lett*; 2011.

Diridollou, S., Patat, F., Gens, F., Vaillant, L., Black, D., Lagarde, J. M., Gall, Y. and Berson, M., "In vivo model of the mechanical properties of the human skin under suction", *Skin Res. Technol*; 6: 214-221, 2000.

Diridollou, S., Vabrey, V., Bersony, M., Vaillantz, L., Black, D., Lagarde, J. M., Gre¤goirey, J. M., Gall, Y. and Pataty, F., "Skin ageing: changes of physical properties of human skin in vivo", *International Journal of Cosmetic Science*, 2001, 23, 353-362

Dinc¸, O. S., Ettles, C. M., Calabrese, S. J. and Scarton, H. A., "Some parameters affecting tactile friction", *J. Tribol*; 113: 512–517, 1991.

Dobrev, H., "Use of cutometer to assess epidermal hydration hydration", *Skin. Res Technol*, 6: 239-244, 2000.

Dowson, D. and Wright, V., "Bio-tribology. In Proceedings of the Conference on The Rheology of Lubrication", *The Institute of Petroleum,The Institution ofMechanical Engineers, and the British Society of Rheology, London*; 81–88, 1973.

Dowson, D., *Tribology and the skin surface*, In: Wilhelm K-P, et al., editors. Bioengineering of the skin: skin surface imaging and analysis. Boca Raton: CRC Press; 159–79, 1997.

Dowson, D., "Bio-tribology", Faraday *Discuss.* 2012; 156, 9-30.

Egawa, M., Hirao, T. and Takahashi, M., "In vivo estimation of Stratum corneum thickness from water concentration profiles obtained with Raman spectroscopy", *Acta Derm Venereol;* 87: 4–8, 2007.

Eldredge, K. R. and Tabor, D., "The mechanism of rolling friction", *I. The plastic range. Proc. R. Soc. Lond*; 229:181-191, 1995.

Elkhyat, A., Courderot-Masuyer, C., Gharbi, T. and Humbert, P., "Influence of the hydrophobic and hydrophilic characteristics of sliding and slider surfaces on friction coefficient: in vivo human skin friction comparison", *Skin Res. Technol*; 10(4): 215–221, 2004).

El-Shimi, A. F., "In vivo skin friction measurements", *J. Soc. Cosmet., Chem.*; 28: 37-51, 1977.

Elsner, P., Wilhelm, D. and Maibach, H. I., "Friction properties of human forearm and vulvar skin: influence of age and correlation with transepidermal water loss and capacitance", *Dermatological*; 181: 88-91, 1990.

Erlandsson, R., Hadziioannou, G., Mate, C. M., McClelland, G. M. and Chaing, S., "Atomic scale friction between the muscovite mica cleavage plane and a tungsten tip:, *J. Chem. Phys*; 89: 5190, 1988.

Escoffier, C., Querleux, B., Rigal, J. d. and Leveque, J., "Age-related mechanical properties of human skin: An in vivo study", *The Journal of Investigative Dermatology*; 93: 353-357, 1989.

Evans, S. L., Holt, C. A., "Measuring the mechanical properties of human skin in vivo using digital image correlation and finite element modelling", *J Strain Anal Eng*; 44(5): 337-345, 2009.

Fercher, A. F., Drexler, W., Hitzenberg, C. K. and Lasser, T., "Optical coherence tomography-pricinples and applications", *Reports On Progress In Physics*; 66: 239-303, 2003.

Fluhr, J., Eisner, P. , Berardesca, E. and Maibach, H. I., *Bioengineering of the Skin, Water and the Stratum Corneum*, 2nd ed.; 105-110, 1994.

Frederick, H. S., Joseph, W. F. and Dale, D., "Viscoelastic properties of human skin and processed dermis", *Skin Research and Technology*; 7: 18-23, 2001.

Friedman, P. M., Skover, G. R., Payonk, G., Kauvar, A. N. and Geronemus, R. G., "3D in-vivo optical skin imaging for topographical quantitative assessment of non-ablative laser technology", *Dermatol Surg*; 28:199-204, 2002.

Fruhstorfer, H., Abel, U., Garthe, C. D., Knüttel, A., "Thickness of the stratum corneum of the volar fingertips*", Clin. Anat*; 13: 429–33, 2000.

Gambichler, T., Jaedicke, V. and Terras, S., "Optical coherence tomography in dermatology*:* technical and clinical aspects*", Arch. Dermatol. Res*; 303: 457-73, 2011.

Gee, M. G., Tomlins, P., Calver, A., Darling, R. H., and Rides, M., "A new friction measurement system for the frictional component of touch", *Wear*; 259: 1437–1442, 2005.

Geerligs, M., *Skin layer mechanics*. PhD Thesis, TU Eindhoven; 2010.

Geerligs, M., Breemen, L. V., Peters, G., Ackermans, P., Baaijens, F. and Oomens, C., "*In vitro indentation to determine the mechanical properties of epidermis"*, *J. Biomech*; 44: 1176–1181, 2011.

Geerligs, M., Oomens, C. W. J., Ackermans, P. A. J., Baaijens, F. P. T. and Peters, G. W. M., "Linear shear response of the upper skin layers", *Biorheology*; 48: 229-45, 2011.

Gerhardt, L. C., Strassle, V., Lenz, A., Spencer, N.D. and Derler, S., "Influence of epidermal hydration on the friction of human skin against textiles", *J. R. Soc. Interface*; 5: 1317–1328, 2008.

Gniadecka, M. and Jemec, G. B. E., "Quantitative evaluation of chronological ageing and photoageing in vivo: studies on skinechogenicityand thickness", *Br. J.Dermatol*; 139,815-821 1998.

Gohar, R. and *Rahnejat. H., Fundamentals of tribology*, Imperial College Press, London; 309-330, 2008.

Grahame, R. and Holt, P. J. L., "The influence of ageing on the in vivo elasticity of human skin", *Gerontologia*; 15: 121–139, 1969.

Grahame, R., "Elasticity of human skin in vivo", *Ann Phys Med*; 10: 130–134, 1969.

Greenwood, J. A. and Tabor, D., "The friction of hard sliders on lubricated rubber the importance of deformation losses", *Proceedings of the Physical Society of London*; 71: 989–1001, 1958.

Guerret-Piécourt, C., Vallayer, J. and Tréheux, D., "Limitation induced by electrical charges effects on micromechanisms", Wear; 254: 950–958, 2003.

Gulati, R. J. and Srinivasan, M. A., "Human fingerpad under indentation I: static and dynamic force reponse", *Bioegineering Conference*; 29: 1995.

Gupta, A. B., Haldar, B. and Bhattacharya, M., "A simple device for measuring skin friction", *Ind. J. Dermatol*; 40(3): 116–121, 1995.

Hall, G., Phillips, T. J., "Estrogen and skin: the effects of estrogen, menopause, and hormone replacement therapy on the skin", *J Am Acad Dermatol*; 53:555–568, 2005.

Han, H. Y., Shimada, A. and Kawamura, S., "Analysis of friction on human fingers and design of artificial fingers", *In IEEE International Conference on Robotics and Automation, Minneapolis, Minnesota*; 3061–3066, 1996.

Hendriks, F. M., Brokken, D., Oomens, C. W. J., and Baaijens, F. P. T., "Influence of hydration and experimental length scale on the mechanical response of human skin in vivo, using optical coherence tomogtpahy", *Skin Research and Technology*; 10: 231-241, 2004.

Hendriks, F. M., Mechanical behaviour of human epidermal and dermal layers in vivo, PhD Thesis. Technische Universiteit , Eindhoven; 2005.

Hendriks, F. M., Brokken, D., Oomens, C. W. J., *Mechanical properties of different layers of skin*, Philips Research Laboratories, Eindhoven and Eindhoven University of Technology; available at: http://www.mate.tue.nl/mate/pdfs/249.pdf.

Hendriks, C. P. and Franklin, S. E., "Influence of Surface Roughness, Material and Climate Conditions on the Friction of Human Skin", *Tribol Lett*; 37: 361-375, 2010.

Highley, D. R., Commey, M., Denbestes, M. and Wolfram, L. J., "Friction properties of skin", *The journal of investigative Dermatology*; 69: 303-305, 1977.

Hof, C. and Hopermann, H., "Comparison of replica-and in vivo-measurement of the microtopography of human skin", *SOFW Journal*; 126: 40-46, 2000.

Holzapfel, G. A., *Biomechanics of soft tissues: handbook of material behaviour*. Available at http://www.biomech. tugraz.at/papers/report7.pdf 2000: 12.

Huang, D., Swanson, E. A., Lin, C. P., Schuman, J. S., Stinson, W. G., Chanf, W., et al, "Optical Coherence Tomography", *Science*; 254: 1178-1181, 1991.

Jacobi, U., Chen, M., Frankowski., Sinkgraven, R., Hund, M., Rzany, B., Sterry, W. and Lademann, J., "In vivo determination of skin surface topography using an optical 3D device", *Skin Research and Technology*; 10; 207-214, 2004.

Jacquemoud, C., Bruyere-Garnier, K. and Coret, M. "Methodology to determine failure characteristics of plantar soft tissues using a dynamic tensile test", *Journal of Biomechanics*; 40: 468-475, 2007.

Johansson, R. S. and Westling, G., "Roles of glabrous skin receptors and sensorimotor memory in automatic control of precision grip when lifting rougher or more slippery objects", *Exp Brain Res*; 56: 550–564, 1984.

Johnson, S. A., Gorman, D. M., Adams, M. J. and Briscoe, B. J., "The friction and lubrication of human stratum corneum," *In: Thin films in tribology. Leeds–Lyon symposium on tribology, Amsterdam: Elsevier Science Publishers*; 663–72, 1993.

Johnson, K. L., *Contact mechanics*, Cambridge University Press, Cambridge, 1985.

Jones, L. A. and Lederman, S. J., *Human hand function*, Oxford University Press, 2006.

Juniper, K. J. and Dykman, R. A., "Skin resistance, sweat gland counts, salivary flow, and gastric secretion: age, race, and sex differences, and intercorrelations", *Psychophysiology*; 4: 216-222, 1967.

Katz, D. A., *Fingerprinting*, 1993, 2002, 2005. Available at: http://www.chymist.com /FINGERPRINTIN G .pdf.

Kinoshita, H., Backstrom, L., Flanagan, J. R. and Johansson, R. S., "Tangential torque effects on the control of grip forces when holding objects with a precision grip", *J. Neuophysiol*; 78: 1619-1630, 1997.

Koudine, A. A. and Barquins, M., "Frictional properties of skin: proposal of a new approach", *International Journal of Cosmetic Science*; 22: 11-20, 2000.

Kwiatkowska, M., Franklin, S. E., Hendriks, C. P. and Kwiatkowski, K., "*Friction and deformation behaviour of human skin", Wear*; 267(5-8): 1264-1273, 2009.

Lagarde, J. M., Rouvrais, C. and Black, D., "Topography and anisotropy of the skin surface with ageing. Skin Res", *Technol*; 11: 110–119, 2005.

Landau, L. D. and Lifshitz, E. M., *Electrodynamics of continuous media*, Pergamon Press, London; 8: 317-318, 1960.

Leveque, J. L., *Bioengingeering of the skin: water and the stratum corneum*, second edition; 15-26, 2005.

Lewis, R., Menardi, C., Yoxall, A., "Langley J. Finger friction: grip and opening packaging", *Wear*; 263(7 - 12): 1124 – 1132, 2007.

Liang, X. and Boppart, S., "Biomechanical properties of in vivo human skin from dynamic optical coherence elastography", *IEEE Trans. Biomed. Eng*; 57: 953-959, 2010.

Li, L., Mac-Mary, S., Marsaut, D., Sainthillier, J.M., Nouveau, S.,Gharbi, T., de Lacharriere, O. and Humbert, P., "Age-related changes in skin topography and microcirculation", *Arch. Dermatol. Re*; 297: 412–416, 2006.

Lodén, M., Olsson, H., AxeÂll, T. and Werner, L. Y., "Friction, capacitance and transepidermal water loss (TEWL) in dry atopic and normal skin", *British Journal of Dermatology*; 126: 137-41, 1992.

Lu, Z. H., Kasaragod, D. K. and Matcher, S. J., "Optic axis determination by fibre-based polarization-sensitive swept-source optical coherence tomography", *Phys. Med. Biol*; 56: 1105-1122, 2011.

Maksic, Z. B. and Orville-Thomas, W. J., "Modern *Modelling of the Chemical Bond", Elsevier*: Amsterdam; 519-536, *1999*.

Man, M. Q., Xin, S. J., Song, S. P., Cho, S.Y., Zhang, X. J., Tu, C. X., Feingold, K. R., Elias, P. M., "Variation of skin surface pH, sebum content and stratum corneum

hydration with age and gender in a large Chinese population", *Skin Pharmacol Physiol*; 22:190–199, 2009.

Marcellier. H., Vescovo, P., Varchon, D., Vacher, P, and Humbert, P., "*Optical analysis of displacement* and *strain fields on human skin", Skin Research and Technology*; 7: 246–253, 2001.

Martin, Y., Abraham, D. W. and Wickramasinghe, H. K., "High resolution capacitance imaging and potentiometry by force microscopy", *Appl. Phys. Lett*; 52: 1103, 1988.

Masen, M. A. "A systems based experimental approach to tactile friction", *J. Mech. Behav. Biomed. Mater*; 4: 1620-6, 2011.

Meyers, M. A., Chen, P. Y., Lin, A. Y. M. and Seki, Y., "Biological materials: Structure and mechanical properties", *Progress in Materials Science*; 53: 1-206, 2008.

Moore, D. F., *The friction and lubrication of elastomers*, Pergamon Press Inc. New York, 1972.

Mossel, W. P. and Roosen, C. P. G., "Friction and the skin", *Contemporary* Ergonomics; 1: 353-358, 1994.

Nakajima, K. and Narasaka, H., "Evaluation of skin surface associated with morphology and coefficient of friction", *International Journal of Cosmetic Science*;15: 135-151, 1993.

Naylor, P. F. D., "The skin surface and friction", *Br J Dermatol*; 67: 239-248, 1955.

Nohara, K., Ueda, Y., Fuji, T., Ohmi, M., and Haruna, M., "Study of dynamics of sweat glands of human fingertip using all-optical fibre high-speed OCT", *Laser and Electro-Optics*; 92-93, 2005.

Nonomura, Y., Fujii, T., Arashi, Y., Miura, T., Maeno, T., Tashiro, K., Kamikawa, Y. and Monchi, R., "Tactile impression and friction of water on human skin", *Colloids Surf. B: Biointerfaces*; 69: 264–267, 2009.

Norlen, L., Emilson, A., and Forilind, B., "Stratum corneum swelling", *Ach Dermatol res*; 289: 506-513, 1997.

Oliver, W. C. and Pharr, G. M., "An improved technique for determining hardness and elastic modulus using load and displacement sensing indentation experiments", *J. Mater. Res*; 7 (6): 1564–83, 1992.

Olsson, H., Åström, K. J., Canudas de Wit, C. Gäfvert, M. and Lischinsky, P., "Friction model and friction compensation", *Publisher: SPRINGER*; 4: 1-37, 1998.

Pailler-Mattei, C. and Zahouani, H., "Study of adhesion force and mechanical properties of human skin in vivo", *J Adhes. Sci. Technol*; 18: 1739-1758, 2004.

Pailler-Mattei, C., Bec, S. and Zahouani, H., "In vivo measurements of the elastic mechanical properties of human skin by indentation tests", *Medical Engineering &Physicas*; 30: 599-606, 2008.

Pailler-Mattei, C., Pavan, S., Vargiolu, R., Pirot, F., Falson, F. and Zahouani, H.,"Contribution of stratum corneum in determining bio-tribological properties of the human skin", *Wear*; 263:1038-1043, 2007.

Pailler-Mattei, C., Nicoli, S., Pirot, E., Vargiolu, R. and Zahouani, H., "A new approach to describe the skin surface physical properties in vivo", *Colloid Surf*; 68: 200–206, 2009.

Pailler-Mattei, C., Guerret-Piécourt, C., Zahouani, H. and Nicoli, S., "Interpretation of the human skin biotribological behaviour after tape stripping", *J R Soc Interface*; 8: 934-941, 2011.

Park, A. and Baddiel, C., "Rheology of stratum corneum-I: a molecular interpretation of the stress-strain curve", *J. Soc. Cosmet. Chem*; 23: 3–12, 1972.

Pasumarty, S., Johnson, S., Watson, S., Adams, M., "Friction of the human finger pad: influence of moisture, occlusion and velocity", *Tribol. Lett*; 44: 117-37, 2011.

Payne, P. A., "Measurement of properties and function of skin", *Clin. Phy. Meas*;12: 105-129, 1991.

Persson, B. N. J., "Capillary adhesion between elastic solids with randomly rough surfaces", *J. Phys. Condens. Matter*; 20: 1–11, 2008.

Peter, A. P., "Measurement of properties and function of skin", Clin. Phys. Physoil. Meas; 12: 105-129, 1991.

Philip, W. W and Bozenma, B. M., *Bioengingeering of the skin: water and the stratum corneum*, second edition; 359-368, 2005.

Prall, J. K., "Instrumental Evaluation of the Effects of Cosmetic Products on Skin Surfaces with Particular Reference to Smoothness", *J. Soc. Cosmet. Chem*; 24: 693-707, 1973.

Rosén, B. G., Blunt, L. and Thomas, T. R., "On in-vivo skin topography metrology and replication techniques", *Phy.: Conf. Ser*; 13: 325-329, 2005.

Ramalho, A., Silva, C. L., Pais, A. A. C. C. and Sousa, J. J. S., "*In-vivo* friction study of human skin: influence of moisturizers on different anatomical sites", *Wear*; 263: 1044–1049, 2007.

Rohr, M. and Schrader, K., "Fast optical in vivo topometry of human Skin (FOITS)-comparative investigation with laser profilometry", *SOFW Journal*; 124: 52-59, 1998.

Sanders, R., “Torsional elasticity of human skin in vivo”, *Pflügers Arch*; 342: 255–260, 1973.

Sato, J., Yanai, M., Hirao, T. and Denda, M., “Water content and thickness of the stratum corneum contribute to skin surface morphology”, *Arch. Dermatol. Res*; 292, 412–417, 2000.

Sarkany, I. and Caron, G. A., “Microtopography of human skin”, J. *Anat*; 99: 359-364, 1965.

Savescu, A. D., Latash, M. L. and Zatsiorsky, V. M., “A technique to determine friction at the finger tips”, *J Appl Biomech*; 24(1): 43–50, 2008.

Scherge, M., Gorb, S. S., “Biological micro- and nano-tribology”, *Nature's solutions. Springer. Proc. R. Soc. Lond.* A: 2004.

Schlangen, L. J. M. and Nuijs, A. M., “Human skin: properties, structure and treatments relevant to skin condition”, *Royal Pilips Electronics N. V*: 2000.

Shuster. S., Black, M. M. and Mcvitie, E., “The influence of age and sex on skin thickness, skin collagen and density”, *British Journal of Dermatology*; 93, 639, 1975.

Sivamani, R. K., Goodman, J., Gitis, N. V. and Maibach, H. I., “Friction coefficient of skin in real-time”, *Skin Research and Technology*; 9: 235-239, 2003.

Sivamani, R. K., Wu, G. C., Gitis, N. V., and Maibach, H. I., “Tribological testing of skin products: gender, age, and ethnicity on the volar forearm”, *Skin Research and Technology*; 9(4): 299–305, 2003.

Silver, F. H., Freeman, J. W. and DeVore, D., “Viscoelastic properties of human skin and processed dermis”, *Skin Res Technol*; 7: 18–23, 2001.

Soneda, T. and Nakano, K., “Investigation of vibrotactile sensation of human fingerpads by observation of contact zone”, *Tribology International*; 43: 210-217, 2010.

Spurr, R. T., “Fingertip friction”, *Wear*; 39: 167-171, 1976.

Stachowiak, G. W. and Batchelor, A. W., *Engineering tribology* , 3rd. Edition, Elsevier, 2005.

Sutton, M. A., Wolters, W. J., Peters, W. H., Ranson, W. F. and McNeill, S. R., “Determination of displacements using an improved digital correlation method”, *Image Vision Computing*; 1(3): 133–139, 1983.

Tada, M., Kanade, T., “An imaging system of incipient slip for modeling how human perceives slip of a fingertip”, *In Proceedings of the 26th Annual Int. Conf. of the IEEE Engineering in Medicine and Biology Society*; 2045-2048, 2004.

Takema, Y., Yorimoto, Y., Kawai, M. and Imokawa, G., "Age-related changes in the elastic properties and thickness of human facial skin", *Br. J. Dermatol*; 131: 641-648, 1994.

Tang, W., Ge, S. R., Zhu, H., Cao, X. C. and Li, N., "The influence of normal load and sliding speed on frictional properties of skin", *Journal of bionic engineering*; 5: 33-38, 2008.

Terekhov, A. V. and Hayward, V., "Minimal adhesion surface area in tangentially loaded digital contacts*",* *J Biomech*; 43: 2508-2510, 2011.

Tomlinson, S. E., Lewis, R. and Carré, M .J., "Review of the frictional properties of finger-object contact when gripping", *Proc. IMechE*; 221: 841-850, 2007.

Tomlinson, S. E., *Understanding the friction between human finger and contacting surfaces* [PhD Thesis]. The University of Sheffield, 2009.

Tomlinson, S. E., Lewis, R. and Carré, M .J., "The effect of normal force and roughness on friction in human finger contact", *Wear*; 267: 1311-1318, 2009.

Tomlinson, S. E., Lewis, R., Liu, X., Texier, C. and Carré, M. J., "Understanding the friction mechanisms between the human finger and flat contacting surfaces in moist conditions", *Tribo Lett* ; 41: 283-294, 2010.

Tomlinson, S. E., Carré, M. J., Lewis, R. and Franklin, S., "Human finger contact with small,triangular ridged surfaces", *Wear*; 271: 2346-2353, 2011.

Treffel, P., Panisset, F., Faivre, B. and Agache, P., "Hydration transepidermal water loss, pH and skin surface parameters: correlations and variations between dominant and non-dominant forearms", *British Journal of Dermatology*; 130: 325-328, 1994.

Tung, S. H. and Sui, C. H., "*Application of digital-image-correlation techniques in analysing cracked cylindrical Pipes", Sadhana*; 35: 557-567, 2010.

van Kuilenburg, J., Masen, M. A., Bana, V., Groenendijk, M., van der Heide, E., "An experimental study on the relation between surface texture and tactile friction", *Tribology International*; 48: 15-21, 2012.

van Kuilenburg, J., Masen, M. A. and van der Heide, E., "The role of the skin microrelief in the contact behaviour of human skin: Contact between the human finger and regular surface textures", Accepted for Publication in *Tribology International*; http://www.utwente.nl/ctw/tr/Staff/Staff/Masen/TribInt_2012.pdf, 2012.

Veijgen, N. K., Masen, M. A. and van der Heide, E., "Relating friction on the human skin to the hydration and temperature of the skin", Accepted for Publication in Tribology Letter; http://www.springerlink.com/content/a6w77365m6124387/full text . pdf, 2012.

Veijgen, N. K., Masen, M. A. and van der Heide, E., "A novel approach to measuring the frictional behaviour of human skin in vivo", *Tribology International*; 54: 38–41, 2012.

Verdier-Sévrain, S. and Bonté, F., "Skin hydration: a review on its molecular mechanisms", *J Cosmet Dermatol*; 6: 75-82, 2007.

Warman, P. W. and Ennos, A. R., "Fingerprints are unlikely to increase the friction of primate fingerpads", *Journal of Experimental Biology*; 212: 2015-2021, 2009.

Welzel, J., Lankenau, E., Birngruber, R. and Engelhardt, R., "Optical coherence tomography of the human skin. Journal of the American Academy of Dermatology", *J. Amer. Acad. Derm*; 37: 958–63, 1997.

Welzel, J., "Optical coherence tomography in dermatology: a review", *Skin Research and Technology*; 7: 1-9, 2008.

Wildnauer, R. H., Bothwell, J. W. and Douglass, A. B., "Stratum corneum biomechanical properties", *Journal of Investigative Dermatology*; 56: 72-78, 1971.

Wolfram, L. J., "Friction of skin", *Journal of the Society of Cosmetic Chemists*; 34: 465-476, 1983.

Wood, E. J. and Bladon, P. T. "The human skin", *Studies in Biology*; 162: 1985.

Wu, K. S., van Osdol, W. W. and Dauskardt, R. H., "Mechanical properties of human stratum corneum: effects of temperature, hydration, and chemical treatment", *Biomaterials*; 27:785–795, 2006.

Wu, W. C., *Tactile sensing of shape: Biomechanics of contact investigated using imaging and modelling* [PhD Thesis]. Massachusetts Institute of Technology, 2006.

Xin, S., Man, W., Fluhr, J. W., Song, S., Elias, P. M., Man, M. Q., "Cutaneous resonance running time varies with age, body site and gender in a normal Chinese population", *Skin Res Technol*; 16:413–421, 2010.

Xydas, N. and Kao, I., "Modeling of contact mechanics and frictionlimit surface for soft fingers in robotics, with experimental results", *Int. Jour. of Robotic Research*; 18(8): 941–950, 1999.

Yoshimune, N., Takaharu , F., Yuichiro, A., Taku, M., Takashi, M., Kaoru, T., et al., "Tactile impression and friction of water on human skin", *Colloids and surfaces B: Biominterfaces*; 69: 264-267, 2009.

Yoneyama, S. and Murasawa, G., "*Experimental mechanics-digital image correlation"*, Available from: http://www.eolss.net/Sample-Chapters/C05/E6-194-04.pdf, 2011. Accessed on 30 August 2012.

Yuan, Y. and Verma, R., "Measuring microelastic properties of stratum corneum", *Colloids and Surfaces B: Biointerfaces. Colloids Surf. B*: *Bioint- erfaces*; *48*: 6–12, *2006*.

Zahouani, H., Boyer, G., Pailler-Mattei, C., Tkaya, M. B. and Vargiolu, R., "Effect of human aging on skin rheology and tribology", *Wear*; 271: 2364-2369, 2011.

Zhang, M. and Mak, A. F. T., "In vivo friction properties of human skin", *Prosthetics and Orthotics International*; 23: 135-141, 1999.

Zhu, Y. H., Song, S. P., Luo, W., Elias, P. M. and Man, M. Q., "Characterization of skin friction coefficient, and relationship to stratum corneum hydration in a normal Chinese population", *Skin Pharmacol. Physiol*; 24: 81–86, 2011.

http://www.moritexusa.com/products/product.php?plid=5&pcid=10&pid=17. Accessed 1/12/2009.

Appendix A – Publications

Liu, X., Lu, Z., Lewis, R., Carré, M. J. and Matcher, S. J., "Feasibility of using Optical Coherence Tomography to study the influence of skin structure on finger friction", *Tribology International*; 63: 34-44, 2013.

Liu, X., Lewis, R., Carré, M. J., Matcher, S. J. and Lu, Z., "Investigation of the contact area for human finger-pads against flat surfaces", *Proceedings of the 9th Tribo Uk Conference*; 24-25, 2012.

Tomlinson, S. E., Lewis, R., Liu, X., Texier, C. & Carré, M. J., "Understanding the friction mechanisms between the human finger and flat contacting surfaces in moist conditions", *Tribology Letters*; 41(1): 283-294, 2010.

Appendix B- Screen of *"NetForce"*

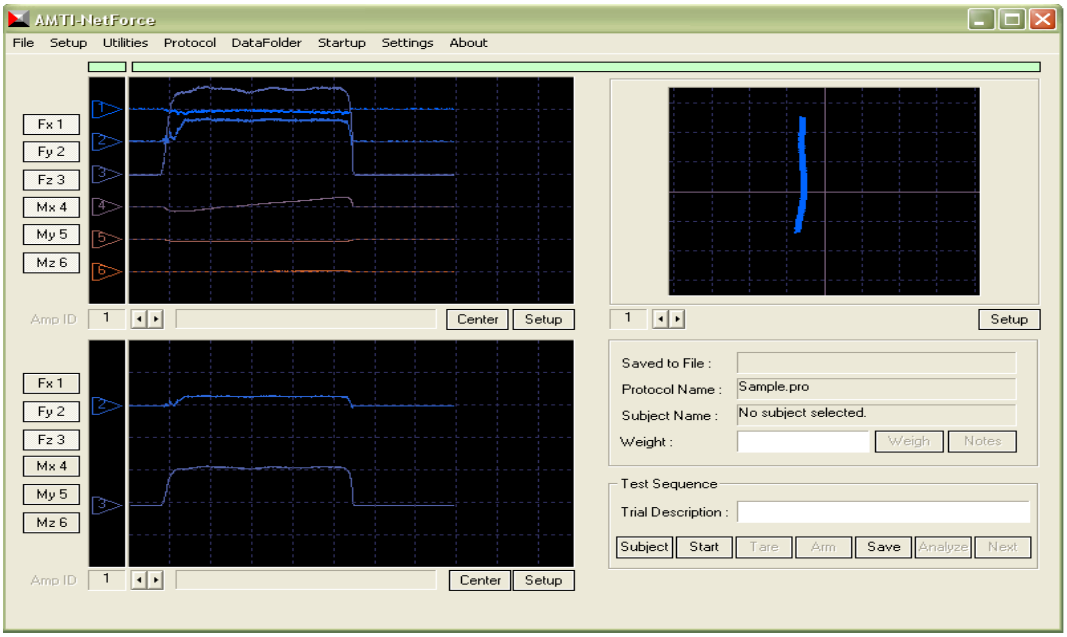

Appendix C –Participant Consent Form from The University of Sheffield

Title of Project: Investigation of the effect of mechanical properties of human skin in the friction coefficient of finger-pads.
Name of Researcher: Xiaoxiao Liu
Participant Identification Number for this project:

Participant ID Number for Questionnaire (if applicable):

Please initial box

1. I confirm that I have read and understood the information sheet for the above project and have had the opportunity to ask questions. ☐
2. I understand that my participation is voluntary and that I am free to withdraw at any time without giving any reason. I may also request that my data/recordings be deleted at any time. ☐
3. I understand that my responses will be anonymised before analysis. I give permission for members of the research team to have access to my anonymised responses. ☐
4. I understand that video footage of task performance will be taken during the testing session and that I am free to stop any video of me being taken. ☐
5. I agree to take part in the above project. ☐

_____	_____	_____
Name of Participant	Date	Signature
_____	_____	_____
Researcher	Date	Signature

Copies:

One copy for the participant and one copy for the Principal Investigator / Supervisor.

Appendix D - User Interface of Pinch Grip Rig and Labview Programme (developed by Peter T Mylon)

User interface:

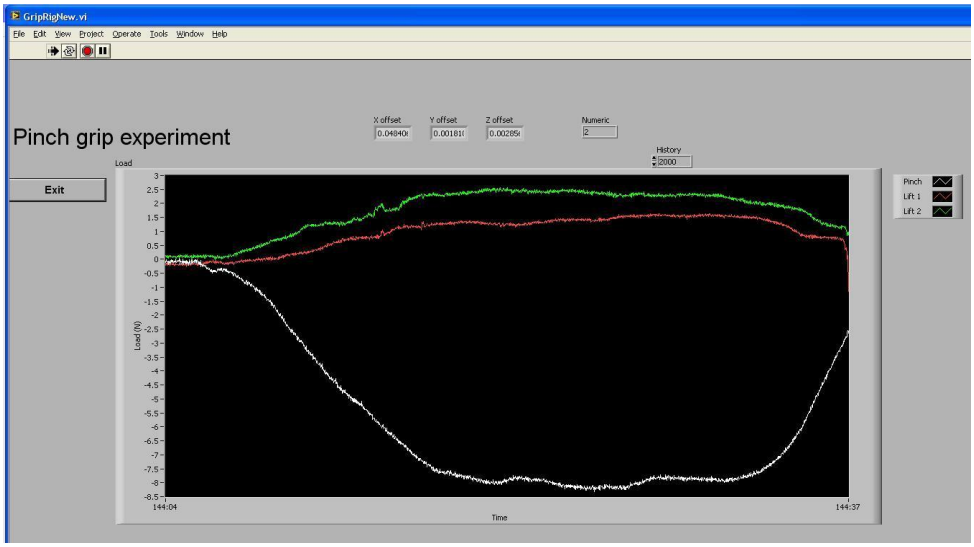

Labview Programme:

```
% find the max and minimum values in a dataset and compile into a
list

fnames = dir('C:\Documents and Settings\Xiaoxiao
Liu\Desktop\pinchGrip\*.txt')
dir_length=length(fnames)
%av_max=[];
%av_min=[];
%sdev_max=[];
%sdev_min=[];

for k=1:dir_length
 file = fnames(k).name
figure
 %file='F:\Pinch Grip Data\pinchGrip_2012-03-26_14-09-34_22.txt'

[time,pinchforce,liftforce1,liftforce2]=textread(file,'%f %f %*f %f
%*f %f','headerlines',23); % read the first two columns into time
and force arrays
%f_length=length(force); % get the length of the force array
ind=[2:2:length(time)];
time(ind)=[];
pinchforce(ind)=[];
liftforce1(ind)=[];
liftforce2(ind)=[];
%[accel]=textread(file,'%*f %f %*f %*f %*f %*f','headerlines',23);
%ind=[1:2:length(accel)];
%accel(ind)=[];
%[max_loc, max_vals]= peakfinder(force)
```

```
%[min_loc, min_vals]= peakfinder(force,[],[],-1)
%max_sort=sort(max_vals,'descend'); % sort max values into a
descending list, i.e highest at top
%min_sort=sort(min_vals,'ascend');  % sort max values into a
ascending list, i.e lowest at top
%v=round(length(max_sort)/5); % this is the number of minimum or max
values selected from the list of peaks / troughs
%w=round(length(min_sort)/5); % this is the number of minimum or max
values selected from the list of peaks / troughs
%max_list=max_sort(1:v) % take the top 'v' values from the list, to
give the biggest peaks
%min_list=min_sort(1:w)

%av_max=[av_max mean(max_vals)]
%av_min=[av_min mean(min_vals)]
%sdev_max=[sdev_max std(max_vals)]
%sdev_min=[sdev_min std(min_vals)]
subplot(2,1,1)
whitebg('white')
%Plot the three graphs in seperate axes on the same figure window:
plot(time,pinchforce,'r')
hold on
plot(time,liftforce1,'g')
hold on
plot(time,liftforce2,'b')
hold on
plot(time,liftforce1 + liftforce2,'k')
xlabel('Time (s)')
%add some axes labels
ylabel('Force (N)')
legend('Pinch Force','Lift Force 1','Lift Force 2','Combined Lift
Force')
%title('Candidate: 4 Sextant: Lower Left Hand Condition: No Gloves')
%end
% subplot(2,1,2)
% whitebg('white')
% %Plot the three graphs in seperate axes on the same figure window:
% plot(time,accel,'r')
% xlabel('Time (s)')
% %add some axes labels
% ylabel('Acceleration (g)')
% title(file)

 end
```

Appendix E – A Sample of Polymer Replica of a Finger-pad

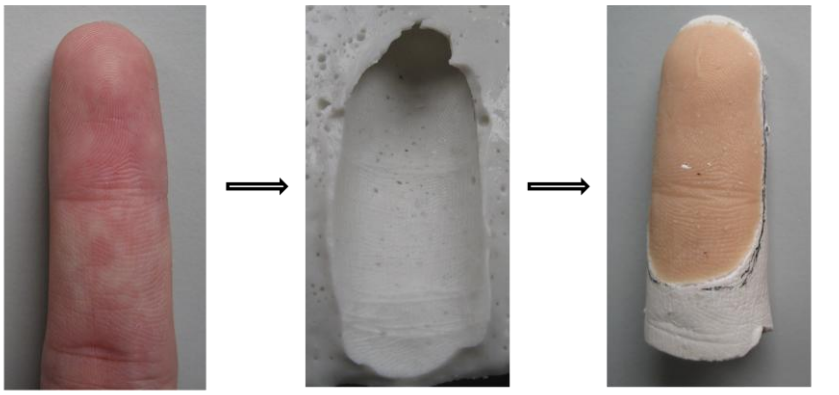

Human real finger Mould Polymer replica finger